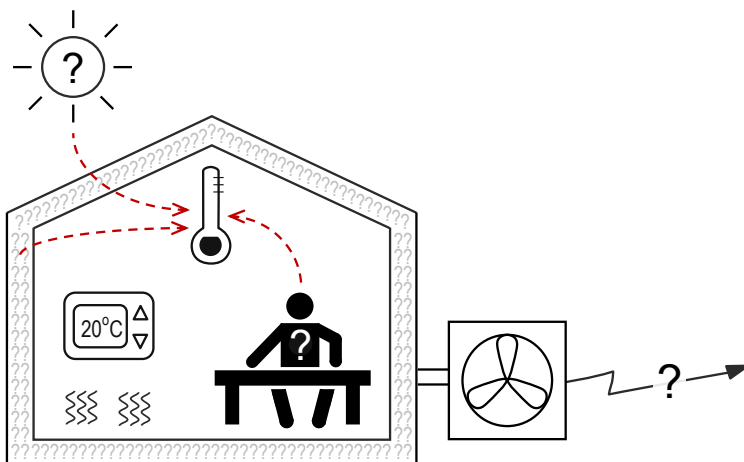


Optimal Operation of Thermostatically Controlled Loads in Residential Buildings under Uncertainty

From a Building to an Electricity System Perspective



Anke Uytterhoeven

Supervisors:
Prof. dr. ir. L. Helsen
Dr. ir. K. Bruninx

Dissertation presented in partial fulfillment of the requirements for the degree of Doctor of Engineering Science (PhD): Mechanical Engineering

February 2022

Optimal Operation of Thermostatically Controlled Loads in Residential Buildings under Uncertainty

From a Building to an Electricity System Perspective

Anke UYTTERHOEVEN

Examination committee:
em. Prof. dr. ir. J.P. Celis, chair
Prof. dr. ir. L. Helsen, supervisor
Dr. ir. K. Bruninx, supervisor
Prof. dr. ir.-arch. D. Saelens
Prof. dr. ir. E. Delarue
Prof. dr. ir. A. Arteconi
Prof. dr. ir. G. Deconinck
Prof. dr. H. Madsen
(DTU)

Dissertation presented in partial fulfillment of the requirements for the degree of Doctor of Engineering Science (PhD): Mechanical Engineering

February 2022

© 2022 KU Leuven – Faculty of Engineering Science
Uitgegeven in eigen beheer, Anke Uytterhoeven, Celestijnenlaan 300 box 2421, B-3001 Leuven (Belgium)

Alle rechten voorbehouden. Niets uit deze uitgave mag worden vermenigvuldigd en/of openbaar gemaakt worden door middel van druk, fotokopie, microfilm, elektronisch of op welke andere wijze ook zonder voorafgaande schriftelijke toestemming van de uitgever.

All rights reserved. No part of the publication may be reproduced in any form by print, photoprint, microfilm, electronic or any other means without written permission from the publisher.

Preface

Een doctoraatstraject afleggen, doe je allesbehalve alleen! Ik wil dan ook heel graag een aantal mensen bedanken, die elk op hun eigen manier een belangrijke rol hebben gespeeld doorheen dit avontuur.

Eerst en vooral... *Lieve*, wat een geluk heb ik gehad om terecht te komen bij een promotor met zo een passie voor het hele energiegebeuren, zo een aanstekelijk enthousiasme, en zo een warm hart voor haar onderzoeksgroep. Ik had bij niemand liever een doctoraat willen maken! Ik zou je oprecht willen bedanken voor alle kansen die je me gegeven hebt, en voor alle keren dat je me uit mijn comfortzone getrokken hebt. Van het zetelen in de Raad van Bestuur van ODE tot een conferentie openen aan jouw zijde... Zonder jouw vertrouwen en aanmoediging zou ik niet staan waar ik vandaag de dag sta. En ons bezoekje aan de lagere school de Zevensprong voor onze warmtepomp-workshop is een herinnering waar ik nog heel lang met een grote glimlach en vol trots aan zal terug denken!

Kenneth, ook jij heel erg bedankt voor je betrokkenheid bij mijn doctoraat, eerst in een informele rol, en later officieel als co-promotor. Jouw inhoudelijke expertise over het hele marktgebeuren is een enorme meerwaarde geweest voor mijn onderzoek! Bedankt voor de vele boeiende en verhelderende discussies, en om steeds opnieuw met even veel enthousiasme mijn talrijke vragen te beantwoorden; geen mail of 'kort' overleg waren ooit te veel, dat heb ik echt enorm geapprecieerd!

Ook *Geert* en *Alessia* wil ik graag bedanken voor hun waardevolle begeleiding als co-promotoren tijdens de eerste fase van mijn doctoraat. Bedankt voor de vele boeiende meetings en goede raad!

I would also like to sincerely thank the members of the jury. *Professor Celis, Lieve, Kenneth, Erik, Dirk, Geert, Alessia* and *professor Madsen*, thank you very much for your thorough review of the text, for the interesting discussions, and for your very valuable suggestions to improve the quality of this dissertation!

Naast mijn (co-)promotor(en) en jury zijn er nog een aantal andere mensen die een zeer waardevolle inhoudelijke bijdrage hebben geleverd tot dit werk. Eerst en vooral, *Robbe*, bedankt voor jouw onmiskenbare bijdrage aan alle wiskundige uitwerkingen doorheen dit werk. Jouw diepgaande wiskundige inzichten en grondige kennis over optimalisatie en ADMM hebben dit werk naar een hoger niveau getild. *Dieter*,

bedankt om me thuis te maken in de hele wereld van vraagzijdemodellering en flexibiliteit, en voor de sterke begeleiding bij de start van mijn doctoraat. *Glenn en Ina*, bedankt voor het delen van alle gebouwmodellen, en om me toch een klein beetje vertrouwd te maken met de principes van gebouwmodellering en bouwfysica. *Steffen*, thanks a lot for your valuable advice regarding ADMM, and for helping me out with the determination of the representative days.

Also *The SySi team* deserves a special place in this preface. It was a great privilege and pleasure to be part of such a nice research group, with such warm and inspiring people, who are always striving to lift the team to a higher level! *Filip*, bedankt voor de vele toffe treinbabbels richting Mechelen, en voor al het (ver)bouwadvies! *Jelger*, bedankt om zo een vrolijke en betrokken collega, bureaugenoot, mede-assistent en mede-thesisbegeleider te zijn. *Javi*, cabrón, thanks for all memorable trips abroad (from playing shuffleboard to almost missing the plane)! *Iago*, thanks for the amazing time in Boulder, and for being my personal Spanish language tutor (with a very particular expertise ;-)). *Damien*, bedankt om mijn visies en inzichten steeds opnieuw uit te dagen met je positief-kritische vragen over mijn onderzoek. *Annelies*, ik heb heel veel van je geleerd als assistente warmteoverdracht, en ik heb enorm genoten van de fijne tijd aan ons 'vrouweneiland'! *Dieter*, ik bewonder enorm wat je met *Duscan* doet, en welk enthousiasme je daarvoor aan de dag legt; ik hoop dat je voor velen (waaronder mezelf) nog lang een inspiratiebron mag zijn! *Bram*, ik heb heel erg genoten van jouw warme persoonlijkheid en gevatte humor, en ik ben nog steeds onder de indruk van jouw talent om les te geven. *Yamid*, your humor and your shared love for plants always brightened up my day. *Wouter*, jouw inzet en gedrevenheid zijn bewonderenswaardig; ik ben er zeker van dat die je nog ver zullen brengen. *Louis en Lucas*, ik wens jullie alle succes toe met jullie startende doctoraten, jullie gaan dat ongetwijfeld goed doen! En het is ongelooflijk fijn om te weten dat dankzij jullie dit werk misschien nog een vervolg zal kennen! Also *Ján*, *Maarten*, *Kristoff*, *Nicholas* and *Deepak*, and *Alessia*, *Rongling* and *Ian*, thanks for sharing this road with me!

To all people at *TME*, thank you for being such amazing co-workers, and for creating such an amiable atmosphere at work! I really treasured this! *Jelger*, *Filip*, *Xu*, *Yamid*, *Annelies*, *Paul*, *Maarten*, *Ján*, *Dries* and *Abdelhalim*, you were all fantastic office mates and members of the 'coffee train'. *Tim*, ook jij ontzettend bedankt, voor alle wandelingen, koffies en vriendschap. Ik ben super blij om dat alles bij de *VREG* te kunnen verder zetten; ik ben blij dat je in mijn tiem, euh, team, zit. ;-)
Dank je wel ook aan *Cindy*, *Marijke*, *Valérie*, *Lieve*, *Regine*, *Nele*, *Natia*, *Marina* en *Jan* voor jullie hulp met alle praktische aangelegenheden!

Ina, ook jij verdient een speciaal plekje in dit dankwoord. Bedankt voor de geweldig toffe samenwerking, je buitengewoon aanstekelijke enthousiasme, en voor alle fijne en eerlijke babbels, over het werk, maar ook over alles daarbuiten!

Cindy en Alexander, Jelle, Thomas en Lisse, Brecht en Annemiek, Stijn, Caroline, Koba, Bastiaan, de Intersoc groep, Team Yodolo, en onze burens, ik zou me echt geen betere vrienden kunnen wensen! Bedankt voor alle steun, en voor de zo welkome afleiding! Iedere babbel, wandeling, etentje, gezelschapsp spel-avond, escape room, The-Block-marathon, padel-match, weekendje weg, skivakantie, ... samen met jullie is telkens weer genieten! *Cindy en Jelle*, jullie wil ik graag nog net dat tikkeltje extra bedanken, om al zó lang mee te bouwen aan twee fantastische vriendschappen, waarvan ik hoop dat er nog heel veel jaren extra op de teller mogen komen!

Ook een oprechte dank je wel aan alle *familie en schoonfamilie*, en in het bijzonder, aan *ons moeke*, voor alle betrokkenheid en interesse, voor alle warmte en gezelligheid, en voor alle goede zorgen en deugddoende kleine attenties.

Mama en papa, "lieve jullie twee, een dikke zoen voor wie jullie zijn en wat jullie doen". Bedankt voor alle kansen die jullie me gegeven hebben, en bedankt om me telkens opnieuw van aan de zijlijn te blijven steunen, motiveren, en aanmoedigen, zoals alleen jullie dat kunnen (●). Bedankt ook voor de ongelooflijk warme thuis die jullie ons geven (waar de koffie en de speculaas nooit ver weg zijn ;-)), en om altijd en overal klaar te staan, niet alleen voor mij en onze Lenn, maar ook voor Robbe, Ilse en ons Kato'tje. Ik ben zo dankbaar en trots om jullie dochter te mogen zijn, en ik hoop dat ik jullie met dit werk ook een beetje trots gemaakt heb.

Lenn en Ilse, ook jullie bedankt om bij te dragen aan ons warme gezin. Het is geweldig hoe jullie deur in Berlaar altijd voor mij en Robbe open staat (en hoe jullie altijd te overtuigen zijn voor een escape room (of zelfs twee!) en sushi ;-)). En *Kato'je*, jij bent de leukste afleiding en beste supporter die ik me tijdens mijn doctoraat had kunnen wensen!

Als laatste, en voornaamste, *Robbe*, dank je wel voor alle liefde en geduld doorheen mijn doctoraat, en om zo goed voor mij te zorgen, zeker tijdens de laatste eindspurt. Ik kon altijd op jou rekenen, voor een luisterend oor, voor hulp bij mijn talloze wiskundige vragen, en zelfs om samen een paper te schrijven (van romantische *life goals* gesproken... ;-)). Ook dank je wel om al zo lang onvoorwaardelijk aan mijn zijde te staan... Ik ben super blij en gelukkig met jou als mijn *partner in crime*, en ik zie jou echt super graag! Ik kijk er ongelooflijk naar uit om samen verder te ontdekken wat het leven nog allemaal voor ons in petto heeft, en om samen verder te bouwen aan onze dromen... De wereld ligt aan onze voeten!

Anke Uytterhoeven
Februari 2022

Abstract

Advanced control strategies, and model predictive control (MPC) in particular, are gaining widespread attention for building climate control, since they can systematically save energy and/or costs with simultaneous thermal comfort improvement, as well as adapt the energy demand in correspondence with the available (renewable/residual) supply via demand response. The performance of any MPC strategy is dependent on the accuracy of the mathematical model describing the thermal loads and on the quality of the forecasts of disturbances, such as weather and occupant behavior. Deviating model parameters and inaccurate disturbance predictions are shown to give rise to increased energy costs and comfort violations if not properly accounted for, and require real-time corrective actions, thereby jeopardizing the participation in possible demand response programs. In contrast to the additive forecast uncertainty, the uncertainty on the building model parameters is typically not explicitly taken into account in MPC applications. Nevertheless, the building controller model is not always capable of capturing the building dynamics in detail, due to the unavailability of sufficient data and/or experts' knowledge to set up the model, and/or due to the impossibility to correctly describe the complexity of the underlying physics. In that case, the parametric uncertainty of the controller model can become non-negligible, and hence, should be accounted for.

Therefore, the main goal of this dissertation is to develop and assess a stochastic model predictive control (SMPC) strategy for building climate control and demand response under combined additive (disturbance forecast) and parametric (model) uncertainty (more specifically referred to as the SMPC^{ap} strategy). The presented approach is tailored to the class of systems represented by a linear time-invariant state space model. Analytically reformulated chance constraints are combined with affine disturbance feedback (ADF) to reduce conservatism.

The SMPC development consists of two important parts. First, starting from the conventional deterministic optimal control problem, a convex stochastic problem formulation is derived, explicitly accounting for additive as well as parametric uncertainties. Second, an appropriate mathematical model of all relevant uncertainties is obtained, serving as an essential input to the stochastic optimal control problem. Here, an important additional contribution, in particular, is the derived probabilistic description of the parameters of a physics-based building controller model. The thermal characteristics of the building envelope, and the derived controller model parameters, are determined based on sparse, publicly available data via the probabilistic characterization method of De Jaeger et al.,

without intensive on-site data collection, which is fundamentally different from what is done in current research.

To fully assess the potential added value of the proposed SMPC^{ap} strategy, its impact is examined at building level, as well as at electricity system level.

At building level, the advantages of the SMPC^{ap} approach are investigated for two different application domains, being optimal control and integrated optimal control and design. Regarding optimal control, the main focus is on the attainable thermal comfort improvement by hedging against uncertainty, and on the associated energy costs. The enhanced uncertainty anticipation of the SMPC^{ap} approach is shown to induce improved thermal comfort in closed-loop simulations compared to the conventional deterministic MPC (DMPC) strategy and the state-of-the-art SMPC^a strategy only accounting for additive uncertainties. These gains are most prominent in buildings equipped with floor heating (representing large thermal inertia) and characterized by the combination of a large model uncertainty and a large nominal heat demand, and this at the expense of limited increases in energy use. For all considered cases, irrespective of the installed heat emission system, 90% of the thermal comfort improvement relative to the DMPC strategy can be realized with a relative increase of at most 9% in energy use. Regarding optimal design, the suitability of the SMPC^{ap} approach for obtaining a more appropriate, yet robust, heat supply system size is illustrated, by incorporating the SMPC^{ap} strategy in an integrated optimal control and design approach. Capacity reductions of 3-5 kW are shown to be achievable in an individual building for a heating system initially sized at 15 kW without increasing thermal discomfort compared to an analogous approach incorporating a DMPC strategy.

At electricity system level, the focus is on the impact of the stochastic control strategy on the resulting demand, and on how this demand of a group of buildings can be coordinated via demand response to lower the system operating cost. Due to the incorporation of ADF in the open-loop control problem, the SMPC^{ap} strategy is able to simultaneously optimally schedule the demand for electrical energy, reserve capacity and real-time flexibility, required to guarantee thermal comfort. This discloses very valuable information for an aggregator or system operator, since the load uncertainty can be revealed and controlled ahead of real time. It is demonstrated that the day-ahead coordination of the demand for reserve capacity in addition to the energy demand is able to reduce the system operating cost, and hence, enables a more cost-efficient electrification of the residential heating sector. Cost reductions up to 10.7% are shown to be achievable for a demand side consisting of 900 000 flexible heat pumps combined with low-temperature radiators. These insights support the discussion on the need for flexibility markets for low-voltage/residential consumers, and demonstrate the added value of implementing the proposed SMPC^{ap} strategy for demand response under uncertainty in this context.

Beknopte samenvatting

Optimale regeling, en modelgebaseerde voorspellende regeling (beter gekend als *model predictive control* (MPC)) in het bijzonder, maakt een opgang voor klimaatregeling in gebouwen. De toenemende interesse valt te verklaren door haar potentieel om energie en/of kosten te besparen en tegelijkertijd het thermische comfort te verbeteren, en om de energievraag aan te passen aan het beschikbare aanbod van (hernieuwbare en/of rest-)energie via vraagsturing. De performantie van een MPC-strategie is afhankelijk van de nauwkeurigheid van het gebruikte wiskundige model van het gebouw, en van de kwaliteit van de voorspellingen van de verstoringen, zoals het weer en het gebruikersgedrag, die mee het binnenklimaat bepalen. Afwijkende modelparameters en onnauwkeurige voorspellingen leiden tot verhoogde energiekosten en thermisch ongemak, en vereisen realtime corrigerende acties waardoor een mogelijke deelname aan vraagsturing in het gedrang komt. In tegenstelling tot de onzekerheid op de voorspellingen van de verstoringen, wordt de onzekerheid op de gebouwmodelparameters doorgaans niet in rekening gebracht bij het bepalen van een optimale regelstrategie. Nochtans is het niet altijd mogelijk om een accuraat gebouwmodel te bekomen, omwille van een gebrek aan voldoende data en/of vakkennis, en/of de onmogelijkheid om alle optredende fysische effecten voldoende in detail te vatten in een wiskundig model. In deze gevallen kan het nodig zijn om zich ook tegen parametrische onzekerheden expliciet in te dekken.

Het hoofddoel van dit doctoraatsonderzoek is dan ook om een stochastische regelstrategie (aangeduid als de SMPC^{ap}-strategie) te ontwikkelen en te evalueren voor de optimale regeling van het binnenklimaat in residentiële gebouwen, en van vraagsturing, onder gecombineerde additieve (voorspellingen van de verstoringen) en parametrische (gebouwmodel) onzekerheden. De uitwerking is gericht op systemen voorgesteld door een lineair, tijdsinvariant *state space model* (letterlijk vertaald als toestand-ruimte-model). De voorgestelde methode combineert analytisch geherformuleerde kansbeperkingen met affiene verstoringsfeedback, om de conservativiteit van de regelstrategie te beperken.

De uitwerking van de SMPC^{ap}-strategie bestaat uit twee onderdelen. Ten eerste moet er een convexe stochastische formulering van het optimaal regelprobleem opgesteld worden vertrekkende van de deterministische formulering, door de impact van onzekerheden expliciet in rekening te brengen. Ten tweede moet er een geschikt wiskundig model van alle relevante onzekerheden gedefinieerd worden, aangezien dit een essentieel onderdeel is van het stochastisch optimaal regelprobleem. Een belangrijke bijdrage wat betreft dit onzekerheidsmodel is de

uitwerking van waarschijnlijkheidsverdelingen voor de modelparameters van een fysica-gebaseerd gebouwmodel. Deze modelparameters worden afgeleid van de thermische eigenschappen van de gebouwschil, die op hun beurt bepaald worden op basis van schaarse, publiek beschikbare gegevens met behulp van de probabilistische karakteriseringsmethode van De Jaeger et al., zonder een intensieve dataverzameling ter plaatse, wat fundamenteel verschilt van de gangbare onderzoeksaanpak.

Om de meerwaarde van de SMPC^{ap}-strategie te evalueren, wordt haar impact onderzocht op het niveau van een individueel gebouw, alsook op het niveau van het elektriciteitssysteem.

Op het niveau van een individueel gebouw worden de voordelen van de SMPC^{ap}-strategie onderzocht voor twee toepassingsdomeinen, met name optimale regeling, en geïntegreerde optimale regeling en ontwerp. Wat betreft optimale regeling ligt de focus op de haalbare verbetering van het thermische comfort door zich in te dekken tegen onzekerheden, en op de mogelijke stijging van de energiekosten die hiermee gepaard gaat. Aan de hand van simulaties wordt aangetoond dat de verhoogde onzekerheidsanticipatie van de SMPC^{ap}-strategie een duidelijke comfortverbetering teweeg brengt ten opzichte van de gangbare deterministische (D)MPC-strategie, alsook ten opzichte van de state-of-the-art SMPC^a-strategie die zich enkel indekt tegen additieve onzekerheden. Deze comfortverbetering is het meest uitgesproken in gebouwen met vloerverwarming (wat gepaard gaat met een grote thermische inertie) die gekenmerkt worden door een grote modelonzekerheid en een hoge nominale warmtevraag, en dit met slechts een beperkt hoger energiegebruik; voor alle bestudeerde gevallen, zowel degene met vloerverwarming als degene met radiatoren, wordt 90% van de comfortverbetering relatief ten opzichte van de DMPC-strategie bereikt met een relatieve stijging van het energiegebruik van maximaal 9%. Wat betreft optimaal ontwerp ligt de focus op de bruikbaarheid van de SMPC^{ap}-strategie om een adequate en robuuste dimensionering van het warmteproductiesysteem te bekomen. Simulaties tonen aan dat het vervangen van een DMPC- door een SMPC^{ap}-strategie in een geïntegreerde optimale regeling- en ontwerpaanpak capaciteitsreducties van 3 tot 5 kW mogelijk maakt voor een systeem initieel gedimensioneerd op 15 kW, met behoud van thermisch comfort.

Op het niveau van het elektriciteitssysteem ligt de focus op de impact van de SMPC^{ap}-strategie op de vraag, en op de coördinatie van deze vraag van een groep van gebouwen via vraagsturing om de werkingskost van het elektriciteitssysteem te verlagen. Dankzij de implementatie van affiene verstoringsfeedback in de SMPC^{ap}-strategie is deze in staat om de vraag naar energie, reservecapaciteit en realtime flexibiliteit simultaan optimaal te plannen. Dit is zeer waardevol voor een aggregator of systeembeheerder, aangezien de onzekerheid op de vraag vooraf (bijvoorbeeld een dag voordien, in plaats van slechts in real time) kan ingeschat, en bovendien ook gecontroleerd kan worden. De day-aheadcoördinatie van deze flexibiliteitsvraag bovenop de energievraag maakt een verlaging van

de totale systeemkosten mogelijk, en garandeert aldus een kostenefficiëntere elektrificatie van de residentiële verwarmingssector. De resultaten tonen aan dat er voor een vraagzijde bestaande uit 900 000 flexibele warmtepompen gecombineerd met laagtemperatuurradiatoren een kostenreductie tot 10.7% gerealiseerd kan worden. Deze bevindingen ondersteunen de hypothese van de behoefte aan flexibiliteitsmarkten voor huishoudelijke consumenten, en bevestigen de meerwaarde van de implementatie van de ontwikkelde SMPC^{aP}-strategie voor vraagsturing onder onzekerheid in deze context.

List of abbreviations

| | |
|------|---|
| A | Ageing |
| ADF | Affine disturbance feedback |
| ADMM | Alternating direction method of multipliers |
| | |
| COP | Coefficient of performance |
| CV | Coefficient of variation |
| | |
| D | Detached |
| DHW | Domestic hot water |
| DMPC | Deterministic model predictive control |
| DR | Demand response |
| DSO | Distribution system operator |
| DZ | Day zone |
| | |
| GEN | Electricity generating unit |
| | |
| HP | Heat pump |
| HVAC | Heating, ventilation and air-conditioning |
| | |
| IOCD | Integrated optimal control and design |
| | |
| KPI | Key performance indicator |
| | |
| L | Large |

| | |
|--------------------|---|
| M | Midsize |
| MPC | Model predictive control |
| NZ | Night zone |
| O | Old |
| OCP | Optimal control problem |
| OPF | Optimal power flow |
| PBMPC | Performance bound MPC |
| PI(D) | Proportional-integral(-derivative) |
| PMV | Predicted mean vote |
| PV | Photovoltaic |
| R | Recent |
| R ² ES | Renewable and residual energy sources |
| RBC | Rule-based control |
| RC | Resistance-capacitance |
| RMI | Royal Belgian Meteorological Institute |
| RMPC | Robust model predictive control |
| RQ | Research question |
| S | Small |
| SC | Space cooling |
| SD | Semi-detached |
| SH | Space heating |
| SMPC | Stochastic model predictive control |
| SMPC ^{ap} | Stochastic model predictive control accounting for additive as well as parametric uncertainties |
| SMPC ^a | Stochastic model predictive control accounting for additive uncertainties |
| SOC | Second order cone |
| SSM | State space model |

| | |
|-----|----------------------------------|
| T | Terraced |
| TCL | Thermostatically controlled load |
| TCV | Thermal comfort violation |
| TED | Thermal energy demand |
| TES | Thermal energy storage |
| WDM | Weighted distance to the mean |
| WWR | Window-to-wall ratio |

List of symbols

Latin characters

| | | |
|-----------|--|--|
| \dot{P} | Electric power | [W] |
| \dot{Q} | Thermal power | [W], or $[\frac{W}{m^2}]$ i.c.o. \dot{Q}_{sol} |
| A | Building model state space matrix A (states) | |
| B | Building model state space matrix B (inputs) | |
| d | Building model disturbances | |
| E | Building model state space matrix E (disturbances) | |
| e | Selection vector | |
| I | Identity matrix | |
| p | Latent variable aggregating all uncertainties | |
| q | Auxiliary variable related to the second order cone constraints on the building model states | $[^{\circ}C^{1/2}]$ |
| r | Auxiliary variable related to the second order cone constraints on the building model inputs | $[W^{1/2}]$ |
| s | Slack variable related to the building model state constraints | $[^{\circ}C]$ |
| T | Transformation matrix | |
| u | Building model inputs | [W] |
| x | Building model states | $[^{\circ}C]$ |
| z | Auxiliary optimization variables (in Chapter 9) | |

| | | |
|--------------|---|--|
| \mathbf{z} | Vector aggregating the vectorized state space matrices (in Chapter 5) | |
| A | Area | $[\text{m}^2]$ |
| a | Element of building model state space matrix A (states) | |
| B | Total number of buildings constituting the demand side | |
| b | Element of building model state space matrix B (inputs) | |
| C | Thermal capacitance | $[\frac{\text{J}}{\text{K}}]$ |
| c | Cost | |
| cap | Capacity of a generator | $[\text{W}]$ |
| COP | Coefficient of performance | |
| D | Demand for electric energy | $[\text{W h}]$ |
| e | Element of building model state space matrix E (disturbances) | |
| G | Total number of (aggregated) generators constituting the supply side | |
| K | Prediction horizon | |
| k | Time (in discrete time domain) | |
| L | (Augmented) Lagrangian | |
| N | Sample size | |
| n | Number/amount | |
| PR | Performance ratio | |
| R | Demand for reserve capacity (in Chapter 9) | $[\text{W}]$ |
| R | Thermal resistance (in Chapter 5 and Chapter 8) | $[\frac{\text{K}}{\text{W}}]$ |
| res | Residual of the iterative ADMM procedure | |
| S | Supply of electric energy | $[\text{W h}]$ |
| T | Temperature | $[\text{°C}]$ |
| t | Time (in continuous time domain) | |
| U | Heat transfer coefficient | $[\frac{\text{W}}{\text{m}^2 \text{K}}]$ |
| V | Supply of reserve capacity (in Chapter 9) | $[\text{W}]$ |

| | | |
|-----|--------------------------|----------------|
| V | Volume (in Chapter 8) | $[\text{m}^3]$ |
| w | System-level uncertainty | $[\text{W}]$ |

WDM Weighted distance to the mean

X Set of constraints restraining χ

Greek characters

α Participation factor defining the affine control scheme of a generator

ϵ Risk level

η Efficiency

λ Dual variable of a constraint

μ Mean

ν Parameter for the adaptive update procedure of the ADMM penalty parameter

ρ ADMM penalty factor

Σ Variance

σ Standard deviation

τ Parameter for the adaptive update procedure of the ADMM penalty parameter

χ Optimization strategy aggregating all optimization variables, including those directly involved in the coupling constraints

Special characters

\mathbb{N} The set of integer numbers

\times Optimization strategy aggregating all optimization variables, except for those directly involved in the coupling constraints

\mathbb{R} The set of real numbers

Subscripts

0 Initial value

amb Ambient

aux Auxiliary resistance heater

| | |
|----------------|--|
| <i>b</i> | Building index |
| <i>BU</i> | The set of all buildings |
| <i>dem</i> | Demand |
| <i>DR</i> | Demand response |
| <i>dual</i> | Dual (feasibility) |
| <i>E</i> | East |
| <i>el</i> | Electric |
| <i>f</i> | Ground floor |
| <i>fi</i> | Internal floor |
| <i>g</i> | Generator index |
| <i>GE</i> | The set of all generators |
| <i>gen</i> | Generation |
| <i>gr</i> | Ground |
| <i>h</i> | Building model disturbance index |
| <i>hp</i> | Heat pump |
| <i>i</i> | Building model state index |
| <i>ia</i> | Indoor air |
| <i>inf,win</i> | Infiltration and transmission losses through windows and doors |
| <i>int</i> | Internal (heat gains) |
| <i>j</i> | Building model input index |
| <i>k</i> | Time index |
| <i>N</i> | North |
| <i>nom</i> | Nominal |
| <i>prim</i> | Primal (feasibility) |
| <i>pv</i> | Solar photovoltaics |
| <i>rad</i> | Radiator |

| | |
|-------------|---------------------------------|
| <i>S</i> | South |
| <i>s</i> | Building sample index |
| <i>sol</i> | Solar (irradiance) |
| <i>sup</i> | Supply |
| <i>surr</i> | Surroundings |
| <i>sys</i> | System level |
| <i>tank</i> | Domestic hot water storage tank |
| <i>tilt</i> | Tilted (solar irradiance) |
| <i>trad</i> | Traditional |
| <i>W</i> | West |
| <i>w</i> | External wall |
| <i>wi</i> | Internal wall |

Superscripts

| | |
|-------------|------------------------------|
| <i>c</i> | Coupling |
| <i>CCV</i> | Comfort constraint violation |
| <i>decr</i> | Decrease |
| <i>dhw</i> | Domestic hot water |
| <i>DZ</i> | Day zone |
| <i>EN</i> | Energy |
| <i>GEN</i> | Generation |
| <i>gi</i> | Grid injection |
| <i>incr</i> | Increase |
| <i>l</i> | ADMM iteration index |
| <i>max</i> | Maximum value |
| <i>min</i> | Minimum value |
| <i>NZ</i> | Night zone |

| | |
|-------|-----------------------------|
| PCV | Power constraint violation |
| r | Root form |
| RE | Reserve capacity |
| REa | Reserve capacity activation |
| REp | Reserve capacity provision |
| sc | Space cooling |
| sco | Self consumption |
| sh | Space heating |
| T | Transpose |

Operators

| | |
|---------------------|---|
| $\tilde{\cdot}$ | Uncertain variable |
| $\bar{\cdot}$ | Mean value |
| $\bar{\cdot}$ | Reference value |
| $\Delta(\cdot)$ | Uncertainty band around the mean value of a stochastic variable |
| $\delta(\cdot)$ | Uncertain portion of a stochastic variable |
| $\mathbb{E}[\cdot]$ | Expected value |
| $cov(\cdot)$ | Covariance |
| $P(\cdot)$ | Probability |
| $vec(\cdot)$ | Vectorization |

Contents

| | |
|---|------------|
| Abstract | v |
| Beknopte samenvatting | vii |
| List of abbreviations | xi |
| List of symbols | xv |
| Contents | xxi |
| 1 Introduction | 1 |
| 1.1 Context and problem statement | 1 |
| 1.2 Research objectives and questions | 4 |
| 1.3 Scope | 6 |
| 1.4 Scientific challenges | 6 |
| 1.5 Outline | 8 |
| 2 Setting the scene – Deterministic MPC as starting point | 11 |
| 2.1 General MPC procedure applied to TCLs | 11 |
| 2.2 Mathematical formulation | 13 |
| 2.3 Problems related to deterministic MPC | 14 |
| 3 Literature review on MPC of TCLs under uncertainty | 15 |
| 3.1 Building climate control under uncertainty | 15 |
| 3.2 (Integrated optimal control and) design under uncertainty | 21 |
| 3.3 Demand response under uncertainty | 22 |

| | | |
|-----------|---|-----------|
| I | SMPC development | 27 |
| 4 | Stochastic OCP formulation | 29 |
| 4.1 | Notation | 29 |
| 4.2 | Introducing uncertainties in the state space equation | 30 |
| 4.3 | Introducing uncertainties in the state constraints | 33 |
| 4.4 | Introducing uncertainties in the input constraints | 35 |
| 4.5 | Resulting stochastic OCP formulation | 38 |
| 4.6 | Conclusion | 39 |
| 5 | Uncertainty characterization | 41 |
| 5.1 | System model specification | 42 |
| 5.2 | Building model parameter uncertainty | 45 |
| 5.2.1 | Background | 45 |
| 5.2.2 | Modeling approach | 46 |
| 5.2.3 | Resulting uncertainty characterization | 50 |
| 5.3 | Weather forecast uncertainty | 69 |
| 5.3.1 | Background | 69 |
| 5.3.2 | Modeling approach | 69 |
| 5.3.3 | Resulting uncertainty characterization | 70 |
| 5.4 | Occupant behavior forecast uncertainty | 71 |
| 5.4.1 | Background | 73 |
| 5.4.2 | Modeling approach | 73 |
| 5.4.3 | Resulting uncertainty characterization | 74 |
| 5.5 | Conclusion | 75 |
| II | SMPC assessment at building level | 79 |
| 6 | Optimal control under uncertainty of a TCL in an individual building | 81 |
| 6.1 | Optimal control performance assessment method | 82 |
| 6.2 | Case study | 86 |
| 6.3 | Results and discussion | 89 |
| 6.3.1 | Thermal comfort improvement and associated increase in energy use | 89 |
| 6.3.2 | Computational effort | 96 |
| 6.4 | Conclusion | 96 |
| 7 | Towards integrated optimal control and design under uncertainty of a TCL in an individual building | 99 |
| 7.1 | Optimal design performance assessment method | 100 |
| 7.2 | Case study | 102 |
| 7.3 | Results and discussion | 102 |
| 7.4 | Conclusion | 110 |

| | | |
|------------|---|------------|
| III | SMPC assessment at system level | 113 |
| 8 | The importance of system integration – The sense and nonsense in maximizing self-consumption with a HP-PV system in an individual building | 115 |
| 8.1 | Self-consumption assessment method | 119 |
| 8.1.1 | Objective function | 119 |
| 8.1.2 | Solar photovoltaic model | 120 |
| 8.1.3 | Heat/cold supply system model | 120 |
| 8.1.4 | Building and heat/cold emission system model | 126 |
| 8.1.5 | Domestic hot water storage tank model | 129 |
| 8.1.6 | Resulting OCP formulation | 131 |
| 8.2 | Case study | 132 |
| 8.3 | Results and discussion | 134 |
| 8.4 | Conclusion | 144 |
| 9 | Optimal collective control under uncertainty of TCLs in a group of buildings | 145 |
| 9.1 | Demand profile induced by the SMPC ^{ap} strategy | 146 |
| 9.2 | Demand response performance assessment method | 151 |
| 9.2.1 | Integrated system-level optimization problem | 152 |
| 9.2.2 | Distributed solution strategy using ADMM | 165 |
| 9.3 | Case study | 180 |
| 9.4 | Results and discussion | 187 |
| 9.5 | Conclusion | 195 |
| 10 | Conclusions and suggestions for future work | 199 |
| 10.1 | Conclusions | 200 |
| 10.1.1 | Development of the SMPC ^{ap} strategy | 200 |
| 10.1.2 | Assessment of the potential added value of the SMPC ^{ap} strategy at building level | 202 |
| 10.1.3 | Assessment of the potential added value of the SMPC ^{ap} strategy at system level | 204 |
| 10.2 | Suggestions for future work | 206 |
| | Appendix | 209 |
| A | Parametric uncertainty characterization for a two-zones nine-states building model | 211 |

| | |
|-----------------------------|------------|
| Bibliography | 221 |
| Curriculum | 241 |
| List of publications | 243 |

Chapter 1

Introduction

1.1 Context and problem statement

In order to mitigate the detrimental effects of global warming and climate change, a drastic reduction of anthropogenic greenhouse gas emissions is required. A crucial sector to be tackled in this context is the residential heating sector. In 2018, the residential sector was responsible for 26.1% of the final energy use in Europe, of which 63.3% was used for space heating; the majority of this energy demand is still being delivered by fossil fuels [1, 2]. To achieve the envisioned reduction of greenhouse gas emissions in the building sector, the European Commission has discerned two important measures. First, the energy efficiency of buildings should be improved, resulting in a reduced energy use. Second, the remaining energy demand should to a large extent be covered by renewable and residual energy sources (R²ES) [2, 3, 4, 5, 6].

Improved energy efficiency for residential space heating can be achieved in different ways. First and foremost, building renovation is an important measure to reduce the space heating demand. [7, 8]. In addition, district heating networks offer an interesting possibility to further improve energy efficiency [9]; this is especially true in areas with a large heat demand per square kilometer, where the thermal losses are limited, thereby guaranteeing the efficiency and profitability of thermal networks [10]. For areas with a smaller heat density, energy-efficient electric heat pumps are the most cost-effective option [9, 11]. Finally, the additional implementation of an overarching advanced control strategy for building climate control, aiming at optimally operating the space heating system, can further reduce energy use; energy savings of 15-50% are reported for numerous simulation or pilot

case studies [12, 13, 14, 15].

Increasing the utilization of R⁽²⁾ES is a challenging task, because of their intermittent character, i.e., their variability and limited predictability, hampering the balance between supply and demand. This issue could be overcome by shifting from a demand-driven to a resource-driven operation of the energy system, by exploiting demand side flexibility in a smart grid context [16, 17]. In this setting, thermostatically controlled loads (TCLs), such as heat pumps, play an important role, because of the high energy use, and the inherent flexibility offered by the thermal storage capacity of the building thermal mass and active energy storage devices if available [18, 19, 20]. The exploitation of this available flexibility to increase the system efficiency¹ and the penetration of R⁽²⁾ES, while safeguarding the operational limits of the system (i.e., the heat pump, network, generation, etc.), can be established via demand response (DR), and can be applied in either electricity networks [22, 23, 24, 25, 26] or district heating networks [27, 28, 29, 30]. The main aim of DR is to let flexible end-consumers change their consumption pattern to better match the available supply, by either shifting loads in time, or changing loads in size [15, 31]. This altered behavior is often achieved via price incentives [31]. Here again, advanced control strategies play an important role, since residential consumers lack the required knowledge about how to optimally schedule the operation of their appliances and heating, ventilation and air-conditioning (HVAC) devices in response to changing price signals [32]. Besides, dynamic pricing without smart appliances, thus requiring manual interventions, is also shown to lead to user fatigue, resulting in very limited behavioral changes [33, 34]. Hence, automated response technologies are recommended to facilitate the implementation of DR [4, 17, 31, 34].

A particular advanced control strategy that is gaining widespread attention in the context of buildings/TCLs, is model predictive control (MPC). MPC is a control method that optimizes the operation of a system over a finite prediction horizon in accordance with a selected objective function, while explicitly taking into account a mathematical model representing the system behavior together with predictions of the relevant boundary conditions. The control strategy is implemented in a receding-horizon fashion, thereby not only exploiting the benefits of feedforward, but also of feedback control. Applied to residential space heating applications, MPC typically optimizes the heating schedule over a number of days, considering the dynamics of the building envelope, heat supply system and heat emission system, together with predictions of the future weather conditions, occupant behavior, and energy prices.

¹ It should be stressed that the application of demand response is not only beneficial/required to increase the utilization of R²ES. The ongoing electrification associated with the energy transition (for example via the increased implementation of heat pumps), also leads to an increased electricity demand, with a high degree of simultaneity among consumers, possibly overloading the grid. Also these issues can be tackled by demand response, by incentivizing consumers to lower their demand and/or shift/spread their demand in time [21].

The indoor temperature is thereby maintained between predefined, user-specified comfort limits, while the exact system operation depends on the user preferences (e.g., minimization of energy use, operational cost, CO₂ emission, ... and/or maximization of thermal comfort). MPC offers numerous advantages compared to other less advanced control logics such as proportional-integral(-derivative) (PI(D)) control or rule-based control (RBC). An important added value is the possibility for a multi-objective optimization of the heating strategy while taking into account the physical constraints of the system, allowing for systematic energy and/or cost savings with simultaneous thermal comfort improvement [12, 13, 14, 35, 36]. The price-responsiveness and anticipative behavior make it moreover an ideal candidate for DR coordination, adapting the energy demand in correspondence with the available supply [26, 32, 37, 38].

The application of MPC for building climate control is currently mostly focused on larger (office/tertiary) buildings, since, among others, the investment cost is more likely to be justified in that case due to higher absolute savings [39]; however, if also taking into account the DR capabilities, and the associated monetary value [40] and benefits for the central energy system, the application of MPC for residential buildings stands to reason.

The performance of any MPC strategy for residential space heating is dependent on the accuracy of the mathematical model describing the thermal loads and the quality of the forecasts of disturbances, such as weather and occupant behavior. Deviating model parameters and inaccurate disturbance predictions are shown to give rise to increased energy costs and comfort violations if not properly accounted for [41, 42, 43, 44, 45], and require real-time corrective actions, thereby jeopardizing the participation in possible demand response programs [46, 47]. To address this issue, dedicated MPC approaches that explicitly take into account uncertainty when determining the optimal control strategy have been developed. These approaches currently mainly focus on the additive disturbance forecast uncertainty [44, 48, 49, 50, 51, 52, 53]. Although the building model parameters are recognized as another important source of uncertainty influencing the building energy performance [54, 55], this uncertainty is typically not explicitly taken into account [43, 56, 57, 58, 59]. Nevertheless, the building controller model is not always capable of capturing the building dynamics in detail, due to the unavailability of sufficient data and/or experts' knowledge to set up the model, and/or due to the impossibility to correctly describe the complexity of the underlying physics [54, 59, 60, 61].

1.2 Research objectives and questions

Given the aforementioned trends and challenges, **the main aim, and main novelty, of this work are to develop and assess an MPC strategy for building climate control and DR under combined additive (disturbance forecast) and parametric (model)² uncertainty.** More particularly, a stochastic MPC (SMPC) approach, tailored to systems subject to probabilistic uncertainty, is pursued. This choice is motivated by the probabilistic descriptions found in literature for the building envelope characteristics [60, 62, 63, 64, 65, 66], weather conditions [51, 55, 64, 67] and occupant behavior [55, 64, 65], and by the fact that thermal comfort is allowed to be occasionally violated, which is confirmed in building standards (see e.g., [68, 69]). The presented approach is tailored to the class of systems represented by a linear time-invariant state space model (SSM).

Two main aspects are embedded in this main research objective, being the SMPC development and the SMPC performance assessment.

The **SMPC development** entails two important underlying objectives. First, starting from the dominating deterministic optimal control problem (OCP), a stochastic (preferably convex) OCP formulation needs to be derived, explicitly accounting for additive as well as parametric uncertainties. Second, an appropriate mathematical description of all relevant uncertainties, serving as an essential part of the stochastic OCP formulation, is required.

The main objective of the **SMPC performance assessment** is to illustrate the potential added value of the proposed SMPC approach for different application domains.

When focusing on an **individual building**, first, the advantages of the proposed SMPC approach for optimal building climate control need to be investigated. Here, the main focus is on the attainable thermal comfort improvement by hedging against uncertainty, and on the associated energy costs, which are the key factors of interest for consumers. In addition, acknowledging the emerging interest to exploit optimal control algorithms for optimal design applications³ [70, 71], the suitability of the proposed SMPC approach to obtain a more appropriate, yet robust, heat supply

² The uncertainty on the building model is limited to parametric uncertainty, i.e., uncertainty on the value of the model parameters. Model-form uncertainty, representing the discrepancy between the complex physical process and the simplified mathematical characterization, is out of scope of this work.

³ A better alignment of control and design via an integrated optimal control and design methodology, properly accounting for the system dynamics, can result in a more appropriate, i.e., less oversized and more cost-optimal, system design [70, 71]. This is in contrast to current engineering practices, that typically consider worst-case static conditions, and/or assign a safety factor to a deterministic load calculated for specific design conditions, leading to serious oversize problems [64, 72, 73, 74, 75].

system size needs to be additionally investigated, by incorporating it in an integrated optimal control and design (IOCD) methodology.

In a next step, the **link with the central energy system** needs to be taken into account, to investigate the advantages of the active DR capabilities of the SMPC strategy. To this end, the SMPC approach needs to be embedded in a system-level optimization problem, involving both the supply and demand side, where the demand side is constituted by a group of TCLs. Here, the main focus is on the impact of the stochastic control strategy on the resulting demand, and on how this demand can be coordinated to lower the total system cost.

Summarizing, the following research questions (RQ) will be answered.

Development of the SMPC strategy:

RQ 1: How does the conventional deterministic OCP formulation for building climate control need to be reformulated in order to explicitly account for additive (disturbance forecast) and parametric (model) uncertainties?

(→ Chapter 4)

RQ 2: How can all relevant uncertainties affecting the building indoor climate be appropriately mathematically modeled in order to include them in the stochastic OCP formulation?

(→ Chapter 5)

Assessment of the potential added value of the SMPC strategy at building level:

RQ 3: Does the SMPC^{ap4} strategy guarantee a thermal comfort improvement compared to the current-practice deterministic MPC (DMPC) strategy, and the state-of-the-art SMPC^a strategy only accounting for additive uncertainties, and at what cost is this improvement obtained?

(→ Chapter 6)

RQ 4: Does the SMPC^{ap} strategy allow for obtaining a more appropriate, yet robust, sizing of the heating system when embedded in an IOCD approach?

(→ Chapter 7)

Assessment of the potential added value of the SMPC strategy at system level:

RQ 5: How does the proposed SMPC^{ap} strategy alter the demand profile, and how can this altered demand profile be coordinated for the benefit of the central energy system?

(→ Chapter 9)

⁴ In the remainder of this dissertation, the proposed approach will more specifically be indicated by the SMPC^{ap} strategy, to emphasize that both additive and parametric uncertainties are being considered, in contrast to the state-of-the-art SMPC^a strategy that is only accounting for additive uncertainties.

1.3 Scope

Model predictive control of TCLs for building climate control and DR is linked to a wide range of research areas. Hence, to guarantee the feasibility of this research, it is required to clearly delineate its scope.

This work specifically focuses on an SMPC strategy for **residential space heating applications**, given the heating-dominated climate in Belgium. For the sake of simplicity, neither space cooling, nor domestic hot water supply are considered (except in Chapter 8). Nevertheless, the presented methodologies for optimal control/design under uncertainty could be transferred to these applications, since they can also be represented with the help of a SSM.

The SMPC strategy is assumed to merely deal with **high-level, supervisory control actions** regarding the supply of space heating (i.e., the optimal indoor temperature profile and the required heat supply to accomplish this). The component-level control is not considered in this work. Consequently, the component models used by the SMPC strategy are rather simple (the detailed configuration of the hydronic system, including all pumps and valves, and associated losses, is for example disregarded), which in turn limits the available degrees of freedom when optimizing the design via an integrated optimal control and design approach.

When linking the demand side to the central energy system, thereby assessing the DR capability of the SMPC strategy, a **system-level perspective** is adopted, minimizing the overall system cost, and assuming perfect competition and perfect knowledge of all involved agents. The analysis considers an **electrification scenario**, motivated by the expected increase in market penetration of heat pumps for residential space heating [76, 77]. Hence, the considered demand side is a group of residential compression heat pumps, each controlled by the proposed SMPC strategy, and the considered supply side is a pool of electricity generation units. The transmission and distribution grid, on the other hand, are not included, but are considered to be a copper plate, not posing any congestion problems, and not showing any losses. DR can only be performed by heat pumps, without competition from other technologies, such as white good appliances, battery storage, electric vehicles, or flexible industrial processes. The available electricity merely stems from generating facilities; import and export of electricity are disregarded.

1.4 Scientific challenges

In order to answer the research questions, some important scientific challenges have to be overcome.

A first challenge is the **mathematical formulation of the stochastic OCP** (Chapter 4). Since the combination of additive and parametric uncertainty gives rise to products of optimization variables, the stochastic OCP in its most general form results in a non-convex formulation. Non-convex problems are generally hard to solve, and do not guarantee a globally optimal solution, which is not desirable in MPC applications. Hence, a convex reformulation needs to be found to ensure tractability when taking into account the parametric uncertainty in addition to the additive uncertainty.

A second challenge is the **uncertainty characterization**, both in terms of data gathering and modeling approach (Chapter 5). For both the additive and parametric uncertainty, a practically relevant uncertainty characterization is pursued, starting from readily available data, and aiming at a practically feasible processing methodology.

Although the additive uncertainty (i.e., weather and occupant behavior forecast uncertainty) has been widely studied, and there is a clear consensus about how to mathematically represent this, the mathematical model cannot straightforwardly be found in literature. Most works provide a clear description of the applied uncertainty characterization method, see e.g., [44, 48, 53, 78, 79], but the actual numerical values are usually not disseminated. Besides, important details such as (auto- and cross-)correlation are often disregarded, thereby omitting valuable information that could otherwise be exploited to improve the control strategy under uncertainty [80, 81]. Hence, a more dedicated data gathering and subsequent processing of the additive forecast uncertainty is required, by using the methods as prescribed in literature. Regarding the parametric uncertainty, the main challenge is that the uncertainty characterization is currently typically derived based on detailed (mostly building-specific) information and/or experts' knowledge. However, in case of a widespread MPC implementation, a lack of detailed and accurate input data is plausible, especially if also the older, existing building stock is involved [54]. Moreover, the need for an expert should be avoided to lower the implementation cost. In this case, one needs to rely upon sparse, publicly available data to characterize the building envelope [60, 62, 63] and subsequently construct the building controller model. This fundamentally different point of view requires revisiting the currently prevailing uncertainty characterization methods, in addition to dedicated data gathering.

A final challenge is the development of a suitable **coordination framework for DR** of a group of TCLs under uncertainty, leveraging the developed SMPC strategy (Chapter 9). An important aspect is the need for an integrated system-level optimization problem, requiring a thorough understanding and reflection of the decision making of all different involved agents, and of their interaction. The elaboration of an appropriate solution strategy of this fairly large problem is a crucial challenge to be tackled.

1.5 Outline

This dissertation consists of ten chapters, which are briefly discussed below. A graphical representation of these chapters is presented in Figure 1.1, highlighting their coherence and interdependency.

The dissertation starts with the discussion of the important background. Following the introduction in Chapter 1, Chapter 2 explains the general working principle of MPC applied to TCLs, elaborates on the mathematical formulation, and highlights the problems related to the dominant deterministic implementation in case high-quality forecasts and/or a high-quality model are lacking. Chapter 3 subsequently gives a concise overview of the literature on the different application domains involving MPC applied to TCLs under uncertainty. This review is moving from building level to system level, thereby successively discussing building climate control under uncertainty, (integrated optimal control and) design under uncertainty, and DR under uncertainty. The main aim of this literature review is to delineate the state-of-the-art regarding the uncertainty incorporation in each of these application domains, and to identify important gaps to be tackled by this dissertation.

The next two chapters constitute Part I of this dissertation, dedicated to the SMPC development. Starting from the deterministic problem formulation presented in Chapter 2, Chapter 4 subsequently derives a stochastic OCP formulation, explicitly accounting for additive as well as parametric uncertainties (**RQ 1**). Chapter 5 continues the SMPC development, by establishing an appropriate mathematical model of all relevant uncertainties, serving as an essential part of the derived stochastic OCP formulation (**RQ 2**). The uncertainty characterization, including dedicated data gathering and subsequent processing steps, is successively discussed for the building model parameters, embodying the parametric uncertainty, and for the weather forecasts and the occupant behavior forecasts, embodying the additive uncertainty.

The next two parts of this dissertation investigate the potential added value of the proposed SMPC strategy in different application domains, either focusing on building level or on system level.

In Part II, Chapter 6 first investigates the effectiveness of the proposed SMPC strategy for optimal building climate control under uncertainty, by examining the attainable thermal comfort improvement, as well as the associated energy costs, compared to the state-of-the-art (**RQ 3**). Chapter 7 in turn discusses the potential of an integrated optimal control and design approach incorporating the proposed SMPC strategy, to obtain a more appropriate, yet robust, heat supply system size under uncertainty (**RQ 4**).

In Part III, Chapter 8 first substantiates the switch from a building-level perspective

towards a system-level perspective, by elaborating on the importance of system integration. To this end, an illustrative study regarding the attainable self-consumption with residential heat pumps in the Belgian heating-dominated climate is presented, highlighting the suboptimality of individual, isolated approaches. Next, Chapter 9 links the proposed SMPC strategy with the central energy system, and investigates the advantages of its DR capabilities. In particular, it is investigated how the SMPC strategy impacts the resulting demand profiles, and how these altered demand profiles could be optimally coordinated for the benefit of the central system (**RQ 5**).

Finally, Chapter 10 presents the conclusions, complemented by the recommendations for future work.

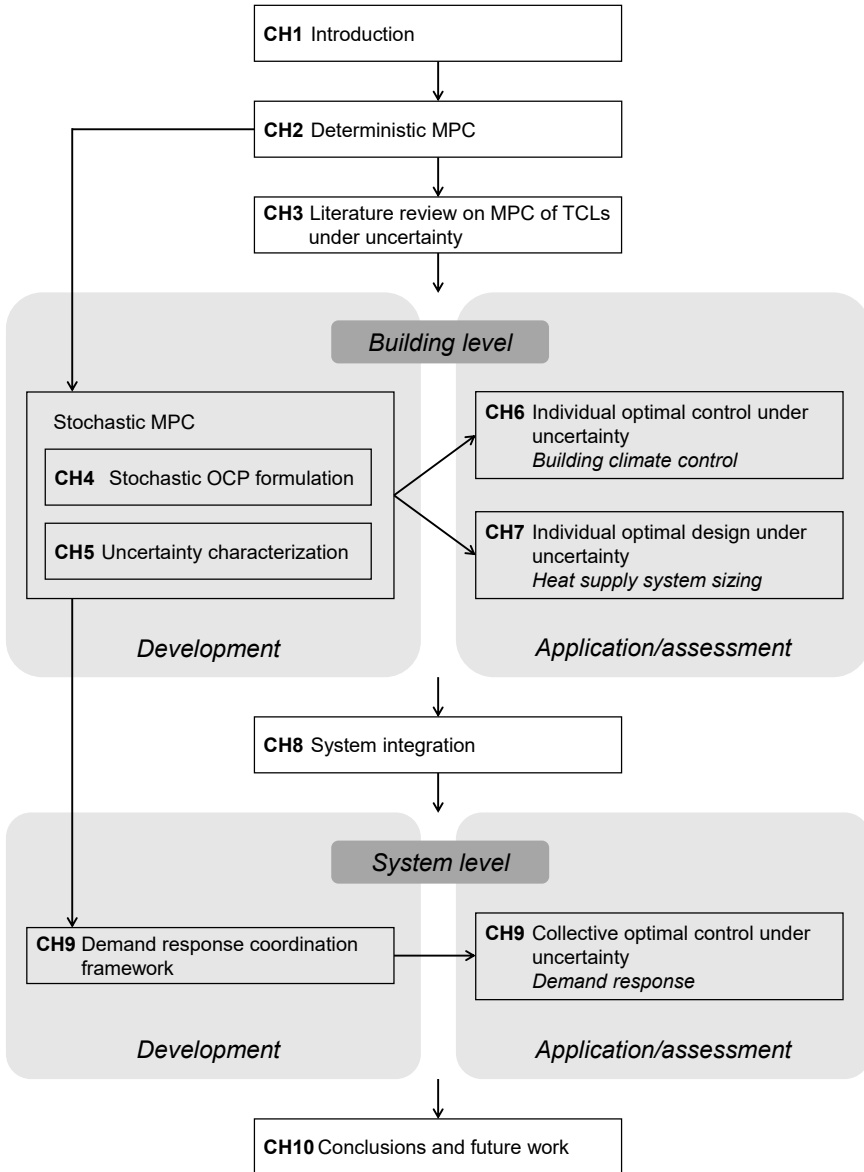


Figure 1.1: A graphical representation of the outline of the dissertation.

Chapter 2

Setting the scene – Deterministic MPC as starting point

This chapter is based on A. Uytterhoeven, R. Van Rompaey, K. Bruninx, and L. Helsen, “Chance Constrained Stochastic MPC for Building Climate Control Under Combined Parametric and Additive Uncertainty,” submitted to Journal of Building Performance Simulation, July 2021.

This introductory chapter briefly explains the general working principle of MPC applied to a TCL in Section 2.1, elaborates on the mathematical formulation in Section 2.2, and highlights the problems related to the dominating deterministic implementation in case high-quality forecasts and/or a high-quality model are lacking in Section 2.3.

2.1 General MPC procedure applied to TCLs

Figure 2.1 illustrates the general MPC procedure for building climate control and DR applied to a TCL. At the current point in time, the heating plan for the next hours up to a few days is determined by solving an open-loop optimal control problem. This open-loop OCP aims at optimizing the heating system operation over

a finite prediction horizon in accordance with a selected objective function (e.g., minimization of energy use, operational cost, CO₂ emissions, ... and/or maximization of thermal comfort), while explicitly taking into account the mathematical model representing the system behavior together with the thermal comfort constraints, and predictions of the relevant boundary conditions. Typically, MPC algorithms are implemented in closed-loop, using the principle of receding horizon control, as shown in Figure 2.1. After solving the OL OCP, the first step of the optimized control sequence is applied to the building. Then, the actual system response is measured and fed back to the OCP, thereby serving as an updated initial condition for the optimization at the next time step [36]. As such, MPC combines both feedforward and feedback.

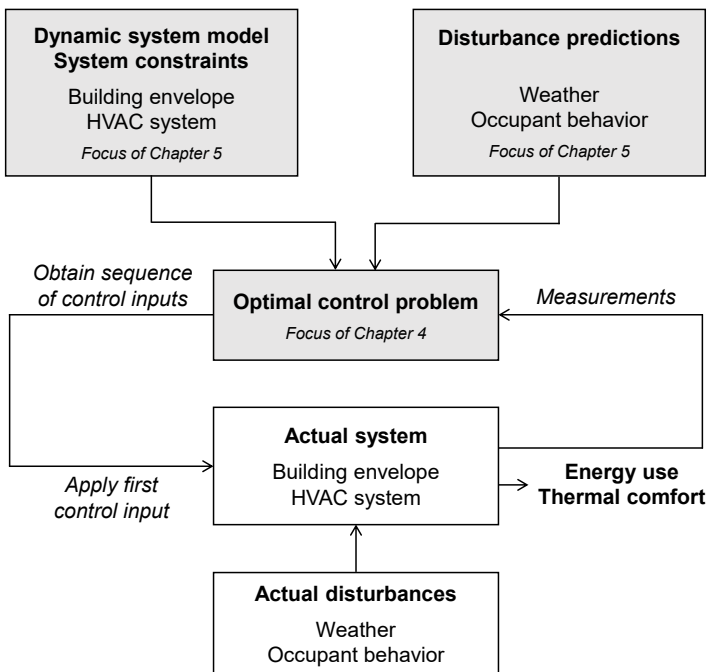


Figure 2.1: The general working principle of MPC applied to a TCL. All relevant parts regarding the SMPC development are highlighted in grey. Adapted from [82].

2.2 Mathematical formulation

The deterministic open-loop OCP for the class of systems represented by a linear time-invariant SSM can be mathematically formulated as follows.

$$\begin{aligned} \min \quad & \phi(\mathbf{x}_k, \mathbf{s}_k, \mathbf{u}_k) \\ & \{\mathbf{x}_k\}_{k=0\dots K+1}, \\ & \{\mathbf{s}_k\}_{k=0\dots K+1}, \\ & \{\mathbf{u}_k\}_{k=0\dots K} \end{aligned}$$

$$s.t. \quad \mathbf{x}_{k+1} = \mathbf{A} \mathbf{x}_k + \mathbf{B} \mathbf{u}_k + \mathbf{E} \mathbf{d}_k \quad \forall k \quad (2.1a)$$

$$\mathbf{x}_k + \mathbf{s}_k \geq \mathbf{x}_k^{min} \quad \forall k \quad (2.1b)$$

$$\mathbf{x}_k - \mathbf{s}_k \leq \mathbf{x}_k^{max} \quad \forall k \quad (2.1c)$$

$$\mathbf{s}_k \geq \mathbf{0}_{n_x} \quad \forall k \quad (2.1d)$$

$$\mathbf{0}_{n_u} \leq \mathbf{u}_k \leq \mathbf{u}_k^{max} \quad \forall k \quad (2.1e)$$

$$\mathbf{x}(0) = \mathbf{x}_0 \quad (2.1f)$$

$$\mathbf{u}(0) = \mathbf{u}_0 \quad (2.1g)$$

Here, $\{\mathbf{x}_k \in \mathbb{R}^{n_x}\}_{k=0\dots K+1}$ represents all system states over the prediction horizon K , being the indoor temperature as well as all relevant temperatures of the building construction elements and of the heating system (which can be easily extended to the complete HVAC system). $\{\mathbf{s}_k \in \mathbb{R}^{n_x}\}_{k=0\dots K+1}$ represents the slack variables relaxing the state constraints. $\{\mathbf{u}_k \in \mathbb{R}^{n_u}\}_{k=0\dots K}$ in turn represents the thermal power inputs delivered by the heat supply system during one time step Δt . Finally, $\{\mathbf{d}_k \in \mathbb{R}^{n_d}\}_{k=0\dots K}$ represents the point forecasts of the disturbances affecting the system, such as weather and occupant behavior.

The state space equation (2.1a) describes the dynamics of the building envelope and heating system with the help of the state space matrices $\mathbf{A} \in \mathbb{R}^{n_x \times n_x}$, $\mathbf{B} \in \mathbb{R}^{n_x \times n_u}$ and $\mathbf{E} \in \mathbb{R}^{n_x \times n_d}$, constituting the building controller model. This constraint determines the evolution of the system states \mathbf{x}_{k+1} as a function of the preceding states \mathbf{x}_k , heat inputs \mathbf{u}_k and disturbances \mathbf{d}_k . The states are constrained by a lower and upper bound, $\{\mathbf{x}_k^{min}\}_{k=0\dots K+1}$ and $\{\mathbf{x}_k^{max}\}_{k=0\dots K+1}$, in Equations (2.1b) and (2.1c). When applied to the indoor temperature, these state constraints (approximately¹) denote the thermal comfort requirements. These requirements

¹ In reality, thermal comfort is determined by a wide variety of factors, such as metabolic factors, humidity level, human body thermal radiation, etc. [83]. However, including detailed comfort models in the OCP could lead to a computationally intractable problem [14, 51].

cannot always be satisfied, e.g., after a perturbation due to an uncertainty manifestation. To prevent the model from becoming infeasible in these cases, the state constraints are relaxed with the help of the slack variables s_k that are penalized in the pursued objective function ϕ at a very high value. The inputs are in turn limited by an upper power bound $\{\mathbf{u}_k^{max}\}_{k=0\dots K}$ in Equation (2.1e), that is typically reflecting the technical limits of the heating system. Finally, the current conditions, represented by \mathbf{x}_0 and \mathbf{u}_0 , are taken into account as initial values for the states and inputs in Equations (2.1f) and (2.1g).

2.3 Problems related to deterministic MPC

Although closed-loop MPC already offers a certain degree of robustness to uncertainties via its feedback mechanism, its conventional deterministic OCP formulation (Equation (2.1)), that is considering the system model $\mathbf{A}, \mathbf{B}, \mathbf{E}$ and disturbance predictions \mathbf{d}_k as perfect representations of reality, typically fails to systematically deal with the impact of uncertainties [84]. This is for example shown in detail by Wang et al. [41], and will also be further illustrated in Chapter 6). Therefore, to obtain a robust control strategy, it is required to additionally adapt the formulation of the open-loop OCP by integrating information about the uncertainties in the problem formulation, which is further discussed in Chapters 4 and 5.

Chapter 3

Literature review on MPC of TCLs under uncertainty

This chapter gives a concise overview of the literature on the different application domains involving MPC applied to TCLs, with a particular focus on the consideration of uncertainties therein. Sections 3.1 and 3.2 consider the application of MPC at building level, in the context of optimal control and of optimal design, respectively. Section 3.3 acknowledges that MPC also plays an important role at system level for the coordination of demand response, thereby adapting the energy demand for the benefit of the central energy system. The main aim of this literature review is to delineate the state-of-the-art regarding the uncertainty incorporation in each of these application domains, and to identify important research gaps to be tackled by this dissertation.

3.1 Building climate control under uncertainty

Because of the acknowledged detrimental impact of uncertainties on thermal comfort and energy use [41, 42, 43, 44, 45], more dedicated MPC approaches for optimal control under uncertainty have been developed. Within MPC literature for building climate control, two main methods are generally considered to explicitly address uncertainty: robust MPC (RMPC) and stochastic MPC (SMPC) [50, 52, 85, 86, 87]. There are also other MPC strategies that take into account uncertainty in a more implicit way, such as offset-free MPC [88], adaptive MPC [89] and learning-based

MPC [90], which are not further considered here. For a detailed review on these methods, see [36].

Robust MPC is tailored to systems subject to bounded uncertainty. It is especially useful for applications where the shape of the distribution is not known (or irrelevant), and when violations are extremely costly. It computes a control policy that guarantees constraint satisfaction for all possible uncertainty realizations, which are treated as equally likely, by optimizing the objective for the worst possible uncertainty realization. This results in a worst-case control strategy, which is rather conservative [48].

Stochastic MPC, on the other hand, is tailored to systems subject to probabilistic uncertainty. It exploits the shape of the probability distributions to find a suitable control strategy under uncertainty, and may allow for acceptable levels of constraint violations during system operation, as set by the user according to his risk averseness, by imposing probabilistic chance constraints, instead of hard constraints. As such, less conservative solutions can be obtained [48].

Two main solution strategies have been adopted for chance constrained problems, being scenario-based approaches and analytical approximation methods [91].

Scenario-based approaches consider a properly chosen number of uncertainty realizations to describe the probability distributions, in order to obtain a finite number of sampled deterministic constraints replacing the original probabilistic constraints. Hence, scenario-based approaches do not involve any assumption on the shape and support of the underlying probability distributions, but they are in general computationally very demanding [86, 91, 92, 93].

Analytical approximation methods, on the other hand, directly reformulate the probabilistic constraints in deterministic terms. Consequently, they result in an OCP of similar complexity as the conventional deterministic problem, thereby ensuring the tractability of the problem. However, this typically comes at the cost of some degree of conservativeness, due to the involved approximations [93, 94]. Nevertheless, for some specific probability distributions, such as normal distributions, exact reformulations can be found [91, 94, 95, 96].

Both RMPC and SMPC applications for building climate control currently mainly focus on the **uncertainty on the weather forecasts** (typically ambient temperature and solar heat gains) **and/or occupant behavior forecasts** (typically equipment-related and metabolic internal heat gains), as indicated by Table 3.1, which gives a summary of the relevant literature.

Maasoumy et al. [97] consider imperfect predictions of the ambient air temperature, solar radiation, and internal heat gains from occupants and equipment, and cope with this uncertainty by adopting an RMPC strategy. To reduce conservatism, they additionally implement affine disturbance feedback; here, the idea is to parametrize the control inputs as affine functions of the preceding uncertainties, in order to

Table 3.1: Summary of the relevant literature regarding RMPC and (scenario-based (scen.) or analytical reformulation based (reformul.)) SMPC applications for building climate control under uncertainty. The considered papers are categorized by considered uncertainty type, MPC strategy, and the consideration of feedback in the open-loop OCP.

| | Additive uncertainty | Parametric uncertainty | RMPC / SMPC (scen./reformul.) | Feedback |
|-------------------------------------|----------------------|------------------------|----------------------------------|----------|
| Maasoumy et al. [97] | x | | RMPC | x |
| Wang et al. [41] | x | | RMPC | |
| Zhang et al. [53] | x | | SMPC - scen. | |
| Zhang et al. [86] | x | | SMPC - scen. | x |
| Ma et al. [51] | x | | SMPC - scen. | x |
| Parisio et al. [49, 78, 98] | x | | SMPC - scen. | |
| Long et al. [48] | x | | SMPC - scen. | |
| Drgoňa et al. [99] | x | | SMPC - scen. | x |
| Ioli et al. [50] | x | | SMPC - scen. | |
| Oldewurtel et al. [44, 79, 79, 100] | x | | SMPC - reformul. | x |
| Zhang et al. [52] | x | | SMPC - reformul. | x |
| Hewing et al. [87] | x | | SMPC - reformul. | x |
| Ma et al. [101] | x | | SMPC - reformul. | x |
| Nagpal et al. [56] | | x | RMPC | x |
| Maasoumy et al [57] | | x | RMPC | x |
| Tanaskovic et al. [58] | | x | (adaptive) RMPC | |
| Yang et al. [59] | x | x | (adaptive) RMPC | x |
| This dissertation | x | x | SMPC - reformul. | x |

mimick the closed-loop corrective behavior of MPC in the open-loop control problem. Also Wang et al. [41] adopt RMPC, with an adaptable robustness level (via cardinality constraints), in order to cope with uncertainties on the outdoor temperature and hot water demand.

Zhang et al. [53] implemented a scenario-based SMPC strategy to account for the uncertainty on the outside air temperature, the wet-bulb temperature and solar radiation, as well as on the equipment-related and metabolic internal heat gains. To replace the original (not directly solvable) probabilistic constraints, a limited number of sampled uncertainty scenarios were considered, leading to a finite number of sampled deterministic constraints replacing the chance constraints. In order to improve the cost function value, some of the sampled scenarios were discarded a posteriori via sample removal. A similar scenario-based approach (but without sample removal), combined with affine disturbance feedback, was adopted by Zhang et al. [86]. Also Ma et al. [51] applied a scenario-based method with sample removal, combined with a feedback linearization scheme, and considered non-Gaussian distributions for the ambient temperature, solar radiation, and the internal thermal loads induced by occupants. The effectiveness of the proposed approach was illustrated by simulations as well as experiments in an MPC lab environment. Parisio et al. [49, 78, 98] also opted for a scenario-based SMPC strategy to limit the impact of the weather and occupancy uncertainty on the thermal comfort. To improve robustness, the proposed SMPC approach dynamically learned the statistics of the weather and occupancy conditions, represented by copulas. The effectiveness of this strategy was demonstrated for a real office building. Other examples of scenario-based approaches accounting for additive forecast uncertainties in building climate control can be found in [48, 50, 99].

In [79], Oldewurtel et al. applied analytically reformulated chance constraints, combined with affine disturbance feedback, to cope with assumed Gaussian uncertainty on the outside air temperature, the wet-bulb temperature and the incoming solar radiation. The SMPC strategy was shown to outperform both conventional rule-based control and deterministic MPC, by achieving a better trade-off between energy use and probability of thermal comfort violations. In related work [44, 79, 100], a tractable approximation of chance constrained SMPC combined with affine disturbance feedback was developed and applied, in order to cope with uncertainty on the weather and occupant behavior; for the proposed methodology to be scalable to large-scale systems, special attention was given to obtaining a linear approximation (rather than second order cone constraints). Another analytical reformulation approach combined with affine disturbance feedback, subject to uncertainty on the outside temperature, the solar radiation and the internal heat gains, can be found in [52], where a simplified control parametrization was implemented to reduce computation time. Also Hewing et al. [87] considered an SMPC method where the chance constraints were translated into tightened

deterministic constraints, to cope with a normally distributed, time-varying and correlated outside temperature sequence. Ma et al. [101] adopted analytically approximated joint¹ chance constraints, which were decoupled into individual chance constraints by using Boole's inequality, to eliminate the negative impact of Gaussian uncertainty on the ambient temperature, solar irradiance and occupancy load. A linear feedback control law was additionally implemented to reduce conservatism. In their approach, not only the control inputs and feedback gain, but also the risk allocations (i.e., the allowable violation) for each individual chance constraint were optimized.

Although the **building model parameters** are recognized as another important source of uncertainty influencing the building energy performance [54, 55], this uncertainty is only occasionally explicitly addressed.

Oldewurtel et al. [43] investigated the sensitivity of the performance of a deterministic MPC, used for climate control of an office room, to model parameter mismatch. By superimposing expert-defined variations on the nominal values of the U-values of the windows ($\pm 10\%$), the heat transmission coefficients ($\pm 15\%$), the energy recovery efficiency of the ventilation ($\pm 15\%$), the building mass ($\pm 10\%$), and the g-value and visual transmission of the windows ($\pm 10\%$), it was shown that building model parameter mismatch results in increased thermal comfort violations and energy costs.

To mitigate these negative effects, Nagpal et al. [56] considered a dedicated RMPC strategy, explicitly accounting for parametric uncertainty, applied to both a residential and an office building. Variations of a selection of the parameters of a one-zone four-states building model, being the heat transfer coefficient between the zone air and internal mass and the heat transfer coefficient between the zone air and ambient temperature, were included in the MPC formulation as polytopic uncertainties, characterized by a minimum and maximum value. The RMPC was shown to better track an imposed reference temperature profile compared to a deterministic MPC, with a relative tracking performance improvement of 17-24%. Maasoumy et al. [57] explicitly accounted for model uncertainty in an RMPC formulation for an office room in two different ways. First, the parametric uncertainty was implicitly handled by updating all model parameters of a one-zone five-states model in an online fashion, based on measurements, resulting in a parameter-adaptive building model. The uncertainty on the estimated parameters was additionally represented by an additive, box-constrained uncertainty with a fixed magnitude. In a simulation setting, the RMPC was able to guarantee a better trade-off between energy use and thermal discomfort compared to rule-based control or deterministic

¹ The constraint satisfaction can either be required for all inequality constraints altogether, over the whole prediction horizon, resulting in joint chance constraints, or for every individual inequality constraint at each distinct time step, also referred to as individual chance constraints [91, 100, 101, 102].

MPC for moderate model uncertainty (i.e., when the model uncertainty ranges between 30% and 67% of its maximum value). However, for very small or very large model uncertainty, the deterministic MPC approach or rule-based controller were found to be more appropriate.

Tanaskovic et al. [58] extended the robust adaptive MPC method of Maasoumy et al. [57] by also making the uncertainty, rather than only the estimated model parameters, adaptive. Starting from an initial set of possible models, a recursive set membership identification method is used to progressively shrink this set. In a case study for an office room, they considered an initial variation of $\pm 50\%$ around a nominal value for the thermal heat capacities of the walls, floor and ceiling, the convective heat transfer coefficients between the building elements and the zone air, and the U-values of the window. They demonstrated via simulations that the robust adaptive MPC was able to guarantee small thermal comfort violations, even during the adaptation phase; as the adaptation phase proceeded, the energy costs decreased, eventually falling below the costs related to a nominal, non-robust and non-adaptive MPC implementation that has model mismatch.

Building further upon the work of Tanaskovic et al. [58], Yang et al. [59] considered a robust adaptive MPC that not only takes into account model uncertainty, but also uncertainty on the disturbance forecasts (more specifically, on the internal heat and moisture gains). Through simulations for an office room represented by a one-zone three-states RC model, their adaptive robust MPC was shown to improve thermal comfort compared to a conventional reactive-based thermostat control, a deterministic MPC, a calibrated deterministic MPC, and a non-robust adaptive MPC; the robust adaptive MPC was the only control strategy achieving an acceptable thermal comfort² during at least 90% of the office hours. The thermal comfort improvement came at the cost of a slight decrease in thermal energy savings relative to the conventional thermostat control, declining from $\sim 20\%$ to 15% for increasing uncertainty levels, with the internal load varying from 0-60% around its nominal value.

Research gap

Despite the limited attention for parametric uncertainty in building climate control applications, the building controller model is not always capable of capturing the building dynamics in detail, due to the unavailability of sufficient data and/or experts' knowledge to set up the model [61]. This is especially true in case of a widespread MPC implementation involving the older, existing building stock [54, 60]. Besides, the impossibility to correctly describe the

² The indoor thermal comfort valuation in [59] was based on the predicted mean vote (PMV) index, where an acceptable PMV was in the range (-0.5,0.5). Overall the PMV values can range from -3 (cold), over -1 (slightly cold), over 0 (neutral), over +1 (slightly warm), to +3 (hot) [83].

complexity of the underlying physics plays an important role regarding model uncertainty [59]. In these cases, the parametric uncertainty of the controller model can become non-negligible, and hence, should be explicitly accounted for by the MPC strategy. Despite the probabilistic descriptions found in literature for the building envelope characteristics [60,62,63,64,65,66], weather conditions [51, 55, 64, 67] and occupant behavior [55, 64, 65], and the fact that thermal comfort is allowed to be occasionally violated [68, 69], building climate control applications have mostly tackled (the combination of additive and) parametric uncertainty via RMPC strategies, leading to conservative approaches. The development and assessment of an SMPC approach for building climate control under combined additive and parametric uncertainty is therefore to be investigated. The SMPC development is the focus of Chapters 4 and 5 of this dissertation, whereas the application of the proposed SMPC strategy for building climate control is discussed in Chapter 6.

3.2 (Integrated optimal control and) design under uncertainty

In order to cope with uncertainties in design applications, and the associated risk for thermal discomfort, current engineering practices typically consider worst-case static conditions, as formulated in heat loss calculations (e.g., [69]), and/or assign a safety factor to a deterministic load calculated for specific design conditions [64, 72, 73, 74, 75]; this safety factor serves to account for more extreme periods than the design conditions, thereby implicitly dealing with uncertainty. An important issue associated with these kind of approaches is that they may lead to oversized systems [64, 72, 73, 74, 75].

In order to overcome this issue, there has been an emerging interest to exploit optimal control algorithms in an optimal design context, because of the close interconnection between both [70, 103]. Indeed, the building envelope design determines the heating and cooling load profiles, and thus, which control actions are required, whereas the HVAC system design determines the technical limits of the heat supply, distribution and emission system, and thus, which control actions are possible [70]. A better alignment of control and design via an integrated optimal control and design methodology, properly accounting for the system dynamics, can result in a more appropriate, i.e., less oversized and more cost-optimal, system design. This is for example shown for an office building by Jorissen et al. [70], or for a district heating network by van der Heijde [71].

Research gap

Although the transition towards IOCD methodologies is a considerable improvement tackling the oversize problem of the static approaches, there is risk that they still result in an inadequate system sizing, since current IOCD approaches typically incorporate a deterministic MPC strategy, thereby overlooking the impact of uncertainties. This could endanger the required thermal comfort, and might moreover drastically reduce the flexibility potential needed in DR programs. These problems could be overcome by using an SMPC (or RMPC) for the optimal control part of the IOCD approach, which is investigated in Chapter 7 of this dissertation.

3.3 Demand response under uncertainty

Also for DR applications, there has been an increasing interest to explicitly consider uncertainties in the decision-making process, in order to guarantee the feasibility and optimality of the determined load schedules in real time [41, 46, 47, 104, 105, 106].

Although there is a vast amount of research available targeting uncertainty in real-time control (see e.g., [46, 107, 108, 109, 110]), the uncertainty is especially important in day-ahead planning problems, since they require forecasts over a longer timescale, which are inevitably more uncertain [105].

Also in this context, the two most common adopted approaches to deal with uncertainties are stochastic optimization and robust optimization [47], or even combinations of both (see e.g., [47, 111]). These approaches are used to cope with a wide variety of uncertainties, including uncertainty on prices, renewable generation and/or loads. The scope of this dissertation is limited to the latter category, and more specifically, to the uncertainty on the flexible demand of residential TCLs.

Several authors have studied the day-ahead coordination of residential TCLs as a DR resource under uncertainty. In the available literature, two major research approaches can be discerned.

A first stream of research assesses the day-ahead optimal planning problem from a **system perspective**, where the flexible load model is part of a larger energy system optimization problem or equilibrium model. Note that, although these approaches can generally not be classified as MPC³, they also use OCP formulations

³ The classification of a control approach as MPC, instead of more generally as optimal control, requires a receding horizon implementation with closed-loop disruptions.

to describe the TCL behavior (similar to MPC). These approaches acknowledge that the demand can be uncertain, and explicitly optimize the actions required to cope with this load uncertainty. The load uncertainty is typically assumed to be known and uncontrollable.

Vrakopoulou et al. [112,113] developed a multi-period chance constrained optimal power flow⁴ (OPF) formulation that co-optimizes energy and reserves provided by both generators and controllable TCLs for the upcoming day to guarantee minimal operating cost, while taking into account uncertainty on the forecasts of the renewable power generation and the TCL behavior via scenarios. In their problem formulation, they explicitly acknowledged that an incorrect appraisal of the demand may cause imbalances, which are corrected for by reserves.

A very similar problem setting was considered by Zhang et al. [106], where the main difference with the work of Vrakopoulou et al. [112,113] lies in the adopted solution strategy; they solve a single-period (instead of a multi-period) chance constrained OPF via distributionally robust optimization, instead of via a robust reformulation of the scenario approach, and as such, do not require a large number of uncertainty samples.

Good et al. [115] assessed the DR problem rather from a market oriented perspective. They looked at aggregated TCLs represented/coordinated by a balancing responsible party, whose market participation was modeled with the help of a two-stage stochastic problem, representing a day-ahead market participation with imbalance responsibility, where the aim is to minimize the overall expected day-ahead energy costs, as well as imbalance costs for deviations from the day-ahead position as a consequence of demand forecast uncertainty. The demand forecast uncertainty is in this work caused by uncertainties on the outdoor temperature (and hence, also the space heating demand), the domestic hot water demand, the electricity consumption from all other appliances, and the dwelling occupancy), all of which are accounted for through the use of scenarios. In addition to the demand uncertainty, also uncertainty on the imbalance prices is accounted for.

Another two-stage stochastic problem can be found in the work of Kou et al. [116], who considered the role of a distribution system operator (DSO) in both the day-ahead and real-time electricity markets. The DSO coordinates the use of the flexibility of a large number of residential TCLs (via an aggregator) to maximize social welfare, while explicitly mitigating the impact of a wide range of uncertainties on the DR performance (including weather uncertainty, i.a., the outdoor temperature affecting the space heating demand and the solar generation affecting the local PV generation, and occupant behavior uncertainty, i.a., the non-responsive load and the hot water consumption, all of which are modeled via scenarios).

Also Bruninx et al. [117,118] explicitly accounted for load uncertainties in a demand

⁴ An optimal power flow problem optimizes how much power should be generated by each considered generation unit, as well as how much power should be sent around a transmission or distribution network in order to meet the demand [114].

response context. In [117], the authors adopted an optimization based approach, by solving a multi-period deterministic unit commitment model⁵ to determine the optimal day-ahead power plant schedule, with probabilistic power balancing and reserve constraints to cope with uncertainties. The considered uncertainties include the stochastic renewable electricity generation, and the limited controllability of the residential electric heating systems providing load shifting and ancillary services (due to inaccuracies in the weather and occupant behavior forecast, and in the load model or due to sub-rational behavior). The uncertainty on the flexible demand is modeled with the help of a proportional and non-proportional component, both of which are assumed to be normally distributed with a fixed standard deviation. In [118], Bruninx et al. assessed a very similar scheduling problem, although this time without reserve provision by the TCLs, via a market-based approach, by studying the strategic interactions between an aggregator, its consumers, and the day-ahead market, with the help of bi-level optimization framework. Here again, chance constraints were used to cope with the uncertainty, forcing the aggregator to procure sufficient electricity in the day-ahead market to be able to cover the demand of its consumers in accordance with the imposed level of risk aversion.

A second stream of research assesses the day-ahead DR scheduling problem under uncertainty via a bottom-up approach, from the **consumer perspective**. These approaches typically implement an MPC strategy that is reacting to an external price signal expressing the DR request. The MPC problem is formulated as a stochastic/robust OCP in order to guarantee thermal comfort, as well as to guarantee the feasibility of the scheduled load profile in real time, despite possible uncertainty manifestations. Remarkably, these consumer-oriented approaches tend to neglect, or even deliberately prohibit the closed-loop corrective behavior of MPC, and thus, do not incorporate affine disturbance feedback⁶. As such, they limit the exposure of the central system to load uncertainty (which is fundamentally different from the approaches described above). Instead, they opt for very conservative control strategies, where the impact of uncertainties is fully managed at consumer level.

Garifi et al. [120] proposed a chance constrained MPC algorithm, which optimally schedules the operation of the combination of an HVAC system, uncontrollable loads, a local PV installation and a battery system in a residential building, in response to a grid load reduction request, at minimal operating cost. Two sets of chance constraints were implemented, to guarantee the satisfaction of the load reduction, as well as of the thermal comfort, with high probability. The considered uncertainties include the available PV power and the outdoor air temperature, which are assumed to be normally distributed (and possibly time-dependent).

⁵ A unit commitment model is an operational model of an electric power system, used to determine the on/off states of the considered generating units, while taking into account their relevant technical constraints [119].

⁶ This is in contrast commonly done for optimal control applications, as discussed in Section 3.1.

Wang et al. [41] considered a robust optimization method for day-ahead household load scheduling in response to a time-varying electricity price profile. Different levels of conservatism were allowed, enabling a trade-off between cost and thermal comfort. The loads considered in the scheduling problem include controllable loads affected by uncertainty (i.e., an air conditioning unit and an electric water heater), uncontrollable loads, uninterruptible loads, interruptible loads, and an (electric) energy storage device. The control strategy explicitly accounts for uncertainties on the outdoor temperature and the hot water demand, which were modeled with the help of uncertainty sets surrounding the forecast values.

Finally, Diekerhof et al. [121] considered a robust MPC as part of a larger hierarchical DR framework, used for the day-ahead scheduling of flexible heat pumps (by implementing the alternating direction method of multipliers for distributed optimization). In the proposed framework, an aggregation service provider coordinates the heat pump demand via an exchange of price vectors, in order to pursue a system-level objective, being either a minimization of the energy procurement cost, or peak shaving. The TCLs, on the other hand, respond to the coordination signals received from the aggregator, while potentially optimizing an additional local objective. The heat pump operation is optimized in a robust way, hedging against uncertainty on the thermal demand of the building, in order to avoid real-time power adjustments to the pre-calculated operational schedule⁷.

Research gap

In the state-of-the-art literature regarding SMPC and RMPC strategies for demand response, real-time adjustments to the scheduled control strategy of TCLs are typically prohibited, thereby fully managing the uncertainty on consumer level. The system-level oriented literature illustrates that load uncertainty, typically assumed to be given and known, can be effectively managed at system level as well. To establish a middle ground between the two streams of research perceived above, this dissertation proposes to explicitly account for the closed-loop feedback aspect in the open-loop OCP of MPC strategies for TCLs participating in DR programs. This can be done by including affine disturbance feedback. This not only allows to characterize the load uncertainty in detail, but moreover allows to optimize it. As such, a trade-off between the degree of uncertainty management at building versus at system level is enabled, which may facilitate a more cost-effective use of the demand side flexibility offered by TCLs. This is investigated in Chapter 9.

⁷ Note that the robust optimization merely focuses on the compliance with the DR request, since no explicit thermal comfort requirements are considered in the work of Diekerhof et al. [121].

Part I

SMPC development

Chapter 4

Stochastic OCP formulation

RQ 1: How does the conventional deterministic OCP formulation for building climate control need to be reformulated in order to explicitly account for additive (disturbance forecast) and parametric (model) uncertainties?

This chapter is based on A. Uytterhoeven, R. Van Rompaey, K. Bruninx, and L. Helsen, "Chance Constrained Stochastic MPC for Building Climate Control Under Combined Parametric and Additive Uncertainty," submitted to Journal of Building Performance Simulation, July 2021.

This chapter focuses on the first part of the SMPC development, being the derivation of the stochastic OCP formulation that explicitly accounts for both additive and parametric uncertainty. First, a short overview of the relevant notation is given in Section 4.1. Subsequently, starting from the conventional deterministic formulation presented in Chapter 2, the stochastic substitute is derived. This derivation is performed in a systematic way, by successively introducing the uncertainties in all relevant parts of the OCP in Sections 4.2 to 4.4. The resulting convex stochastic OCP formulation is presented in Section 4.5, after which conclusions are drawn in Section 4.6.

4.1 Notation

Bold face upper case letters refer to matrices, bold face lower case letters refer to vectors, and regular lower case letters refer to scalars. Letters with superscript

tilde $\tilde{\cdot}$ refer to uncertain parameters or variables with mean $\bar{\cdot}$ and uncertain portion $\delta\cdot$. $\mathbb{E}[\cdot]$ is the expected value operator, $P(\cdot)$ represents a probability. \mathbb{R} represents the set of real numbers, and \mathbb{N} the set of integer numbers. $\mathbf{0}_{i \times j}$ is the $i \times j$ zero matrix, $\mathbf{0}_i$ is an all-zeros vector of size i , \mathbf{I}_i is the $i \times i$ identity matrix, $\mathbf{1}_i$ is an all-ones vector of size i , and \mathbf{e}_i is a selection vector containing a one on the i th position and zeros elsewhere. $\text{vec}(\cdot)$ denotes the vectorization of a matrix stacking all its columns in one vector. \otimes denotes the Kronecker product.

4.2 Introducing uncertainties in the state space equation

Uncertainties turn the parameters of the building controller model and the disturbance predictions into stochastic quantities, whose distribution can be characterized by a mean value $\bar{\cdot}$ and a covariance Σ .

$$\begin{aligned} \mathbf{A} &\rightarrow \tilde{\mathbf{A}} \triangleq \bar{\mathbf{A}} + \delta\mathbf{A} \\ &\text{with } \bar{\mathbf{A}} \triangleq \mathbb{E}[\tilde{\mathbf{A}}] \text{ and } \Sigma_{\mathbf{A}} \triangleq \mathbb{E}[\text{vec}(\delta\mathbf{A}) \text{vec}(\delta\mathbf{A})^T] \end{aligned} \quad (4.1a)$$

$$\begin{aligned} \mathbf{B} &\rightarrow \tilde{\mathbf{B}} \triangleq \bar{\mathbf{B}} + \delta\mathbf{B} \\ &\text{with } \bar{\mathbf{B}} \triangleq \mathbb{E}[\tilde{\mathbf{B}}] \text{ and } \Sigma_{\mathbf{B}} \triangleq \mathbb{E}[\text{vec}(\delta\mathbf{B}) \text{vec}(\delta\mathbf{B})^T] \end{aligned} \quad (4.1b)$$

$$\begin{aligned} \mathbf{E} &\rightarrow \tilde{\mathbf{E}} \triangleq \bar{\mathbf{E}} + \delta\mathbf{E} \\ &\text{with } \bar{\mathbf{E}} \triangleq \mathbb{E}[\tilde{\mathbf{E}}] \text{ and } \Sigma_{\mathbf{E}} \triangleq \mathbb{E}[\text{vec}(\delta\mathbf{E}) \text{vec}(\delta\mathbf{E})^T] \end{aligned} \quad (4.1c)$$

$$\begin{aligned} \mathbf{d}_k &\rightarrow \tilde{\mathbf{d}}_k \triangleq \bar{\mathbf{d}}_k + \delta\mathbf{d}_k \quad \forall k \\ &\text{with } \bar{\mathbf{d}}_k \triangleq \mathbb{E}[\tilde{\mathbf{d}}_k] \text{ and } \Sigma_{\mathbf{d}_k} \triangleq \mathbb{E}[\delta\mathbf{d}_k \delta\mathbf{d}_k^T] \end{aligned} \quad (4.1d)$$

By incorporating these probabilistic parametric ($\tilde{\mathbf{A}}, \tilde{\mathbf{B}}, \tilde{\mathbf{E}}$) and additive ($\tilde{\mathbf{d}}_k$) uncertainties in the deterministic OCP (2.1) presented in Chapter 2, the deterministic state space equation (2.1a) is transformed into its stochastic counterpart

$$\begin{aligned} \tilde{\mathbf{x}}_{k+1} &= \tilde{\mathbf{A}} \tilde{\mathbf{x}}_k + \tilde{\mathbf{B}} \mathbf{u}_k + \tilde{\mathbf{E}} \tilde{\mathbf{d}}_k \\ &= (\bar{\mathbf{A}} + \delta\mathbf{A})(\bar{\mathbf{x}}_k + \delta\mathbf{x}_k) + (\bar{\mathbf{B}} + \delta\mathbf{B})\mathbf{u}_k + (\bar{\mathbf{E}} + \delta\mathbf{E})(\bar{\mathbf{d}}_k + \delta\mathbf{d}_k) \end{aligned}$$

$$\begin{aligned} &\approx (\bar{\mathbf{A}} \bar{\mathbf{x}}_k + \bar{\mathbf{B}} \mathbf{u}_k + \bar{\mathbf{E}} \bar{\mathbf{d}}_k) + \\ &(\delta \mathbf{A} \bar{\mathbf{x}}_k + \bar{\mathbf{A}} \delta \mathbf{x}_k + \delta \mathbf{B} \mathbf{u}_k + \delta \mathbf{E} \bar{\mathbf{d}}_k + \bar{\mathbf{E}} \delta \mathbf{d}_k) \end{aligned} \quad (4.2)$$

where the products of stochastic variables (i.e., second order terms) are neglected in the third step to ensure mathematical tractability.

Because of the explicit dependency of the states \mathbf{x}_k on the introduced uncertainties, imposed by the state space equation, the states are also transformed to stochastic variables. Based on Equation (4.2), the mean and covariance can then be allocated as

$$\bar{\mathbf{x}}_{k+1} = \bar{\mathbf{A}} \bar{\mathbf{x}}_k + \bar{\mathbf{B}} \mathbf{u}_k + \bar{\mathbf{E}} \bar{\mathbf{d}}_k \quad (4.3)$$

and

$$\begin{aligned} \Sigma_{\mathbf{x}_{k+1}} = \mathbb{E}[(\delta \mathbf{A} \bar{\mathbf{x}}_k + \bar{\mathbf{A}} \delta \mathbf{x}_k + \delta \mathbf{B} \mathbf{u}_k + \delta \mathbf{E} \bar{\mathbf{d}}_k + \bar{\mathbf{E}} \delta \mathbf{d}_k) \\ (\delta \mathbf{A} \bar{\mathbf{x}}_k + \bar{\mathbf{A}} \delta \mathbf{x}_k + \delta \mathbf{B} \mathbf{u}_k + \delta \mathbf{E} \bar{\mathbf{d}}_k + \bar{\mathbf{E}} \delta \mathbf{d}_k)^T], \end{aligned} \quad (4.4)$$

erving as the stochastic substitute for Equation (2.1a).

Note that the inputs \mathbf{u}_k , in contrast to the states, do not explicitly depend on any of the imposed uncertainties. Hence, for now, the deterministic form of the inputs is retained, but this will be revisited when introducing the uncertainties in the input constraints.

Further elaboration of Equation (4.4) in its current form would result in a non-convex expression, due to the cross-products of optimization variables. To overcome this issue, two manipulations are proposed in this work to convexify the constraint: the introduction of a latent variable aggregating all uncertainties, and a transformation of the covariance by using a square root notation.

First, all stochastic quantities are aggregated in the latent random variable $\tilde{\mathbf{p}} \in \mathbb{R}^{n_p}$ with mean $\bar{\mathbf{p}}$ and covariance $\Sigma_{\tilde{\mathbf{p}}}$, i.e.,

$$vec(\tilde{\mathbf{A}}) = \mathbf{T}_{\mathbf{A}} \tilde{\mathbf{p}} \text{ with } \mathbf{T}_{\mathbf{A}} \in \mathbb{R}^{n_x^2 \times n_p} \quad (4.5a)$$

$$vec(\tilde{\mathbf{B}}) = \mathbf{T}_{\mathbf{B}} \tilde{\mathbf{p}} \text{ with } \mathbf{T}_{\mathbf{B}} \in \mathbb{R}^{n_x n_u \times n_p} \quad (4.5b)$$

$$vec(\tilde{\mathbf{E}}) = \mathbf{T}_{\mathbf{E}} \tilde{\mathbf{p}} \text{ with } \mathbf{T}_{\mathbf{E}} \in \mathbb{R}^{n_x n_d \times n_p} \quad (4.5c)$$

$$\tilde{\mathbf{d}}_k = \mathbf{T}_{\mathbf{d}_k} \tilde{\mathbf{p}} \text{ with } \mathbf{T}_{\mathbf{d}_k} \in \mathbb{R}^{n_d \times n_p} \quad \forall k \quad (4.5d)$$

where $\mathbf{T}_{\mathbf{A}}$, $\mathbf{T}_{\mathbf{B}}$, $\mathbf{T}_{\mathbf{E}}$ and $\mathbf{T}_{\mathbf{d}_k}$ are appropriate selection matrices.

Consequently, any stochastic parameter $\tilde{\mathbf{f}} \in \{\tilde{\mathbf{A}}, \tilde{\mathbf{B}}, \tilde{\mathbf{E}}, \tilde{\mathbf{d}}_k\}$ can be expressed as

$$\text{vec}(\tilde{\mathbf{f}}) = \text{vec}(\bar{\mathbf{f}}) + \text{vec}(\delta\mathbf{f}), \quad (4.6)$$

with

$$\text{vec}(\bar{\mathbf{f}}) = \mathbb{E}[\text{vec}(\tilde{\mathbf{f}})] = \mathbf{T}_f \bar{\mathbf{p}} \quad (4.7a)$$

and

$$\Sigma_f = \mathbb{E}[\text{vec}(\delta\mathbf{f}) \text{vec}(\delta\mathbf{f})^T] = \mathbf{T}_f \Sigma_p \mathbf{T}_f^T \quad (4.7b)$$

being the (vectorized¹) mean and covariance of $\tilde{\mathbf{f}}$, respectively. In addition, the covariance between two stochastic quantities $\tilde{\mathbf{f}}, \tilde{\mathbf{g}} \in \{\tilde{\mathbf{A}}, \tilde{\mathbf{B}}, \tilde{\mathbf{E}}, \tilde{\mathbf{d}}_k\}$ that are correlated with one another, can be written as

$$\Sigma_{f,g} = \mathbb{E}[\text{vec}(\delta\mathbf{f}) \text{vec}(\delta\mathbf{g})^T] = \mathbf{T}_f \Sigma_p \mathbf{T}_g^T. \quad (4.8)$$

Second, the covariance matrix Σ_p is decomposed by using a square root notation as follows

$$\Sigma_p = \Sigma_p^{1/2} \Sigma_p^{1/2T}, \quad (4.9)$$

where $\Sigma_p^{1/2} \in \mathbf{R}^{n_p \times n_p}$ is the square root of Σ_p , unique up to an orthogonal transformation of its columns². With the help of the square root notation, the covariance between two stochastic quantities $\tilde{\mathbf{f}}, \tilde{\mathbf{g}} \in \{\tilde{\mathbf{A}}, \tilde{\mathbf{B}}, \tilde{\mathbf{E}}, \tilde{\mathbf{d}}_k\}$ can be decomposed as

$$\Sigma_{f,g} = \mathbf{T}_f \Sigma_p \mathbf{T}_g^T = \left(\mathbf{T}_f \Sigma_p^{1/2} \right) \left(\Sigma_p^{1/2T} \mathbf{T}_g^T \right) = \Sigma_f^r \Sigma_g^r{}^T. \quad (4.10)$$

Here, the more general notation \cdot^r is used to refer to the root form instead of $\cdot^{1/2}$, since the matrices Σ_f^r and Σ_g^r are not necessarily square, and hence are not actual square roots of the considered matrices.

By applying the two manipulations discussed above to Equation (4.4), and by furthermore using following relation between the vectorization of a matrix and the Kronecker product³

$$\text{vec}(\mathbf{A}\mathbf{X}\mathbf{B}^T) = (\mathbf{B} \otimes \mathbf{A}) \text{vec}(\mathbf{X}) \quad (4.11)$$

¹ The vectorized notation is introduced for arguments of simplicity, to prevent the use of tensors. Indeed, by writing all uncertainties in vector format, it is possible to use covariance matrices, rather than covariance tensors, of all stochastic quantities.

² Since the covariance matrix Σ_p is per definition a positive (semi-)definite matrix, this square root form can for example be obtained via the Cholesky factorization [122].

³ The Kronecker product of an $m \times n$ matrix \mathbf{A} and a matrix \mathbf{B} is defined as

$$\mathbf{A} \otimes \mathbf{B} = \begin{bmatrix} a_{1,1}\mathbf{B} & \dots & a_{1,n}\mathbf{B} \\ \vdots & \ddots & \vdots \\ a_{m,1}\mathbf{B} & \dots & a_{m,n}\mathbf{B} \end{bmatrix}.$$

the covariance $\Sigma_{\mathbf{x}_{k+1}}$ can be rewritten in square root form as follows

$$\begin{aligned} \Sigma_{\mathbf{x}_{k+1}}^r &= (\bar{\mathbf{x}}_k^T \otimes \mathbf{I}_{n_x}) \Sigma_{\mathbf{A}}^r + \bar{\mathbf{A}} \Sigma_{\mathbf{x}_k}^r + (\mathbf{u}_k^T \otimes \mathbf{I}_{n_x}) \Sigma_{\mathbf{B}}^r + \\ &\quad (\bar{\mathbf{d}}_k^T \otimes \mathbf{I}_{n_x}) \Sigma_{\mathbf{E}}^r + \bar{\mathbf{E}} \Sigma_{\mathbf{d}_k}^r. \end{aligned} \quad (4.12)$$

By using Equation (4.3) in combination with the square root form of the covariance, as presented by Equation (4.12), as the stochastic substitute for Equation (2.1a), the constraints are now linear in the optimization variables \mathbf{u}_k , $\bar{\mathbf{x}}_k$ and $\Sigma_{\mathbf{x}_k}^r$ (rather than $\Sigma_{\mathbf{x}_k}$), thereby guaranteeing the convexity of the problem.

4.3 Introducing uncertainties in the state constraints

By integrating the stochastic information in the state constraints, the hard state constraints (2.1b) and (2.1c) are transformed to chance constraints, as presented by Equation (4.13), which are seen as the key characteristic of stochastic model predictive control formulations.

$$P(\tilde{\mathbf{x}}_k + \mathbf{s}_k \geq \mathbf{x}_k^{min}) \geq 1 - \epsilon_{\mathbf{x}_k} \quad \forall k \quad (4.13a)$$

$$P(\tilde{\mathbf{x}}_k - \mathbf{s}_k \leq \mathbf{x}_k^{max}) \geq 1 - \epsilon_{\mathbf{x}_k} \quad \forall k \quad (4.13b)$$

Note that the slack variables \mathbf{s}_k are retained to guarantee feasibility under unbounded uncertainties [91].

The rationale behind chance constraints is the following. Since the open-loop stochastic OCP needs to decide upon an optimal control strategy before the actual values of the stochastic quantities are known, it tries to guarantee constraint satisfaction for possible realizations of the stochastic quantities in a probabilistic sense, by exploiting the knowledge of their distributions. The probability of constraint satisfaction is determined by the user-predefined risk-attitude⁴ $\{\epsilon_{\mathbf{x}_k}\}_{k=0\dots K+1}$ (or risk-averseness level $1 - \epsilon_{\mathbf{x}_k}$), which enables a systematic trade-off between control performance and constraint satisfaction; $\epsilon \rightarrow 0$ corresponds to a very conservative

⁴ Although the majority of applications impose a user-predefined level of constraint satisfaction, it is also possible to consider the risk level ϵ as an additional optimization variable that is determined via optimal risk allocation, see for example [101].

attitude⁵, whereas $\epsilon = 0.5$ reduces the chance constraints to their deterministic equivalent without any uncertainty anticipation [84, 123].

The constraint satisfaction can either be required for all inequality constraints altogether, over the whole prediction horizon K , resulting in joint chance constraints, or for every individual inequality constraint at each distinct time step, also referred to as individual chance constraints [91, 100, 101, 102]. Joint chance constraints typically become non-convex, for which an exact tractable representation might not exist [91], and hence are highly computationally intensive [100, 101]. Therefore, this work focuses on individual chance constraints.

As discussed in detail in Section 3.1, two main solution strategies have been adopted for chance constrained problems, being scenario-based approaches and analytical approximation methods [91]. In this work, the analytical approximation method is pursued. According to this approach, chance constraints can be generally reformulated as deterministic ones by enforcing tightened constraints on the expected values of the states as follows

$$\bar{\mathbf{x}}_k + \mathbf{s}_k \geq \mathbf{x}_k^{min} + \mathbf{q}_k(1 - \epsilon_{\mathbf{x}_k}) \quad \forall k \quad (4.14a)$$

$$\bar{\mathbf{x}}_k - \mathbf{s}_k \leq \mathbf{x}_k^{max} - \mathbf{q}_k(1 - \epsilon_{\mathbf{x}_k}) \quad \forall k, \quad (4.14b)$$

based on the idea that part of the tail of the distribution is allowed to violate the imposed bounds, as visualized in Figure 4.1. The exact expression for the constraint tightening level $\mathbf{q}_k(1 - \epsilon_{\mathbf{x}_k})$ is dependent on the distribution of the considered uncertainties [91]. In the most general case, where the distribution of \mathbf{x}_k is not specified, one can resort to distributionally robust chance constraints, resulting in a more conservative approach [91, 95, 96]. In the specific case where the marginal distributions of the different states $\tilde{x}_{i,k} = \mathbf{e}_i^T \tilde{\mathbf{x}}_k \forall i \in \mathbb{N}^{n_x}$ can be approximated as normal distributions, the individual chance constraints can be equivalently (and exactly) reformulated as deterministic constraints as follows

$$\bar{x}_{i,k} + s_{i,k} \geq x_{i,k}^{min} + \Phi^{-1}(1 - \epsilon_{x_{i,k}}) \sqrt{\Sigma_{x_{i,k}}^r \Sigma_{x_{i,k}}^r{}^T} \quad \forall i, k \quad (4.15a)$$

$$\bar{x}_{i,k} - s_{i,k} \leq x_{i,k}^{max} - \Phi^{-1}(1 - \epsilon_{x_{i,k}}) \sqrt{\Sigma_{x_{i,k}}^r \Sigma_{x_{i,k}}^r{}^T} \quad \forall i, k \quad (4.15b)$$

where Φ^{-1} denotes the inverse normal cumulative probability density function of $\tilde{x}_{i,k}$. The justification of using marginal normal distributions in this work will be

⁵ Note that $\epsilon = 0$ corresponds to a robust optimization problem, where the constraints need to hold for all possible values of the stochastic quantities [123]. Under these conditions, a solution can only be found under the assumption that $\tilde{\mathbf{x}}_k$ is bounded [91]. Only the support of the distribution is considered in that case, without taking advantage of the actual shape of the distribution.

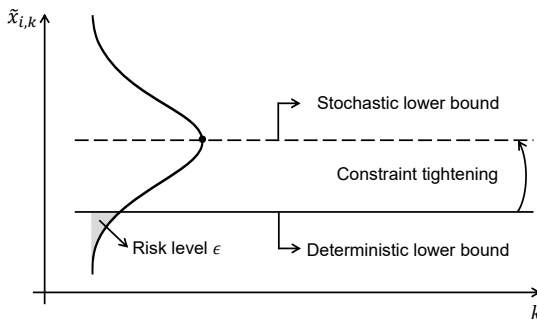


Figure 4.1: The visualization of the constraint tightening resulting from the analytical reformulation of chance constraints.

further discussed in Chapter 5, and will be numerically tested/validated in Chapters 6 and 7.

The constraints (4.15a) and (4.15b) can be further recast to obtain efficiently solvable second order cone (SOC) constraints, by introducing an auxiliary optimization variable $\{\mathbf{q}_k \in \mathbb{R}^{n_x}\}_{k=0 \dots K+1}$

$$\bar{x}_{i,k} + s_{i,k} \geq x_{i,k}^{min} + \Phi^{-1}(1 - \epsilon_{x_{i,k}}) q_{i,k} \quad \forall i, k \quad (4.16a)$$

$$\bar{x}_{i,k} - s_{i,k} \leq x_{i,k}^{max} - \Phi^{-1}(1 - \epsilon_{x_{i,k}}) q_{i,k} \quad \forall i, k \quad (4.16b)$$

$$q_{i,k} \geq \|\Sigma_{x_{i,k}}^r\|_2 \quad \forall i, k \quad (4.16c)$$

where $\Sigma_{x_{i,k}}^r$ corresponds to the root form of the covariance of the system states as defined by Equation (4.12). The first two constraints (Equations (4.16a) and (4.16b)) define a half space in the optimization variables and the last constraint (Equation 4.16c) defines a second order cone, which all together define a convex set.

The combination of Equations (4.16a) - (4.16c) replaces Equations (2.1b) and (2.1c) in the deterministic OCP formulation to form the stochastic OCP.

4.4 Introducing uncertainties in the input constraints

For the input constraints two approaches are possible to incorporate the uncertainties.

First, one can retain the nominal power constraints (2.1e), leading to a computationally attractive formulation. According to this approach, the future control actions are only a function of the current situation, and not of the future disturbance and state realizations. The disadvantage of this approach is that it results in highly conservative behavior, since the OCP neglects the closed-loop feedback aspect of MPC. As such, it disregards the possibility to intermediately react against manifested realizations of the uncertainties (i.e., perturbations), and tries to hedge against the accumulative effect of the uncertainties over the whole prediction horizon [92, 100].

To reduce conservatism, it is recommended to introduce affine disturbance feedback (ADF). Following this approach, the control inputs are reformulated as an affine function of the preceding uncertainty manifestations, thereby mimicking the closed-loop behavior of the MPC in the open-loop control problem [52, 79, 84, 91, 92, 97, 100]. Using the previously introduced notation, this can be written as follows.

$$\begin{aligned} \mathbf{u} &\rightarrow \tilde{\mathbf{u}} = \bar{\mathbf{u}} + \delta\mathbf{u} \\ \text{with } \tilde{\mathbf{u}} &= [\tilde{\mathbf{u}}_0^T \dots \tilde{\mathbf{u}}_k^T \dots \tilde{\mathbf{u}}_K^T]^T \\ \bar{\mathbf{u}} &= \mathbb{E}[\tilde{\mathbf{u}}] \\ \Sigma_{\mathbf{u}} &= \mathbb{E}[\delta\mathbf{u} \delta\mathbf{u}^T] = \mathbf{T}_{\mathbf{u}} \Sigma_{\mathbf{p}} \mathbf{T}_{\mathbf{u}}^T \end{aligned} \quad (4.17)$$

Note that the inputs are rewritten in the same way as the stochastic quantities in Equations (4.1) and (4.7). However, the important difference is that the mean $\bar{\mathbf{u}}$ as well as the selection matrix $\mathbf{T}_{\mathbf{u}}$ are now optimization variables, rather than fixed, predefined parameters. The selection matrix $\mathbf{T}_{\mathbf{u}}$ should be interpreted as a feedback gain matrix, that guarantees causality by ensuring that the control input at time step k can only react to the uncertainty manifestations up to time $k - 1$. Also note that the first control input is not a function of any uncertainty, since it is assumed that at the first time step, the currently prevailing states and inputs are known [91, 92].

Since the inputs now also become functions of stochastic random variables, characterized by an unbounded value range, the input constraints can no longer be guaranteed for all possible uncertainty realizations. This would result in an infeasible optimization problem, unless $\mathbf{T}_{\mathbf{u}} = \mathbf{0}_{n_u K \times n_p}$. To overcome this issue, the hard input constraints (2.1e) need to be relaxed, and hence, are also replaced by chance constraints on the individual inputs $\tilde{u}_{j,k} = \mathbf{e}_j^T \tilde{\mathbf{u}}_k \forall j \in \mathbb{N}^{n_u}$, similarly to Equation (4.16) (see (*), p. 38). However, in contrast to the thermal comfort requirements, the input constraints cannot just be violated, since they represent restrictive technical system limits. Hence, to closely resemble the hard constraints, small values need to be assigned to $\epsilon_{\mathbf{u}_k}$, so that the original requirements are met

with a high probability⁶ [79,92]. Because of the structure of \mathbf{T}_u , the reformulation of the input constraints has nevertheless no impact on the constraints imposed for the first time step, which still remain hard constraints. As such, when implementing the MPC in closed-loop, the technical system limits will never be actually violated [92].

The introduction of ADF requires a slight adaptation to the structure of the latent variable $\tilde{\mathbf{p}}$. To allow for a proper reaction against the uncertainty realizations in Equation (4.17) via the feedback gain matrix \mathbf{T}_u , it should be made explicit that the model uncertainties persist, and thus reoccur every single time step. Hence, they should be repeated in $\tilde{\mathbf{p}}$, $\tilde{\mathbf{p}}$ and Σ_p ⁷.

This adaptation leads to the covariance matrix presented by Equation (4.18). Note that the covariance of the state space matrices $\tilde{\mathbf{A}}$, $\tilde{\mathbf{B}}$ and $\tilde{\mathbf{E}}$ on the one hand, and of the disturbances $\{\mathbf{d}_k\}_{k=0\dots K}$ on the other hand, are grouped into a larger covariance matrix, to account for possible correlations between their elements.

$$\Sigma_p = \left[\begin{array}{cccc|c} \Sigma_{\mathbf{A},\mathbf{B},\mathbf{E}} & \mathbf{0} & \cdots & \mathbf{0} & \\ \mathbf{0} & \Sigma_{\mathbf{A},\mathbf{B},\mathbf{E}} & \cdots & \mathbf{0} & \\ \vdots & \vdots & \ddots & \vdots & \\ \mathbf{0} & \mathbf{0} & \cdots & \Sigma_{\mathbf{A},\mathbf{B},\mathbf{E}} & \\ \hline & \mathbf{0} & & & \Sigma_{\{\mathbf{d}_k\}_{k=0\dots K}} \end{array} \right] \quad (4.18)$$

The structure of the associated feedback gain matrix \mathbf{T}_u , consisting of two strictly lower block triangular matrices, is represented by Equation (4.19); here, the dots • indicate the non-zero sub-matrices.

$$\mathbf{T}_u = \left[\begin{array}{cccc|cccc} \mathbf{0} & \mathbf{0} & \cdots & \mathbf{0} & \mathbf{0} & \mathbf{0} & \cdots & \mathbf{0} \\ \bullet & \mathbf{0} & \cdots & \mathbf{0} & \bullet & \mathbf{0} & \cdots & \mathbf{0} \\ \vdots & \vdots & \ddots & \vdots & \vdots & \vdots & \ddots & \vdots \\ \bullet & \cdots & \bullet & \mathbf{0} & \bullet & \cdots & \bullet & \mathbf{0} \end{array} \right] \quad (4.19)$$

It should be stressed that the dimension of $\tilde{\mathbf{p}}$ has a large impact on the number of optimization variables (mainly via \mathbf{T}_u and $\Sigma_{\mathbf{x}_k}^r$). Hence, the repetition of the parametric uncertainty for each time step can easily blow up the problem size, especially for systems with large time constants, such as buildings, requiring a sufficiently long prediction horizon (see also Section 6.3.2). One possible way to reduce the computation time, is by restricting the optimizable degrees of freedom of the feedback gain matrix, or by rather relying upon pre-computed matrices, as is for example done in [44,92,99]; this is nevertheless not considered in this work.

⁶ Throughout this dissertation, ϵ_{u_k} is consistently equal to 0.999.

⁷ Be aware that an adaptation of the structure of $\tilde{\mathbf{p}}$ also affects the associated selection matrices.

Finally, since the inputs \mathbf{u}_k are no longer considered in their deterministic form, the previously derived formulation for the covariance of the states, as presented by Equation (4.12), needs to be altered using Equation (4.17), leading to

$$\begin{aligned} \Sigma_{\mathbf{x}_{k+1}}^r &= (\bar{\mathbf{x}}_k^T \otimes \mathbf{I}_{n_x}) \Sigma_{\mathbf{A}}^r + \bar{\mathbf{A}} \Sigma_{\mathbf{x}_k}^r + (\bar{\mathbf{u}}_k^T \otimes \mathbf{I}_{n_x}) \Sigma_{\mathbf{B}}^r + \bar{\mathbf{B}} \Sigma_{\mathbf{u}_k}^r + \\ &(\bar{\mathbf{d}}_k^T \otimes \mathbf{I}_{n_x}) \Sigma_{\mathbf{E}}^r + \bar{\mathbf{E}} \Sigma_{\mathbf{d}_k}^r. \end{aligned} \quad (4.20)$$

4.5 Resulting stochastic OCP formulation

Combining all previously introduced steps, the following stochastic OCP formulation, explicitly accounting for both additive and parametric uncertainties, is obtained.

$$\min_{\times} \phi(\times) \quad (4.21a)$$

with

$$\begin{aligned} \times &= \{ \{ \bar{\mathbf{x}}_k \}_{k=0 \dots K+1}, \{ \Sigma_{\mathbf{x}_k}^r \}_{k=0 \dots K+1}, \{ \mathbf{q}_k \}_{k=0 \dots K+1}, \{ \mathbf{s}_k \}_{k=0 \dots K+1} \\ &\{ \bar{\mathbf{u}}_k \}_{k=0 \dots K}, \mathbf{T}_{\mathbf{u}}, \{ \mathbf{r}_k \}_{k=0 \dots K} \} \end{aligned} \quad (4.21b)$$

subject to

$$\bar{\mathbf{x}}_{k+1} = \bar{\mathbf{A}} \bar{\mathbf{x}}_k + \bar{\mathbf{B}} \bar{\mathbf{u}}_k + \bar{\mathbf{E}} \bar{\mathbf{d}}_k \quad \forall k \quad (4.21c)$$

$$\begin{aligned} \Sigma_{\mathbf{x}_{k+1}}^r &= (\bar{\mathbf{x}}_k^T \otimes \mathbf{I}_{n_x}) \Sigma_{\mathbf{A}}^r + \bar{\mathbf{A}} \Sigma_{\mathbf{x}_k}^r + \\ &(\bar{\mathbf{u}}_k^T \otimes \mathbf{I}_{n_x}) \Sigma_{\mathbf{B}}^r + \bar{\mathbf{B}} \Sigma_{\mathbf{u}_k}^r + \\ &(\bar{\mathbf{d}}_k^T \otimes \mathbf{I}_{n_x}) \Sigma_{\mathbf{E}}^r + \bar{\mathbf{E}} \Sigma_{\mathbf{d}_k}^r \quad \forall k \end{aligned} \quad (4.21d)$$

$$\bar{x}_{i,k} + s_{i,k} \geq x_{i,k}^{min} + \Phi^{-1}(1 - \epsilon_{x_{i,k}}) q_{i,k} \quad \forall i, k \quad (4.21e)$$

$$\bar{x}_{i,k} - s_{i,k} \leq x_{i,k}^{max} - \Phi^{-1}(1 - \epsilon_{x_{i,k}}) q_{i,k} \quad \forall i, k \quad (4.21f)$$

$$q_{i,k} \geq \|\Sigma_{x_{i,k}}^r\|_2 \quad \forall i, k \quad (4.21g)$$

$$s_{i,k} \geq 0 \quad \forall i, k \quad (4.21h)$$

$$\bar{u}_{j,k} \geq \mathbf{0}_{n_u} + \Phi^{-1}(1 - \epsilon_{u_{j,k}}) r_{j,k} \quad \forall j, k \quad (*) \quad (4.21i)$$

$$\bar{u}_{j,k} \leq u_{j,k}^{max} - \Phi^{-1}(1 - \epsilon_{u_{j,k}}) r_{j,k} \quad \forall j, k \quad (*) \quad (4.21j)$$

$$r_{j,k} \geq \|\Sigma_{u_{j,k}}^r\|_2 \quad \forall j, k \quad (4.21k)$$

$$\Sigma_{\mathbf{u}}^r = \mathbf{T}_{\mathbf{u}} \Sigma_{\mathbf{p}}^r \quad (4.21l)$$

$$\mathbf{x}(0) = \mathbf{x}_0 \quad (4.21m)$$

$$\mathbf{u}(0) = \mathbf{u}_0 \quad (4.21n)$$

Since only linear constraints and second order cone constraints are added compared to the convex, deterministic OCP (2.1), the derived stochastic OCP (4.21) remains convex if $\phi(\mathbf{x})$ is convex in \mathbf{x} .

4.6 Conclusion

In this chapter, a convex stochastic open-loop OCP formulation is derived for building climate control and DR under combined additive (disturbance forecast) and parametric (model) uncertainty, tailored to the class of systems represented by a linear time-invariant state space model.

The derivation takes the conventional deterministic formulation, as presented in Chapter 2, as a starting point, and is performed in a systematic way, by successively introducing the uncertainties in all relevant parts of the optimal control problem. The derived stochastic OCP formulation is obtained in a convex form by applying following manipulations: i) the introduction of the latent variable $\tilde{\mathbf{p}}$, aggregating all uncertainties, ii) the switch to a root form notation, iii) the introduction of chance constraints, and, iv) the implementation of affine disturbance feedback, and with the help of following assumptions: i) the original deterministic OCP formulation is convex, ii) the products of stochastic variables are neglected, and, iii) the chance constraints are reformulated for every distinct state and input based on its marginal distribution, which is assumed to be normal.

The derivation of the stochastic OCP formulation constitutes the first part of the SMPC development. In a next step, the mathematical description of all relevant additive and parametric uncertainties in terms of their mean and covariance needs to be further specified, which is the focus of the next chapter.

Chapter 5

Uncertainty characterization

RQ 2: How can all relevant uncertainties affecting the building indoor climate be appropriately mathematically modeled in order to include them in the stochastic OCP formulation?

This chapter is based on A. Uytterhoeven, I. De Jaeger, K. Bruninx, D. Saelens, and L. Helsen, “Data-driven estimation of parametric uncertainty of reduced order RC models for building climate control,” in Proceedings of the Building Simulation (BS) Conference 2021, Bruges, Belgium, International Building Performance Association (IBPSA), 2021, and, A. Uytterhoeven, R. Van Rompaey, K. Bruninx, and L. Helsen, “Chance Constrained Stochastic MPC for Building Climate Control Under Combined Parametric and Additive Uncertainty,” submitted to Journal of Building Performance Simulation, July 2021.

The mathematical model of the uncertainties is an essential part of the stochastic OCP formulation derived in Chapter 4. This chapter further elaborates on how the different stochastic quantities $\tilde{\mathbf{A}}$, $\tilde{\mathbf{B}}$, $\tilde{\mathbf{E}}$ and $\tilde{\mathbf{d}}_k$ can be properly represented by their mean and covariance, delineating the underlying probability density functions.

Regarding the parametric uncertainty, this chapter aims to come up with a substantiated uncertainty characterization without relying upon detailed building-specific information or experts' knowledge, to acknowledge the plausibility of a lack of information in case of a widespread MPC implementation. Since this point of view is fundamentally different from what is commonly done, the currently prevailing uncertainty characterization methods first need to be revisited, before deriving

a suitable characterization of $\tilde{\mathbf{A}}, \tilde{\mathbf{B}}, \tilde{\mathbf{E}}$. Hence, the contribution of this chapter regarding the parametric uncertainty not only lies in the obtained uncertainty model, but also in the proposed uncertainty characterization method.

In contrast, regarding the additive uncertainties, there is clear consensus on how to mathematically represent them. However, although most works provide a clear description regarding the applied uncertainty characterization method, they rarely disseminate the resulting uncertainty model in terms of numerical values. Hence, regarding the additive uncertainties, the focus of this chapter is mostly on determining and disseminating - to the best extent possible - the mean and covariance of $\tilde{\mathbf{d}}_k$ ¹, by applying the methods from literature.

Since the exact controller model structure determines which specific form $\tilde{\mathbf{A}}, \tilde{\mathbf{B}}, \tilde{\mathbf{E}}$ and $\tilde{\mathbf{d}}_k$ take, the considered model structure is first presented in Section 5.1. Next, an uncertainty characterization method is presented for each of the considered uncertainties, which is subsequently applied to a case study in order to give insight in the resulting uncertainty model. Section 5.2 focuses on the uncertainty characterization of the building model parameters, whereas Section 5.3 and Section 5.4 focus on the uncertainty characterization of the forecasts of the disturbances, being the weather and occupant behavior. Finally, the most important findings are summarized in Section 5.5.

5.1 System model specification

Before proceeding with the uncertainty characterization, this section first specifies the building model structure, and hence, the form of $\tilde{\mathbf{A}}, \tilde{\mathbf{B}}, \tilde{\mathbf{E}}$ and $\tilde{\mathbf{d}}_k$, that will be considered throughout this dissertation. Due to the fact that the mathematical complexity (i.e., the number of optimization variables and constraints) of the stochastic OCP formulation (4.21) highly depends on the order of the building controller model, because of the repetition of the parametric uncertainty in the latent variable $\tilde{\mathbf{p}}$ (see Equation (4.18)), a reduced order model of sufficiently low order is preferred.

Model orders as low as two or three are shown to be sufficient to adequately represent the general thermal dynamics of buildings [14, 126, 127, 128, 129]. In this work, based on the findings of Reynders et al. [126, 130], a building model of

¹ Note that it is also possible to incorporate more advanced stochastic forecasting (grey-box) models for the disturbances in the MPC framework, as is for example done by Thilker et al. [124, 125]; this is nevertheless not further considered in this dissertation.

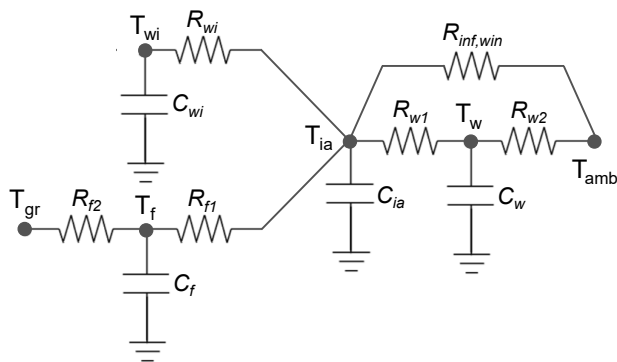


Figure 5.1: The model structure of the studied reduced order one-zone four-states resistance-capacitance model, representing a residential dwelling. Note that the shown RC model merely focuses on the representation of the building envelope, without specifying the installed emission system; also the heat inputs coming from the solar heat gains and the internal heat gains, are not indicated. Adapted from [130].

order four is used^{2,3}, which is shown in Figure 5.1. This resistance-capacitance (RC) model uses an electric circuit analogy to represent a residential dwelling. It serves as a good compromise between complexity and interpretability, since it is of sufficiently low order, but still distinguishes between all fundamentally different construction elements and boundary conditions⁴.

The model approximates the building as one thermal zone, represented by four states, being the temperatures of the indoor air (T_{ia}), external walls (T_{wi}), internal walls (T_w) and floor (T_f). The associated thermal capacitances and resistances (same indices as the states) are shown in Figure 5.1. The windows are not represented by an individual state, because of their negligible thermal mass compared to the massive building structure; as such, the resistance $R_{inf,win}$ not only refers to the heat losses via infiltration/ventilation, but also to the transmission losses via the windows and

² Throughout this work, the building model parameters are theoretically calculated. Hence, the building model should be interpreted as a highly simplified white-box model. Nevertheless, the optimal model structure was determined by Reynders et al. [126] via a grey-box modeling approach.

³ A similar analysis regarding the building model parametric uncertainty was performed using an analogous but slightly more complex two-zones building model. The results of this analysis can be found in Appendix A.

⁴ The difference in occupation (and hence, thermal comfort requirements) between the day and night zone, and the associated difference in utilization of the thermal mass between the two zones, is nevertheless discarded by the one-zone model, possibly leading to an overestimation of the effective thermal capacity.

doors. The heat emission system that is incorporated in the building can be either an underfloor heating system or a low-temperature radiator system, and is assumed to be ideal, with a 100% efficiency. In case the installed heat emission system is a low-temperature radiator system, an additional state is considered (T_{rad})⁵. The heat input delivered to the heat emission system is coming from a single heat supply system⁶, \dot{Q}_{sup} , and is assumed to be a heat pump in this work. The system is subject to seven disturbances, being the ambient temperature T_{amb} , the ground temperature T_{gr} , the solar irradiance on the vertical planes along the four cardinal directions \dot{Q}_{solN} , \dot{Q}_{solE} , \dot{Q}_{solS} and \dot{Q}_{solW} , and the internal heat gains from the occupants \dot{Q}_{int} . The solar heat gains are distributed over the capacitances of the different states in proportion to their surface area, relative to the total surface area of all building construction elements, by using distribution coefficients. The fraction of the solar heat gains associated with the windows is assigned to the internal air capacitance. For the internal heat gains, on the other hand, a distinction is made between the convective fraction, which is allocated to the internal air capacitance, and the radiative fraction, which is allocated to the capacitances of the different states by using area weighted distribution coefficients (similarly to the solar heat gains) [126, 132].

Summarizing, $\tilde{\mathbf{x}}_k$, $\tilde{\mathbf{u}}_k$ and $\tilde{\mathbf{d}}_k$ take the form as expressed by Equation (5.1) in this work. The state space matrices $\tilde{\mathbf{A}}$, $\tilde{\mathbf{B}}$, and $\tilde{\mathbf{E}}$ are defined as in Figure 5.1, constituting a linear(ized) model. Depending on the installed heat emission system, they take a different form, to correctly represent all heat exchanges.

$$\tilde{\mathbf{x}}_{k+1} = \tilde{\mathbf{A}} \tilde{\mathbf{x}}_k + \tilde{\mathbf{B}} \tilde{\mathbf{u}}_k + \tilde{\mathbf{E}} \tilde{\mathbf{d}}_k \quad \forall k$$

$$\text{with } \tilde{\mathbf{x}}_k = \begin{bmatrix} \tilde{T}_{ia,k} \\ \tilde{T}_w,k \\ \tilde{T}_{wi,k} \\ \tilde{T}_f,k \\ (\tilde{T}_{rad,k}) \end{bmatrix}, \quad \tilde{\mathbf{u}}_k = [\tilde{Q}_{sup,k}], \quad \tilde{\mathbf{d}}_k = \begin{bmatrix} \tilde{T}_{amb,k} \\ \tilde{T}_{gr,k} \\ \tilde{Q}_{solN,k} \\ \tilde{Q}_{solE,k} \\ \tilde{Q}_{solS,k} \\ \tilde{Q}_{solW,k} \\ \tilde{Q}_{int,k} \end{bmatrix} \quad (5.1)$$

⁵ The consideration of a radiator as heat emission system requires an additional (linearized) heat balance, supplementing the SSM: $C_{rad} \frac{T_{rad,k+1} - T_{rad,k}}{\Delta t} = \dot{Q}_{sup,k} - UA_{rad}(T_{rad,k} - T_{ia,k}) \quad \forall k$. Here, C_{rad} represents the thermal capacitance of the radiator, determined by the combined thermal capacitance of its dry mass and water content; UA_{rad} represents the overall heat transfer coefficient, obtained by linearizing the radiator formula around the design supply temperature [131].

⁶ Since only one heat input is considered, the index j is omitted from now on.

As a final important remark, it should be highlighted that the radiative temperatures of the surrounding building components are not explicitly considered in the chosen building model. Consequently, thermal comfort is assessed based on the indoor air temperature (i.e., the state associated with the air thermal capacitance of the building model) in this work, instead of on the operative temperature (which is typically used in comfort standards [83]). The implications of this point of view will be further discussed in Intermezzo 6.1.

5.2 Building model parameter uncertainty

This section focuses on the uncertainty characterization of the building model parameters. After some background discussed in Section 5.2.1, Section 5.2.2 describes the applied modeling approach. Next, Section 5.2.3 presents the resulting uncertainty characterization. Here, nine existing buildings are presented as case studies for which the parametric uncertainty is determined and compared.

5.2.1 Background

The uncertainty characterization of the parameters of the building model $\tilde{\mathbf{A}}$, $\tilde{\mathbf{B}}$ and $\tilde{\mathbf{E}}$ depends on the pursued modeling method, and the stance taken on the available information. The values of the building model parameters can either be obtained via a physics-based [129, 132, 133] or via a data-driven [124, 126, 127, 132] approach. In order to include domain knowledge and thus maximize insight, this work adopts a physics-based approach, that links the stochasticity of the parameters of a reduced order white-box model to the underlying uncertainty of the physical properties. It should be stressed that this choice does not detract from the more general applicability of the proposed stochastic OCP formulation. Indeed, also data-driven modeling approaches, such as grey-box modeling, result in uncertain parameter estimations⁷ [124, 134], that can be characterized by a covariance matrix [124, 135], and as such, can be directly incorporated in the proposed SMPC approach.

The stochasticity of the parameters of a physics-based building controller model is caused by a lack of knowledge about the building envelope. Since the building geometry and construction year can often be derived from the building

⁷ In case of a data-driven modeling approach, the uncertainty of the parameter estimation process emerges from the non-smoothness of the objective function expressing the difference between the measured (actual) and calculated (modeled) system behavior, due to unavoidable fluctuations and noise in the measurement data. This non-smoothness can lead to many local minima, making the search for the most optimal estimate of the model parameters very difficult, and possibly resulting in large confidence intervals for the individual estimated parameters [134].

address based on geographic information systems data and cadastral data, the uncertainties can be mainly attributed to the building thermal properties [63]. This uncertainty has already been addressed in several studies, where the uncertainty characterization is typically derived based on detailed (mostly building-specific) information and/or experts' knowledge [54,60,136]. However, in case of a widespread MPC implementation, a lack of detailed and accurate input data is plausible, especially if also the older, existing building stock is involved. In this case, one needs to rely upon sparse, publicly available data (i.e., construction year, building location and building geometry) to characterize the building envelope, and subsequently construct the building controller model. This fundamentally different point of view requires a revisitation of the prevailing uncertainty characterizations. This was done by De Jaeger et al. [62,63], who recently developed a statistical, data-driven building characterization method that leverages governmental databases of the energy performance of buildings to obtain probability distributions, as well as correlated samples, of the U-values of the ground floor, external walls, windows and roof and of the window-to-wall ratio (WWR) for a particular dwelling. As such, a building can be statistically characterized without intensive on-site data collection. Building further upon that work, a substantiated estimate of the parametric uncertainty of a theoretical physics-based building controller model can be derived, which is the focus of the remainder of this section. Since neither detailed building-specific information on the thermal properties, nor experts' knowledge is incorporated, the obtained uncertainty characterization can be seen as a worst-case appraisal. Note that the obtained uncertainty characterization can be further improved by using it as a starting point for local learning approaches. However, this is not further considered in this dissertation.

5.2.2 Modeling approach

To be able to characterize the building model parametric uncertainty, the publicly available information (i.e., construction year, building location and building geometry) needs to be transformed into a (probabilistic) building controller model. This can be achieved via the procedure explained below, which is summarized in Figure 5.2.

Step 1: Extracting building thermal quality data

Based on the building location, geometry and construction year (where the latter two characteristics can be derived from the building address based on geospatial and cadastral data), information on the building thermal properties can be obtained with the help of the probabilistic building envelope characterization method developed

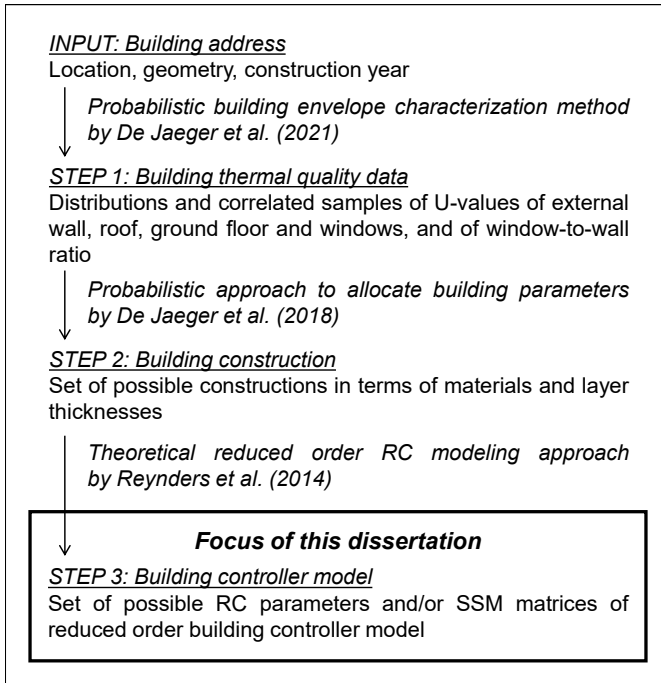


Figure 5.2: The pursued methodology to come up with the uncertainty characterization of the building model parameters, starting from publicly available data.

by De Jaeger et al. [63]. This method generates distributions of the U-values of the external walls, roof, ground floor and windows, as well as of the WWR, by applying a quantile regression method on the Flemish energy performance certificates database, which contains building envelope thermal quality data of Flemish single-family dwellings. The correlations between the different variables are included by building multivariate distributions from the distinct marginal distributions, and by subsequently drawing correlated samples of the U-values and WWR on building level. These correlated samples can be seen as possible realizations of a specific dwelling with a fixed location, geometry and age.

Since advanced control strategies for building climate control and DR are mostly focusing on heat pump systems, only the realizations with a sufficiently low nominal heat demand⁸ are considered (i.e., $\dot{Q}_{nom} \lesssim 15 \text{ kW}$), restricting the considered domain of the obtained distributions.

⁸ The nominal heat demand is quantified following NBN EN 12831 [137].

Step 2: Converting building thermal quality data to building construction

In order to be able to derive a building controller model, the obtained U-values and WWR need to be converted to material layers composing the building envelope. Following the methodology of De Jaeger et al. [62], we derive the building construction, in terms of materials and layer thicknesses, by gradually adjusting an initial (heavy-weight) construction, representative for Flemish buildings, with predefined upgrades until the targeted U-values are reached. More specifically, for the roof and for the ground floor, these adjustments imply gradually adding insulation. For the wall, first, the thickness of the heavy masonry composing the internal walls is increased up to a maximum value, after which a non-ventilated air cavity is provided between the internal and external walls; finally, if needed, an insulation layer with appropriate thickness is added between the internal walls and the air cavity. For the windows, the most appropriate glazing out of a list of discrete options is chosen.

This conversion process is repeated for all correlated samples spanning the domain of the distribution of the U-values and WWR obtained in the previous step, leading to a set of possible constructions for a dwelling with a fixed location, geometry and age.

Step 3: Converting building construction to building controller model

The building controller model can be obtained based on the specified construction, by using a theoretical, physics-based modeling approach. In this work, the approach of Reynders et al. [132] is used, resulting in a reduced order RC model, with a model structure as shown in Figure 5.1. This building controller model can be either directly characterized in terms of the RC parameters, or in terms of the (discretized) SSM matrices derived therefrom.

Note that, for the sake of simplicity, without loss of generality, the determination of the RC parameters merely focuses on the RC parameters related to the building construction, making abstraction of the installed heat emission system.

Building controller model in terms of RC parameters

The building model RC parameters are related to the building construction as follows. The thermal capacitances, representing the active thermal mass, are determined by the material layers within the insulation barrier. In line with this, the thermal resistances of the external walls and ground floor are split in two components: an internal resistance (index 1, see also Figure 5.1) up to, but excluding, the insulation layer, and an external resistance (index 2, see also Figure 5.1). For the

Table 5.1: The dependency of the RC parameters of the studied building controller model on the probabilistic U-values and WWR, illustrating their stochastic character.

| | $R_{\text{int,win}}$ | $R_{\text{w}(1/2)}$ | R_{wi} | $R_{\text{f}(1/2)}$ | C_{w} | C_{wi} | C_{f} | C_{ia} |
|-----------------------------|----------------------|---------------------|-----------------|---------------------|----------------|-----------------|----------------|-----------------|
| $U_{\text{external walls}}$ | | x | | | x | | | |
| $U_{\text{ground floor}}$ | | | | x | | | | |
| U_{roof} | | x | | | x | | | |
| U_{windows} | x | | | | | | | |
| WWR | x | x | | | x | | | |

internal walls, the thermal resistance is taken equal to 50% of the total resistance of the wall, since the thermal mass is equally accessible from both sides. The heat capacitance of the internal air is determined as the product of the specific heat capacity of the air at constant pressure, the density of the indoor air and the air volume, multiplied by a correction factor (set equal to five [138]) to account for the additional furniture thermal capacitance. Finally, the UA-values of the windows and doors are combined with the ventilation and infiltration losses to represent an additional thermal resistance [132].

By repeating the model identification for the whole set of possible constructions obtained in the previous step, the resulting set of RC parameters may be interpreted as a statistical characterization of the building controller model.

To summarize the whole conversion process, Table 5.1 clarifies the relation between the probabilistic U-values and WWR characterizing the building envelope, and the RC parameters of the building controller model, illustrating the probabilistic character of the latter. Logically, only the RC parameters related to the building exterior are affected by the uncertainty on the building thermal quality.

Building controller model in terms of SSM elements

Finally, the obtained correlated samples and probability distributions of the RC parameters, representing all possible dwelling realizations, still need to be converted into a statistical description of the discrete-time⁹ state space matrices $\tilde{\mathbf{A}}$, $\tilde{\mathbf{B}}$ and $\tilde{\mathbf{E}}$, in terms of their mean and covariance, in order to incorporate them in the stochastic OCP formulation (4.21). Since the SSM elements $\{a_{i,i'}\}_{i,i'=1\dots n_x}$, $\{b_{i,j}\}_{i=1\dots n_x, j=1\dots n_u}$ and $\{e_{i,h}\}_{i=1\dots n_x, h=1\dots n_d}$, which can be directly derived from the RC parameters by writing down the energy balances

⁹ In this dissertation, a discretization time step of one hour is considered.

in state-space form and subsequently discretizing the obtained SSM matrices, are found to more closely approximate a normal distribution compared to the RC parameters, these SSM elements are used to build up $\bar{\mathbf{p}}$. The covariance $\Sigma_{\mathbf{A},\mathbf{B},\mathbf{E}}$ can be straightforwardly determined by considering all samples of all SSM elements altogether. The mean values $\bar{\mathbf{A}}, \bar{\mathbf{B}}$ and $\bar{\mathbf{E}}$, on the other hand, should not be determined in the conventional way, precisely because of the existing correlation between the different SSM elements (although this is rarely considered in literature [60]). Simply calculating the mean values of the individual distributions of the distinct SSM elements would disregard their correlation, and would result in a wrong representation of the building dynamics when combining the individual mean values into a SSM. To overcome this issue, the average state space matrices $\bar{\mathbf{A}}, \bar{\mathbf{B}}$ and $\bar{\mathbf{E}}$ are replaced by reference state space matrices $\bar{\bar{\mathbf{A}}}, \bar{\bar{\mathbf{B}}}$ and $\bar{\bar{\mathbf{E}}}$, which closely approximate the average model, but also respect the actual dynamics. The reference SSM is determined by selecting the sampled SSM $\mathbf{z}_s \ni \{\mathbf{A}_s, \mathbf{B}_s, \mathbf{E}_s\}$ that has the lowest weighted distance to the average model $\bar{\mathbf{z}}$, where this weighted distance to the mean (WDM) for a particular sample s is defined as

$$WDM_s = (\mathbf{z}_s - \bar{\mathbf{z}})^T \Sigma_{\mathbf{z}}^{-1} (\mathbf{z}_s - \bar{\mathbf{z}}), \quad (5.2a)$$

with

$$\mathbf{z}_s = \begin{bmatrix} \text{vec}(\mathbf{A}_s) \\ \text{vec}(\mathbf{B}_s) \\ \text{vec}(\mathbf{E}_s) \end{bmatrix}, \quad \bar{\mathbf{z}} = \begin{bmatrix} \text{vec}(\bar{\bar{\mathbf{A}}}) \\ \text{vec}(\bar{\bar{\mathbf{B}}}) \\ \text{vec}(\bar{\bar{\mathbf{E}}}) \end{bmatrix}, \quad \Sigma_{\mathbf{z}} = \text{cov}(\bar{\bar{\mathbf{z}}}, \bar{\bar{\mathbf{z}}}). \quad (5.2b)$$

This weighting (via $\Sigma_{\mathbf{z}}^{-1}$) is needed to account for the fact that different state space elements - even within the same state space matrix - can have very different dimensions.

Combining the reference SSM $\bar{\bar{\mathbf{A}}}, \bar{\bar{\mathbf{B}}}$ and $\bar{\bar{\mathbf{E}}}$ with the (actual) covariance $\Sigma_{\mathbf{A},\mathbf{B},\mathbf{E}}$ results in a mathematical description of the stochasticity of the building model parameters that can be implemented in the stochastic OCP formulation. It should be stressed that this combination results in a slightly changed distribution compared to the actual distribution of the different SSM elements. Nevertheless, the impact of this modification is limited, exactly because the distance to the mean is being minimized.

5.2.3 Resulting uncertainty characterization

To give an idea about the order of magnitude of uncertainty on the building thermal properties to be expected when starting from publicly available data, and about how this uncertainty propagates into the building model parameters, a case study

is set up, determining the parametric uncertainty of the building controller model for a set of residential buildings, by applying the methodology described above.

5.2.3.1 Case study

To maximize insight, the statistical characterization of a building controller model is repeated for multiple dwellings for which the main characteristics determining the thermal quality (i.e., geometry and construction year) are sufficiently different. Nine buildings of varying age (old (O) (<1950), ageing (A) (1950-1990) or more recent (R) (>1990)) are selected from the suburban residential areas of the City of Genk in Flanders (Belgium). For each building type (i.e., terraced (T), semi-detached (SD) and detached (D)), three buildings are selected with a varying floor area, ranging from small (S), over midsize (M), to large (L). Their main characteristics are summarized in Table 5.2. As a final remark, it should be noted that all buildings are assumed to have the same air infiltration rate of $0.4 \frac{1}{h}$; this assumption is based on the fact that, in case of renovation, the decrease of infiltration is compensated by the introduction of mechanical ventilation, which is assumed to result in a similar total air change rate.

For each dwelling in Table 5.2, 100 correlated samples of the U-values and WWR are generated¹⁰, leading to 100 possible building controller models per considered dwelling.

5.2.3.2 Results and discussion

In this section, the uncertainty on the building thermal properties, as well as on the derived building model parameters, is determined for the nine dwellings introduced above, starting from publicly available information, by applying the proposed uncertainty characterization method. Since the different uncertain variables have different orders of magnitude, the whole assessment is done in terms of the standardized coefficient of variation (CV)¹¹. Note that we performed a similar analysis regarding the parametric uncertainty in previous work [139] for a slightly more complex two-zones nine-states variant of the model described in Section 5.1. The results of this analysis can be found in Appendix A.

The discussion about the parametric uncertainty primarily focuses on the inverse of the RC parameters, rather than on the RC parameters themselves, or on the

¹⁰ The choice to pursue 100 samples is based on the findings of De Jaeger [60], who showed that a sample size of ~ 60 is advisable to come up with an adequate uncertainty characterization.

¹¹ The coefficient of variation is equal to the ratio of the standard deviation to the mean, and serves as a unit-independent statistical measure of the dispersion of a variable.

Table 5.2: Overview of the main characteristics of the nine dwellings for which the building model parametric uncertainty is investigated. The label refers to the building type, size, and age, and will be used throughout this dissertation.

| Label | Building type [-] | Net floor area [m ²] | Protected volume [m ³] | Ground floor area [m ²] | Façade area [m ²] | Roof area [m ²] | Construction year [-] |
|--------|----------------------|-------------------------------------|---------------------------------------|--|----------------------------------|--------------------------------|--------------------------|
| T_S_O | Terraced (T) | 129 (S) | 406 | 87 | 80 | 95 | <1950 (O) |
| T_M_O | Terraced (T) | 193 (M) | 531 | 97 | 92 | 116 | <1950 (O) |
| T_L_A | Terraced (T) | 244 (L) | 844 | 145 | 116 | 161 | 1950-1990 (A) |
| SD_S_A | Semi-detached (SD) | 155 (S) | 546 | 96 | 171 | 101 | 1950-1990 (A) |
| SD_M_A | Semi-detached (SD) | 210 (M) | 692 | 105 | 140 | 122 | 1950-1990 (A) |
| SD_L_O | Semi-detached (SD) | 275 (L) | 742 | 200 | 226 | 154 | <1950 (O) |
| D_S_A | Detached (D) | 163 (S) | 559 | 94 | 202 | 112 | 1950-1990 (A) |
| D_M_O | Detached (D) | 260 (M) | 716 | 139 | 181 | 187 | <1950 (O) |
| D_L_R | Detached (D) | 301 (L) | 752 | 151 | 167 | 173 | > 1990 (R) |

derived SSM matrices. The reason for this is that the conversion process up to the inverse of the RC parameters is clearly physically interpretable. The last two conversion steps, in contrast, merely entail strict mathematical manipulations (i.e., inversion and discretization), making the subsequent analysis less insightful.

However, one important aspect regarding the SSM matrices that should nevertheless be discussed, is the appropriateness of the assumption of normality. This consideration is important to justify the assumption that the different states and inputs each follow a normal distribution, which is key in the derivation of the stochastic OCP formulation in Chapter 4. Since the sum of independent normal random variables is normally distributed, the distribution of the states (see Equation (4.2)) as well as the distribution of the inputs (see Equation (4.17)) can be assumed normal if the distinct uncertainty contributions are normal. Nevertheless, it should be stressed that the normality of the distinct uncertainty contributions is not required to guarantee the normality of the states and inputs, since also the sum of non-normal random variables can give rise to a normal distribution.

Note furthermore that, for the discussion of (the inverse of) the RC parameters, abstraction can be (and is) made of the installed heat emission system¹². This is nevertheless not possible when investigating the SSM elements, since the A- and B-matrix of the SSM take another form depending on the heat emission system, to correctly represent all heat exchanges.

Uncertainty on the inverse of the RC parameters

Figure 5.3 and 5.4 respectively show the distributions of the U-values and WWR, and the resulting set of RC parameters for the nine considered dwellings. In order not to overload Figure 5.4, only the most important uncertain parameters characterizing the building envelope are shown. To be able to analyze the results, first, a proper understanding of the uncertainty on the building thermal properties is needed, followed by an in-depth assessment of how this uncertainty propagates into the model parameters.

When comparing the thermal properties of the different dwellings, an interesting trend can be observed in Figure 5.3. Because of the imposed cap on the nominal heat demand, the total heat loss coefficient of transmission (i.e., the total sum of the UA-values of the building), presented in the last plot of Figure 5.3, spans approximately the same range for all considered dwellings (although terraced dwellings can have slightly smaller heat losses because of the smaller total loss area). These similar UA-values break down in small buildings with a large range of admissible U-values, or in larger, renovated buildings, for which only the lowest U-values are allowed,

¹²In case of floor heating, the RC model exactly corresponds to the model shown in Figure 5.1, since the floor is an integral part of the building construction. However, in case of radiators, an additional state, and associated RC values, are required, which are for convenience not further discussed.

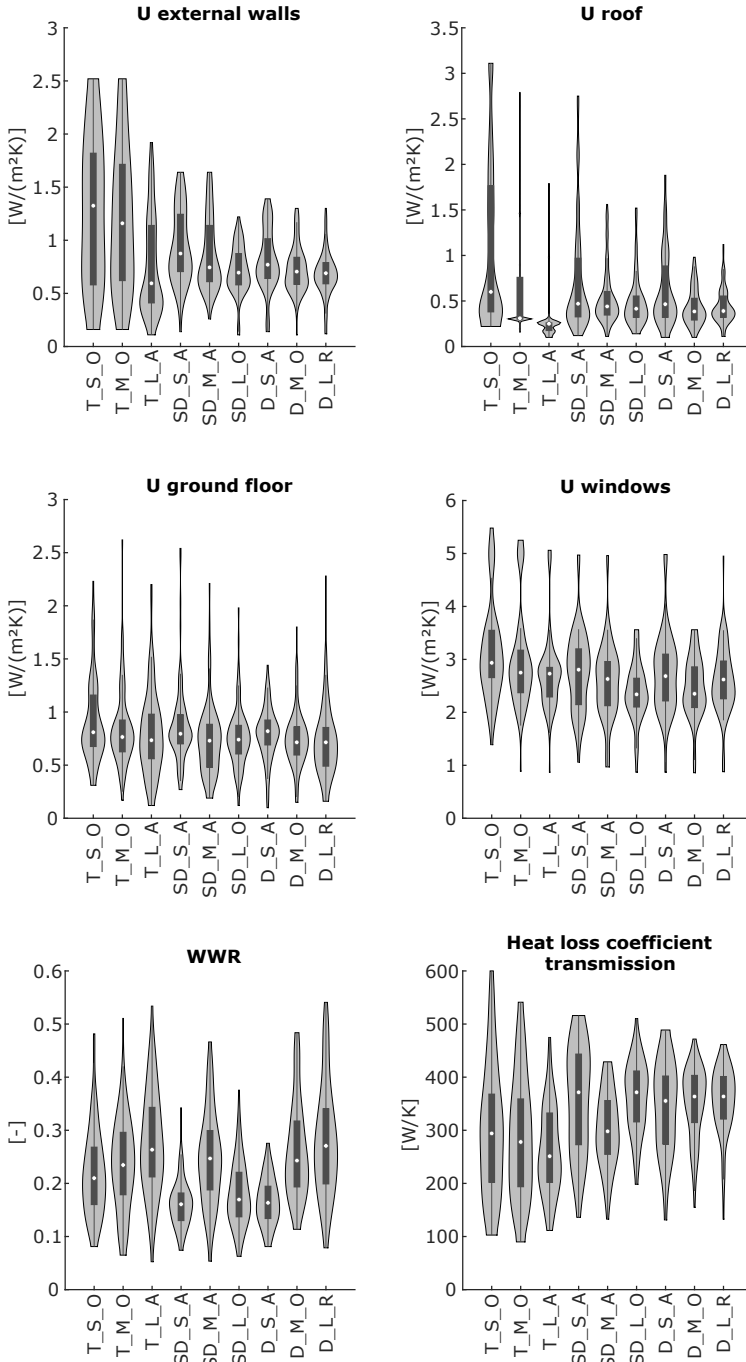


Figure 5.3: The probability distributions of the U-values of the external walls, roof, ground floor and windows, as well as of the window-to-wall ratio and of the heat loss coefficient of transmission for the nine considered dwellings.

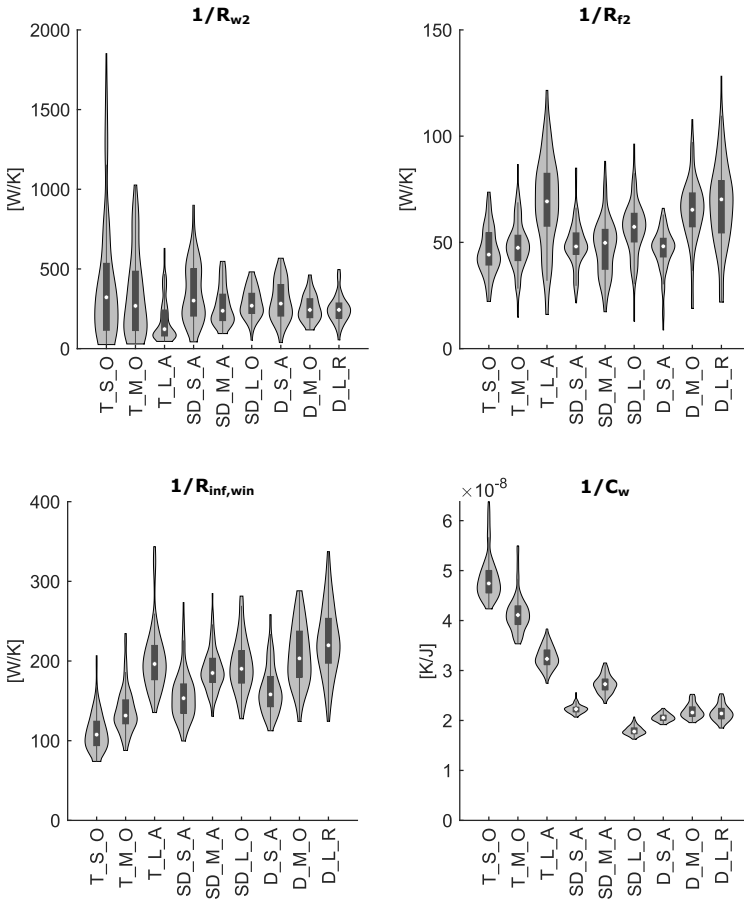


Figure 5.4: The probability distributions of the inverse of the most significant uncertain RC parameters characterizing the building envelope of the nine considered dwellings.

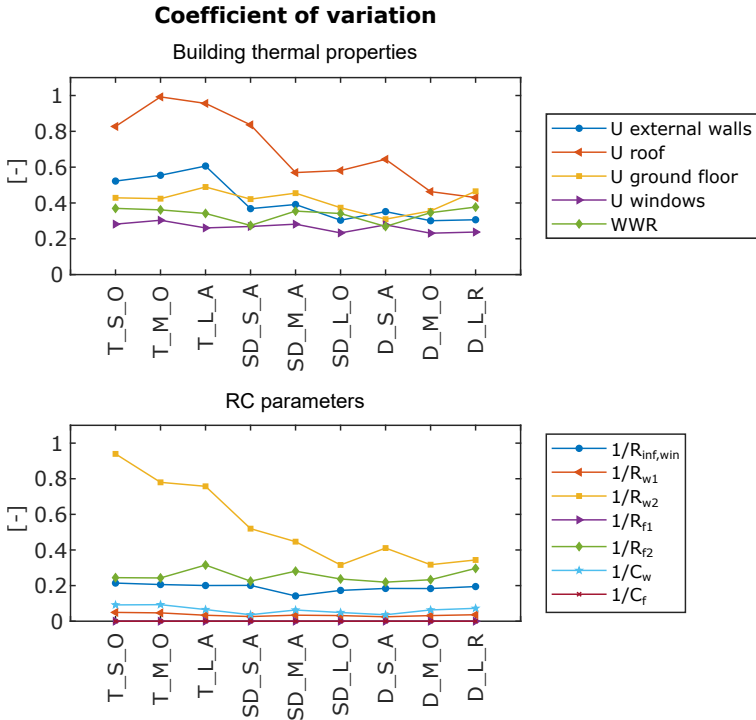


Figure 5.5: The coefficient of variation of the U-values and of (the inverse of) the derived RC parameters for the nine considered dwellings.

as shown in Figure 5.3. Due to this effect, the nine considered dwellings can also be interpreted as nine cases of increasing confidence about the building thermal quality. This is confirmed by Table 5.3 and Figure 5.5. Figure 5.5 clearly shows that this effect predominantly manifests itself for the U-value of the external walls (CV 0.30-0.61) and roof (CV 0.43-0.99). For the U-value of the ground floor (CV 0.31-0.49), the tendency is less clear, since the low probability of invasive floor renovations leads to more similar distributions for all dwellings [60], which is confirmed by Figure 5.3. Also for the windows (CV 0.23-0.30), the difference in uncertainty is less pronounced, since window glazing can only have a limited number of discrete U-value options; the significantly lower absolute value of the CV of the U-value of the window compared to the other U-values, on the other hand, can be explained by the significantly higher average U-value for windows compared to opaque parts.

The lower bounds of the CV ranges for all U-values are of the same order (~ 0.3) as the values reported in literature for older buildings [54], and as such, can be roughly

Table 5.3: The coefficient of variation of the U-values and window-to-wall ratio, the UA-values, and the RC parameters for the nine considered dwellings.

| | U external walls | U roof | U ground floor | U windows | WWR | UA external walls | UA windows | $1/R_{w1}$ | $1/R_{w2}$ | $1/R_{f1}$ | $1/R_{f2}$ | $1/R_{inf,win}$ | $1/C_w$ | $1/C_f$ |
|--------|------------------|--------|----------------|-----------|------|-------------------|------------|------------|------------|------------|------------|-----------------|---------|---------|
| T_S_O | 0.52 | 0.83 | 0.43 | 0.28 | 0.37 | 0.54 | 0.42 | 0.05 | 0.94 | 0.00 | 0.24 | 0.21 | 0.09 | 0.00 |
| T_M_O | 0.55 | 0.99 | 0.42 | 0.30 | 0.36 | 0.57 | 0.43 | 0.05 | 0.78 | 0.00 | 0.24 | 0.21 | 0.09 | 0.00 |
| T_L_A | 0.61 | 0.96 | 0.49 | 0.26 | 0.34 | 0.62 | 0.46 | 0.03 | 0.76 | 0.00 | 0.32 | 0.20 | 0.07 | 0.00 |
| SD_S_A | 0.37 | 0.84 | 0.42 | 0.27 | 0.27 | 0.37 | 0.38 | 0.03 | 0.52 | 0.00 | 0.22 | 0.20 | 0.04 | 0.00 |
| SD_M_A | 0.39 | 0.57 | 0.45 | 0.28 | 0.35 | 0.40 | 0.39 | 0.03 | 0.45 | 0.00 | 0.28 | 0.14 | 0.06 | 0.00 |
| SD_L_O | 0.30 | 0.58 | 0.37 | 0.23 | 0.34 | 0.31 | 0.36 | 0.03 | 0.32 | 0.00 | 0.24 | 0.17 | 0.05 | 0.00 |
| D_S_A | 0.35 | 0.64 | 0.31 | 0.28 | 0.27 | 0.36 | 0.35 | 0.02 | 0.41 | 0.00 | 0.22 | 0.18 | 0.04 | 0.00 |
| D_M_O | 0.30 | 0.46 | 0.36 | 0.23 | 0.35 | 0.31 | 0.35 | 0.03 | 0.32 | 0.00 | 0.23 | 0.18 | 0.06 | 0.00 |
| D_L_R | 0.31 | 0.43 | 0.47 | 0.24 | 0.38 | 0.34 | 0.36 | 0.04 | 0.34 | 0.00 | 0.30 | 0.19 | 0.07 | 0.00 |

considered as expected values of the uncertainty for existing, (partly) renovated, heavy-weight dwellings. It should be stressed that these uncertainty ranges are worst case estimates, since the followed approach relies upon very limited building-specific information.

When converting the U-values of the different construction elements into RC parameters for a particular dwelling, the uncertainty is affected by the different processing operations. First, the uncertainty is altered due to the conversion of U-values into UA-values describing the heat transfer with the surroundings. This operation only has an impact in case of a variable area (i.e., for the external walls and windows due to the variable WWR); otherwise, the mean and standard deviation are simply scaled by the same factor. Next, splitting up the heat transfer in the material layers inside and outside the insulation barrier further impacts the CV. Finally, an inverting operation is needed, since the heat transfer coefficients are related to the inverse of the RC parameters. However, the inverting operation is not considered here, since it results in distorted distributions with increased skewness due to exacerbated outliers, thereby making the analysis more difficult.

For the external walls, the CV of the UA-value is slightly increased compared to the U-value due to the impact of the WWR, resulting in a variation between 0.31 and 0.62 (see Table 5.3). The internal resistance $1/R_{w1}$ and the capacitance $1/C_w$ are hardly impacted by this uncertainty, with a CV in the order of 10^{-2} . This is to be expected, since the large differences in U(A)-values are mainly attributed to different insulation levels of the exterior, whereas the inner parts don't change much when converting U-values to layers and materials with the method of De Jaeger et al. [62]. Hence, the uncertainty is mainly transferred to the external resistance $1/R_{w2}$, as can also clearly be seen in Figure 5.5. For $1/R_{w2}$, the conversion from UA to $1/R$ results in an even higher CV for all nine cases, with values ranging from 0.32 to 0.94. This increase can be (partially) explained by the additional incorporation of the uncertainty of the U-value of the roof in $1/R_{w2}$.

For the ground floor, the uncertainty of the U-values does not affect the internal resistance $1/R_{f1}$ or the capacitance $1/C_f$ ($CV = 0$), since the corresponding material layers, tiles and screed, are fixed. The external resistance $1/R_{f2}$, on the other hand, has a mildly varying CV ranging from 0.22 to 0.32, which is a clear decrease compared to the CV of the U-value.

Finally, for the windows and doors, the CV of the UA-value is increased compared to the U-value due to the varying WWR, resulting in a CV in the range of 0.35 up to 0.46. This uncertainty is then absorbed by the resistance $1/R_{inf,win}$, resulting in a CV between 0.14 and 0.21. This reduction in CV is due to the fact that $R_{inf,win}$ does not only account for transmission losses via windows and doors, but also for infiltration losses, which are assumed to be known.

Summarizing, the uncertainty is predominantly transferred to the external resistances containing the insulation layer; more specifically, for the ground floor and windows, the CV decreases when moving from U to $1/R$, whereas for the external walls and roof, it increases. It should be stressed that the results above depend on i) the underlying input data (being the energy performance data of the Flemish building stock), ii) the subsequent processing (being the methods of De Jaeger et al. [62,63]), and iii) the imposed building model structure (being the single-zone four-states reduced order RC model developed by Reynders et al. [126]). In order to further consolidate the presented results, a more differentiated assessment is recommended, where the uncertainty on the $U(A)$ -values and derived model parameters is further explored for different U -value distributions, and for other building model structures. Nevertheless, the presented analysis offers important insights regarding the order of magnitude of the uncertainty on the building thermal properties to be expected when starting from publicly available information, the impact of increasing confidence about the building thermal quality, and finally, which building model parameters are the most uncertain ones.

Uncertainty on SSM elements

For arguments of interpretability, the discussion about the parametric uncertainty has mainly focused on the inverse of the RC parameters. However, one important aspect that still needs to be discussed, are the distributions of the stochastic discretized SSM elements $\{a_{i,i'}\}_{i,i'=1\dots n_x}$, $\{b_{i,j}\}_{i=1\dots n_x, j=1\dots n_u}$ and $\{e_{i,h}\}_{i=1\dots n_x, h=1\dots n_d}$, derived from the uncertain RC parameters. This consideration is important to assess the validity of assuming a normal distribution for the different states and inputs, imposed in Chapter 4 when analytically reformulating the chance constraints, as already explained above. As can be expected, the SSM elements do not exactly follow a normal distribution. The aim of this discussion is not to prove (quasi-)normality via formal normality tests (such as the Shapiro Wilk test [140, 141]), but rather to illustrate the appropriateness of assuming a normal distribution. To this end, two interesting parameters to consider are the kurtosis and the skewness, which are both descriptive statistics characterizing the shape of a distribution.

Intermezzo 5.1

Kurtosis and skewness as descriptive statistics characterizing the shape of a distribution

The kurtosis is a measure of the extent to which the density of observations of a distribution differs from the probability densities of a normal distribution, or in other words, how outlier-prone a distribution is. For a normal distribution, the kurtosis is equal to three; a kurtosis value larger than three indicates that there are more extreme values than characteristic for a normal curve, and vice versa for a value smaller than three [142, 143]. The kurtosis can be calculated with the help of Equation (5.3a) for (the samples x_i from) a population of a variable x [143].

$$\text{kurtosis} = [\textit{population version}] \quad \frac{\mathbb{E}[(x - \mu)^4]}{\sigma^4} \quad (5.3a)$$

$$[\textit{sample version}] \quad \frac{\frac{1}{N} \sum_{i=1}^N (x_i - \bar{x})^4}{\left(\frac{1}{N} \sum_{i=1}^N (x_i - \bar{x})^2\right)^2} \quad (5.3b)$$

The skewness, on the other hand, is a measure of the asymmetry in a distribution. For a normal distribution, which is perfectly symmetrical, the skewness amounts to zero; a negative skew indicates that the data spread out more to the left of the distribution (i.e., the mean lies to the left of the peak), and vice versa for a positive skew [142]. It can be calculated with the help of Equation (5.4a) for (the samples x_i from) a population of a variable x [144].

$$\text{skewness} = [\textit{population version}] \quad \frac{\mathbb{E}[(x - \mu)^3]}{\sigma^3} \quad (5.4a)$$

$$[\textit{sample version}] \quad \frac{\frac{1}{N} \sum_{i=1}^N (x_i - \bar{x})^3}{\left(\sqrt{\frac{1}{N} \sum_{i=1}^N (x_i - \bar{x})^2}\right)^3} \quad (5.4b)$$

For sufficiently large sample sizes (i.e., $N > 300$), the values of the kurtosis and skewness give a direct indication about the normality of the distribution. As a rule of thumb, absolute kurtosis values larger than seven, and absolute skew values larger than two indicate substantial non-normality; for smaller sample sizes, a z-test is required to accept/reject the null hypothesis of normality [145].

To get a compact overview of the (non-)normality of the distributions of all SSM elements, Figure 5.6 shows the kurtosis and skewness of the distributions of all SSM elements (in one plot per building type) as a function of their CV (each dot represents the distribution of a particular $\{a_{i,i'}\}_{i,i'=1\dots n_x}$, $\{b_{i,j}\}_{i=1\dots n_x, j=1\dots n_u}$ or $\{e_{i,h}\}_{i=1\dots n_x, h=1\dots n_d}$). The reference kurtosis and skewness value of a normal distribution are indicated by the horizontal dotted line. The figure makes a distinction between the case with radiators and with floor heating, since a different SSM is obtained depending on the considered heat emission system (as explained in Section 5.1). The figure confirms that most distributions are not exactly normal, as was to be expected. However, a more detailed inspection of the distinct distributions, as is for example done in Figures 5.7, 5.8 and 5.9 for the terraced, midsize, older (but renovated) (T_M_O) dwelling equipped with floor heating (characterized by the most frequent, large deviations from the kurtosis and skewness values characterizing a normal distribution in Figure 5.6), suggests that the assumption of normality for the states and inputs, based on the observed distributions for the SSM elements, might be reasonable¹³. Figures 5.7, 5.8 and 5.9 show the histograms, fitted normal probability density functions, and shifted normal probability density functions (using the values corresponding to the reference model, rather than the distinct mean values, as the centre of the probability density functions, thereby taking into account the correlation between all different SSM elements of the A-, B- and E-matrix, as explained in Section 5.2.2) of all SSM elements. As can be seen, the normal distribution approximately covers the domain covered by the different model realizations.

¹³ This assumption will be further numerically tested/validated in Chapters 6 and 7.

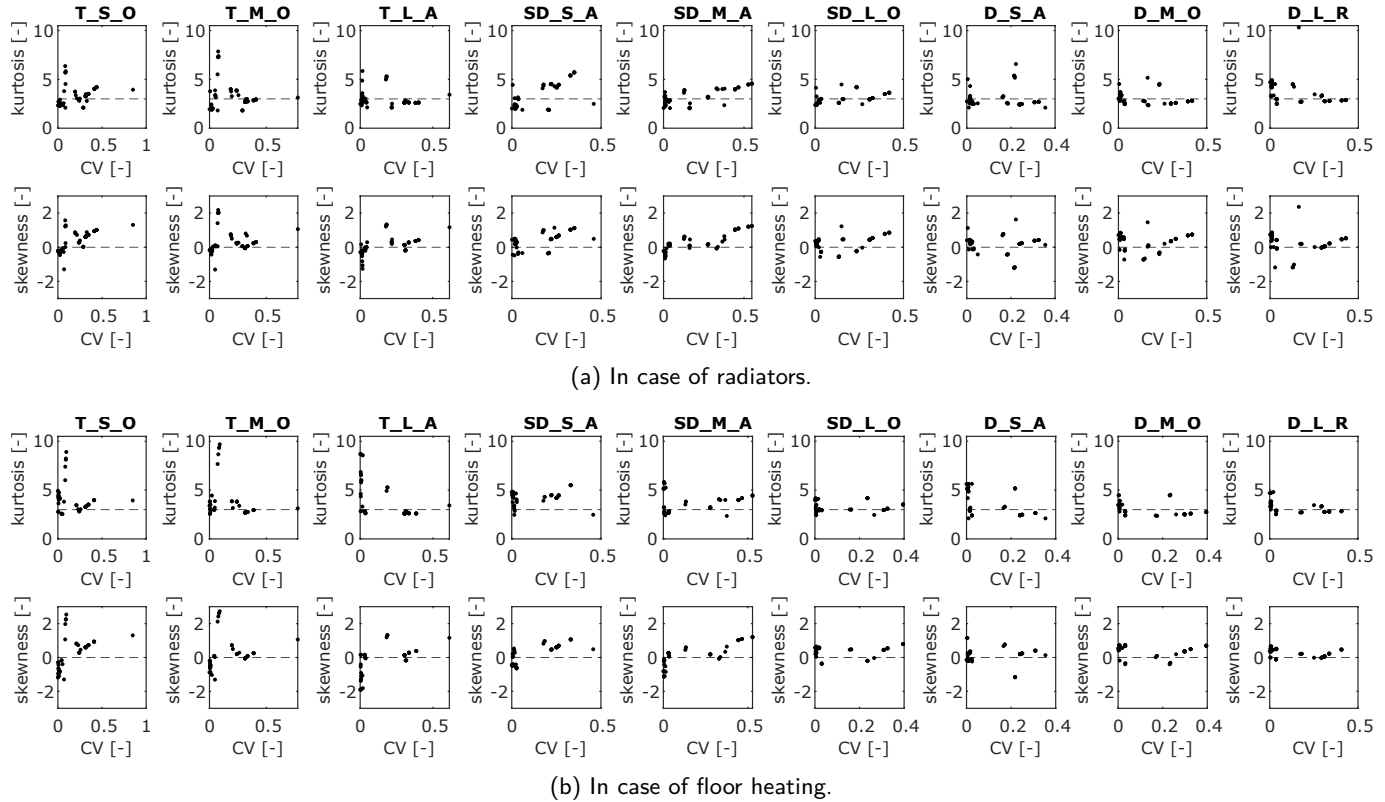


Figure 5.6: The kurtosis and skewness of the distributions of the SSM elements $a_{i,j}$, $b_{i,k}$ and $e_{i,j}$ of the nine considered dwellings, either equipped with radiators or floor heating as heat emission system, as a function of the coefficient of variation. Each dot represents (the kurtosis or skewness of) the distribution of a particular SSM element.

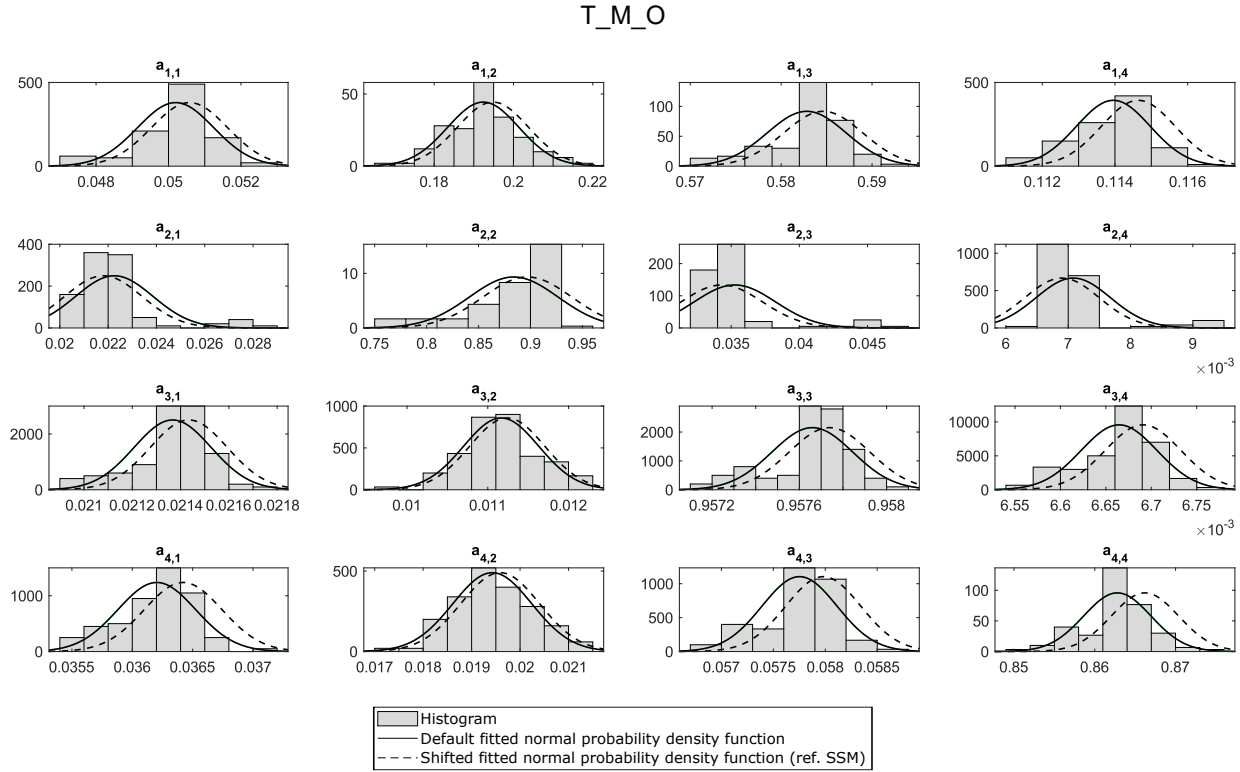


Figure 5.7: The histograms and (default and shifted) fitted normal probability density functions for the SSM elements of the A-matrix of the considered terraced, midsize, older (but renovated) dwelling equipped with floor heating.

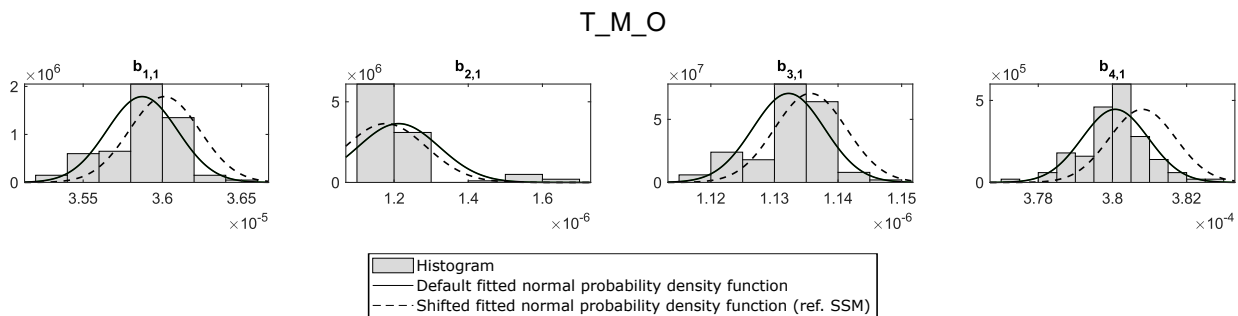


Figure 5.8: The histograms and (default and shifted) fitted normal probability density functions for the SSM elements of the B-matrix of the considered terraced, midsize, older (but renovated) dwelling equipped with floor heating.

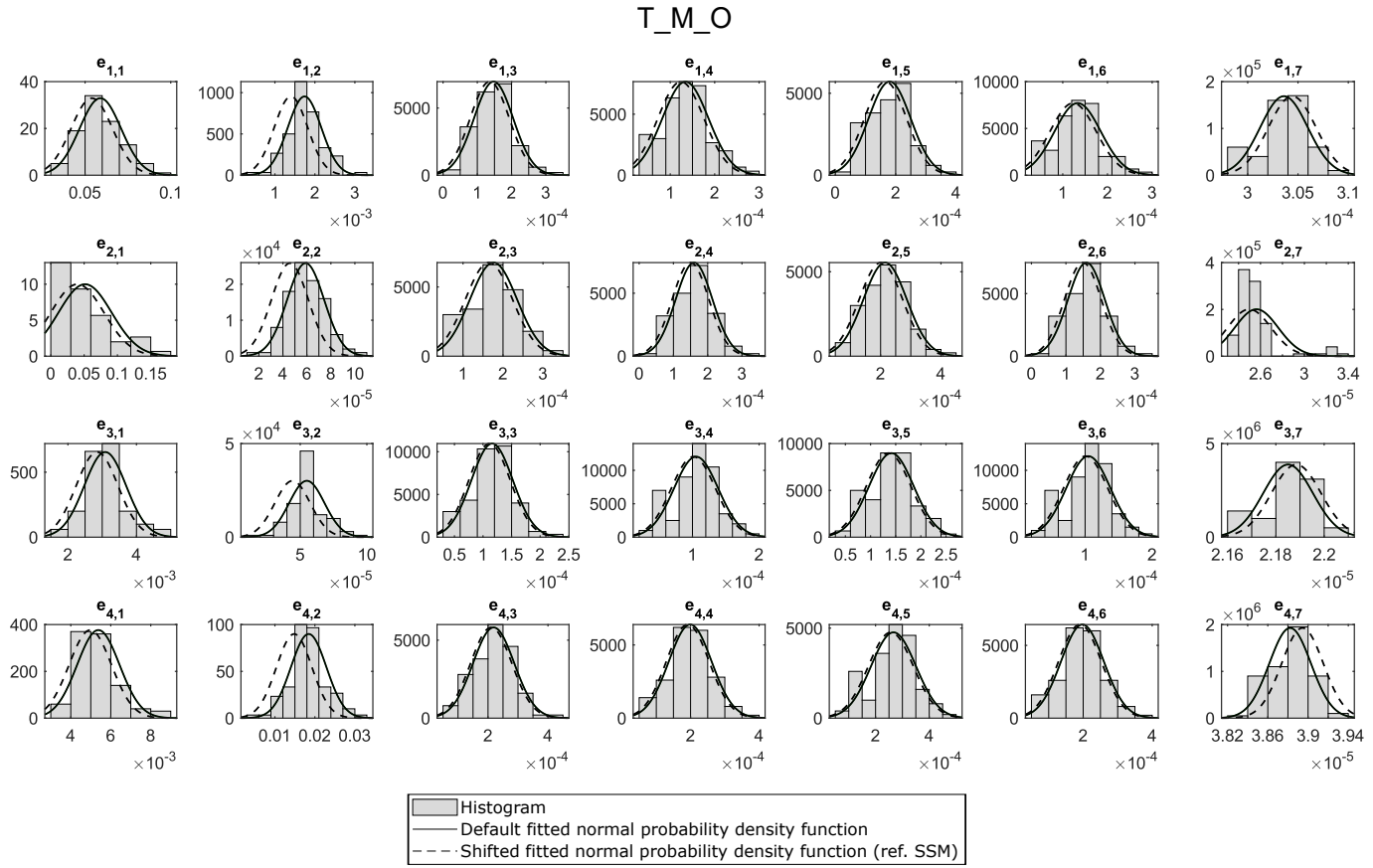


Figure 5.9: The histograms and (default and shifted) fitted normal probability density functions for the SSM elements of the E-matrix of the considered terraced, midsize, older (but renovated) dwelling equipped with floor heating.

Intermezzo 5.2

Preliminary assessment of the impact of the parametric uncertainty on the MPC performance

Building further upon the analysis above, an important additional question to be raised is how big the impact of the parametric uncertainty exactly is. To already get a first indication about this^a, the impact of the obtained variation in building model parameters on the thermal energy demand is investigated via a Monte Carlo analysis. More specifically, an optimal space heating strategy is determined by deterministic optimal control for the complete set of possible building controller models that may be representative for a specific dwelling with a fixed geometry, location and age. The aim is to investigate the variation in overall yearly demand, as well as in dynamic behavior in terms of timing and peak demand.

As an important remark, it should be stressed that this analysis was initially performed for a two-zones nine-states building controller model (see [139] and Appendix A). Since the results for the further reduced one-zone four-states building model derived therefrom would reflect the same general trends, the analysis was not repeated for this simpler model, and the original results for the two-zones nine-states building controller model are discussed here. The most important difference of this model compared to the one-zone four-states model, is the explicit distinction between a day zone (DZ), consisting of all rooms in which the occupants are active during the day, and a night zone (NZ), mainly consisting of the bedrooms.

The formulation of the considered optimal control problem, aiming at guaranteeing thermal comfort at minimal energy use, is equal to the deterministic OCP formulation described in Chapter 2. The considered optimization spans a whole year^b, with an additional week for initialization purposes^c. The time step is equal to one hour. The upper bound for the heat inputs is taken equal to the nominal heat demand of the building; as such, the heating system is assumed to be ideal, with a 100% efficiency and perfect modulation. Perfect predictions of the disturbances are assumed, resulting in a theoretical bound on the performance that any real controller can achieve. The absence of a receding horizon approach with closed-loop disruptions is also why the considered implementation is referred to as optimal control, rather than as MPC. For the weather data (i.e., ambient temperature and solar heat gains), measurement data of the year 2016 of the Vliet test building of the KU Leuven Laboratory of Building Physics, located in Leuven (Belgium), are used. For the occupancy behavior (i.e., internal heat gains and comfort requirements

in terms of setpoint temperatures for different zones), profiles characterizing a four-persons-household are generated with the help of the open web tool StROBe (Stochastic Residential Occupancy Behaviour) of Baetens et al. [146]. The setpoint temperatures are used as a lower thermal comfort bound. The upper thermal comfort bound, on the other hand, is of minor importance, since the controller is compelled to stick to the lower temperature bound as it aims to minimize the energy use.

Figure 5.10 illustrates how the different samples of the detached, midsize, older (but renovated) (D_M_O) dwelling equipped with radiators, arbitrarily chosen as an example out of the nine considered dwellings, result in different energy demand profiles for a particular day (start of January). The different model realizations entail different estimates of the time constants of the building, thereby requiring a different heat supply to the radiator system, both in terms of timing, and in terms of peak demand. The difference in peak demand between the considered 100 possible dwelling realizations exceeds 4 kW for the shown 24h-profile.

The yearly energy use for the 100 dwelling realizations of the D_M_O case ranges from 9757 kWh to 26702 kWh, resulting in a CV of 0.22. For the other considered dwellings equipped with radiators, the CV is higher; their variation in yearly energy use is summarized in Figure 5.11.

The substantial variation in resulting space heating control strategies, both in terms of dynamic effects and total yearly energy use, is a first indication that the obtained uncertainty characterization is not accurate enough to be directly used for deterministic building level control, and that an adapted control strategy explicitly accounting for the uncertainty, and/or additional data acquisition (e.g., via experts or learning) narrowing down the range of feasible model parameters, is indeed needed.

^a A more thorough and complete investigation of the impact of the parametric uncertainty on the MPC performance can be found in Chapter 6.

^b To ensure mathematical tractability, the full-year optimization is performed by considering consecutive weekly optimizations, with a receding horizon of 7 days, and a prediction horizon of 7.5 days (to impede end-of-horizon effects).

^c For the one-week initialization problem, cyclic boundary conditions are imposed.

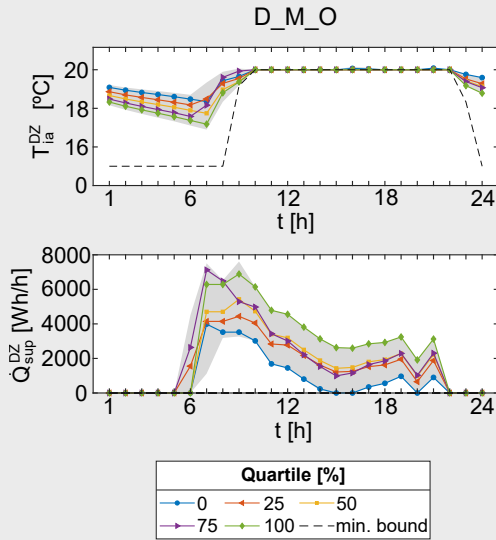


Figure 5.10: 24h-profiles of the indoor temperature T_{fa}^{DZ} and heat input to the emission system \dot{Q}_{sup}^{DZ} (averaged over one hour) for the day zone for five dwelling realizations of the considered detached, midsize, older (but renovated) dwelling equipped with radiators; the shaded area indicates the range of solutions spanned by all 100 possible dwelling realizations.

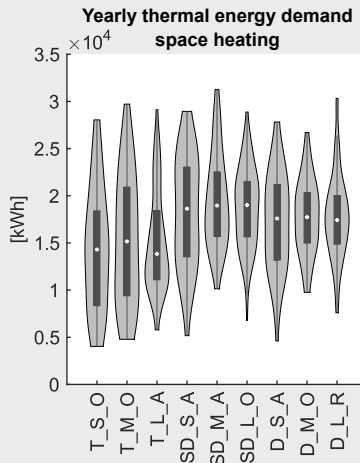


Figure 5.11: The distribution of the optimized yearly energy demand for space heating for the nine considered dwellings when equipped with radiators.

5.3 Weather forecast uncertainty

This section focuses on the uncertainty characterization of the weather forecasts. Section 5.3.1 first gives some background about weather uncertainty modeling. Section 5.3.2 then describes the considered uncertain variables and the applied modeling approach, after which the uncertainty characterization resulting from this approach is discussed in Section 5.3.3.

5.3.1 Background

In contrast to the building model parameters, there is a clear consensus on how to model the weather forecast uncertainty, covering the ambient temperature and solar heat gains, since it is unequivocally defined by the difference between the forecast and the actual weather conditions. Despite this clear definition, the required mathematical model cannot straightforwardly be found in literature. Most works provide a clear description of the applied uncertainty characterization method, see e.g., [44, 48, 53, 78, 79], but the actual numerical values are often not disseminated. Besides, even if the weather forecast uncertainty model is fully disclosed, see e.g., [51, 67, 147], these models are often not readily reusable. Either, they are very detailed, but case-specific, and hence not readily applicable to the considered conditions, or they neglect important details, such as the time-dependency of the stochastic characteristics. Also the (auto- and cross-)correlation of the forecast errors is most often disregarded [80, 81]. By using these simplified representations of the weather forecast uncertainty, valuable information is omitted that could otherwise be exploited by the SMPC to further improve its control strategy.

To overcome these issues, a thorough weather data analysis was performed by Lambrichts [148], who compared the actual weather conditions recorded at the Vliet test building of the KU Leuven Laboratory of Building Physics, located in Leuven (Belgium), with the corresponding weather forecasts made for Leuven by the Royal Belgian Meteorological Institute (RMI) for a full year. The forecast errors collected by Lambrichts are further processed in this work, in order to come up with an accurate characterization of the weather forecast uncertainty.

5.3.2 Modeling approach

The weather information required by the building controller model described in Section 5.1 includes the ambient temperature, the ground temperature, and the solar heat gains on the vertical planes along the four cardinal directions (see Equation (5.1)). In this dissertation, the considered uncertain variables are limited to the

ambient temperature and the solar irradiance, since this information is relatively easy to measure, and often available from local weather stations¹⁴ [126]. The uncertainty on the ground temperature, on the other hand, is not considered in this work, since the forecasts and actual measurement data required for a proper uncertainty characterization are hard to obtain [148]. In fact, the temporal variation of the ground temperature is not even considered, as argued in [126], since it is unrealistic that local measurements can be actually used as an input to the building controller model; rather, a constant value of 10 °C is used throughout this work.

To come up with an accurate uncertainty characterization of the selected weather variables, the forecast errors collected by Lambrichts are further processed. First, they are split up in different datasets according to the moment of the day when the forecast is made, so that this impact on the forecast uncertainty can be taken into account. Besides, within one dataset, an explicit distinction is made between forecasts made for different look-ahead times, thereby acknowledging that the uncertainty is likely to increase with an increasing forecast horizon. Since the RMI provides forecasts with a prediction horizon of 60 hours, which are being updated every 6 hours, four different datasets are distinguished, each containing 60 h-forecasts for both the ambient temperature and solar heat gains. Each of these datasets is used to characterize the probability distributions of the weather forecast errors in terms of their (time-dependent) mean and covariance, accounting for both the auto-correlation and cross-correlation. This information is subsequently used to constitute $\bar{\mathbf{d}}_k$ and $\Sigma_{\mathbf{d}_k}^t$, which will take different values depending on the moment of the day when the OCP is being solved, and on the considered prediction horizon.

As a final remark, it should be stressed that the mean value $\bar{\mathbf{d}}_k$ is determined by the combination of the weather forecast and its corresponding mean forecast error, and not merely by the forecast error itself. Hence, also weather forecasts are needed. In this dissertation, these are obtained via a reverse engineering approach, by generating correlated samples from the forecast error distributions, and by subsequently subtracting them from the available measurement data at the Vliet test building. Although this reverse engineering approach obviously would not work in real-life applications requiring dedicated forecast algorithms, it suffices for the setting considered here, without loss of generality, to illustrate the functionality of the SMPC approach under discrepancies between forecasts and actual data.

5.3.3 Resulting uncertainty characterization

This section particularly focuses on two additional aspects supplementing the detailed discussion of Lambrichts about (the time dependency of) the statistics of

¹⁴ The solar irradiance on the vertical planes along the four cardinal directions can either be directly measured, or can be derived from global horizontal irradiance data via pre-processing [126, 148].

the weather forecast uncertainty in [148].

A first important contribution is the consideration of the auto- and cross-correlation of the different forecast errors when determining the (co)variance, which was not taken into account by Lambrichts, resulting in a more accurate representation of the weather forecast uncertainty. The four derived covariance matrices, one corresponding to each moment of the day when a forecast is being made (i.e., $t = 0\text{ h}$, 6 h , 12 h or 18 h), are made available online¹⁵ to maximize reusability.

The second contribution is a more nuanced view on the assumption of normality of the forecast errors. To this end, the kurtosis and skewness of the different distributions of the weather forecast errors are again considered, similar to what was done for the building model parameter uncertainty. For each of the forecast error distributions, corresponding to the combination of a particular moment of the day when the forecast is made (i.e., $t = 0\text{ h}$, 6 h , 12 h or 18 h) and a particular lookahead time (i.e., $t = 1\text{ h} \rightarrow 60\text{ h}$), the kurtosis and skewness are plotted in Figure 5.12, but now as a function of the standard deviation, instead of as a function of the CV, since the latter is an inappropriate measure for average values amounting to zero. Given that the sample size is now large enough (i.e., $N > 300$) for the kurtosis and skewness to give a direct indication about normality, as explained in Intermezzo 5.1, the region of quasi-normality is explicitly indicated by the grey shaded region. From the figure, it is clear that - as already shown by Lambrichts - the forecast errors of the ambient temperature are mostly (quasi-)normally distributed. However, this does not always hold for the solar heat gains, where primarily the errors of forecasts made at the beginning or the end of the day do not follow a normal distribution. However, as can be seen from Figure 5.12, these specific forecast errors are also characterized by a small dispersion (i.e., small standard deviation), thereby restraining the adverse impact of assuming a normal distribution anyway. These observations again suggest that the assumption of normality for the states and inputs might be reasonable; this assumption will be further numerically tested/validated in Chapters 6 and 7.

5.4 Occupant behavior forecast uncertainty

This section focuses on the uncertainty characterization of the occupant behavior forecasts. We again first start with some background about the modeling of occupant behavior forecast uncertainty in Section 5.4.1. Section 5.4.2 then describes the considered uncertain occupant-related variables, and how this uncertainty can be modeled, after which the resulting uncertainty characterization is discussed in Section 5.4.3.

¹⁵<https://gitlab.kuleuven.be/u0117233/weather-forecast-uncertainty.git>.

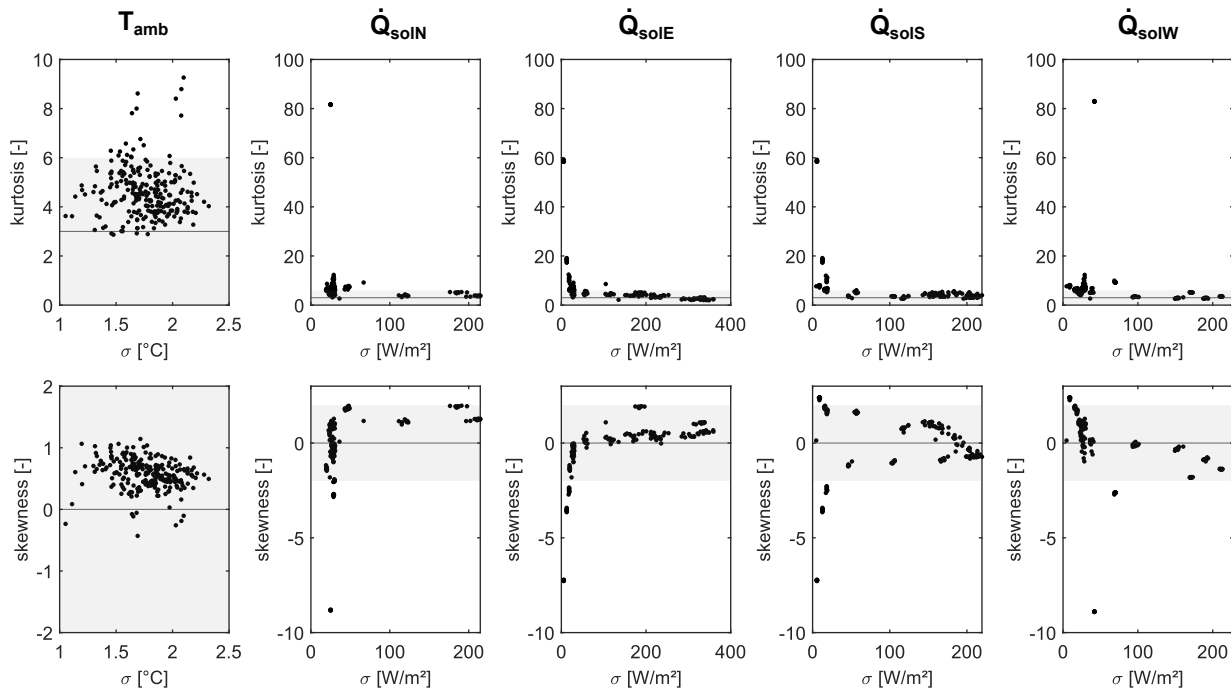


Figure 5.12: The kurtosis and skewness of the distributions of the forecast errors of the ambient temperature, and the solar irradiance on the vertical planes along the four cardinal directions. Each dot represents (the kurtosis or skewness of) the distribution of a particular error, corresponding to the combination of a particular moment of the day when the forecast is made and a particular lookahead time. The grey shaded area indicates the region of quasi-normality [145].

5.4.1 Background

The uncertainty on the occupant-related disturbance forecasts, can be defined in the same way as the weather forecast uncertainty. However, finding and/or defining a proper uncertainty characterization is even more difficult, due to the complex stochastic nature of human behavior, which is determined by many personal factors [149]. Dedicated approaches can be found in literature, implementing rigorous occupancy models combined with real-time, on-site measurements. This is for example done by Mady et al. [150], who implemented a stochastic occupancy model based on Markov chains as an input of an MPC algorithm, where the computation of the occupancy sequence is revisited at every time step. Another valuable approach is the learning-based approach, see e.g., [78], where the statistics of the uncertainties are continuously and dynamically inferred from real data.

5.4.2 Modeling approach

The occupant-related variables considered by the building controller model described in Section 5.1 are the thermal comfort requirements in terms of setpoint temperatures, and the equipment-related and metabolic internal heat gains. In this dissertation, the temperature setpoints are assumed to be deterministic, and hence, fixed and known. This is motivated by the findings of Guerra et al. [149], who observed that in dwellings with programmable thermostats, occupants take fewer deliberate actions, and leave the control to the thermostat. Nevertheless, if desired, the uncertainty on the setpoints can be straightforwardly included by also writing \tilde{x}_k^{min} and \tilde{x}_k^{max} as stochastic quantities in Equation (4.13), and by treating $\tilde{x}_k^* = \tilde{x}_k - \tilde{x}_k^{min}$ or $\tilde{x}_k^* = \tilde{x}_k - \tilde{x}_k^{max}$ (rather than \tilde{x}_k) as a stochastic variable in the elaboration discussed in Chapter 4. The internal heat gains, on the other hand, are considered as stochastic variables, and hence, require an uncertainty characterization.

Although the development of detailed occupancy forecast models are out of scope of this thesis, the working principle of such an approach can be imitated via a workaround as follows. With the help of the open web tool StROBe (Stochastic Residential Occupancy Behaviour)¹⁶ [146], an explicit occupancy modeling toolbox developed at the KU Leuven Building Physics Section, a yearly profile for the internal heat gains with a one hour time step can be generated¹⁷. This yearly profile

¹⁶ Note that in this work, an updated StROBe version is used, extended by Jansen, to include the metabolic heat rates in addition to the heat gains caused by appliances and lighting; see https://github.com/jelgerjansen/StROBe/tree/output_occupancy_profiles.

¹⁷ Although an explicit occupancy model is indeed available in the form of the open-source StROBe toolbox, it is out of scope of this work to incorporate this toolbox as an integral part of the MPC framework.

is considered as a proxy for an actually measured profile, and is subsequently used to determine an average daily¹⁸ profile and associated variance, determined by the deviations from the average daily profile. The average daily profile can then be used as a forecast for the internal heat gains (with a zero mean forecast error), and as such can be directly incorporated in $\bar{\mathbf{d}}_k$; the (square root of the) variance, on the other hand, can be used to constitute $\Sigma_{\mathbf{d}_k}^r$.

It should be stressed that this approach is based on a very important and limiting assumption, being that direct measurements of the internal heat gains are available, which are in practice difficult to obtain. A more plausible approach would be to use the domestic electricity use, available from digital/smart meter data, as an alternative input for the internal heat gains, as is for example suggested by Reynders et al. [126]. However, in this dissertation, we are bound to the set-up of the selected theoretical building model in Section 5.1, where the internal heat gains, rather than the electricity use (or any other suitable alternative), is used as an occupancy-related disturbance input.

5.4.3 Resulting uncertainty characterization

Figure 5.13 shows an example of the daily average profile and associated uncertainty (in terms of the standard deviation) of the internal heat gains derived from a StROBe profile for a four-persons-household, consisting of two full-time employed adults and two school-age children.

The approach to derive the uncertainty characterization of the internal heat gains fundamentally differs from the approach used for the building model parameter uncertainty and weather forecast uncertainty. Where the latter is based on a rigorous and extensive data-analysis, the uncertainty on the internal heat gains is merely a representation of the variation induced by the underlying modeling tool and its associated assumptions, due to the lack of actually measured profiles¹⁹. As such, it can also not be used to further consolidate the assumption that the states are normally distributed. Nevertheless, it should be stressed that the imprecise uncertainty characterization of the internal heat gains does not detract from the general purpose of this thesis, which is the development and assessment of an SMPC strategy that is able to cope with different types of discrepancies between the actual situation and what the model assumes.

¹⁸ The reason why a daily average is considered, without considering more details by for example making a distinction between weekdays and weekend days, is because the occupancy profiles generated by the considered version of the StROBe toolbox, and the profiles for the metabolic heat gains derived therefrom (but not the equipment-related heat gains), consist of a one-week profile (which depends on the household characteristics) repeated 52 times.

¹⁹ The statistics used in the StROBe toolbox to generate profiles are nevertheless based on actual data regarding household activity, collected via surveys [146].

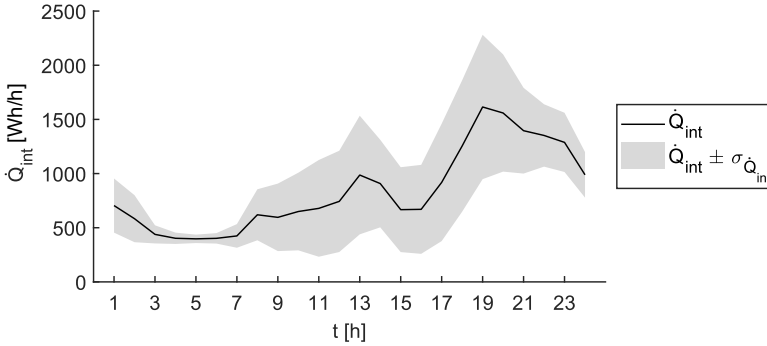


Figure 5.13: An example of the forecast (i.e., the daily average profile, with a one hour time step) and associated uncertainty (i.e., the standard deviation) of the internal heat gains, derived from a StROBe profile of a four-persons-household, consisting of two full-time employed adults and two school-age children.

5.5 Conclusion

As a second part of the SMPC development, this chapter derives a mathematical model of the model parameter and forecast uncertainty, serving as an essential part of the stochastic OCP formulation.

The model parameter uncertainty is derived with the help of the probabilistic building characterization method of De Jaeger et al. [62, 63]. This method generates a statistical characterization of the building envelope based on the building geometry, location and construction year, without intensive on-site data collection. By using the theoretical physics-based modeling approach of Reynders et al. [132], this information is subsequently converted into a reduced order one-zone four-states RC model. The parametric uncertainty can be derived in terms of the mean and (co)variance of (the inverse of) the RC parameters, as well as in terms of the reference SSM $\bar{\bar{A}}$, $\bar{\bar{B}}$ and $\bar{\bar{E}}$, and associated covariance $\Sigma_{\bar{\bar{A}}, \bar{\bar{B}}, \bar{\bar{E}}}$, where the latter can be directly incorporated in the stochastic OCP formulation discussed in Chapter 4. The presented approach leads to a worst-case estimation of the parametric uncertainty, acknowledging the possible lack of information about the building envelope, e.g., in case the older, existing building stock is involved. This is fundamentally different from what is done in current research, where the uncertainty characterization is typically derived based on detailed (building-specific) information and/or experts' knowledge.

The uncertainty characterization is applied to nine disparate, (partly) renovated dwellings. Analysis of the results of the uncertainty characterization shows that the proposed methodology results in rather large distributions for the thermal properties. A coefficient of variation in the order of 0.3 is recognized as a lower bound for all U-values for all considered dwellings. The uncertainty on the U-values of the ground floor and windows is found to fluctuate around the same value, whereas the uncertainty on the U-values of the external walls and roof can vary considerably. Since the exact set of building model parameters derived from the building envelope characteristics depends on the imposed building model structure, the most important takeaway from the parametric uncertainty analysis is the insight in how the uncertainty on the building thermal properties propagates into the RC parameters, rather than exact values for the parametric uncertainty. It is observed that the uncertainty is predominantly transferred to the external resistances containing the insulation layer; more specifically, for the ground floor and windows, the CV decreases when moving from U to 1/R, whereas for the external walls and roof, it increases. Finally it is also shown that the conversion into a discrete-time SSM with a time step of one hour results in distributions that can be roughly approximated by a normal distribution for the gross of the state space matrix elements, which substantiates the normality assumption imposed in Chapter 4.

The forecast uncertainty encompasses the uncertainties on the weather conditions and on the occupant-behavior, which together determine the mean $\bar{\mathbf{d}}_k$ and (the root form of) the covariance $\Sigma_{\mathbf{d}_k}^r$.

To come up with a substantiated estimate of the weather forecast uncertainty, and more specifically of the uncertainty on the forecasts of the ambient temperature and solar irradiance, we build further upon the work of Lambrichts [148], who detailedly compared the actual weather conditions recorded at the Vliet test building of the KU Leuven Laboratory of Building Physics, located in Leuven (Belgium), to the corresponding weather forecasts made by the Royal Belgian Meteorological Institute (RMI) for a full year. Based on this information, four covariance matrices (one for each moment of the day when a prediction is being made) are derived, taking into account the auto- and cross-correlation of the forecast errors, which are often disregarded.

In contrast to the building model parametric uncertainty and the weather forecast uncertainty, the uncertainty on the occupant-related disturbance forecasts, and on the internal heat gains in particular, is much harder to characterize, due to the complex nature of human behavior, but also due to the lack of actually measured profiles. As a workaround, a yearly profile, simulated with the open web tool StROBe, is used to deduce a daily average profile and associated variance, to nevertheless get a loose representation of the occupancy-related uncertainty to be incorporated in $\bar{\mathbf{d}}_k$ and $\Sigma_{\mathbf{d}_k}^r$. Although it is acknowledged that this uncertainty

characterization is imprecise, it does not detract from the general purpose of this thesis, which is the development and assessment of an SMPC strategy that is able to cope with different types of discrepancies between the actual situation and the model assumptions.

Now that all relevant uncertainties are characterized, the development of the SMPC strategy is complete. The next important step is to assess its performance, thereby appraising its potential added value. This is the focus of the next chapters.

Part II

SMPC assessment at building level

Chapter 6

Optimal control under uncertainty of a TCL in an individual building

RQ 3: Does the SMPC^{ap} strategy guarantee a thermal comfort improvement compared to the current-practice DMPC strategy, and the state-of-the-art SMPC^a strategy only accounting for additive uncertainties, and at what cost is this improvement obtained?

This chapter is based on A. Uytterhoeven, R. Van Rompaey, K. Bruninx, and L. Helsen, "Chance Constrained Stochastic MPC for Building Climate Control Under Combined Parametric and Additive Uncertainty," submitted to Journal of Building Performance Simulation, July 2021.

The goal of this chapter is to investigate the effectiveness of the proposed SMPC strategy for optimal building climate control under uncertainty. The main focus is on the attainable thermal comfort improvement by hedging against additive as well as parametric uncertainties in an optimal control context, and on the related energy costs. Section 6.1 discusses the general set-up of the performance assessment. Section 6.2 then introduces the specific case study used to evaluate the performance, for which the results are discussed in Section 6.3. Finally, the most important conclusions are summarized in Section 6.4.

6.1 Optimal control performance assessment method

The optimal control performance assessment is done based on two performance metrics, being the specific thermal energy demand (TED), and the thermal comfort violations (TCV).

The total specific thermal energy demand is determined by the heat input delivered by the heat supply system, expressed relative to the net floor area of the building.

$$TED = \sum_{k=0 \dots K} \frac{\bar{u}_k \Delta t}{A_{floor}} \quad (6.1)$$

The thermal comfort is determined by the condition of the state representing the indoor air temperature $x_{i,k} = T_{ia,k}$, with respect to the imposed lower and upper temperature bounds. The implications of this point of view regarding the assessment of thermal (dis)comfort are further discussed in Intermezzo 6.1.

Because of the particular setting considered in this chapter, focusing on optimal space heating at minimal energy use, the controller is compelled to stick to the lower temperature bound, implying that the upper bound is of minor importance here¹. Therefore, the violations of the upper thermal comfort bound are not explicitly considered in Equation (6.2).

$$TCV = \sum_{k=0 \dots K} \max(x_{i,k}^{min} - \bar{x}_{i,k}, 0) \Delta t \quad (6.2)$$

Intermezzo 6.1

The simplified assessment of thermal (dis)comfort

It is important to stress that the assessment of thermal comfort in this dissertation is based on some simplifying assumptions.

First, as already discussed in Section 5.1, the thermal comfort is assessed based on the indoor air temperature, instead of on the operative temperature, which is used in comfort standards [83]. This simplification is required because the

¹ Also in Chapter 7, again considering a controller aiming for an energy use minimization in a space heating context, the upper thermal comfort bound will be neglected. However, be aware that this simplification is not generally acceptable. Indeed, if the objective is not to minimize energy use, as is for example the case in Chapter 8 and Chapter 9, both the lower and upper thermal comfort bounds play an important role, as they determine the valid operating region for the controller, and as such, the available flexibility.

radiative temperatures of the building components are not explicitly considered in the chosen building model (see Section 5.1). Consequently, the impact of the temperatures of the surfaces surrounding the occupants on thermal comfort is not taken into account. This hampers a profound comparison of the thermal comfort achieved by radiators versus by floor heating, since the impact of the difference in temperature of the heat emission system itself (due to a different water supply temperature), as well as in temperature of the surrounding construction elements (due to a different loading of the building thermal mass), is neglected [151].

Second, thermal discomfort is based on the cumulative violations of the imposed thermal comfort bounds in this dissertation (see Equation (6.2)); the impact of the duration, frequency and severeness of the temperature violations is not further differentiated. Also the impact of the rate of change of the temperature profile (even when not exceeding the comfort bounds) on the perceived thermal comfort, is neglected.

Finally, a wide variety of other factors which affect thermal comfort in practice, such as humidity level, air velocity, metabolic factors, clothing level, etc. [83, 151], are not further considered.

All statements regarding thermal (dis)comfort mentioned throughout this dissertation should be interpreted in light of these simplifications.

To obtain a profound insight in the potential added value of the proposed SMPC approach compared to the state-of-the-art, its control performance is compared to the following control strategies:

- **Performance Bound (PB) MPC** PBMPC assumes perfect knowledge of the system dynamics and future disturbance realizations in the OCP, i.e., the uncertainty is absent and the stochastic quantities are equal to their actual, future values. Hence, the system is not subject to closed-loop perturbations. This is not a controller, but rather a theoretical concept, that can serve as a benchmark for other control strategies; it illustrates the best possible (but not actually attainable) MPC performance.
- **Deterministic (D) MPC** DMPC, also known as certainty equivalence MPC, considers the deterministic OCP formulation (2.1) without uncertainty anticipation, i.e., the chance constraints are solved for $\epsilon = 0.5$, and all predictions are assumed to be correct (i.e., equal to certain). Uncertainties are nevertheless present in the closed-loop simulations, causing the actual model parameters and disturbances to differ from the nominal values assumed in the OCP. This strategy follows common practice.

- Stochastic MPC** SMPC explicitly accounts for the uncertainties in the OCP formulation (4.21), in order to limit the detrimental impact of the closed-loop perturbations. A distinction is made between SMPC only accounting for additive (disturbance forecast) uncertainty, SMPC^a, which is the current state-of-the-art strategy for building climate control, and SMPC taking into account both additive and parametric (model) uncertainty, SMPC^{ap}, corresponding to the proposed novel strategy.

The difference in information used by the different controllers in the OCP formulation is summarized in Table 6.1.

Table 6.1: The information used in the OCP formulation by the different MPC strategies for which the MPC performance regarding building climate control under uncertainty is compared.

| | | Actual value | Covariance |
|--------------------|----------------------------|----------------------|------------|
| | | Mean/reference value | |
| PB MPC | Weather forecast | x | |
| | Occupant behavior forecast | x | |
| | Building model | x | |
| DMPC | Weather forecast | | x |
| | Occupant behavior forecast | | x |
| | Building model | | x |
| SMPC ^a | Weather forecast | x | x |
| | Occupant behavior forecast | x | x |
| | Building model | x | |
| SMPC ^{ap} | Weather forecast | x | x |
| | Occupant behavior forecast | x | x |
| | Building model | x | x |

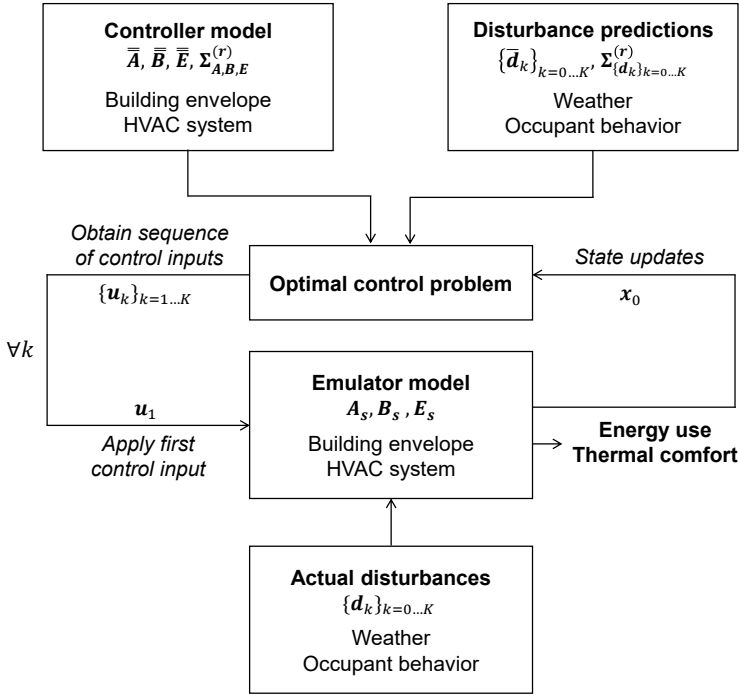


Figure 6.1: The general working principle of MPC applied to a TCL. Adapted from [82].

To assess the control performance by simulations, all MPC strategies are implemented in closed-loop, using a receding horizon, as explained in Section 2.1 and illustrated by Figure 2.1, which is repeated here for convenience in a slightly adapted form as Figure 6.1. Since no model-structure uncertainty is considered, the emulator model representing the actual system, and used for the state updates, is characterized by the same model equations, but different model parameters, as the controller model used in the OCP formulation (except for the PBMP strategy, where the controller and emulator model are equal). Perfect state updates and full state information are assumed, to avoid additional interference of noise introduced by a state estimator. Thereby, the impact of measurement errors, system errors, and the like are ruled out. As such, it is possible to unequivocally assess how the different MPC strategies (merely) cope with the stochasticity of the parameters of the controller model and of the disturbance forecasts. For the state updates, all controllers use the same information, being the actual building model parameters, the actual weather realizations and the actual internal heat gain realizations.

Table 6.2: The most important characteristics regarding construction year (known), geometry (known) and thermal quality (uncertain) of the terraced, small, older (but renovated) building for which the MPC performance for building climate control under uncertainty is investigated.

| | |
|-------------------------------------|----------|
| Construction year [-] | <1950 |
| Detachment level [-] | Terraced |
| Net floor area [m ²] | 129 |
| Protected volume [m ³] | 406 |
| Ground floor area [m ²] | 87 |
| Façade area [m ²] | 80 |
| Roof area [m ²] | 95 |
| UA building [W/K] | 130-668 |

6.2 Case study

In this chapter, the TCV and TED of the different MPC strategies are evaluated by closed-loop simulations for a residential dwelling for one week, during the first seven days of January 2016². All controllers pursue an energy use minimization, and consider a time step of 1 h and a prediction horizon of 60 h, restricted by the characteristics of the available disturbance forecasts. For the SMPC approaches, different risk-averseness levels regarding thermal comfort ($1 - \epsilon = 0.6 \rightarrow 0.999$) are considered, in order to fully cover their possible operating region.

The considered residential building in this study is selected from the set of heavy-weight dwellings for which the parametric uncertainty is studied in detail in Chapter 5. Here, the terraced, small, older (but renovated) (T_S_O) dwelling is considered, characterized by the largest parametric uncertainty. The most important characteristics are repeated in Table 6.2. Both radiators and floor heating are considered separately as installed heat emission system.

The controller model used to represent this building in the OCP formulation, as explained in Section 5.2, is either the reference SSM $\bar{\mathbf{A}}, \bar{\mathbf{B}}, \bar{\mathbf{E}}$ (in case of the DMPC, SMPC^a or SMPC^{ap} strategy), combined with the corresponding covariance matrix $\Sigma_{\mathbf{A},\mathbf{B},\mathbf{E}}$ for the SMPC^{ap} strategy, or the emulator model (in case of the

² These closed-loop simulations are preceded by an initialization procedure, where the starting values for the different states are determined by solving an OCP with cyclic boundary conditions for the states. The prediction horizon for the initialization is chosen equal to the maximum number of full days (being two days) that fits in the actual prediction horizon, to minimize the impact of presuming cyclic boundary.

PBMPC strategy), where the emulator model corresponds to a sampled SSM \mathbf{A}_s , \mathbf{B}_s , \mathbf{E}_s . To maximize insight, the performance assessment considers different emulator models, representing different cases of model uncertainty. Seven different SSMs, each representing a possible realization of the T_S_O building, are selected from the total set of 100 possible building controller models obtained in Section 5.2; their characteristics are summarized in Table 6.3. The first one is the reference, with the smallest WDM (Equation (5.2)); this in fact corresponds to the case without model uncertainty. Then, two building samples with a moderate WDM are selected, one with a smaller nominal heat demand³, \dot{Q}_{nom} , than the reference building, and one with a larger one. The same is done for two building samples with a large WDM. Finally, also the building samples with the overall smallest and largest nominal heat demand are included, so that also the 'best-case' and 'worst-case' possible building realizations are considered in the analysis. It should be stressed that, depending on the heat emission system, the WDM ranking of the sampled SSMs is different. Hence, the reference model in case of radiators and in case of floor heating differs. For arguments of convenience, the other selected SSM samples are nevertheless chosen to be the same, independent of the installed heat emissions system, since they reflect a moderate or large model uncertainty in either case.

The upper thermal power bound to be used as a constraint in the OCP formulation is determined by the capacity of the heat supply system in place, which is assumed to be sized according to the nominal heat demand of the building. In case model uncertainty is being considered (i.e., in all cases except for the PBMPC strategy), the sizing is done based on the reference model and takes into account a safety factor of 1.5, to acknowledge that there may exist a significant discrepancy between the reference model and real-world⁴.

For the actual ambient temperature and solar heat gains realizations, measurement data of the year 2016 are used, recorded at the Vliet test building of the KU Leuven Laboratory of Building Physics, located in Leuven (Belgium). For the actual internal heat gain realizations, a StROBe profile of a four-persons-household, consisting of two full-time employed adults and two school-age children, is used. As explained in Section 5.4.2, the thermal comfort requirements are considered to be fixed. In this study, a minimum temperature of 20 °C is requested during daytime (i.e., 07:00 - 23:00), combined with a night setback of 16 °C. Note that the maximum allowed temperature is of minor importance in this case study, since a week in January is

³ The nominal heat demand is quantified following NBN EN 12831, considering an extremely cold day (according to the Belgian climate) with an outside temperature of -8 °C, a ground temperature of 10 °C, and an indoor temperature of 20 °C [137].

⁴ The point of view adopted in this dissertation differs from the one adopted in current practice, where one typically assumes that a sufficiently accurate building model is available. To account for the impact of the significant parametric uncertainty in this work, a high safety factor is used on top of the worst-case static design conditions.

Table 6.3: The most important characteristics distinguishing the seven considered sampled SSMs of the terraced, small, older (but renovated) building, either equipped with radiators or with floor heating, for which the MPC performance for building climate control under uncertainty is investigated.

Rather than mentioning the actual WDM value, the WDM is represented by an index, ranging from 1 for the reference building, to 100 for the realization that differs the most from the reference.

| Sample | <i>In case of radiators</i> | | | <i>In case of floor heating</i> | | |
|--------|-------------------------------|------------------|----------------------|---------------------------------|------------------|----------------------|
| | \dot{Q}_{nom} [W] | WDM index [-] | UA building [W/K] | \dot{Q}_{nom} [W] | WDM index [-] | UA building [W/K] |
| A | 4080 (min) | 81 | 130 | 4080 (min) | 67 | 130 |
| B | 6334 | 95 | 214 | 6334 | 95 | 214 |
| C | 8582 | 50 | 360 | 8582 | 55 | 360 |
| REF | 9033 | 1 | 295 | 9371 | 1 | 400 |
| D | 11996 | 53 | 457 | 11996 | 48 | 457 |
| E | 11303 | 100 | 480 | 11303 | 89 | 480 |
| F | 14959 (max) | 96 | 668 | 14959 (max) | 98 | 668 |

chosen where the controller will try to stick to the lower temperature bound as it tries to minimize the energy use.

The expected value and covariance of the disturbance forecasts are derived by applying the methods described in Chapter 5. Since the proposed uncertainty characterization method for the occupant behavior forecast is not underpinned by actual data⁵, and turns out to result in a very large variance, the control performance assessment is done twice, one time with and one time without uncertainty on the internal heat gains, where the truth is expected to lie somewhere in between. By considering these two cases, the impact of the balance between the additive and parametric uncertainty is taken into account, allowing for a more nuanced view on the added value of the SMPC^{ap} strategy.

6.3 Results and discussion

The discussion of the results focuses on the attainable thermal comfort improvement by hedging against additive as well as parametric uncertainties in a building climate control context, and on the related costs. This cost is mainly assessed in terms of energy use in Section 6.3.1, but also the computational effort associated with the more complex SMPC^{ap} strategy is briefly touched upon in Section 6.3.2.

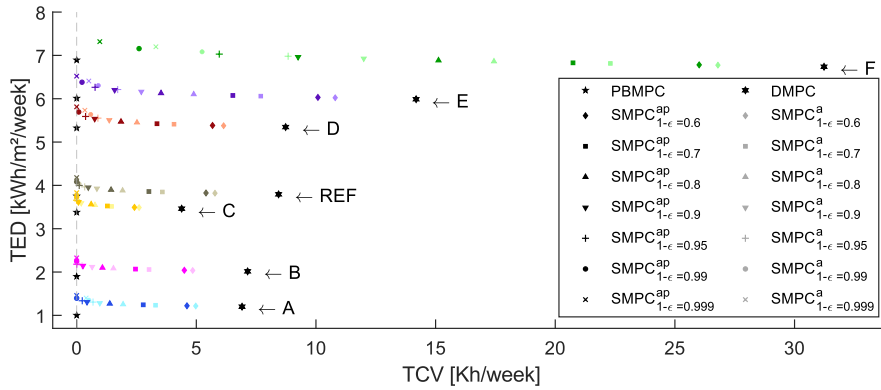
6.3.1 Thermal comfort improvement and associated increase in energy use

As we will illustrate below, the SMPC^{ap} approach yields thermal comfort improvements at the expense of limited increases in energy use. These gains are most prominent in buildings equipped with floor heating and characterized by the combination of a large model uncertainty and a large nominal heat demand, and this at a limited cost.

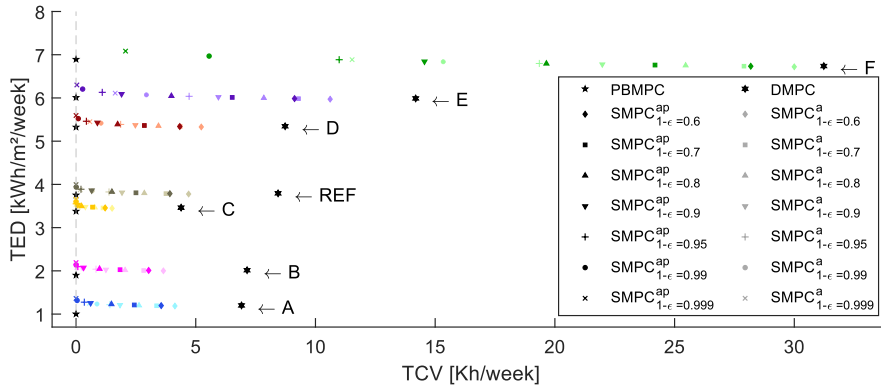
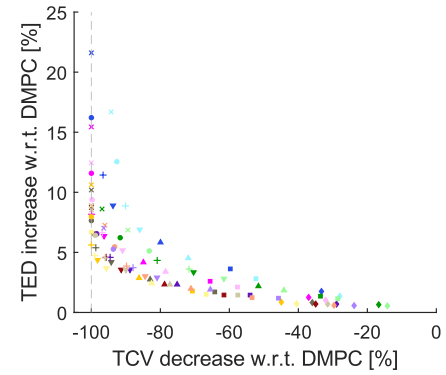
Figures 6.2 and 6.3 summarize the performance, in terms of thermal comfort violations and specific thermal energy demand, of the PBMPC, DMPC, SMPC^a and SMPC^{ap} strategies, for the first week of January 2016⁶. For each considered realization of the studied T_S_O building, either equipped with radiators (Figure

⁵ In contrast to the uncertainty characterization of the building model parameters and weather forecasts, which are both based on a rigorous and extensive data-analysis.

⁶ The results shown in this chapter focus on the overall performance in terms of thermal comfort violations and specific thermal energy demand. A more detailed analysis of the underlying time-dependent system behavior associated with the different MPC strategies will be discussed in Section 7.3.



(a) With uncertainty on the occupant behavior.



(b) Without uncertainty on the occupant behavior.

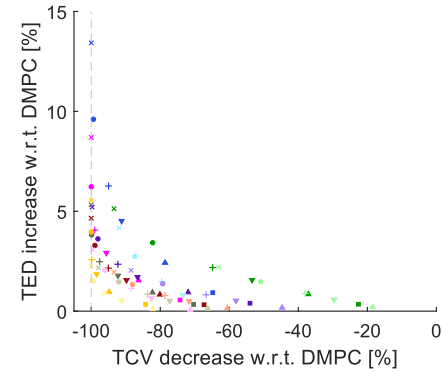
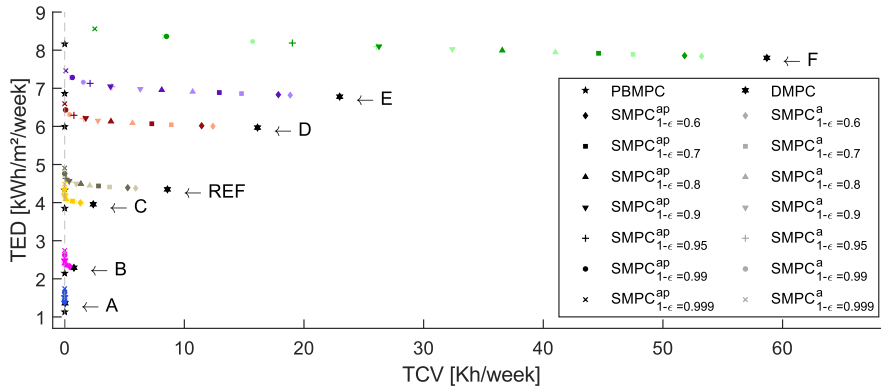
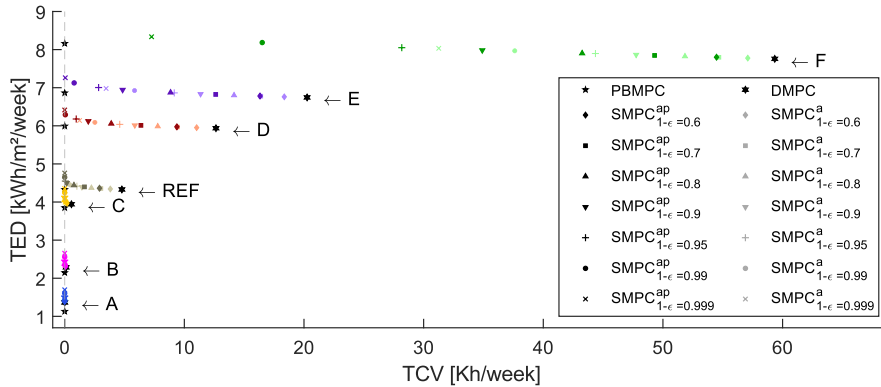
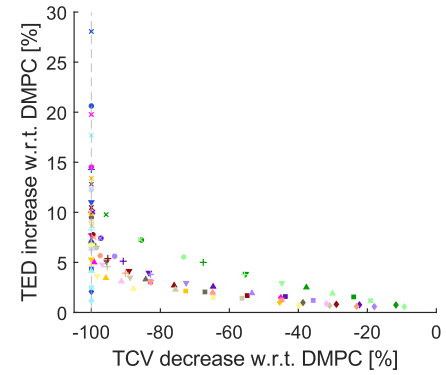


Figure 6.2: The trade-off curves of the thermal comfort violations versus the specific thermal energy demand during the first week of January, for different possible realizations of the terraced, small, old building, equipped with radiators.



(a) With uncertainty on the occupant behavior.



(b) Without uncertainty on the occupant behavior.

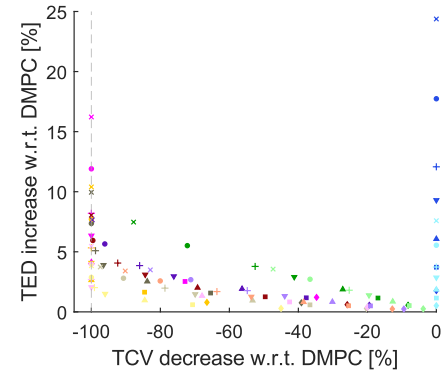


Figure 6.3: The trade-off curves of the thermal comfort violations versus the specific thermal energy demand during the first week of January, for different possible realizations of the terraced, small, old building, equipped with floor heating.

6.2) or with floor heating (Figure 6.3), the figures visualize i) the best-case (theoretical) control performance of the PBMPIC strategy (\star), guaranteeing no thermal comfort violations ($TCV = 0$) at the lowest energy use, ii) the worst-case control performance of the DMPC strategy (\star), and iii) the intermediate control performance of the SMPC^a and SMPC^{ap} approaches, subject to a trade-off between TCV and TED, depending on the value of the risk-averseness level regarding thermal comfort $1 - \epsilon$. For these intermediate cases, the horizontal distance with respect to the DMPC strategy depicts the realized thermal comfort improvement, whereas the vertical distance depicts the increase in energy use required to accomplish the enhanced thermal comfort. Figures 6.2 and 6.3 each time show the results of the two different performance assessments proposed in Section 6.1: one where the uncertainty on the occupant behavior forecasts is considered (Figures 6.2a and 6.3a), and one where this uncertainty is ignored (both in the OCP and in the closed-loop simulations) (Figures 6.2b and 6.3b)).

From both Figure 6.2 and 6.3 it is immediately clear that there is considerable value in switching from current-practice to stochastic approaches (either an SMPC^a or SMPC^{ap} strategy), because of the clear reduction in thermal comfort violations, indicated by the horizontal span of the trade-off curves. This thermal comfort gain is most pronounced for the cases with a large model uncertainty (indicated by a high WDM index, see Table 6.3), where the nominal heat demand of the considered building realization is larger than that of the reference model, i.e., especially for samples E and F, and also sample D in case of floor heating. Indeed, for these cases, the error induced by disregarding the uncertainties in the DMPC approach is the largest, because of the combined effect of the incorrect forecasts, the underestimation⁷ of the required heat relative to the reference model considered in the OCP, and the incorrect assessment of the moment this heat needs to be delivered (due to an incorrect appraisal of the building dynamics). Nevertheless, also for the other samples, i.e., samples A, B and C, a considerable improvement of thermal comfort is possible, especially in case of radiators. In case of floor heating, on the other hand, the combination of the large time constants and the overestimation of the heat demand by using the reference model as a controller model for these building samples, having a smaller actual nominal heat demand, already implicitly triggers a considerable amount of anticipation, even without actually hedging against the impact of possible uncertainties via a stochastic approach; indeed, the overestimation of the heat demand results in a large initial heating peak, after which the indoor temperature is situated sufficiently far away from the thermal comfort bounds (under the condition that the thermal comfort band is sufficiently wide), allowing the indoor temperature to float freely for multiple time steps, even

⁷ A slight overestimation of the heat demand is less of a problem (of course only if combined with a proper estimation of the building dynamics), since this steers the indoor temperature further away from the minimum bound, thereby implicitly hedging against the impact of possible downward perturbations causing a temperature drop.

under the influence of possible (either upward or downward) uncertainty realizations. Hence, there is little thermal comfort improvement possible by switching to a stochastic approach for building realizations with a small nominal heat demand equipped with floor heating. However, for building realizations with a large nominal heat demand equipped with floor heating, a correct uncertainty anticipation is all the more important, exactly because of the large time constants. This is confirmed by the very large thermal comfort gains realized by the stochastic approaches in this case, as illustrated by Figure 6.3, which significantly exceed the comfort gains realized for buildings equipped with radiators (as also indicated by the difference in scale of the x-axis of Figures 6.2 and 6.3).

A large part of the thermal comfort improvement of the stochastic approaches (either an SMPC^a or SMPC^{ap} strategy) can be attained at the cost of a limited increase of energy use, as indicated by the gentle, almost flat, slope of the trade-off curves. For all building samples, irrespective of the installed heat emission system, 90% of the thermal comfort improvement relative to the DMPC strategy can be realized with an increase of at most 9% in energy use. However, for larger risk averseness levels ($1 - \epsilon \geq 0.9$), the trade-off between enhanced thermal comfort and additional energy use becomes more pronounced.

Overall, for the dwelling realizations equipped with radiators, the increase in energy use of the SMPC^a strategy relative to the DMPC strategy for the case with the occupant behavior forecast uncertainty included ranges between 0.6% (samples D, E, F, $1 - \epsilon = 0.6$) and 16.7% (sample A, $1 - \epsilon = 0.999$, but with a relative TCV decrease compared to the DMPC strategy of -94.3%), whereas the relative energy use increase of the SMPC^{ap} approach ranges between 0.7% (samples D, E, F, $1 - \epsilon = 0.6$) and 21.6% (sample A, $1 - \epsilon = 0.999$, with complete elimination of thermal discomfort). It should nevertheless be stressed that the SMPC^{ap} strategy can already guarantee zero thermal discomfort at a relative energy use increase of 16.2% for sample A and $1 - \epsilon = 0.99$; further increasing the risk-averseness level actually results in an unnecessarily conservative control strategy, that does not realize any further thermal comfort improvement, but nevertheless requires more energy. For the case without occupant behavior forecast uncertainty, the relative energy use increase of the SMPC^a approach compared to the DMPC approach ranges between -1.1%⁸ (sample A, $1 - \epsilon = 0.6$) and 4.2% (sample A, $1 - \epsilon = 0.999$, but with a relative TCV decrease compared to the DMPC strategy of -91.9%), whereas the relative energy use increase of the SMPC^{ap} approach ranges between -0.3% (samples A, B, $1 - \epsilon = 0.6$) and 13.4% (sample A, $1 - \epsilon = 0.999$, with complete elimination of thermal discomfort); the lower energy use compared to the case with uncertainty on the occupant behavior forecast is to be expected, since

⁸ The negative value of the relative energy use increase of the SMPC approach compared to the DMPC approach indicates that the energy use due to the closed-loop corrections of the DMPC approach outweighs the energy use due to the more conservative (anticipating) control strategy of the SMPC approach in this particular case.

the omission of part of the uncertainty results in a lower constraint tightening level. For the dwelling realizations equipped with floor heating, on the other hand, the increase in energy use of the SMPC^a strategy relative to the DMPC strategy for the case with the occupant behavior forecast uncertainty included ranges between 0.6% (sample F, $1 - \epsilon = 0.6$) and 17.7% (sample A, with complete elimination of thermal discomfort). It should again be stressed that the latter percentage is actually an overestimation, since it corresponds to an overly conservative strategy; if only considering the cases that still realize an actual further thermal comfort improvement when increasing the risk-averseness level, the relative energy use increase remains limited to 8.7% (sample REF, $1 - \epsilon = 0.999$). The relative energy use increase of the SMPC^{ap} approach ranges between 0.7% (sample F, $1 - \epsilon = 0.6$) and 28.1% (sample A, $1 - \epsilon = 0.999$); if again neglecting the overly conservative cases, the relative TED increase only amounts to 10.0% (sample E, $1 - \epsilon = 0.999$). For the case without occupant behavior forecast uncertainty, the relative increase in energy use of the SMPC^a strategy compared to the DMPC strategy ranges between 0.2% (sample E, $1 - \epsilon = 0.6$) and 7.6% (sample A, $1 - \epsilon = 0.999$, with complete elimination of thermal discomfort), or between 0.2% and 3.7% (sample REF, $1 - \epsilon = 0.999$, with a relative TCV decrease compared to the DMPC strategy of -97.4%) when omitting the overly conservative cases. Analogously, the relative energy use increase of the SMPC^{ap} approach ranges between 0.6% (sample E, $1 - \epsilon = 0.6$) and 24.4% (sample A, $1 - \epsilon = 0.999$, with complete elimination of thermal discomfort), or between 0.6% and 8.1% (sample D, $1 - \epsilon = 0.999$, with complete elimination of thermal discomfort), respectively.

The relative TED increase and TCV decrease of the stochastic approaches compared to the DMPC approach for all building samples and risk-averseness levels are depicted in the subfigures on the right hand side of Figures 6.2 and 6.3. Interestingly, in each of these subfigures, all relative trade-off curves of all different building samples more or less coincide; only the curves of samples A and F, being the building samples with the smallest and largest nominal heat demand, show a slightly deviating behavior. Hence, the trends followed by the relative trade-off curves suggest the existence of a rule of thumb when assessing the associated energy cost of an envisioned thermal comfort improvement.

When focusing on the mutual comparison of the two stochastic approaches, SMPC^a and SMPC^{ap}, a more detailed analysis of Figure 6.2 shows that for the bulk of the possible building realizations equipped with radiators, the added value of the SMPC^{ap} strategy compared to the SMPC^a strategy is limited. If thermal comfort improvements by moving from the SMPC^a strategy to the SMPC^{ap} strategy of less than 1 K h over an entire week are deemed insufficient, the SMPC^{ap} approach with uncertainty on the occupant behavior forecast included realizes a considerable thermal comfort improvement only for sample F, reducing the TCV from 3.3 K h to 1.0 K h for $1 - \epsilon = 0.999$. When increasing the relative share of the model uncertainty

relative to the additive uncertainty, by omitting the uncertainty on the occupant behavior forecast, the improvement brought about by the SMPC^{ap} strategy for sample F is significantly amplified, with a TCV reduction from 11.5 K h to 2.1 K h, as shown in Figure 6.2b. Moreover, also the thermal comfort improvement for sample E becomes substantial, with a TCV reduction from 1.6 K h to 0.0 K h. The reason why the SMPC^{ap} strategy is hampered to fully distinguish itself from the SMPC^a strategy in the considered case with radiators, is threefold, namely i) because of the small time constants associated with radiators, ii) because the stochastic OCP is re-solved for every subsequent time step, and iii) because the heat supply system has sufficient heating capacity available (due to the imposed safety factor of 1.5). These three aspects all obviate the added value of a correct uncertainty anticipation, which is the most important asset of the SMPC^{ap} approach.

When comparing the SMPC^a and SMPC^{ap} strategies for the building realizations equipped with floor heating, shown in Figure 6.3, the picture completely changes. In this case, due to the larger time constants associated with floor heating, the SMPC^{ap} strategy can make the most of its enhanced uncertainty anticipation to improve thermal comfort under uncertainty. Again considering thermal comfort improvements by moving from the SMPC^a strategy to the SMPC^{ap} strategy of less than 1 K h over an entire week as insufficient, the SMPC^{ap} strategy is now able to guarantee a significant improvement in thermal comfort for sample F compared to the SMPC^a strategy, shifting the TCV from 8.3 K h over an entire week towards 2.5 K h for $1 - \epsilon = 0.999$. When omitting the uncertainty on the occupant behavior forecast, the thermal comfort improvement becomes even more substantial, with a TCV reduction for samples D, E and F from 1.2 K h, 3.5 K h and as much as 31.3 K h, towards 0.0 K h, 0.1 K h and 7.3 K h, respectively.

These results show that despite the simplifying assumptions introduced in Chapter 4 (such as the omission of the products of stochastic variables, and the assumption that every distinct state and input is characterized by a marginal normal distribution) to derive the open-loop stochastic OCP formulation, the developed SMPC^{ap} approach is able to guarantee improved thermal comfort compared to the state-of-the-art in closed-loop simulations. The impact of these assumptions could be more profoundly investigated by performing Monte Carlo simulations, to check whether the thermal comfort constraints are actually met by a probability of $1 - \epsilon$. However, this would require a large number of closed-loop simulations, to be able to make profound, substantiated statements with sufficient confidence. Given the mathematical complexity of the stochastic OCP, and the associated calculation effort, this is not further pursued in this dissertation.

6.3.2 Computational effort

To finalize the discussion about the performance of the SMPC^{ap} strategy, it should be acknowledged that the increased thermal comfort does not only come at the cost of a higher energy use, but also at the cost of a higher computational complexity. In the particular setting considered in this chapter, solving one open-loop OCP of the SMPC^a approach requires less than 1 minute on a 2.3 GHz core with 192 GB RAM, whereas the solution of the OCP of the SMPC^{ap} approach takes approximately 10 minutes. This considerable difference is due to the repetition of the parametric uncertainty for each time step in the latent variable $\tilde{\mathbf{p}}$ for the SMPC^{ap} approach, markedly increasing the problem size. Indeed, by including the parametric uncertainty, in addition to the additive uncertainty, in $\tilde{\mathbf{p}}$, its dimension increases from $n_p = n_d K = 420$ to $n_p = n_d K + n_x (n_x + n_u + n_d) K = 3300$ (in case of floor heating) or $n_p = n_d K + n_x (n_x + n_u + n_d) K = 4320$ (in case of radiators⁹), which impacts the dimension of the optimization variables $\Sigma_{\mathbf{x}_k}^r \in \mathbb{R}^{n_x \times n_p}$ and $\mathbf{T}_{\mathbf{u}} \in \mathbb{R}^{n_u K \times n_p}$. Hence, an important downside of the proposed SMPC^{ap} strategy is its scalability. This can nevertheless be partially overcome by discarding the full optimization of the feedback gain matrix, and rather relying upon pre-computed matrices, as discussed in Section 4.4; this is nevertheless not further considered in this dissertation.

6.4 Conclusion

This chapter investigates the potential added value of the SMPC^{ap} strategy, developed in this dissertation, for building climate control under combined additive and parametric uncertainty.

In a case study, the performance of the SMPC^{ap} strategy, in terms of thermal comfort violations and the specific thermal energy demand, is compared to that of the theoretical performance bound MPC strategy, the conventional deterministic MPC strategy and the state-of-the-art SMPC^a strategy only accounting for additive uncertainties. This is done by performing closed-loop simulations, where a building, controlled by one of these control strategies, is subject to perturbations due to (additive/parametric) uncertainty manifestations. The different control strategies are all aiming at guaranteeing thermal comfort while minimizing energy use during the first week of January 2016. To maximize insight, the analysis is repeated for different building realizations of the terraced, small, older (but renovated) dwelling, either equipped with radiators or with floor heating, for which the parametric uncertainty is derived in Chapter 5.

⁹ Recall that the consideration of radiators requires an additional state, as discussed in Section 5.1.

The results of the case study indicate that the enhanced uncertainty anticipation of the developed SMPC^{ap} strategy brings about improved thermal comfort compared to the current-practice deterministic MPC strategy and the state-of-the-art SMPC^a strategy, and this at the expense of a limited increase in energy use; for the considered cases, 90% of the thermal comfort improvement compared to the deterministic MPC can be attained with a relative increase of at most 9% in energy use, irrespective of the installed heat emission system.

The thermal comfort gains are most prominent in buildings equipped with floor heating and characterized by the combination of a large model uncertainty and a large nominal heat demand. Here, for the most extreme building realization in terms of model uncertainty and nominal heat demand (i.e., sample F), the thermal discomfort can be decreased from as much as 31.3 K h over an entire week down to 7.3 K h by simply switching from the SMPC^a to the SMPC^{ap} strategy (for a risk averseness level of 0.999). For buildings with a small nominal heat demand equipped with floor heating, on the other hand, the thermal comfort gains by switching to a stochastic approach (either an SMPC^a or an SMPC^{ap} strategy) are negligible.

Also for buildings equipped with radiators, both characterized by a small as well as a large nominal heat demand and/or model uncertainty, a thermal comfort improvement is possible, especially if the model uncertainty predominates the additive uncertainty. In this case, switching from an SMPC^a to an SMPC^{ap} strategy can induce a thermal discomfort reduction from 11.5 K h down to 2.1 K h for the most extreme building realization in terms of model uncertainty and nominal heat demand (i.e., sample F) (for a risk-averseness level of 0.999). Nevertheless, for all considered building realizations equipped with radiators, the SMPC^{ap} strategy is hampered to fully distinguish itself from the SMPC^a strategy, for three reasons, namely i) because of the small time constants associated with radiators, ii) because the stochastic OCP is re-solved for every subsequent time step, and iii) because the heat supply system has sufficient heating capacity available (due to the imposed safety factor of 1.5). These three aspects all limit the added value of a correct uncertainty anticipation, which is the most important asset of the SMPC^{ap} strategy.

Chapter 7

Towards integrated optimal control and design under uncertainty of a TCL in an individual building

RQ 4: Does the SMPC^{ap} strategy allow for obtaining a more appropriate, yet robust, sizing of the heating system when embedded in an IOCD approach?

This chapter is based on A. Uytterhoeven, R. Van Rompaey, K. Bruninx, and L. Helsen, "Chance Constrained Stochastic MPC for Building Climate Control Under Combined Parametric and Additive Uncertainty," submitted to Journal of Building Performance Simulation, July 2021.

This chapter aims to explore the potential of an IOCD approach and the added value of considering parametric and additive uncertainties therein when sizing the heat supply system. Similar to the previous chapter, Section 7.1 discusses the general set-up of the performance assessment. Section 7.2 subsequently sets up the case study used to evaluate the possible added value of an IOCD methodology incorporating the SMPC^{ap} strategy. Section 7.3 then covers the results of this case study, after which conclusions are drawn in Section 7.4.

7.1 Optimal design performance assessment method

Rather than setting up an IOCD approach by fully implementing a nested design-control optimization (as for example done by Jorissen [152] via a genetic algorithm optimization), which is out of scope of this work, the outer optimization loop steering the design decisions is replaced by a set of predetermined design scenarios, focusing on high-level decisions regarding the size of the heat supply system, as shown in Figure 7.1. Note that more detailed design choices, e.g., related to the heat emission system sizing and lay-out, cannot be considered here, since this information is not contained in the simplified controller model (in contrast to more detailed, high-order building models), as a consequence of the linearization and model order reduction.

For the lower-level control loop, the same MPC approaches are compared as for the optimal control performance assessment in Chapter 6, being the PBMPC, DMPC, SMPC^a and SMPC^{ap} approaches, all minimizing the overall energy use. As such, the description of the MPC implementation in Section 6.1 remains valid here; the only difference now is that the upper thermal power bound is no longer determined by the nominal heat demand of the reference building multiplied by a safety factor (i.e., in all cases except for the PBMPC strategy, where the nominal heat demand of the sampled SSM is simply used for the upper thermal power bound), but rather by the heat supply system size as imposed by the considered design scenarios. The PBMPC strategy, or any other open-loop deterministic alternative, can be considered as the current state-of-the-art in an IOCD context; it considers the dynamic system behavior in a predefined setting, for a postulated set of boundary conditions. Due to the negligence of uncertainties, this approach is likely to result in a too strictly (under)sized system. To correct for this, a closed-loop approach is considered¹, where the impact of the perturbations (either due to additive or due to parametric uncertainties) is taken into account. This can be considered as the dynamic equivalent of the safety factor used in static design methods. Here, both DMPC and SMPC strategies are looked at.

To assess and compare the suitability of the different control strategies to be used in an optimal design context (and to investigate the potential added value of using the SMPC^{ap} approach), the most appropriate heat supply system size for each of the four control strategies is determined via a simplified IOCD application, and subsequently compared, as follows. Given a particular installed thermal power (design decision), and a particular risk-averseness level regarding thermal comfort (control decision) ($1 - \epsilon = 0.5$ for the PBMPC and DMPC strategies, or $0.5 < 1 - \epsilon \leq 0.999$ for the SMPC^a and SMPC^{ap} strategies), the chosen MPC approach is applied in an

¹ For this assessment, historical forecasts and historical actual data should be used in a simulation-based setting.

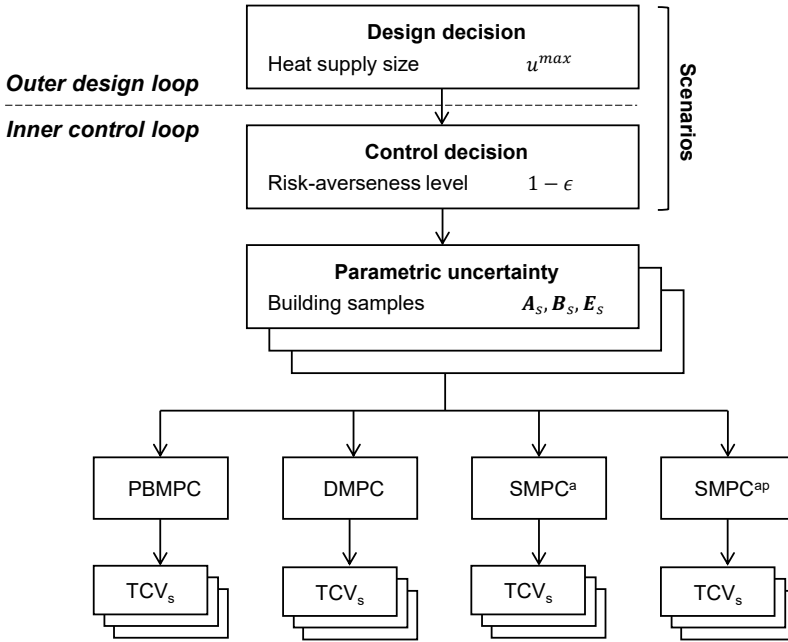


Figure 7.1: Schematic representation of the adopted procedure for the integrated optimal control and design, where the outer optimization loop steering the design decisions is replaced by a set of predetermined scenarios.

optimal control setting, after which the resulting thermal discomfort is determined in terms of TCV (see Equation (6.2) and Intermezzo 6.1). To account for the parametric uncertainty, this is repeated for different building samples (i.e., emulator models) of a particular dwelling with a given geometry, location and age, thereby acknowledging that in reality, the exact building sample is not known. As such, a thermal discomfort range, rather than one single value for the thermal discomfort, is obtained for this dwelling. This procedure is repeated for different heat supply sizes, and risk-averseness levels (as far as the SMPC approaches are concerned), thereby mimicking the functioning of a genetic algorithm [152], resulting in a whole set of thermal discomfort ranges, that can be used to make proper design decisions. For every MPC strategy, the heat production capacity is then selected that guarantees the lowest (preferably zero) thermal discomfort range for all considered building samples of a particular dwelling. The adopted procedure is summarized in Figure 7.1.

7.2 Case study

The thermal discomfort range resulting from the implementation of the different MPC strategies (i.e., the PBMPC, DMPC, SMPC^a or SMPC^{ap} strategy) for a specific dwelling, heat supply system size, and risk-averseness level regarding thermal comfort is again determined via closed-loop simulations. Ideally, the optimal control part should be run for a full year, or at least for a set of representative days, in order to make sure that the different operating regimes that the system might encounter, are sufficiently covered [71]. However, since this is only an exploratory case study, the evaluation is restricted to one day², where challenging weather conditions according to the Belgian climate apply. Here, the 18th of January 2016 is chosen, characterized by temperatures that are well below zero throughout the entire day. Apart from the different time period, altered weather conditions and upper thermal power bounds, the simulation set-up is equal to that of the first case study³, discussed in Section 6.2, in terms of the considered residential building (i.e., the terraced, small, older (but renovated) (T_S_O) dwelling, either equipped with radiators or floor heating, see Table 6.2), considered building samples (see Table 6.3) and considered occupant behavior.

7.3 Results and discussion

Figure 7.2 visualizes the thermal discomfort ranges to be used to make a design decision, resulting from the application of the PBMPC, DMPC, SMPC^a or SMPC^{ap} strategy to the T_S_O dwelling, either equipped with radiators (Figure 7.2a) or with floor heating (Figure 7.2b), during the 18th of January 2016, for different capacities of the heat supply system. Multiple observations can be made indicating the added value of using the SMPC^{ap} strategy for optimal design applications.

From Figure 7.2, it becomes clear that depending on the applied MPC strategy, a different heat supply system size will be chosen.

For the case with radiators, according to the PBMPC (which is the current state-of-the-art for IOCD applications), a heat supply system with a thermal power of 13 kW is able to guarantee thermal comfort for all building samples. However, this is a false promise; when taking into account the closed-loop impact of the uncertainties, by rather looking at the results of the DMPC strategy, it is clear that this system

² The closed-loop simulations are again preceded by an initialization procedure, where the starting values for the different states are determined by solving an OCP with cyclic boundary conditions for the states, for a prediction horizon of two days.

³ However, note that in this chapter, the case without uncertainty on the occupant behavior forecast is no longer considered.

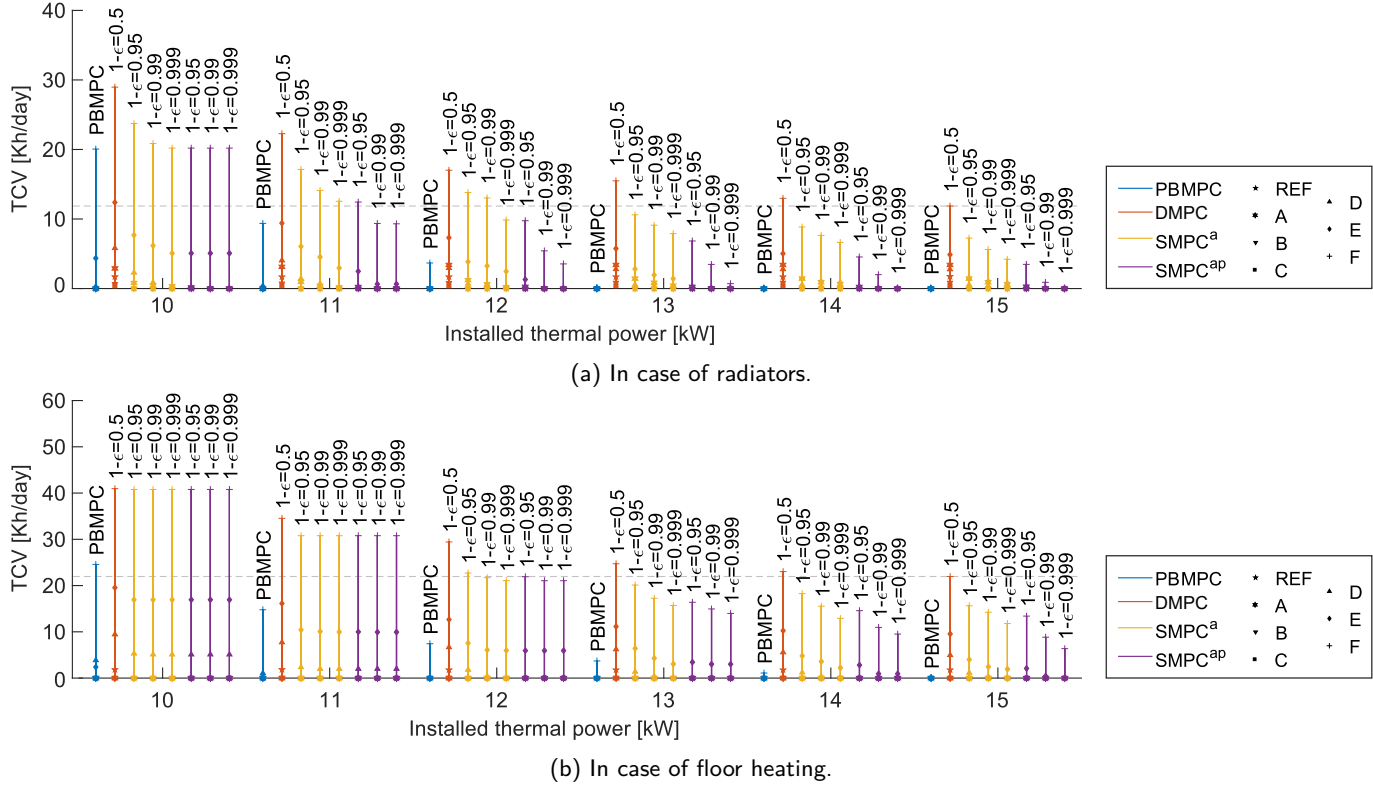


Figure 7.2: The thermal discomfort ranges showing the TCV for different possible realizations of the terraced, small, older (but renovated) building, as a function of the installed thermal power of the heat supply system, applied MPC strategy (i.e., the PBMPC, DMPC, SMPC^a or SMPC^{ap} strategy) and imposed risk averseness level.

size in reality leads to thermal discomfort. For the DMPC strategy, this thermal discomfort can be decreased, but evidently never eliminated⁴, by switching to a larger system size, where the design guaranteeing the lowest TCV is the largest considered size of 15 kW. When looking at the SMPC^a and SMPC^{ap} approaches, where the closed-loop impact of (part of) the uncertainties is not only taken into account, but also explicitly anticipated for, Figure 7.2 shows that these MPC strategies can further reduce the thermal discomfort, where the SMPC^{ap} strategy is even able to truly guarantee zero thermal discomfort for all building samples for a risk-averseness level $1 - \epsilon = 0.999$ and an installed thermal power of 14 kW, in contrast to the PB MPC, DMPC or SMPC^a strategy. Taking the thermal discomfort of the DMPC approach with a system size of 15 kW as a reference, indicated by the grey dashed horizontal line in Figure 7.2a, the same degree of thermal comfort can be achieved with a heat supply system size of 11-12 kW for the SMPC^a strategy, and of 10-11 kW for the SMPC^{ap} strategy, depending on the applied risk-averseness level⁵.

For the case with floor heating, similar observations can be made. Here, the SMPC^{ap} strategy is able to guarantee zero thermal discomfort for all building samples, except for sample F, for a risk-averseness level of $1 - \epsilon = 0.99$ and an installed thermal power of 15 kW. Again taking the thermal discomfort of the DMPC approach with a system size of 15 kW as a reference, the same degree of thermal discomfort only occurs at a system size of 11-12 kW for both the SMPC^a and SMPC^{ap} strategies, depending on the applied risk-averseness level.

The reason why the stochastic approaches are able to longer avoid thermal discomfort, is because of their fundamentally different operating principles compared to a deterministic approach. This is illustrated in Figures 7.3 and 7.4, showing the closed-loop indoor temperature profiles and heat input profiles realized by the DMPC, SMPC^a and SMPC^{ap} strategies during the 18th of January for sample E (chosen as an arbitrary example) of the terraced, small, older (but renovated) dwelling, either equipped with radiators (Figure 7.3) or floor heating (Figure 7.4), for different installed thermal powers of the heat supply system.

Figures 7.3 and 7.4 clearly show that the DMPC strategy does not anticipate⁶ for any uncertainty in its open-loop OCP, and hence waits until the last possible moment to start heating, to subsequently fully exploit the maximum available

⁴ Deterministic approaches do not hedge against uncertainty, making thermal discomfort due to closed-loop perturbations inevitable.

⁵ Similar thermal discomfort levels can be obtained for different combinations of system sizes and risk averseness levels (where the risk-averseness level is rather a control preference characteristic to the user), illustrating the interchangeability between control and design.

⁶ Note that the DMPC strategy in Figures 7.3 and 7.4 nonetheless shows a certain degree of anticipation. However, this anticipation has nothing to do with uncertainties, but is merely due to the fact that the decreasing installed thermal power becomes insufficient to deliver an instantaneous thermal power peak.

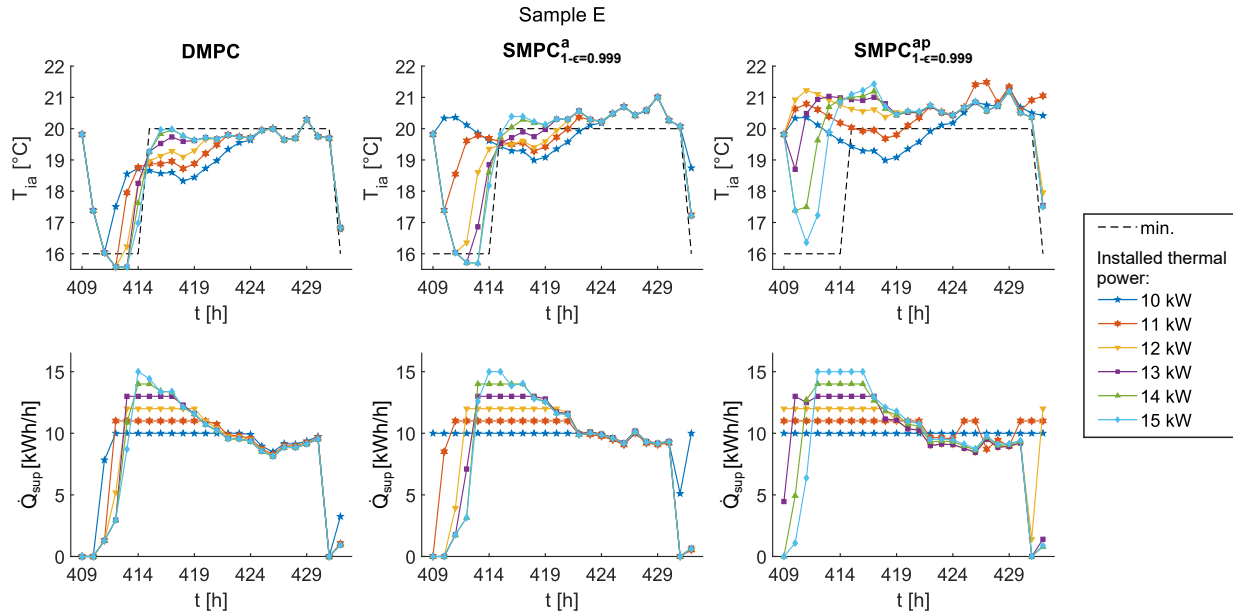


Figure 7.3: The closed-loop indoor temperature profiles and heat input profiles (averaged over one hour) realized by the DMPC, SMPC^a and SMPC^{ap} strategies during the 18th of January for sample E of the terraced, small, older (but renovated) dwelling equipped with radiators, for different installed thermal powers of the heat supply system.

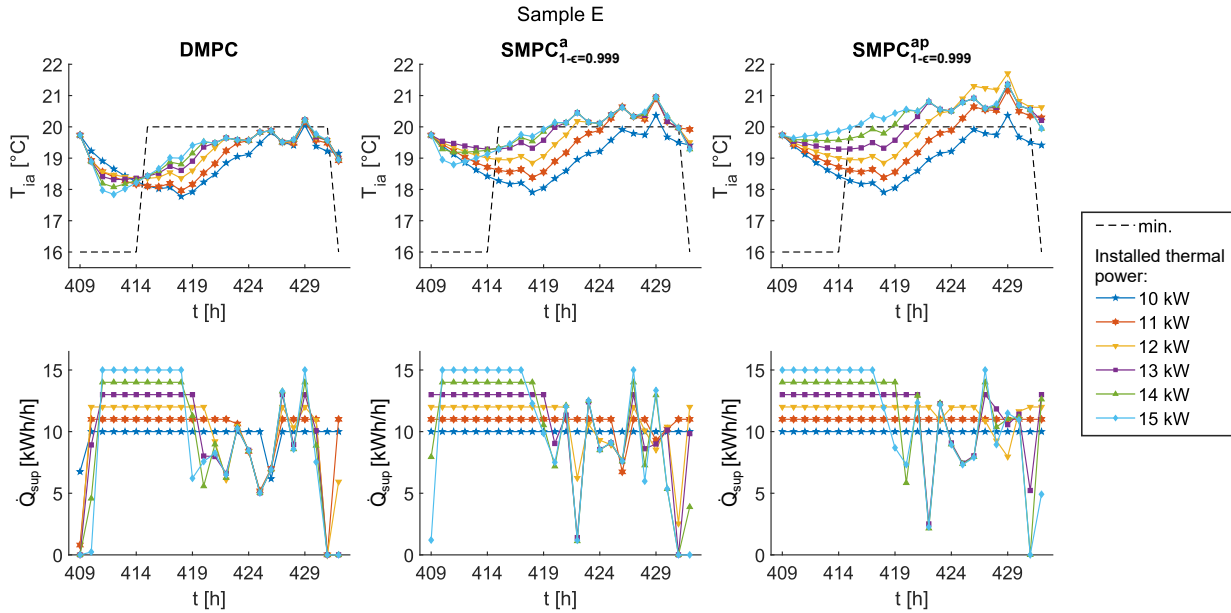


Figure 7.4: The closed-loop indoor temperature profiles and heat input profiles (averaged over one hour) realized by the DMPC, SMPC^a and SMPC^{ap} strategies during the 18th of January for sample E of the terraced, small, older (but renovated) dwelling equipped with floor heating, for different installed thermal powers of the heat supply system.

power. If the required real-time correction/additional heating thereupon exceeds the capacity of the heating system, thermal discomfort occurs. This effect (evidently) becomes more pronounced for smaller heat supply system sizes, for which the risk that the required real-time heating power exceeds the available capacity increases. This explains the need for larger system sizes in case of a DMPC strategy: to be able to correct for non-optimal control strategies, real-time flexibility is required in the form of spare capacity.

In contrast, SMPC approaches explicitly optimize both the anticipation for⁷ as well as the reaction against uncertainties (via ADF) in their open-loop OCP. As such, they deploy the available thermal power in a better way, as illustrated in more detail in Intermezzo 7.1. The pronounced anticipative behavior of the stochastic approaches, and of the SMPC^{ap} strategy in particular, can be clearly distinguished in Figures 7.3 and 7.4, especially for smaller heating capacities.

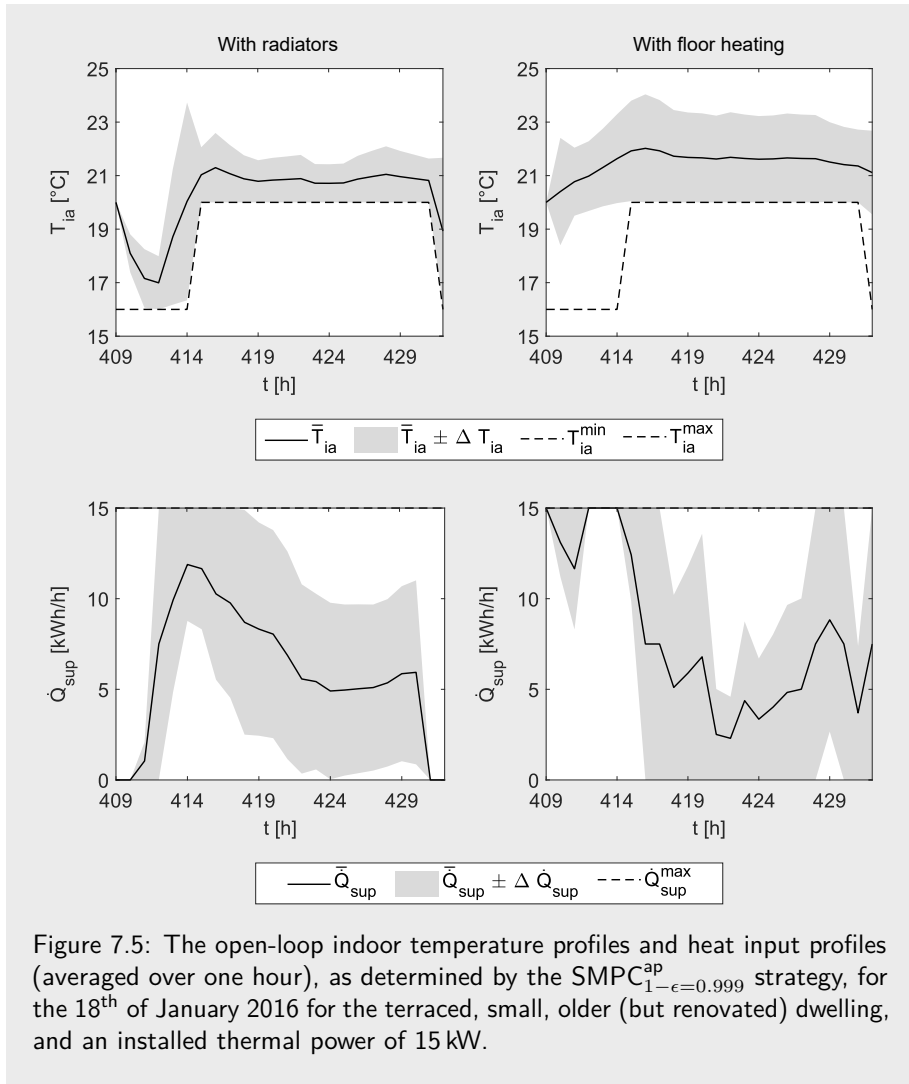
Intermezzo 7.1

The open-loop system behavior induced by SMPC strategies incorporating ADF

To better understand how SMPC strategies incorporating ADF are able to more appropriately deploy the available thermal power compared to a DMPC strategy, this intermezzo briefly explores in more detail the open-loop system behavior induced by such approaches. Where Figures 7.3 and 7.4 focus on the closed-loop system behavior, Figure 7.5 shows the corresponding optimized open-loop system behavior determined by the SMPC^{ap} strategy for the first time step of the receding horizon. Figure 7.5 clearly shows that due to the incorporation of ADF, the reaction against uncertainties is explicitly taken into account in the open-loop OCP. Indeed, the SMPC^{ap} strategy establishes an uncertainty band around the mean heat input profile (depicted by the grey shaded area in Figure 7.5), representing the possibly required real-time reactions against additive and/or parametric uncertainty manifestations. As such, it forces the mean heat input profile to stay further away from its upper bound, in order to make sure that there is still capacity available to accommodate real-time corrective actions.

A more detailed discussion of this induced system behavior, and of the interpretation of the uncertainty band, will be covered in Chapter 9.

⁷ This is done by increasing the temperature by operating the heating system at nominal capacity before the disturbance is expected to occur.



The above-mentioned observations confirm the assertion made during the discussion of the results of the optimal control performance assessment in Chapter 6, stating that the added value of the SMPC^{ap} strategy compared to the SMPC^{a} strategy depends on the required degree of anticipation, which is, among others, influenced by the available heating capacity. To more clearly show the impact of the heat supply system size on the differentiation between the SMPC^{a} and SMPC^{ap} strategies in case of radiators, the information depicted by Figure 7.2a is recast in Figure

7.6⁸, illustrating the TCV as a function of the installed thermal power for samples D, E and F; the choice of these specific samples is motivated by the fact that their nominal heat demand is exceeding the heat demand of the reference building. Figure 7.6 clearly shows that, because the SMPC^{ap} strategy is able to longer avoid thermal discomfort compared to the SMPC^a strategy, the difference in TCV between the two approaches becomes more pronounced for decreasing heating capacities, up to the point where also the SMPC^{ap} strategy is no longer able to guarantee thermal comfort. Figure 7.6 also clearly illustrates that the SMPC^a strategy is never able to fully eliminate thermal discomfort (in contrast to the SMPC^{ap} strategy); for an increasing capacity of the heat supply system, the TCV rather stagnates. Indeed, even when there is spare capacity available to react against uncertainty manifestations, a complete elimination of thermal discomfort can only be achieved by correctly hedging against uncertainty manifestations, prior to reacting to them. Finally, Figure 7.6 shows that this improved performance of the SMPC^{ap} strategy comes at the cost of a higher TED, due to the increased losses associated with the more pronounced anticipative behavior.

The final decision about the most appropriate design is a complex issue, depending on different (and possibly conflicting) factors, including: i) the user's and designer's preference regarding the level of thermal discomfort that is allowed (i.e., is it preferred to guarantee thermal comfort for all possible building realizations, or are certain building realizations - e.g., the most uncertain/extreme ones - rather disregarded when making a design decision?), ii) the desired level of controllability (i.e., oversizing a modulating heat pump might disable the modulation capability, leading to on/off behavior, in case the requested operation corresponds to the operating regime near/below the minimum modulation level), iii) the investment cost, determined by the heat supply system size, and iv) the operational cost, determined by the control choices (i.e., which MPC strategy, and which risk-averseness level). Especially the latter two aspects require a careful balancing, since a smaller heating capacity results in a smaller investment cost, but requires a control approach enforcing increased anticipative behavior, resulting in a higher energy use (which may increase operational costs). In analogy with the vision adopted for chance constrained optimal control, this whole sizing problem could be tackled via a chance constrained optimal design problem, by properly implementing an IOCD approach, where the investment costs and operational costs are weighed up under the consideration of a probabilistic guarantee of thermal comfort. Based on the auspicious results obtained in this exploratory case study, this is considered as a valuable future research track, that is out of scope of this dissertation.

⁸ To highlight the link with Figure 7.2, the same color code and symbols are used.

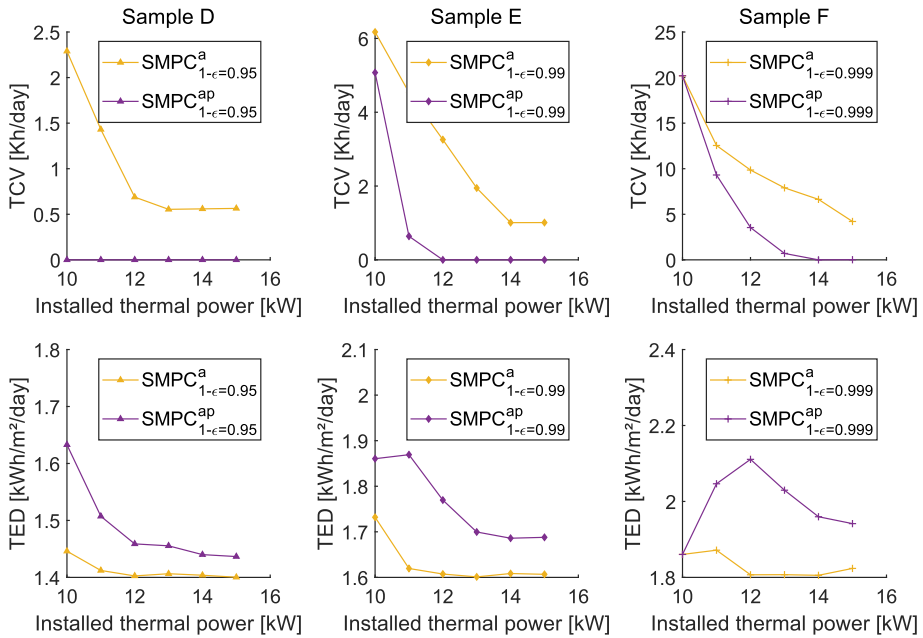


Figure 7.6: The differentiation between the control performance of the SMPC^a and SMPC^{ap} strategies in terms of TCV and TED as a function of the installed thermal power for samples D, E and F of the terraced, small, older (but renovated) building, equipped with radiators.

7.4 Conclusion

As a second MPC application domain, this chapter investigates the potential of IOCD approaches, and the added value of considering additive and parametric uncertainties therein.

Rather than fully implementing a nested design-control optimization, the outer optimization loop steering the design decisions is replaced by a set of predetermined design scenarios, focusing on high-level decisions about the size of the heat supply system. For the lower-level control loop, different MPC approaches are considered and compared. A first option is the current state-of-the-art open-loop performance bound MPC strategy. In addition, different closed-loop approaches are being considered, to account for the impact of uncertainties, including the deterministic MPC strategy, the SMPC^a strategy or the SMPC^a strategy. The different lower-level control strategies are all aiming at guaranteeing thermal comfort at minimal energy use under uncertainty during the 18th of January 2016; this day is chosen because

of the challenging weather conditions, characterized by temperatures that are well below zero throughout the entire day, which are decisive for the required heat supply system size. The analysis is again tailored to the terraced, small, older (but renovated) dwelling, for which the parametric uncertainty is derived in Chapter 5.

The case study shows that the current-practice open-loop performance bound MPC strategy results in a too strictly sized system, that is not able to guarantee thermal comfort under uncertainty. In contrast, the incorporation of the developed SMPC^{ap} strategy in an IOCD approach guarantees a robust sizing of the heat supply system, able to truly guarantee thermal comfort under combined additive and parametric uncertainty for (almost) all building possible realizations, if desired. Moreover, the SMPC^{ap} strategy also allows for a more appropriate system sizing (i.e., right-sizing the system, rather than over-/undersizing it), because of the capability of the SMPC^{ap} strategy to longer avoid a thermal comfort deterioration. When taking the thermal discomfort of a deterministic MPC approach combined with a heat supply system size of 15 kW as a reference, the SMPC^{ap} strategy allows for size reductions of 4-5 kW in case of radiators, and of 3-4 kW in case of floor heating, without increasing thermal discomfort.

Part III

SMPC assessment at system level

Chapter 8

The importance of system integration – The sense and nonsense in maximizing self-consumption with a HP-PV system in an individual building

This chapter is based on A. Uytterhoeven, A. Arteconi, and L. Helsen, "De digitale meter en warmtepompen. Verhoging zelfverbruik & gevolgen voor dimensionering (in Dutch)," presented at *General Assembly Meeting Flemish Heat Pump Platform, Kortenberg, Belgium, 24 May 2019*¹, and, A. Uytterhoeven, G. Deconinck, A. Arteconi, and L. Helsen, "The Added Value of Heat Pumps for Grid Stability via Demand Response," in *IEA Heat Pumping Technologies Magazine, vol 37, no2, August 2019*, Heat Pump Centre, 2019.

¹ The results presented here differ from the originally presented results, due to modifications made to the considered setting, and due to an improvement of the component model of the heat/cold supply system.

Up to now, this dissertation has mainly focused on the application of MPC for building climate control at building level. However, MPC can yet serve another purpose in a residential heating/cooling context, being the exploitation of demand side flexibility to aid the balancing between supply and demand. Given the rising share of intermittent (and hence less controllable) renewable energy sources in the energy supply, this aspect is becoming increasingly important. In this context, a popular approach is to use MPC to control residential heat pumps (HPs) such that they make maximum use of the electricity produced by locally installed solar photovoltaic (PV) panels. However, as this chapter will demonstrate, these kind of individual, isolated approaches can lead to non-optimal solutions from a system perspective. Rather than focusing on building level, the energy system should be considered as a whole, by taking into account the interaction between the supply and demand side. Hence, this chapter advocates the importance of system integration, thereby stressing the importance of the switch from a building-level perspective towards a system-level perspective in the last part of this dissertation.

First, Intermezzo 8.1 gives a short introduction about the exploitation of the demand side flexibility in a residential heating/cooling context, by using residential heat pumps coupled to thermal energy storage (TES) systems to balance the available supply and demand, and more particularly, to increase self-consumption of electricity locally produced by PV panels. Section 8.1 then proposes an assessment method that can be used to determine the maximally attainable self-consumption of residential HP-PV installations. Next, Section 8.2 sets up a case study, considering a typical Belgian residential building equipped with a PV installation and an air-to-water heat pump supplying space heating (SH), space cooling (SC) and domestic hot water (DHW). The aim of this case study is to quantify the realizable self-consumption, as well as to investigate how the heating system behavior is altered to accomplish this. The results of this case study, and the (un)reasonableness to aim for maximal self-consumption with residential HP-PV systems, are discussed in Section 8.3, after which conclusions are drawn in Section 8.4.

Before starting the discussion, it is important to stress that this chapter adopts a rather rudimentary point of view, in order to highlight (and even partly exaggerate) the potential issues regarding the use of HP-PV installations in a context where the main objective is to maximize self-consumption. To get a correct and profound view on the actual value of local PV production, a more nuanced approach is required, considering a more appropriate objective function, which correctly evaluates the cost and value of purchased and injected electricity at each moment in time (thus taking into account the link with the rest of the energy system).

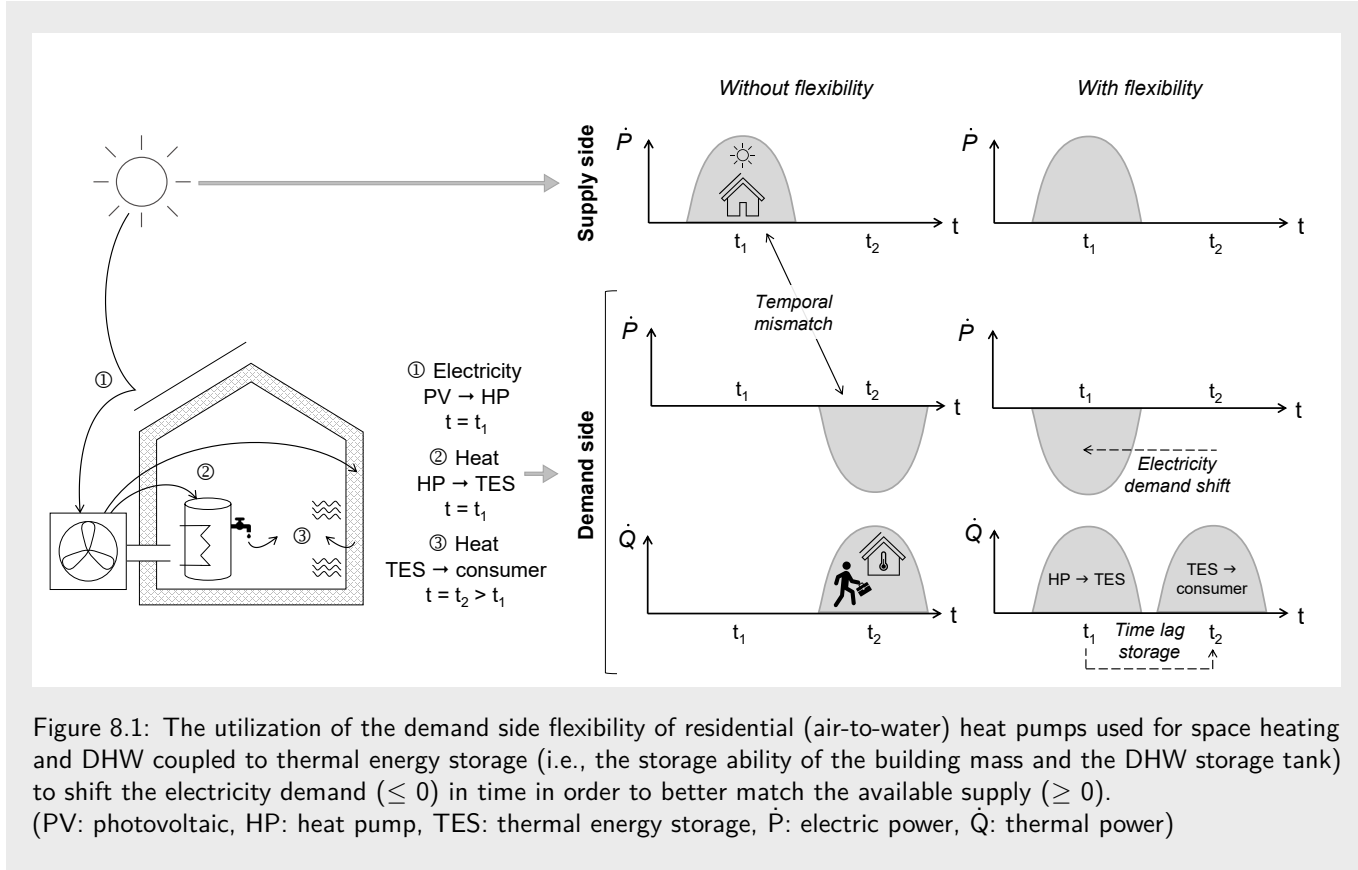
Intermezzo 8.1

Demand side flexibility of residential heat pumps coupled to TES

In the context of residential heating/cooling applications, where compression heat pumps are used for space heating, space cooling and DHW provision, the inherent flexibility offered by the thermal storage ability of the building mass, and by active storage devices if available, allows for a temporal decoupling of the thermal and electric power demand. This flexibility can be exploited to change the electricity demand in time and/or size in order to better match the available supply, without jeopardizing the requested thermal comfort. This concept is explained in Figure 8.1, for an illustrative case. In the situation depicted in Figure 8.1, the electricity generation provided by locally installed PV panels peaks at noon (t_1), when solar radiation is maximal. The heat demand for space heating and/or DHW, on the other hand, only occurs in the evening (t_2), when people get home from work. In the case without flexibility, this heat demand needs to be delivered (quasi-)^ainstantaneously by the heat pump, to avoid thermal discomfort. This results in a mismatch between the electricity generated by the PV panels at noon, and the electricity required by the heat pump in the evening. One possible way to cope with this, is the exploitation of demand side flexibility. By using the thermal storage ability of the building thermal mass and the DHW storage tank, the electricity demand can be shifted (advanced) towards noon, after which the heat is temporarily stored and subsequently delivered to the end consumer at a later point in time. As such, the balance between the supply of and demand for electricity is restored, and the requested heat demand is still being fulfilled.

The explanation above is focusing on local electricity generation by solar PV, which is the focus of this chapter, but it should be stressed that the same reasoning holds for any other form of local/central renewable/non-renewable electricity generation. As already mentioned, leveraging residential HP-PV installations to maximize self-consumption might in fact not be ideal, especially in heating dominated climates [18, 154], despite the fact that it is a popular set up in research (see e.g., [155, 156]), and that it is also encouraged in practice (e.g., due to the difference in injection and offtake tariffs). This non-optimality will be more profoundly illustrated below, with the help of a case study.

^a The time lag between the heat supply and heat emission is dependent on the time constant of the considered emission system, with radiators being characterized by significantly lower time constants (~ 15 min) than floor heating (multiple hours) [153].



8.1 Self-consumption assessment method

The aim of this section is to come up with an assessment method that can be used to determine the attainable self-consumption of HP-PV installations. One possible way to do this, is to consider a deterministic optimal control problem, which is a best-case assessment, resulting in a theoretical bound on the actually achievable self-consumption. The formulation of the considered OCP is an altered/extended version of the deterministic OCP formulation (2.1) described in Chapter 2, merely focusing on space heating. Indeed, to ensure nuanced and fair results, it is acknowledged in this particular chapter that heat pumps can not only provide space heating, but also space cooling and DHW. Neglecting the latter two aspects when assessing the attainable self-consumption would lead to an overly negative representation, due to the seasonal mismatch between the space heating demand and the PV electricity production.

To be able to cover the demand and supply of electricity as well as of space heating/cooling and DHW, supplementary component models are needed, in addition to the building model considered so far, which is the focus of the next sections. For each component model, a linear representation is being pursued. Although more complex, mixed-integer or non-linear problems might be more accurate representations of reality, they require significant computational effort. Moreover, non-linear problems can exhibit multiple local minima, thereby no longer guaranteeing global optimality, in contrast to linear (convex) problems [131, 157].

8.1.1 Objective function

The imposed objective function determining the optimal control actions should promote the maximal usage of the locally generated electricity by the solar PV. However, rather than simply maximizing the self-consumption, it is chosen to minimize the grid electricity demand, which is the difference between the total electricity demand $\dot{P}_{dem,k}$ and the self-consumption $\dot{P}_{pv,k}^{sco}$, as expressed by Equation (8.1). This objective not only tries to maximally exploit the PV electricity generation, but also fosters a rational energy use, especially when there is no locally produced electricity available. Note that an additional term penalizing thermal comfort violations is added, as explained in Section 2.2.

$$\min \sum_{k=1}^K (\dot{P}_{dem,k} - \dot{P}_{pv,k}^{sco}) \Delta t + (c^{CCV} \mathbf{1}_{n_x}^T) \mathbf{s}_k^{sh/sc} \quad (8.1)$$

8.1.2 Solar photovoltaic model

To account for the local electricity generation, a simplified PV model [158] is included, presented by Equation (8.2). This model converts the incident solar irradiance per unit surface area, $\dot{Q}_{soltilt,k}$, hitting a tilted PV panel with area A_{pv} at a time instance k , into electric power, $\dot{P}_{pv,k}$. The attainable electricity generation depends on the solar panel yield, η_{pv} , as well as on the performance ratio, PR_{pv} , accounting for all possible losses.

$$\dot{P}_{pv,k} = PR_{pv} A_{pv} \eta_{pv} \dot{Q}_{soltilt,k} \quad \forall k \quad (8.2)$$

The generated electricity can be either injected into the grid, $\dot{P}_{pv,k}^{gi}$, or used for self-consumption, $\dot{P}_{pv,k}^{sco}$, where the self-consumption cannot exceed the total local electricity demand, $\dot{P}_{dem,k}$. No curtailment is being considered.

$$\dot{P}_{pv,k} = \dot{P}_{pv,k}^{gi} + \dot{P}_{pv,k}^{sco} \quad \forall k \quad (8.3)$$

$$\dot{P}_{pv,k}^{sco} \leq \dot{P}_{dem,k} \quad \forall k \quad (8.4)$$

It should be stressed that the proposed PV model is a considerable simplification of reality, since the generated electricity also highly depends on the weather variables (not only solar irradiance, but also ambient temperature and local wind speed), and on material and system-dependent properties [159], which are not accounted for by Equation (8.2). However, this level of detail is not taken into account in this illustrative case study.

8.1.3 Heat/cold supply system model

Since the focus of this study is on the electric rather than on the thermal demand, a model of the electric heating/cooling supply system needs to be added, defining the local electricity demand, as well as the heat/cold supply. The heat/cold supply system is assumed to be a modulating air-to-water heat pump, assisted by a back-up electric resistance heater.

The heat pump is used to provide hot water for space heating and DHW purposes. Hot water temperatures up to a maximum temperature T_{hp}^{max} of 55 °C can be achieved, after which the heat pump performance significantly deteriorates² [160]. Besides, the heat pump can also provide cold water for cooling purposes, with

² An exception to this is the high temperature heat pump, which can achieve water temperatures up to 80 °C [131].

supply temperatures down to a minimum temperature T_{hp}^{min} of 18 °C, where this lower bound is imposed to prevent condensation issues.

The auxiliary electric resistance heater is mainly used for DHW purposes, to further heat up the water above T_{hp}^{max} , up to the maximum allowed temperature of the DHW tank, T_{tank}^{max} , typically 90 °C [131]. It also serves to assist the heat pump for space heating during very cold days. Indeed, to avoid oversizing of heat pumps³, the code of good practice in Belgium recommends to size heat pumps to meet 80% of the nominal heat demand⁴, \dot{Q}_{nom} , where the remainder of the peak demand is supposed to be covered by the auxiliary resistance heater, which is very seldom necessary [160].

The electric power consumed by the heat pump, $\dot{P}_{hp,k}^{sh/sc/dhw}$, and by the auxiliary resistance heater, $\dot{P}_{aux,k}^{sh/dhw}$, constitute the total local electricity demand, $\dot{P}_{dem,k}$, as expressed by Equation (8.5), thereby linking the PV model and the heat/cold supply system model.

$$\dot{P}_{dem,k} = (\dot{P}_{hp,k}^{sh} + \dot{P}_{hp,k}^{sc} + \dot{P}_{hp,k}^{dhw}) + (\dot{P}_{aux,k}^{sh} + \dot{P}_{aux,k}^{dhw}) \quad \forall k \quad (8.5)$$

The electricity demand, and the associated heat/cold supply, are further elaborated upon for each distinct technology in Sections 8.1.3.1 and 8.1.3.2.

8.1.3.1 Heat pump model

The heat pump model relates the consumed electric power, $\dot{P}_{hp,k}$, to the delivered thermal power, $\dot{Q}_{hp,k}$. Moreover, the technical system limits need to be accounted for, by including the maximum electric power input to the heat pump in the model.

With the help of the coefficient of performance ($COP = \frac{\dot{Q}_{hp}}{\dot{P}_{hp}}$), characterizing the heat pump efficiency, the attainable heat/cold supply of the heat pump can be determined as follows.

³ Oversizing of heat pumps should be avoided for multiple reasons. A smaller sizing compels the heat pump to operate over a longer time period, thereby avoiding large fluctuations in heat pump power and in supply water temperatures, leading to a better (part load) efficiency [157, 161]. Besides, regarding cooling, a more sustained operation of the heat pump over a longer period can better control the moisture level inside [162]. Finally, smaller heat pumps also have a lower investment cost [160].

⁴ The nominal heat demand is quantified following NBN EN 12831, considering an extremely cold day (according to the Belgian climate) with an outside temperature of -8 °C, a ground temperature of 10 °C, and an indoor temperature of 20 °C [137].

$$\dot{Q}_{hp,k}^{sh} = COP_k^{sh} \dot{P}_{hp,k}^{sh} \quad \forall k \quad (8.6)$$

$$\dot{Q}_{hp,k}^{sc} = COP_k^{sc} \dot{P}_{hp,k}^{sc} \quad \forall k \quad (8.7)$$

$$\dot{Q}_{hp,k}^{dhw} = COP_k^{dhw} \dot{P}_{hp,k}^{dhw} \quad \forall k \quad (8.8)$$

The COP of modulating heat pumps highly depends on the modulation, supply temperature and source temperature. However, this aspect is neglected in this dissertation. Moreover, also the dependency on the supply temperature is omitted, since the consideration of this influence would result in a non-linear, non-convex representation. Therefore, the supply temperature is assumed to be constant, and equal to its nominal value, T_{sup}^{nom} (i.e., 45 °C in case of radiator heating, 35 °C in case of underfloor heating, 18 °C in case of underfloor cooling, and 55 °C in case of DHW provision). Although this simplification is indispensable to guarantee linearity, it should be stressed that neglecting the dependency of the heat pump efficiency on the supply temperature leads to a control strategy that tends to concentrate the heat pump operation in certain time periods, as shown by Verhelst et al. [157]. This results in high actual supply temperatures, and hence, lower actual performance and increased energy costs. This problem could be overcome by penalizing power peaks, e.g., by considering the square of the predicted energy use/cost in the cost function. This manipulation is nevertheless not implemented, as the focus is on the maximization of self-consumption, thereby balancing (local) supply and demand, for which demand peaks might actually be desirable.

The resulting COP correlation is based on the work of Verhelst et al. [157], leading to a quadratic function of the ambient temperature, $T_{amb,k}$. This expression is extended with one additional term in this work, containing an arc tangent, in order to capture the efficiency drop of an air-coupled heat pump around 0 °C due to defrosting⁵, resulting in Equation (8.9). The coefficients a_i , listed in Table 8.1, are determined by fitting manufacturer data at full load [163]. The deviation of the fit from the data is at maximum 7.1%⁶.

$$COP_k = a_0 + a_1 T_{amb,k} + a_2 T_{sup}^{nom} + a_3 (T_{amb,k})^2 + a_4 (T_{sup}^{nom})^2 + a_5 T_{amb,k} T_{sup}^{nom} + a_6 \operatorname{atan}(T_{amb,k}) \quad \forall k \quad (8.9)$$

The COP obtained with the help of Equation (8.9) is subsequently averaged out over the considered prediction horizon, leading to a constant value. This manipulation is

⁵ At temperatures around 0 °C, the relative humidity of the ambient air is rather high. As a consequence of the low air temperature, ice is formed on the outdoor unit, which is highly undesirable. To remove this ice, the heat pump is temporarily operated in reverse mode, sending hot refrigerant to the outdoor unit in order to thaw it. As a consequence of this defrost cycle, the performance is negatively affected in this specific temperature window.

⁶ When omitting the arc tangent, the maximum relative error of the COP correlation increases to 9.6%

Table 8.1: The coefficients a_i and b_i of the fitted correlations for the COP (Equation (8.9)) and the maximum power input $\dot{P}_{hp,k}^{max}$ (Equation (8.10)) characterizing the performance of a modulating air-to-water heat pump. A distinction is made between the supply of heat, either for space heating (SH) or domestic hot water (DHW) purposes, and the supply of cold, for space cooling (SC) purposes.

The Daikin Altherma heat pump ERLQ008CV03, with a heating capacity between 3.24 kW and 13.81 kW, is used as a reference. The correlations for SH and DHW are valid for a (wet bulb) ambient temperature between -20°C and 20°C , and a supply water temperature between 30°C and 55°C ; the correlations for SC are valid for a (dry bulb) ambient temperature between 20°C and 43°C , and a supply water temperature between 7°C and 22°C .

To model heat pumps with a different heating capacity, the same COP correlation can be used; the correlation of the maximum power input, on the other hand, needs to be rescaled according to the heating capacity.

| | SH/DHW | SC | | SH/DHW | SC |
|-------|------------------------|------------------------|-------|------------------------|------------------------|
| a_0 | 6.76 | -3.27×10^1 | b_0 | 3.10×10^{-2} | 3.82×10^2 |
| a_1 | 1.74×10^{-1} | -1.68×10^{-1} | b_1 | -5.01×10^{-3} | 1.14 |
| a_2 | -1.36×10^{-1} | 8.33×10^{-2} | b_2 | 9.55×10^{-2} | -2.51×10^{-2} |
| a_3 | 6.44×10^{-4} | 1.25×10^{-3} | b_3 | 2.51×10^{-4} | -1.41×10^{-2} |
| a_4 | 9.22×10^{-4} | 1.99×10^{-3} | b_4 | -7.03×10^{-4} | -5.98×10^{-4} |
| a_5 | -1.93×10^{-3} | -1.01×10^{-3} | b_5 | -3.97×10^{-5} | 6.66×10^{-4} |
| a_6 | -4.97×10^{-2} | 2.50×10^1 | b_6 | 2.63×10^{-3} | -2.61×10^2 |

based on the findings of Patteeuw [131] and Verhelst et al. [157]. Patteeuw [131] illustrated that the simplified heat pump model using a constant, averaged COP, instead of a COP that is a function of the ambient temperature, guarantees a smaller deviation with respect to the results of the detailed physical emulator model, and improves computation time. Besides, in a case study presented by Verhelst et al. [157], a constant and linear COP formulation were shown to perform equally when considering an optimization towards minimal cost, whereas the constant COP formulation performed better when considering an optimization towards minimal energy use.

As a final intervention, in order to prohibit that the heat pump delivers specific services outside of the associated operating regions (i.e., no space heating for ambient temperatures larger than 20°C , and no space cooling for ambient temperatures smaller than 22°C [163]), the constant values of the COP (and of the maximum power input, see further) are reduced to zero for the time instances when the operating conditions are violated. This intervention might lead to situations where the COP is not entirely constant over the considered prediction horizon, especially during mid-season. Consequently, the heat pump operation might again be a bit

more concentrated in certain time periods, which negatively affects the performance. This is nevertheless deemed acceptable, since this intervention exactly prohibits the heat pump from operating in very unfavorable conditions, which would not benefit the heat pump performance either.

To model the maximum electric power input, $\dot{P}_{hp,k}^{max}$, a similar approach is pursued, leading to an additional correlation, as presented by Equation (8.10). The numerical values of the coefficients b_i can also be found in Table 8.1. The deviation of the fit from the data is at maximum 5.8%⁷.

$$\begin{aligned} \dot{P}_{hp,k}^{max} = & b_0 + b_1 T_{amb,k} + b_2 T_{sup}^{nom} + b_3 (T_{amb,k})^2 + b_4 (T_{sup}^{nom})^2 + \\ & b_5 T_{amb,k} T_{sup}^{nom} + b_6 atan(T_{amb,k}) \quad \forall k \end{aligned} \quad (8.10)$$

The maximum power input restricts the electricity demand of the heat pump to provide space heating, $\dot{P}_{hp,k}^{sh}$, or space cooling, $\dot{P}_{hp,k}^{sc}$, and/or DHW, $\dot{P}_{hp,k}^{dhw}$, as expressed by Equations (8.11) to (8.14). Note that, due to the dependency of the maximum electric power input on the supply water temperature, individual bounds are imposed on the power inputs for the different services, because of the different supply water temperatures associated with the supply of space heating, space cooling and DHW. Moreover, Equation (8.14) bounds the total power input. This intervention serves to impede simultaneity of different services to the best extent possible⁸; nevertheless, complete elimination of simultaneity can only be achieved at the expense of introducing binary variables, resulting in a mixed-integer problem. This is not considered in this dissertation for arguments of computational efficiency.

$$\dot{P}_{hp,k}^{sh} \leq \dot{P}_{hp,k}^{sh,max} \quad \forall k \quad (8.11)$$

$$\dot{P}_{hp,k}^{sc} \leq \dot{P}_{hp,k}^{sc,max} \quad \forall k \quad (8.12)$$

$$\dot{P}_{hp,k}^{dhw} \leq \dot{P}_{hp,k}^{dhw,max} \quad \forall k \quad (8.13)$$

$$\dot{P}_{hp,k}^{sh} + \dot{P}_{hp,k}^{sc} + \dot{P}_{hp,k}^{dhw} \leq \max(\dot{P}_{hp,k}^{sh,max}, \dot{P}_{hp,k}^{sc,max}, \dot{P}_{hp,k}^{dhw,max}) \quad \forall k \quad (8.14)$$

$$\dot{P}_{hp,k}^{sh}, \dot{P}_{hp,k}^{sc}, \dot{P}_{hp,k}^{dhw} \geq 0 \quad \forall k \quad (8.15)$$

⁷ When omitting the arc tangent, the maximum relative error of the maximum power input correlation increases to 8.1%

⁸ Note that the manipulation of the COP and maximum power input to avoid that the heat pump delivers services outside of the operating regions associated with these services also serves this purpose. However, this manipulation mainly prohibits simultaneous space heating and cooling. The simultaneity of heating/cooling on the one hand, and DHW provision on the other hand, cannot be avoided by this manipulation, as their respective operating regions overlap.

8.1.3.2 Auxiliary resistance heater model

In line with the heat pump model, the auxiliary resistance heater model needs to relate the consumed electric power, $\dot{P}_{aux,k}$, to the delivered thermal power, $\dot{Q}_{aux,k}$, and needs to specify the maximum electric power that can be consumed by the resistance heater.

With the help of the efficiency ($\eta_{aux} = \frac{\dot{Q}_{aux}}{\dot{P}_{aux}}$), the attainable heat supply of the electric resistance heater can be determined, as expressed by Equations (8.16) and (8.17). Based on the principle of conservation of energy, all incoming electric power needs to be converted into heat, leading to a conversion efficiency of 100%; in other words, for electric resistance heaters, the consumed electric power and delivered thermal power always coincide.

$$\dot{Q}_{aux,k}^{sh} = \eta_{aux} \dot{P}_{aux,k}^{sh} \stackrel{(\eta_{aux}=1)}{=} \dot{P}_{aux,k}^{sh} \quad \forall k \quad (8.16)$$

$$\dot{Q}_{aux,k}^{dhw} = \eta_{aux} \dot{P}_{aux,k}^{dhw} \stackrel{(\eta_{aux}=1)}{=} \dot{P}_{aux,k}^{dhw} \quad \forall k \quad (8.17)$$

Consequently, the maximum electric power input is determined by the thermal power output the auxiliary resistance heater is deemed to deliver.

Regarding space heating, the auxiliary resistance heater should be able to completely replace the heat pump on very cold days. Hence, it is sized to be able to cover the nominal heating demand, \dot{Q}_{nom} , as imposed by Equation (8.18).

Regarding DHW, the auxiliary resistance heater should be able to heat up the water, with density ρ and specific heat capacity c_p , contained in the (perfectly mixed) DHW storage tank with volume V_{tank} , from the cold water tap temperature, T_{tap}^{cold} , to the hot water tap temperature, T_{tap}^{hot} , in a reasonable time span, as expressed by Equation (8.19); the DHW heating time, Δt_{dhw} , is typically equal to 2 hours [161]. The final sizing of the auxiliary resistance heater is then determined by the maximum of these two requisites, as presented by Equation (8.20) [161].

$$\dot{P}_{aux}^{sh,max} = \dot{Q}_{aux}^{sh,max} = \dot{Q}_{nom} \quad (8.18)$$

$$\dot{P}_{aux}^{dhw,max} = \dot{Q}_{aux}^{dhw,max} = \rho c_p V_{tank} \frac{T_{tap}^{hot} - T_{tap}^{cold}}{\Delta t_{dhw}} \quad (8.19)$$

$$\dot{P}_{aux}^{max} = \dot{Q}_{aux}^{max} = \max(\dot{Q}_{aux}^{sh,max}, \dot{Q}_{aux}^{dhw,max}) \quad (8.20)$$

The sizing of the auxiliary resistance heater bounds its total electricity demand to provide space heating, $\dot{P}_{aux,k}^{sh}$, and/or DHW, $\dot{P}_{aux,k}^{dhw}$, as expressed by Equation (8.21).

$$\dot{P}_{aux,k}^{sh} + \dot{P}_{aux,k}^{dhw} \leq \dot{P}_{aux}^{max} \quad \forall k \quad (8.21)$$

$$\dot{P}_{aux,k}^{sh}, \dot{P}_{aux,k}^{dhw} \geq 0 \quad \forall k \quad (8.22)$$

Note that the efficiency and maximum electric power input of the auxiliary heater are independent of the supply water temperature and ambient temperature, and hence, always have the same value. Consequently, no individual bounds are imposed on the power inputs for the distinct services, in contrast to the heat pump model. (Equations (8.11) to (8.13)).

8.1.4 Building and heat/cold emission system model

In order to model the space heating/cooling demand, a building model, including a heat/cold emission system, needs to be considered, similar to what was already done in the rest of this dissertation. In this chapter, the considered heat/cold emission system is an underfloor heating system, as this heat/cold emission system allows for both space heating and cooling (in contrast to radiators).

The constraints of the generic deterministic OCP formulation (2.1) described in Chapter 2, focusing on the space heating demand, mostly still apply, and are repeated below as Equations (8.23) to (8.29). However, note that the constraint on the thermal power inputs (8.27) is slightly different from the original constraint (2.1e), in order to allow the thermal power inputs to take negative values to provide space cooling.

$$\mathbf{x}_{k+1}^{sh/sc} = \mathbf{A}^{sh/sc} \mathbf{x}_k^{sh/sc} + \mathbf{B}^{sh/sc} \mathbf{u}_k^{sh/sc} + \mathbf{E}^{sh/sc} \mathbf{d}_k^{sh/sc} \quad \forall k \quad (8.23)$$

$$\mathbf{x}_k^{sh/sc} + \mathbf{s}_k^{sh/sc} \geq \mathbf{x}_k^{sh/sc,min} \quad \forall k \quad (8.24)$$

$$\mathbf{x}_k^{sh/sc} - \mathbf{s}_k^{sh/sc} \leq \mathbf{x}_k^{sh/sc,max} \quad \forall k \quad (8.25)$$

$$\mathbf{s}_k^{sh/sc} \geq \mathbf{0}_{n_x} \quad \forall k \quad (8.26)$$

$$\mathbf{u}_k^{sh/sc,min} \leq \mathbf{u}_k^{sh/sc} \leq \mathbf{u}_k^{sh/sc,max} \quad \forall k \quad (8.27)$$

$$\mathbf{x}^{sh/sc}(0) = \mathbf{x}_0^{sh/sc} \quad (8.28)$$

$$\mathbf{u}^{sh/sc}(0) = \mathbf{u}_0^{sh/sc} \quad (8.29)$$

Another important modification in this particular chapter compared to the rest of this dissertation, is the consideration of a slightly more elaborate two-zones

nine-states building controller model⁹. This model structure was proposed by Reynders et al. [132] to model archetype buildings representing the Belgian residential building stock, based on the typology data obtained from the European TABULA-project [164, 165].

The two-zones nine-states model represents a residential dwelling with two zones, being a day zone (DZ), consisting of all rooms in which the occupants are active during the day, and a night zone (NZ), mainly consisting of bedrooms. The corresponding RC model structure is shown in Figure 8.2. The model set-up is analogous to the set-up described in Section 5.1, except for the explicit distinction between the two zones in the states, inputs and disturbances, as expressed by Equation (8.30).

$$\mathbf{x}_{k+1}^{sh/sc} = \mathbf{A}^{sh/sc} \mathbf{x}_k^{sh/sc} + \mathbf{B}^{sh/sc} \mathbf{u}_k^{sh/sc} + \mathbf{E}^{sh/sc} \mathbf{d}_k^{sh/sc} \quad \forall k$$

$$\text{with } \mathbf{x}_k^{sh/sc} = \begin{bmatrix} T_{ia,k}^{DZ} \\ T_{w,k}^{DZ} \\ T_{wi,k}^{DZ} \\ T_{f,k}^{DZ} \\ T_{f,k}^{DZ-NZ} \\ T_{ia,k}^{NZ} \\ T_{w,k}^{NZ} \\ T_{wi,k}^{NZ} \\ T_{f,k}^{NZ-DZ} \\ (T_{rad,k}^{DZ}) \\ (T_{rad,k}^{NZ}) \end{bmatrix}, \mathbf{u}_k^{sh/sc} = \begin{bmatrix} \dot{Q}_{sup,k}^{DZ} \\ \dot{Q}_{sup,k}^{NZ} \end{bmatrix}, \mathbf{d}_k^{sh/sc} = \begin{bmatrix} T_{amb,k} \\ T_{gr,k} \\ \dot{Q}_{solN,k} \\ \dot{Q}_{solE,k} \\ \dot{Q}_{solS,k} \\ \dot{Q}_{solW,k} \\ \dot{Q}_{int,k}^{DZ} \\ \dot{Q}_{int,k}^{NZ} \end{bmatrix} \quad (8.30)$$

Finally, since the heat/cold supply system is explicitly accounted for in this chapter, $\dot{Q}_{sup,k}^{DZ}$ and $\dot{Q}_{sup,k}^{NZ}$ can be further specified with the help of Equations (8.31) to (8.35), thereby linking the building and heat/cold emission system model to the heat/cold supply system model. The goal of the optimization problem is to decide how to distribute the heat/cold supply of the heat pump and auxiliary resistance heater over the two zones, as expressed by Equations (8.33) to (8.35).

⁹ The two-zones nine-states building model is the basis for the one-zone four-states building model, introduced in Section 5.1, and considered throughout the rest of this dissertation (except for Intermezzo 5.2, where the two-zones nine-states building controller model was already considered to determine the impact of the parametric uncertainty on the thermal energy demand for space heating). The reason for using the simpler one-zone model (derived from the two-zones model by applying model order reduction) is to ensure mathematical tractability when implementing the SMPC strategy, as explained in Section 5.1

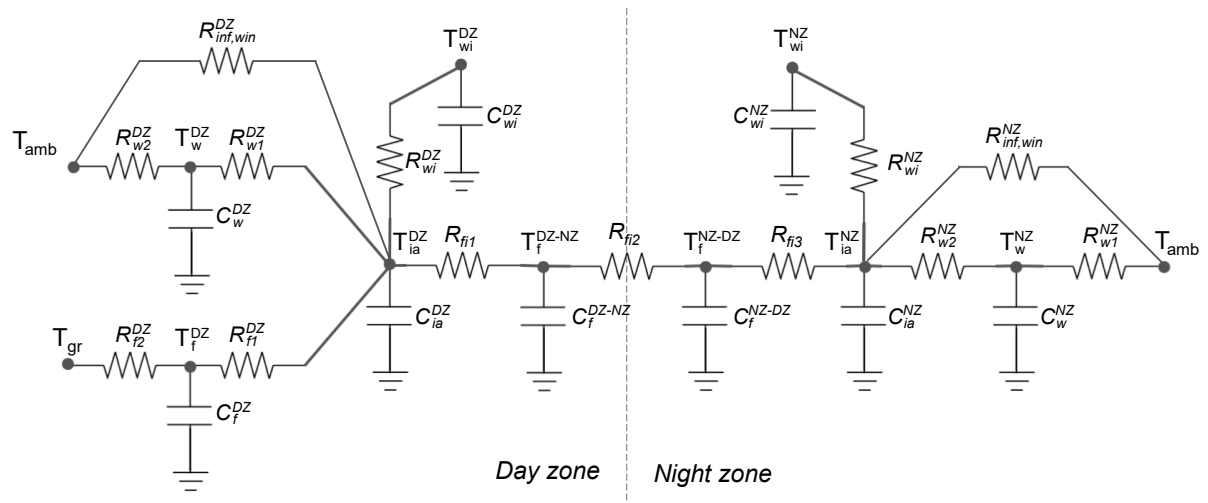


Figure 8.2: The model structure of the studied reduced order two-zone nine-states resistance-capacitance model, representing a residential dwelling as two zones (a day zone (DZ) and a night zone (NZ)). Note that the shown RC model merely focuses on the representation of the building envelope, without specifying the installed emission system; also the heat inputs coming from the solar heat gains and the internal heat gains, are not indicated. Adapted from [132].

$$\dot{Q}_{sup,k}^{DZ} = \dot{Q}_{hp,k}^{sh,DZ} + \dot{Q}_{aux,k}^{sh,DZ} - \dot{Q}_{hp,k}^{sc,DZ} \quad \forall k \quad (8.31)$$

$$\dot{Q}_{sup,k}^{NZ} = \dot{Q}_{hp,k}^{sh,NZ} + \dot{Q}_{aux,k}^{sh,NZ} - \dot{Q}_{hp,k}^{sc,NZ} \quad \forall k \quad (8.32)$$

$$\dot{Q}_{hp,k}^{sh} = \dot{Q}_{hp,k}^{sh,DZ} + \dot{Q}_{hp,k}^{sh,NZ} \quad \forall k \quad (8.33)$$

$$\dot{Q}_{hp,k}^{sc} = \dot{Q}_{hp,k}^{sc,DZ} + \dot{Q}_{hp,k}^{sc,NZ} \quad \forall k \quad (8.34)$$

$$\dot{Q}_{aux,k}^{sh} = \dot{Q}_{aux,k}^{sh,DZ} + \dot{Q}_{aux,k}^{sh,NZ} \quad \forall k \quad (8.35)$$

8.1.5 Domestic hot water storage tank model

In order to model the DHW demand, an additional energy balance for the DHW storage tank is added, as presented in discretized form by Equation (8.36) [131]. The tank, with volume V_{tank} , is assumed to be perfectly stirred, meaning that all water in the tank, with density ρ and specific heat capacity c_p , is at the same temperature $T_{tank,k}$ at a certain time instance k . During a time step Δt , the water in the tank is heated up by the heat supply $\dot{Q}_{sup,k}^{dhw}$, which is either supplied by a heat pump, or by an auxiliary resistance heater. Heat is extracted from the tank through the demand for hot water, $\dot{Q}_{dem,k}^{dhw}$, or through (conductive¹⁰) heat losses to the surroundings at a constant temperature T_{surr}^{dhw} .

$$\rho c_p V_{tank} \frac{T_{tank,k+1} - T_{tank,k}}{\Delta t} = \dot{Q}_{sup,k}^{dhw} - \dot{Q}_{dem,k}^{dhw} - UA_{tank} (T_{tank,k} - T_{surr}^{dhw}) \quad \forall k \quad (8.36)$$

Since the heat pump can only supply warm water up to a temperature T_{hp}^{max} of 55 °C, whereas the auxiliary resistance can heat the water up to the maximum allowed temperature of the DHW tank, T_{tank}^{max} , typically 90 °C, the energy balance is split up in two parts, represented by Equations (8.37) and (8.38). As such, a distinction is being made between the part of the tank temperature that is affected by the heat pump, $T_{tank,k}^{hp}$, and an additional temperature increase above 55 °C, merely realized by the auxiliary resistance heater, $dT_{tank,k}^{aux}$, as shown by Equation (8.39). Note that the auxiliary resistance heater can affect both the heat pump influenced temperature via $\dot{Q}_{aux1,k}^{dhw}$, as well as the auxiliary heater influenced temperature via $\dot{Q}_{aux2,k}^{dhw}$. The heat extracted from the tank to supply

¹⁰ The thermal resistance corresponding to the insulation layer of the DHW storage tank is the dominant resistance in the heat transfer process [131].

DHW to the end consumer also needs to be split up, leading to a heat extraction related to the heat pump influenced temperature via $\dot{Q}_{dem1,k}^{dhw}$, and one related to the auxiliary heater influenced temperature via $\dot{Q}_{dem2,k}^{dhw}$. Again, it is up to the optimization problem to decide on this allocation, as expressed by Equations (8.40) and (8.41) [131].

$$\rho c_p V_{tank} \frac{T_{tank,k+1}^{hp} - T_{tank,k}^{hp}}{\Delta t} = (\dot{Q}_{hp,k}^{dhw} + \dot{Q}_{aux1,k}^{dhw}) - \dot{Q}_{dem1,k}^{dhw} - UA_{tank} (T_{tank,k}^{hp} - T_{sur}^{dhw}) \quad \forall k \quad (8.37)$$

$$\rho c_p V_{tank} \frac{dT_{tank,k+1}^{aux} - dT_{tank,k}^{aux}}{\Delta t} = \dot{Q}_{aux2,k}^{dhw} - \dot{Q}_{dem2,k}^{dhw} - UA_{tank} (dT_{tank,k}^{aux}) \quad \forall k \quad (8.38)$$

$$T_{tank,k} = T_{tank,k}^{hp} + dT_{tank,k}^{aux} \quad \forall k \quad (8.39)$$

$$\dot{Q}_{dem,k}^{dhw} = \dot{Q}_{dem1,k}^{dhw} + \dot{Q}_{dem2,k}^{dhw} \quad \forall k \quad (8.40)$$

$$\dot{Q}_{aux,k}^{dhw} = \dot{Q}_{aux1,k}^{dhw} + \dot{Q}_{aux2,k}^{dhw} \quad \forall k \quad (8.41)$$

As already explained above, the temperatures $T_{tank,k}^{hp}$ and $dT_{tank,k}^{aux}$ are constrained by the maximum attainable hot water temperature by the heat pump, T_{hp}^{max} , and the maximum allowed tank temperature, T_{tank}^{max} , respectively, as expressed by Equations (8.42) and (8.43).

$$T_{tank,k}^{hp} \leq T_{hp}^{max} \quad \forall k \quad (8.42)$$

$$T_{hp}^{max} + dT_{tank,k}^{aux} \leq T_{tank}^{max} \quad \forall k \quad (8.43)$$

The tank temperature is also restricted by a lower bound, which is determined by the DHW demand. Indeed, given that this chapter considers a deterministic OCP formulation, the DHW demand is assumed to be perfectly known, and hence, can be used to derive temperature setpoints for the DHW tank¹¹, as follows. Since the tank is assumed to be perfectly mixed, the whole tank has to be heated up to at least the hot water tap temperature T_{tap}^{hot} , whenever there is a demand for DHW by the end consumer. On the other hand, whenever there is no DHW demand, the tank temperature is allowed to decrease down to the cold tap water temperature,

¹¹ The derivation of setpoints for the DHW tank temperature based on the DHW demand is a quite contrived intervention, as it is rather unlikely that the DHW demand can be accurately predicted, let alone be perfectly known, beforehand. The difficulty to come up with appropriate DHW demand forecasts is also the reason why the DHW supply is not considered in the remainder of this dissertation, when focusing on a stochastic, instead of a deterministic, setting.

T_{tap}^{cold} . This requirement is imposed by Equations (8.44) and (8.45), where $b_{dhw,k}^{dem}$ is a binary parameter, which is equal to one whenever DHW is requested, and zero otherwise [131]. Note that the hot and cold water temperatures are assumed to be constant, and equal to 50 °C and 10 °C, respectively.

$$T_{tank,k}^{min} = T_{tap}^{hot} b_{dhw,k}^{dem} + T_{tap}^{cold} (1 - b_{dhw,k}^{dem}) \quad (8.44)$$

$$T_{tank,k}^{min} \leq T_{tank,k} \quad \forall k \quad (8.45)$$

8.1.6 Resulting OCP formulation

The resulting deterministic OCP formulation, combining all component models introduced above, and used to assess the maximally attainable self-consumption with residential HP-PV systems, is summarized below. Note that a distinction is being made between expressions that do not contain any decision variables, and hence can be evaluated in a pre-processing step prior to solving the OCP, and actual constraints supplementing the OCP formulation.

Pre-processing (generating inputs):

- Solar PV model: (8.2)
- Heat pump model: (8.9) and (8.10)
- Auxiliary resistance heater model: (8.18) to (8.20)
- DHW storage tank model: (8.44)

Optimal control problem formulation:

- Objective function: (8.1)
- Independent decision variables:

$$\{\dot{P}_{pv,k}^{sco}\}_{k=0\dots K}, \{\mathbf{x}_k^{sh/sc}\}_{k=0\dots K}, \{\mathbf{s}_k^{sh/sc}\}_{k=0\dots K}, \{\dot{Q}_{hp,k}^{sh,DZ}\}_{k=0\dots K},$$

$$\{\dot{Q}_{hp,k}^{sh,NZ}\}_{k=0\dots K}, \{\dot{Q}_{hp,k}^{sc,DZ}\}_{k=0\dots K}, \{\dot{Q}_{hp,k}^{sc,NZ}\}_{k=0\dots K}, \{\dot{Q}_{aux,k}^{sh,DZ}\}_{k=0\dots K},$$

$$\{\dot{Q}_{aux,k}^{sh,NZ}\}_{k=0\dots K}, \{T_{tank,k}^{hp}\}_{k=0\dots K}, \{dT_{tank,k}^{aux}\}_{k=0\dots K}, \{\dot{Q}_{hp,k}^{dhw}\}_{k=0\dots K},$$

$$\{\dot{Q}_{aux1,k}^{dhw}\}_{k=0\dots K}, \{\dot{Q}_{aux2,k}^{dhw}\}_{k=0\dots K}, \{\dot{Q}_{dem1,k}^{dhw}\}_{k=0\dots K}, \{\dot{Q}_{dem2,k}^{dhw}\}_{k=0\dots K}$$
- Constraints:
 - Solar photovoltaic model: (8.3) and (8.4)
 - Heat/cold supply system model: (8.5)

- Heat pump model: (8.6) to (8.8) and (8.11) to (8.15)
- Auxiliary resistance heater model: (8.16), (8.17), (8.21) and (8.22)
- Building and heat/cold emission system model: (8.23) to (8.35)
- Domestic hot water storage tank model: (8.37) to (8.43) and (8.45)

8.2 Case study

To investigate the (un)reasonableness of maximizing the self-consumption of residential HP-PV systems coupled to TES, a case study is set-up. The case study considers a HP-PV installation installed in a typical Belgian residential building, for which the achievable self-consumption is determined by solving the deterministic open-loop OCP, described in Section 8.1, over an entire year¹², with an additional week for initialization purposes¹³. The optimization time step is equal to one hour.

The PV installation considered in this study is oriented southwards¹⁴, with a tilt angle of 35° [166,167,168,169]. The solar panels have a surface area of 1.6 m², and a peak power of 295 Wp. To maximize insight, different PV systems of increasing size are being considered, as summarized in Table 8.2¹⁵. The solar irradiance on the tilted PV panels is derived from historical weather data of the year 2017 provided by Darksy [170], with the help of processing code developed by Damien Picard.

The considered residential building is a typical Belgian, detached, single-family dwelling, built after 2005, as identified in the Tabula project [132,165]. The most important characteristics are summarized in Table 8.3. The building is assumed to be equipped with an underfloor heating/cooling system, supplied by an air-to-water heat pump¹⁶, which is sized to meet 80% of the nominal heat demand and is assisted by an auxiliary resistance heater, as explained in Section 8.1.3. The heating/cooling system is assumed to be ideal, with a perfect modulation. For the

¹² To ensure mathematical tractability, the full-year optimization is performed by considering consecutive weekly optimizations, with a receding horizon of 7 days, and a prediction horizon of 7.5 days (to impede end-of-horizon effects).

¹³ For the one-week initialization problem, cyclic boundary conditions are imposed.

¹⁴ The orientation of the PV panels is an important parameter affecting the attainable self-consumption. In the considered case study, a south-facing set-up is chosen, since this guarantees the highest total electricity generation. However, admittedly, from a building-level perspective, it might be better to opt for a combination of east- and west-facing panels, resulting in a smoothed generation curve with more production during the morning and evening hours (instead of a peak at noon), possibly better matching the time-dependent demand.

¹⁵ The upper bound restricting the considered capacity is very loosely based on [168].

¹⁶ Another possibility is the consideration of an air-to-air heat pump, which can also provide both space heating and cooling. However, since these systems more directly interact with the indoor air, they are less suited for flexibility purposes.

Table 8.2: The different considered sizes of the PV system, in terms of number of panels, total surface area and peak capacity, when assessing the attainable self-consumption with HP-PV systems.

| | Number of panels [-] | Total area [m ²] | Peak capacity [Wp] |
|------------|-------------------------|---------------------------------|-----------------------|
| Scenario 1 | 0 | 0 | 0 |
| Scenario 2 | 5 | 8 | 1475 |
| Scenario 3 | 10 | 16 | 2950 |
| Scenario 4 | 15 | 24 | 4425 |
| Scenario 5 | 20 | 32 | 5900 |

Table 8.3: The most important characteristics regarding construction year, geometry and thermal quality of the typical Belgian single-family dwelling for which the attainable self-consumption of the PV system, generating electricity to be used by an air-to-water heat pump providing space heating, cooling and DHW, is investigated.

| | |
|-------------------------------------|----------|
| Construction year [-] | >2005 |
| Detachment level [-] | Detached |
| Net floor area [m ²] | 269.6 |
| Protected volume [m ³] | 741.4 |
| Ground floor area [m ²] | 132.0 |
| Façade area [m ²] | 173.2 |
| Roof area [m ²] | 152.3 |
| UA building [W/K] | 312.6 |

weather data affecting the building indoor climate (i.e., ambient temperature and solar heat gains, see Equation (8.30)), Darksky data of the year 2017 are used [170]. For the occupancy behavior (i.e., internal heat gains and comfort requirements in terms of setpoint temperatures for different zones), StROBe profiles characterizing a four-persons-household, consisting of two full-time employed adults and two school-age children, are used [146]. The setpoint temperatures are used as a lower thermal comfort bound. The maximum allowed indoor temperature, on the other hand, is set to 26 °C [83].

Finally, the considered DHW tank is selected from the Vitocell 100V series of Viessmann. This type of storage tank contains an internal heat exchanger, and

hence, is suited to be combined with a heat pump [171]. The selected tank has a volume of 300 L and a UA-value of $1.53 \frac{\text{W}}{\text{K}}$ [172,173]. It is assumed to be located in an environment at a constant temperature of $15 \text{ }^\circ\text{C}$ ¹⁷. The DHW demand is obtained with the help of the StROBe toolbox [146], similar to the other occupancy-related parameters.

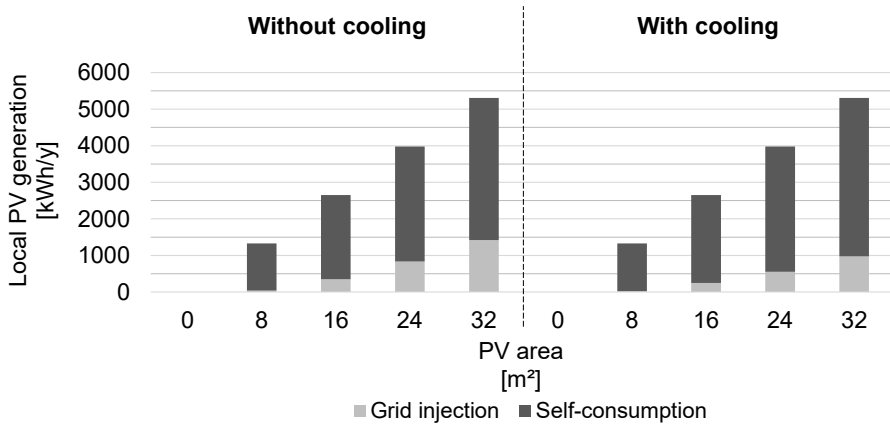
8.3 Results and discussion

The aim of this section is to gain insight in the realizable self-consumption for the case study described in Section 8.2, as well as in how the system behavior is altered to accomplish this. Recall that the assessment uses a deterministic optimal control problem approach, based on perfect disturbance predictions, aiming at the maximal exploitation of the locally available electricity, resulting in an ultimate best-case assessment of the attainable self-consumption. Hence, the emphasis is rather on the trends and insights, instead of on the exact numerical values. Besides, it is important to stress that the results are strictly related to the considered case study, and thus correspond to heating-dominated climate conditions, which highly influence the energy use profile as well as the PV generation profile. Finally, note that an explicit distinction is being made between the case without and with active cooling, as cooling is in general not implemented in Belgian households.

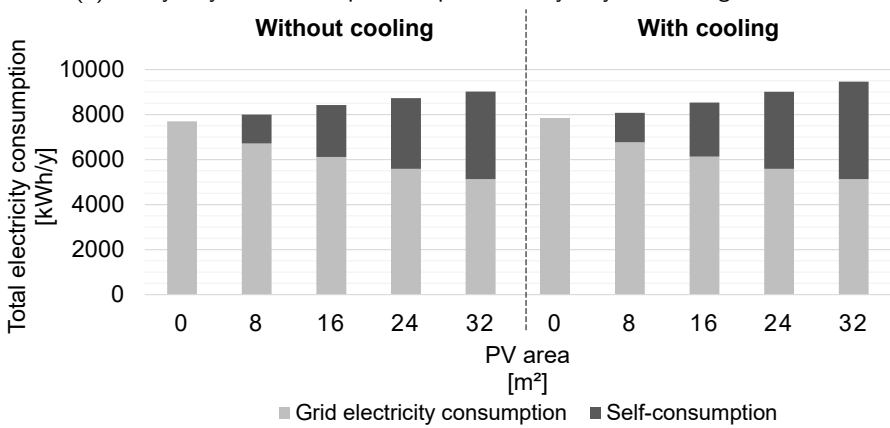
Figure 8.3 shows the share of the attainable self-consumption in the total local PV generation (i.e., adopting a supply perspective), as well as in the total local electricity consumption (i.e., adopting a demand perspective), for an increasing PV capacity, for a whole year. This information is merged in Figure 8.4 in relative terms. Note that the self-consumption relative to the local PV generation shown in Figure 8.4 is very high (amounting to 73.2% for the case without cooling and a PV area of 32 m^2 , and 81.6% for the equivalent case with cooling), due to the optimal control approach assuming perfect knowledge, striving for maximal exploitation of the locally available electricity; the exact impact of this approach will become more clear throughout the discussion below, when analyzing the system behavior in more detail.

When assessing the self-consumption from a supply perspective, Figure 8.3a shows that an increasing PV capacity elevates the self-consumption, but also increases the grid injection due to an oversupply, resulting in a decreasing share of the self-consumption relative to the PV generation in Figure 8.4. The increasing grid injection is less pronounced in the cases with cooling. Nevertheless, despite the higher level of self-consumption, the relative share with respect to the local generation is

¹⁷This is for example approximately the case when the DHW storage tank is located in the basement.



(a) The yearly self-consumption as part of the yearly local PV generation.



(b) The yearly self-consumption as part of the yearly total electricity consumption.

Figure 8.3: The attainable yearly self-consumption for a PV installation with increasing capacity, installed in a typical Belgian detached single-family dwelling equipped with an air-to-water heat pump. A distinction is being made between the case where the heat pump merely provides heat for space heating and DHW, and the case where the heat pump additionally provides active cooling.

still decreasing for increasing PV capacities, as can be seen in Figure 8.4. When assessing the self-consumption from a demand perspective, Figure 8.3b demonstrates that an increasing PV capacity results in a decreasing grid electricity consumption, as well as an increasing self-consumption. Interestingly, Figure 8.3b also indicates that the total electricity consumption is slightly increasing.

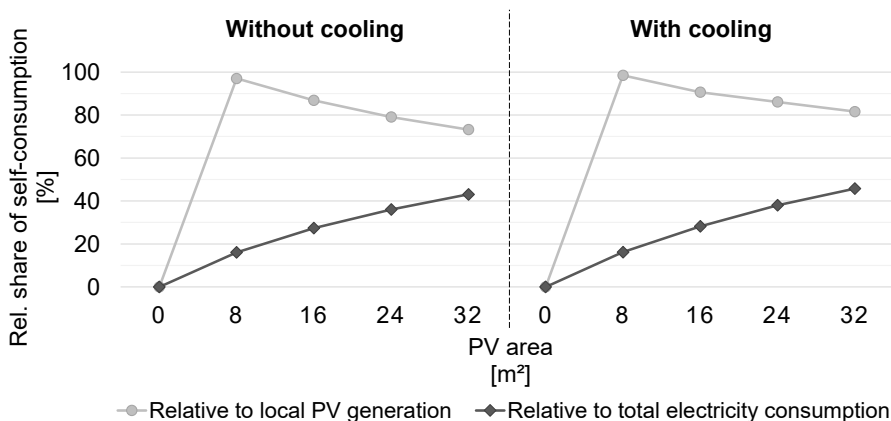


Figure 8.4: The attainable yearly self-consumption, relative to the yearly local PV generation and the yearly total electricity consumption, for a PV installation with increasing capacity, installed in a typical Belgian detached single-family dwelling equipped with an air-to-water heat pump. A distinction is being made between the case where the heat pump merely provides heat for space heating and DHW, and the case where the heat pump additionally provides active cooling.

To get more insight in the trends described above, Figures 8.5 and 8.6 assess the attainable self-consumption in more detail on a monthly basis, for the case without and with active cooling, respectively.

When again looking at the results from a supply perspective, Figures 8.5a and 8.6a show that in winter and mid-season, the locally generated electricity is (quasi) completely locally consumed for all considered cases. However, in summer, there is a clear oversupply, which already materializes for the smallest installed PV capacities for the case without cooling. For the case with cooling, the take-up of the locally generated electricity is slightly better, but is nevertheless not enough to avoid oversupply. This can be explained by the fact that the majority of the demand concerns space heating in winter, as also clearly demonstrated by Figure 8.7, showing the heat/cold supply by the heat pump and/or auxiliary resistance heater for the different end uses (i.e., space heating, space cooling and DHW). These results pinpoint that the underlying problem explaining the decreasing share of self-consumption relative to local PV generation is the seasonal mismatch between the PV electricity production and the demand, indicating the unsuitability of maximizing self-consumption with HP-PV systems.

The seasonal mismatch can also be clearly discerned in Figures 8.5b and 8.6b, assessing the attainable self-consumption on a monthly basis from a demand perspective. Both figures clearly show that in winter, the total electricity consumption is much higher than the available local PV generation. Consequently,

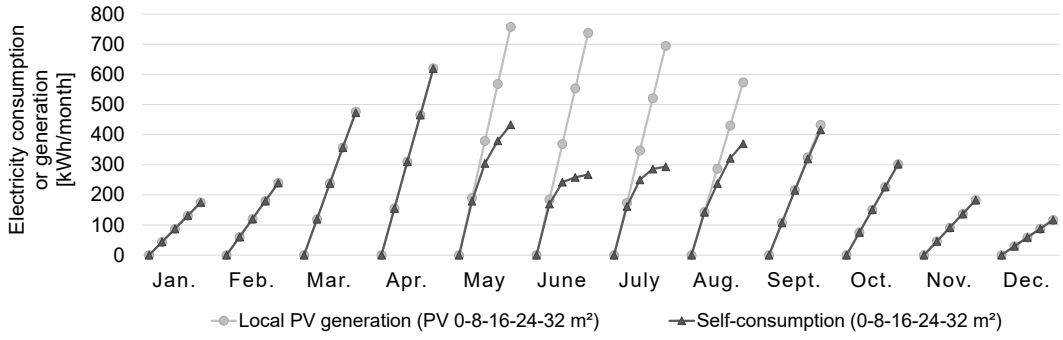
for increasing PV capacities, a part of the electricity requested from the grid is simply replaced by the locally generated electricity, without altering the total electricity demand. Hence, an increase in PV capacity unequivocally results in an increase in self-consumption, and a decrease in grid electricity consumption, substantiating, and already partly explaining, the trends observed in Figures 8.3b and 8.4. In mid-season, on the other hand, the local PV generation does not suffice to cover the demand, but the local supply and demand are nevertheless close together. For increasing PV capacities, the system is shown to be able to guarantee a higher self-consumption. As can also be seen in Figures 8.5b and 8.6b, this increased take-up of local generation goes along with an increase in total electricity demand. Finally, in summer, the electricity consumption can be completely covered by the local generation in most cases. Also here, the self-consumption, as well as the total electricity consumption, are rising for an increasing PV capacity. The observations for the mid-season and summer again confirm the trends observed in Figures 8.3b and 8.4.

Finally, to provide insight in how the increase in self-consumption in mid-season and summer is exactly achieved, and what is causing the increase in total electricity demand, Figures 8.8 and 8.9 show the detailed time-dependent system behavior throughout the day for a week during mid-season (13/03/2017-19/03/2017), and a week during summer (17/07/2017-23/07/2017), for the case with active cooling¹⁸. More specifically, Figures 8.8 and 8.9 depict the detailed time profiles of the indoor air temperature in the day zone, and of the DHW tank temperature, together with the associated heat/cold supply. Also relevant boundary conditions are shown, such as the ambient air temperature, serving as an indicator of the heating/cooling need¹⁹, and the incoming solar irradiance on a tilted surface, serving as an indicator of the availability of locally generated electricity. In order to be able to investigate how the system behavior is being altered to increase self-consumption, Figures 8.8 and 8.9 compare two cases, presented in different colors in the same plot. The first case (PV 0 m²) is the case where no PV is being installed, meaning that the controller simply aims to minimize the energy use, and as such, reflects the minimal needs of the system to guarantee thermal comfort (both in terms of indoor temperature and in terms of DHW temperature). The second case (PV 32 m²) is the case with the largest installed PV capacity, meaning that the controller aims to maximize the exploitation of the locally generated electricity.

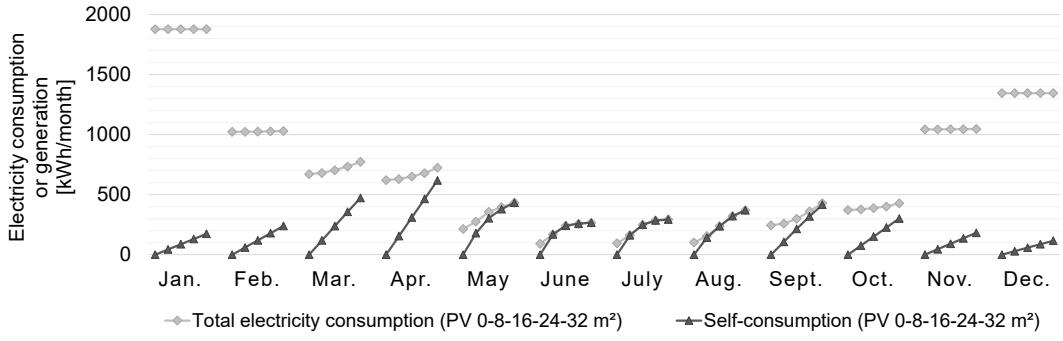
When comparing the results without and with PV for the considered week during mid-season, shown in Figure 8.8, we can see that the heat supply for space heating and for DHW (and hence, also the associated electricity consumption) is shifted for

¹⁸ The results for the case without active cooling are not shown, as they would not provide any additional insight.

¹⁹ The heating/cooling need is determined by many external factors, including the ambient temperature, the ground temperature, the solar heat gains, and the internal heat gains. However, in order not to overload the figures, not all of these factors are shown.

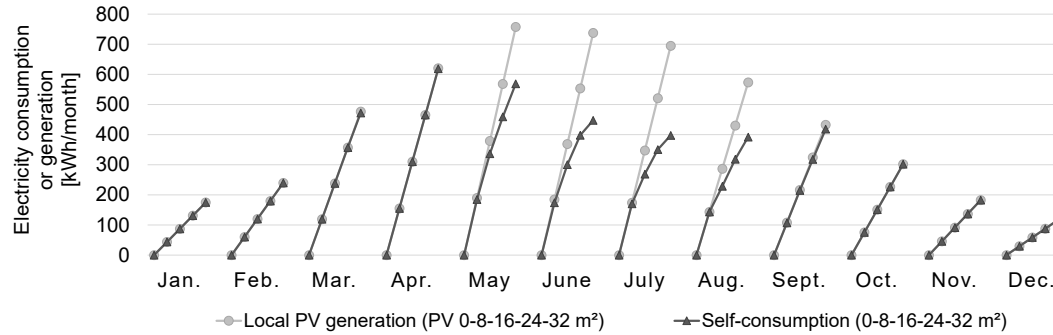


(a) The monthly self-consumption versus the monthly local PV generation.

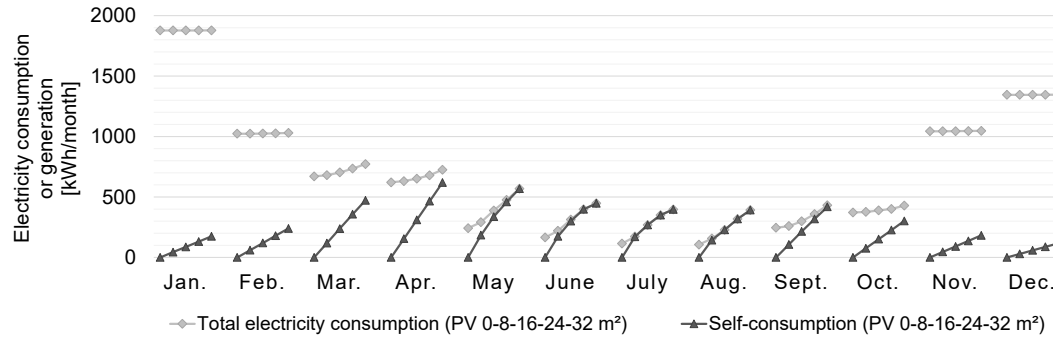


(b) The monthly self-consumption versus the monthly total electricity consumption.

Figure 8.5: The attainable monthly self-consumption for a PV installation with increasing capacity, installed in a typical Belgian detached single-family dwelling equipped with an air-to-water heat pump, for the case without active cooling.

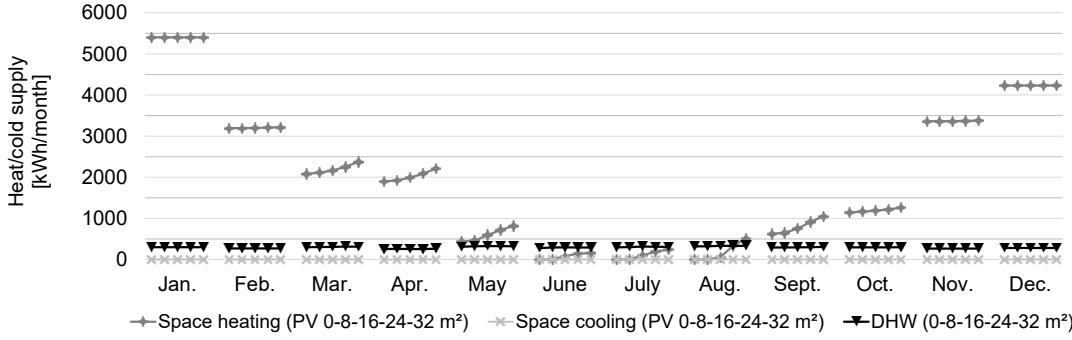


(a) The monthly self-consumption versus the monthly local PV generation.

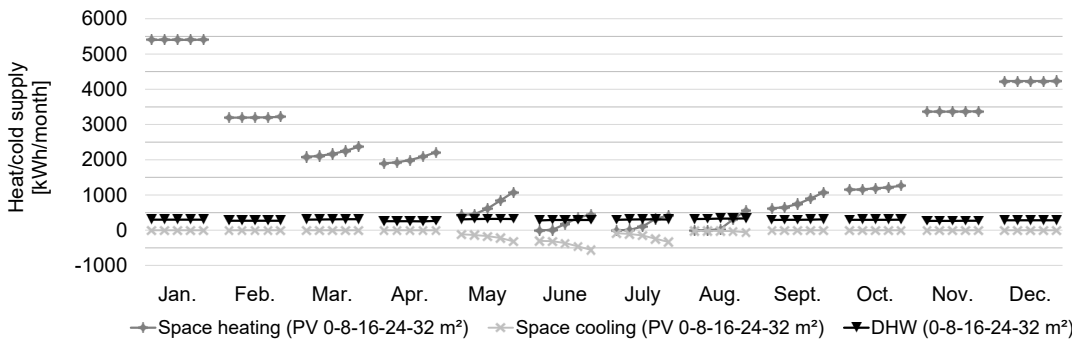


(b) The monthly self-consumption versus the monthly total electricity consumption.

Figure 8.6: The attainable monthly self-consumption for a PV installation with increasing capacity, installed in a typical Belgian detached single-family dwelling equipped with an air-to-water heat pump, for the case with active cooling.



(a) Without active cooling.



(b) With active cooling.

Figure 8.7: The heat/cold supply by the air-to-water heat pump and/or auxiliary resistance heater installed in a typical Belgian detached single-family dwelling.

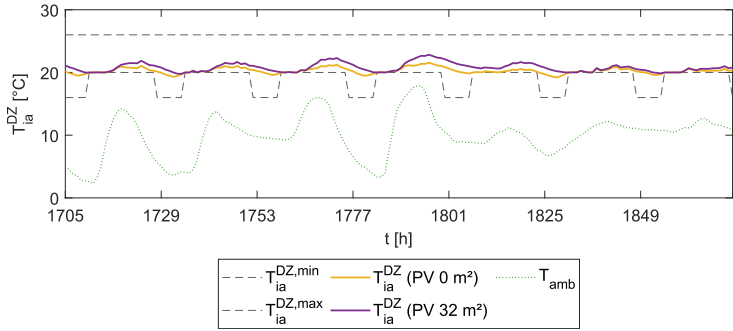
the case with PV to better match the solar irradiance, and thus, the local electricity generation. In other words, the demand profile is adapted to increase the self-consumption, by exploiting the flexibility offered by the building thermal mass and the DHW storage tank. This TES utilization results in momentary temperature increases, both for the indoor climate and the DHW tank. These elevated temperatures go along with increased storage losses, explaining the increased electricity consumption during mid-season.

Figure 8.9 shows the equivalent results for the summer week. Here, the heat/cold supply is not only shifted compared to the case without PV, but also significantly increased. In order to make as much use of the locally available PV generation as possible, even unnecessary measures are being implemented, such as heating during summer^{20,21}, needlessly pushing the indoor temperature towards the upper temperature bound by the end of the prediction horizon. Also the temperature of the DHW tank is now increased well above 55 °C, by activating the less efficient electric resistance heater, fed by locally generated PV electricity.

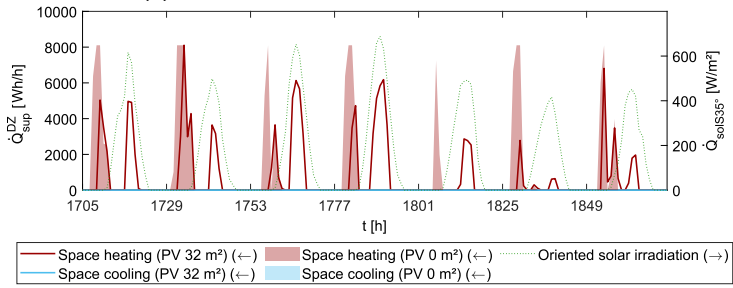
Summarizing, the increase in self-consumption, as well as the increase in total electricity consumption during mid-season and summer can be attributed to two effects, being the exploitation of demand side flexibility and the associated storage losses, as well as the additional unnecessary measures further using (and even spilling) the available electricity. Consequently, it should be stressed that the values in Figure 8.4 are definitely putting a gloss on the attainable self-consumption, in addition to the fact that the optimal control approach assuming perfect knowledge already results in a best-case assessment.

²⁰ Nevertheless, recall that space heating is only allowed for ambient temperatures up to 20 °C.

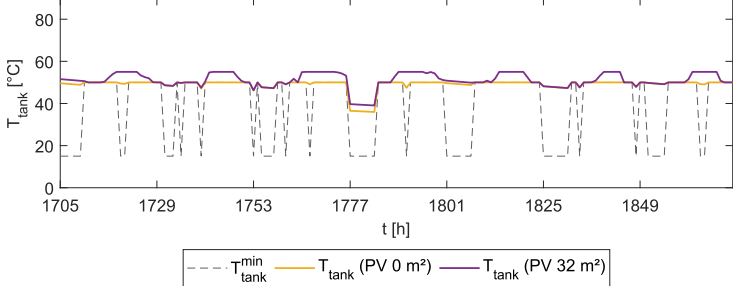
²¹ The paradoxical emergence of space heating during summer for increasing PV capacities is also clearly visible in Figure 8.7.



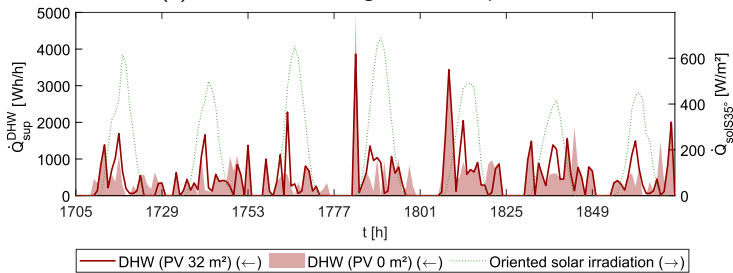
(a) The indoor temperature in the day zone.



(b) The heat/cold supply to the heat emission system in the day zone.

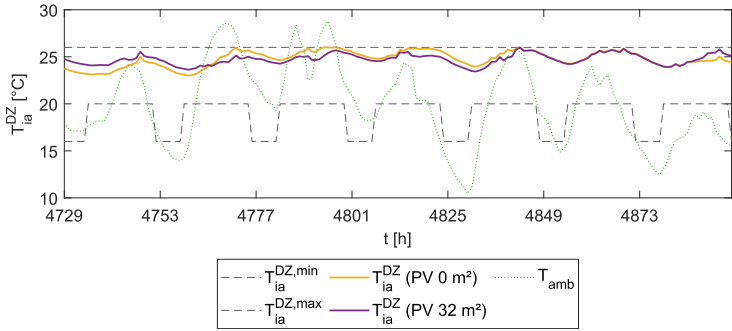


(c) The DHW storage tank temperature.

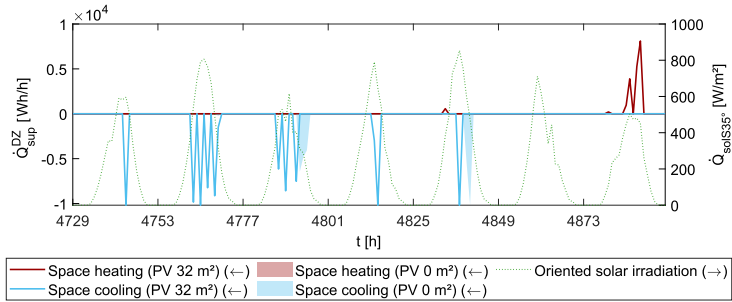


(d) The heat supply to the DHW storage tank.

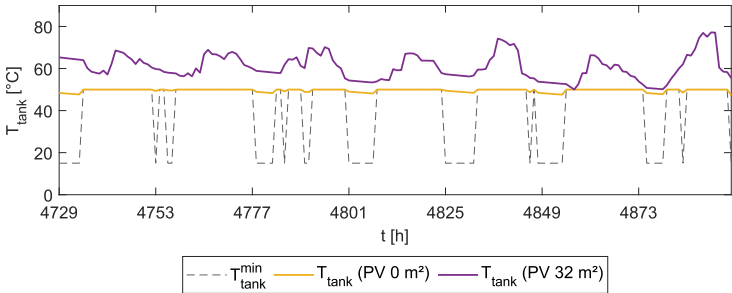
Figure 8.8: The detailed time-dependent system behavior of the HP-PV system installed in a typical Belgian detached single-family dwelling, during a week in mid-season (13/03/2017-19/03/2017), for the case with active cooling.



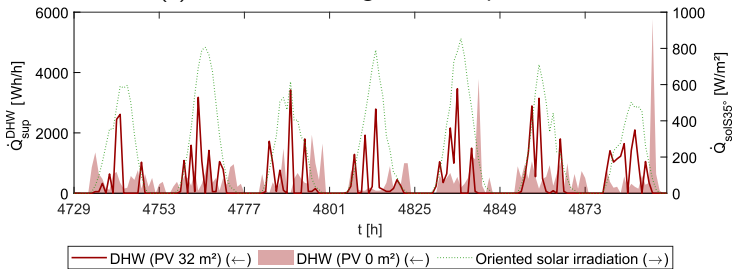
(a) The indoor temperature in the day zone.



(b) The heat/cold supply to the heat emission system in the day zone.



(c) The DHW storage tank temperature.



(d) The heat supply to the DHW storage tank.

Figure 8.9: The detailed time-dependent system behavior of the HP-PV system installed in a typical Belgian detached single-family dwelling, during a week in summer (17/07/2017-23/07/2017), for the case with active cooling.

8.4 Conclusion

After having merely focused on the application of MPC for individual building climate control, this chapter moves to another application domain of MPC in buildings, being the exploitation of demand side flexibility to aid the balancing between supply and demand.

In this context, a popular approach is to use MPC to maximize the self-consumption of residential HP-PV systems coupled to thermal energy storage. The main aim of this chapter is to investigate the (un)reasonableness of such individual, isolated approaches. To this end, an assessment method is proposed to evaluate the attainable self-consumption, and the associated dynamic system behavior, with the help of a deterministic optimal control problem. This method is applied to a case study, considering a typical Belgian detached residential single-family home, built after 2005, equipped with an air-to-water heat pump that provides heat/cold to the underfloor heating/cooling system, and supplies DHW to a storage tank. To maximize insight, the attainable self-consumption is determined for different PV capacities. Additionally, a distinction is made between the case without and with active cooling.

A detailed analysis of the results of the case study, on a yearly, monthly and daily basis, leads to multiple observations demonstrating the impracticality of individually optimizing residential HP-PV systems, aiming at a maximal usage of the locally generated electricity. A first important observed problem is the seasonal mismatch between the solar availability and the demand, which predominantly concerns space heating. Hence, in summer, there is a clear oversupply, for which the end-use is not being considered. Besides, in winter, there is a large residual demand, which is currently not being optimized to match the available supply at grid level, leaving the demand side flexibility untapped. In addition, the analysis also reveals that maximizing the self-consumption ultimately leads to a waste of energy, especially in mid-season and summer, for which other useful applications (e.g., cooling dominated buildings) might exist when considering the larger energy system, and thus results in a non-optimal exploitation of the available electricity generation.

These insights substantiate the switch from a building-level perspective towards a system-level perspective, properly accounting for the interaction between supply and demand, which is the focus of the last part of this dissertation.

Chapter 9

Optimal collective control under uncertainty of TCLs in a group of buildings

RQ 5: How does the proposed SMPC^{ap} strategy alter the demand profile, and how can this altered demand profile be coordinated for the benefit of the central energy system?

This chapter is based on A. Uytterhoeven, R. Van Rompaey, K. Bruninx, and L. Helsen, “Distributed Optimization of the Stochastic Load of Residential Heat Pumps for Demand Response,” in progress, to be submitted to Applied Energy.

The aim of this chapter is to assess the added value of the proposed SMPC^{ap} strategy for DR under additive (disturbance forecast) and parametric (model) uncertainty, and to investigate how the response of a group of TCLs, each controlled by the SMPC^{ap} strategy, can be coordinated for the benefit of the central energy system. As such, the focus in this chapter is shifted from the building-level perspective, where the main concern was thermal comfort, towards the system-level perspective, where the detailed demand profiles provoked by the SMPC^{ap} strategy become of prime importance, since they need to be balanced by the available supply. Therefore, Section 9.1 first investigates in more detail the impact of the SMPC^{ap} strategy on the resulting demand profile for an individual building, and which opportunities this presents. Section 9.2 discusses the adopted method to evaluate the added value of the proposed SMPC^{ap} strategy for DR under uncertainty. More particularly, an

integrated system-level optimization problem is set up, linking the demand side with the supply side, to investigate in detail whether the day-ahead coordination of the particular demand profile induced by the SMPC^{ap} strategy can benefit the central energy system. The analysis considers an electrification scenario of the residential heating sector, where the demand side is constituted by a set of residential buildings equipped with compression heat pumps for space heating (thus neglecting DHW production), and the supply side is constituted by electricity generating facilities. Section 9.3 sets up a case study used to evaluate the attainable benefits. The results of this case study are discussed in Section 9.4. Finally, the most important conclusions are summarized in Section 9.5.

9.1 Demand profile induced by the SMPC^{ap} strategy

When deriving the stochastic OCP formulation in Chapter 4, ADF was incorporated in the open-loop OCP in order to reduce conservatism of the SMPC^{ap} strategy. This particular intervention fundamentally impacts the resulting control strategy and associated demand profiles, which will be analyzed in detail in this section¹.

The impact of incorporating ADF is clearly illustrated in Figure 9.1, showing the stochastic open-loop indoor temperature profiles and heat input profiles induced by the SMPC^{ap} strategy developed in this dissertation which incorporates ADF (right hand side of Figure 9.1), and an equivalent strategy without ADF (left hand side of Figure 9.1), for an illustrative example. More particularly, the results correspond to an open-loop energy use minimization for the terraced, small, older (but renovated) dwelling equipped with radiators, inhabited by a four-persons-household consisting of two full-time employed adults and two school-age children, during the 18th of January 2016, for a risk-averseness level regarding thermal comfort of $1 - \epsilon = 0.99$.

The plots on the left hand side of Figure 9.1 clearly demonstrate the conservative system behavior when omitting ADF, caused by prohibiting the closed-loop feedback aspect of MPC (meaning that all uncertainty needs to be managed at building level, as also discussed in Section 3.3). In this case, the uncertainty on the indoor air temperature is steadily growing as time proceeds, due to the accumulative effect of the additive and/or parametric uncertainties over the whole prediction horizon. This growing uncertainty results in an increasing constraint tightening level (see Equations (4.15) and (4.16)), which requires the mean indoor temperature $\bar{T}_{i,a,k}$ to be progressively pushed further away from the lower bound, resulting in a rather high thermal energy demand.

¹ Recall that this was already briefly touched upon in Intermezzo 7.1.

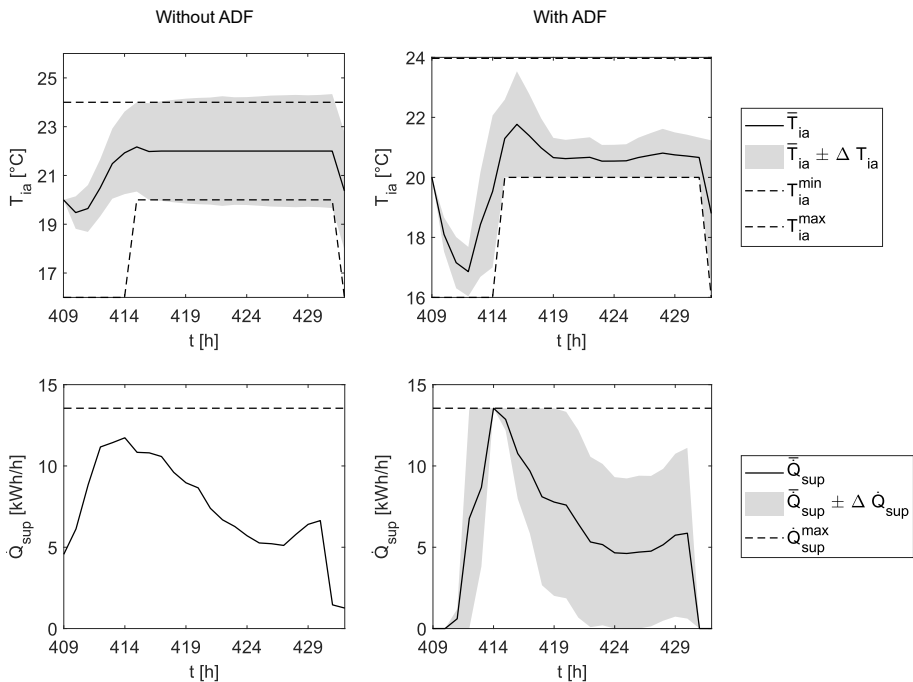


Figure 9.1: The impact of incorporating ADF in SMPC on the open-loop indoor temperature profile and heat input profile (averaged over one hour) realized by an SMPC_{1- ϵ =0.99}^{ap} strategy, aiming to minimize energy use during the 18th of January for the terraced, small, older (but renovated) dwelling equipped with radiators.

When incorporating ADF, on the other hand, the time profiles of both the indoor temperature and the heat input, shown on the right hand side of Figure 9.1, differ significantly from their equivalent profiles on the left hand side, which can be explained as follows. In order to account for the closed-loop feedback aspect of MPC in the open-loop control problem, intermediate reactions against the additive and/or parametric uncertainties are enabled by ADF (meaning that the load uncertainty needs to be (partly/completely) managed at system level, as also discussed in Section 3.3). This is achieved by reformulating the control inputs as an affine function of the preceding perturbations with the help of the feedback gain matrix \mathbf{T}_u (see Equation (4.17)), serving as an additional optimization variable in case ADF is incorporated. This enables a reduction of the uncertainty on the system states (see Equation (4.20)), explaining the reduced conservativeness of this approach. Since the actually required corrective action depends on how severely the additive and/or parametric uncertainties manifest themselves in real time, which is not known beforehand, the heat input now also becomes a stochastic variable

(in contrast to the case without ADF), represented by a mean value $\bar{Q}_{sup,k}$, and a variance $\Sigma_{\dot{Q}_{sup,k}}$ at each time step k , which can be interpreted as follows. The time profile established by the mean values $\{\bar{Q}_{sup,k}\}_{k=0\dots K}$ should be viewed as the heat supply profile sustaining the optimized mean/reference indoor air temperature profile $\{\bar{T}_{ia,k}\}_{k=1\dots K+1}$. The variance $\Sigma_{\dot{Q}_{sup,k}}$ at each time step k , on the other hand, characterizes the distribution of the possibly required real-time reaction against additive and/or parametric uncertainties that actually manifest themselves during $t = [0, k - 1]$ in real time, in order to bring the perturbed temperature each time back to its reference profile at time step $k + 1$.

Note that in Figure 9.1, and in all subsequent figures that will follow throughout this chapter, the uncertainty is comprehensibly represented by an uncertainty band, referred to as $\Delta(\cdot)$, surrounding the mean/reference profile. Instead of considering a band of \pm one standard deviation², it is chosen to consider the band set by the constraint tightening level of the chance constraints, i.e., $\Delta T_{ia,k} = \Delta x_{i,k} = \pm \Phi^{-1}(1 - \epsilon_{x_{i,k}}) q_{i,k}$ and $\Delta \dot{Q}_{sup,k} = \Delta u_k = \pm \Phi^{-1}(1 - \epsilon_{u_k}) r_k$ (see Equation (4.21); the index j is omitted here since only one heat input is considered). As such, the uncertainty bands delineate the intervals within which the actual values of the indoor temperature and heat input will fall with a probability of $1 - 2\epsilon_{x_{i,k}}$ and $1 - 2\epsilon_{u_k}$, respectively³. This particular choice for the uncertainty band is made for arguments of interpretability, as the constraint tightening level unequivocally reflects the operational freedom - either in the form of allowed temperature deviations or in the form of spare capacity - that needs to be provided to guarantee constraint satisfaction when subject to real-time perturbations in correspondence with the imposed risk-averseness level⁴.

The observations above reveal a very important asset of the SMPC^{ap} strategy incorporating ADF. Indeed, thanks to the incorporation of ADF in the open-loop

² It should be stressed that the optimized auxiliary variables $q_{i,k}$ and r_k determining the constraint tightening level of the considered chance constraints on the states and control inputs are linked to their respective standard deviation via inequality constraints (see Equation (4.21)), meaning that they are strongly related, but not necessarily equal. Hence, be aware when interpreting the figures throughout this chapter that the course of the uncertainty band over the prediction horizon is partly determined by the evolution of the associated standard deviation, but also partly due to additional, not necessarily physically explainable effects triggered by the optimization procedure, which might especially appear when the tightened chance constraints affecting the uncertainty band are not binding.

³ Analogously, a band of \pm one standard deviation defines the interval within which the actual value of the stochastic variable will fall with a probability of 68.27%.

⁴ Consequently, this particular choice for the uncertainty band also allows to clearly discern whether the chance constraints are satisfied or not. This is especially important for the chance constraints on the indoor temperature, as these constraints are allowed to be relaxed with the help of slack variables. This constraint relaxation might for example be required in case ADF is disabled, since the accumulative effect of the additive and/or parametric uncertainties can in that case result in a wide uncertainty band towards the end of the prediction horizon exceeding the allowed temperature range as imposed by the lower and upper bounds (as can for example be discerned in Figure 9.1).

OCP, not only the flexible⁵ demand for energy (determined by $\bar{Q}_{sup,k}$ during a time step Δt), but also the flexible demand for reserve capacity and real-time flexibility i.e., the activation of the scheduled reserve capacity in real time (both determined by $\Sigma_{\dot{Q}_{sup,k}}$)⁶ are made explicit in the open-loop OCP, thereby disclosing very valuable information regarding system planning and operation. More importantly, since not only the mean $\{\bar{Q}_{sup,k}\}_{k=0\dots K}$, but also the covariance $\{\Sigma_{\dot{Q}_{sup,k}}\}_{k=0\dots K}$ can now be optimized (via the feedback gain matrix \mathbf{T}_u), an additional controllable/price-responsive demand becomes available, which enables a trade-off between the degree of uncertainty management at building level versus at system level⁷, while guaranteeing thermal comfort (in correspondence with the imposed risk-averseness level). In other words, the incorporation of ADF unlocks an additional degree of freedom characterizing the demand side flexibility that can be coordinated for the benefit of the central energy system when harnessing the DR capability of the SMPC^{AP} strategy.

The controllability of both $\{\bar{Q}_{sup,k}\}_{k=0\dots K}$ and $\{\Sigma_{\dot{Q}_{sup,k}}\}_{k=0\dots K}$ is demonstrated in Figure 9.2, showing the stochastic open-loop indoor temperature profiles and heat input profiles resulting from an open-loop operational cost minimization by the SMPC^{AP} strategy incorporating ADF for three different cases⁸: in the first case, a constant cost is attributed to $\{\Sigma_{\dot{Q}_{sup,k}}\}_{k=0\dots K}$, which is twice as high as the constant cost attributed to $\bar{Q}_{sup,k}$; in the second case, this price ratio is reversed, making $\{\Sigma_{\dot{Q}_{sup,k}}\}_{k=0\dots K}$ twice as cheap as $\{\bar{Q}_{sup,k}\}_{k=0\dots K}$; in the third and final case, $\{\Sigma_{\dot{Q}_{sup,k}}\}_{k=0\dots K}$ can be provided for free whereas a constant cost is still attributed to $\{\bar{Q}_{sup,k}\}_{k=0\dots K}$. The results are again presented for the terraced, small, older (but renovated) dwelling equipped with radiators, inhabited by a four-persons-household consisting of two full-time employed adults and two school-age children, during the 18th of January 2016, for a risk-averseness level regarding thermal comfort of $1 - \epsilon = 0.99$.

Figure 9.2 confirms that the relative cost ratio has an indisputable impact on the share of the demand for energy versus the demand for reserve capacity and real-time flexibility, thereby demonstrating their controllability/price-responsiveness, and their interchangeability. Indeed, either the energy demand for space heating is

⁵ Recall that the demand side flexibility stems from the inherent flexibility offered by the thermal storage capability of the building thermal mass, as explained in Intermezzo 8.1.

⁶ The demand for reserve capacity and for real-time flexibility both stem from the uncertainty on the energy demand, where the first one is related to the forward planning aspect (i.e., the open-loop OCP), and the second one is related to the real-time operational aspect (i.e., the closed-loop OCP).

⁷ Recall the discussion in Section 3.3.

⁸ In all three cases, the cost of providing $\bar{Q}_{sup,k}$ during a time step Δt is taken equal to 1 EUR/MWh. However, note that the exact value of this absolute cost level is of minor importance compared to the relative cost ratio of $\bar{Q}_{sup,k}$ and $\Sigma_{\dot{Q}_{sup,k}}$.

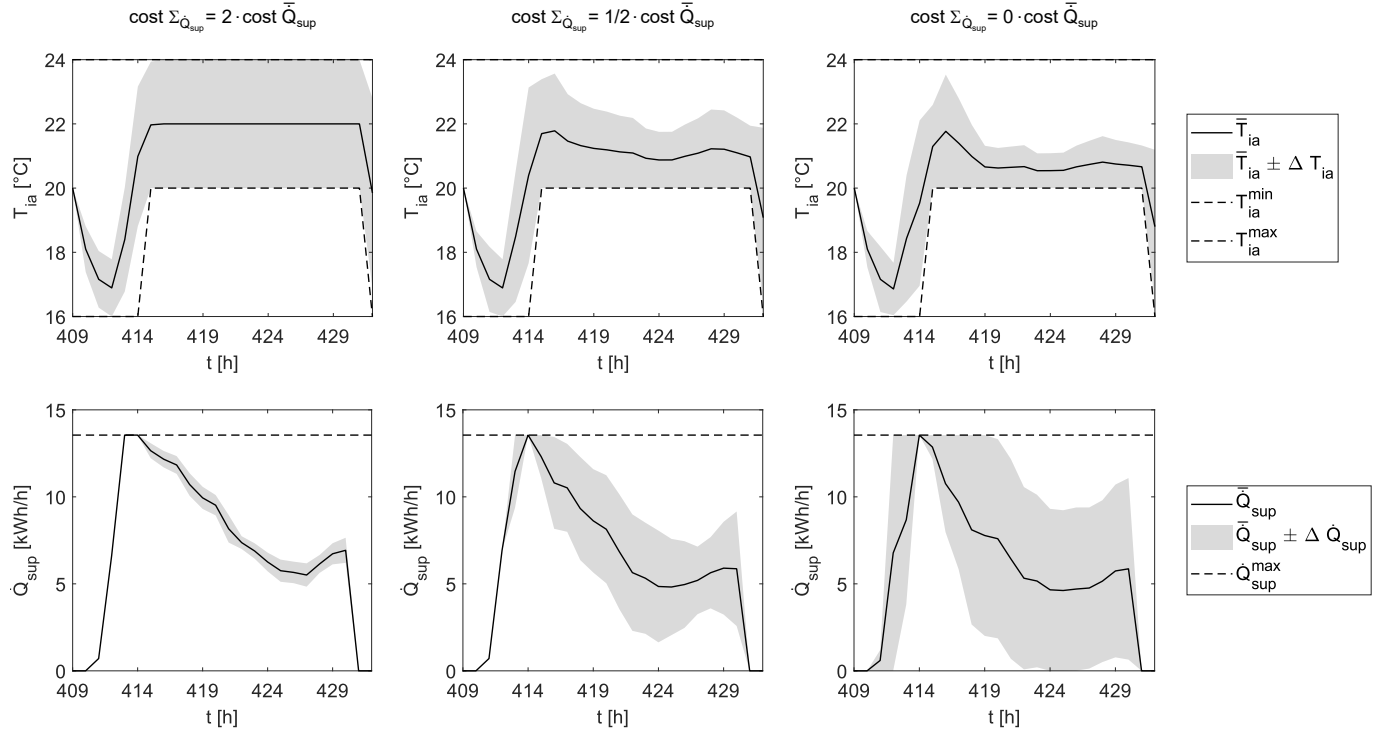


Figure 9.2: The open-loop indoor temperature profiles and heat input profiles (averaged over one hour) realized by an $\text{SMPC}_{1-\epsilon=0.99}^{\text{ap}}$ strategy, aiming to minimize the operating cost during the 18th of January for the terraced, small, older (but renovated) dwelling equipped with radiators, for three different (constant) cost levels attributed to $\bar{Q}_{sup,k}$ and $\Sigma \dot{Q}_{sup,k}$.

higher, in order to steer the temperature further away from its lower bound, so that thermal comfort is still guaranteed despite downward perturbations without requiring any further actions, or the energy demand is exchanged for real-time flexibility, which can be exploited to counteract the detrimental impact of additive and/or parametric uncertainty manifestations in real time. It is exactly this controllability and interchangeability of the demand for energy and the demand for reserve capacity and real-time flexibility that will be further exploited throughout this chapter in a DR context.

9.2 Demand response performance assessment method

As Section 9.1 unveiled, the proposed SMPC^{ap} strategy is not only able to optimize the demand for energy, but also the demand for reserve capacity and real-time flexibility, thanks to the incorporation of ADF in the open-loop control problem. The main aim of this section is to analyze in detail whether the exploitation of this additional degree of freedom, unlocked by the proposed SMPC^{ap} strategy, can benefit the central energy system in a DR context.

To this end, it is investigated whether the coordination of the demand of a group of TCLs controlled by the proposed SMPC^{ap} strategy can reduce the overall system operating cost compared to an equivalent case without ADF, where the coordination of the demand for reserve capacity and real-time flexibility is disabled. The strategy without ADF can be considered as the current state-of-the-art for DR with MPC under uncertainty [41,120,121], albeit with the additional consideration of parametric uncertainties. The overall system operating cost serves as the key performance indicator (KPI) of the DR performance assessment⁹.

Given the expected increase in market penetration of heat pumps for residential space heating [76,77], the analysis considers an electrification scenario, where residential buildings are equipped with compression heat pumps that can deliver services to the electric power system (shortly, power system).

Since the interaction between the demand side and the supply side is of paramount importance when investigating the effects of DR [24,34,174], an integrated system-level optimization problem needs to be considered to properly determine the overall system operating cost. This problem formulation is set up in Section 9.2.1, linking the demand side, consisting of residential buildings equipped with heat pumps, each controlled by the SMPC^{ap} strategy, to the supply side, consisting of electricity

⁹ The overall system operating cost will be further defined in Section 9.2.1.2.

generation units. Subsequently, in Section 9.2.2, a distributed solution approach is proposed to solve this mathematically complex problem.

9.2.1 Integrated system-level optimization problem

The integrated system-level optimization problem merges two problems. The first one is the optimization problem representing the demand side, which is an extended version of the stochastic OCP formulation derived in Chapter 4. The second one is the optimization problem representing the supply side, which is an economic dispatch problem. This problem mimics the day-to-day operation of the power system, and schedules available electricity generation assets to meet the demand at minimum cost. In the considered context, this day-ahead generation schedule comprises of a supply of energy for the upcoming day, as well as of a supply of reserve capacity, where the latter is a common way to cope with load uncertainty (and thus, to accommodate demand for real-time flexibility).

The integrated system-level optimization problem, resulting from the combination of these two subproblems, can be represented in a simplified form as in Problem (9.1)¹⁰.

$$\min_{\substack{\{\chi_b\}_{b=1\dots B} \\ \{\chi_g\}_{g=1\dots G}}} \sum_{g=1}^G c_g^{EN} + c_g^{REp} + c_g^{REa} \quad (9.1a)$$

subject to

$$\left\{ \begin{array}{l} \text{Demand side constraints:} \\ \quad (\bar{\mathbf{D}}_b, \mathbf{R}_b, \times_b) = \chi_b \in X_b \quad \forall b \\ \text{Supply side constraints:} \\ \quad (\bar{\mathbf{S}}_g, \mathbf{V}_g, \times_g) = \chi_g \in X_g \quad \forall g \\ \text{Coupling constraints:} \\ \quad \{\bar{\mathbf{S}}_g\}_{g=1\dots G} \leftrightarrow \{\bar{\mathbf{D}}_b\}_{b=1\dots B}, \bar{\mathbf{D}}_{trad} \\ \quad \{\mathbf{V}_g\}_{g=1\dots G} \leftrightarrow \{\mathbf{R}_b\}_{b=1\dots B}, \sigma_{sys} \end{array} \right. \quad (9.1b)$$

In Equation (9.1), the objective is to minimize the total operating cost of the electric power supply system, comprising of the day-ahead (and hence *expected*) costs of

¹⁰ Note that the notation adopted in Problem (9.1) to refer to the demand and supply variables does not comply with the convention to use upper case letters for matrices, and lower case letters for vectors or scalars, as introduced in Section 4.1. However, this intervention is inevitable to guarantee a clear and unambiguous naming of the different variables.

energy, c_g^{EN} , reserve capacity provision, c_g^{REp} , and reserve capacity activation (i.e., balancing actions in real time), c_g^{REa} . These costs are determined by the stochastic supply scheduled for each generator g , $\tilde{\mathbf{S}}_g = \{\tilde{S}_{g,k} + \delta S_{g,k}\}_{k=0\dots K}$, which is split up in a supply of energy, $\tilde{\mathbf{S}}_g$, and a supply of reserve capacity, \mathbf{V}_g (related to Σ_{S_g}). The same distinction is made for the stochastic, flexible demand of each building b accommodating flexible heat pumps for space heating, $\tilde{\mathbf{D}}_b = \{\tilde{D}_{b,k} + \delta D_{b,k}\}_{k=0\dots K}$, resulting in a demand for energy $\tilde{\mathbf{D}}_b$, and a demand for reserve capacity, \mathbf{R}_b (related to Σ_{D_b}). Since the focus of the integrated system-level problem is on the day-ahead scheduling, the *actual* activation of the scheduled reserve capacity in real time, or said differently, the demand for real-time flexibility, is not further considered¹¹.

The supply of energy, $\{\tilde{\mathbf{S}}_g\}_{g=1\dots G}$, is supposed to cover the flexible demand for energy, $\{\tilde{\mathbf{D}}_b\}_{b=1\dots B}$, as well as the traditional electricity demand, $\tilde{\mathbf{D}}_{trad}$, encompassing all residual¹² electricity demand (i.e., the remaining demand after the subtraction of the available renewable generation) apart from the flexible demand of the heat pumps. This traditional demand is assumed to be fixed (i.e., non-flexible), since only heat pumps are allowed to offer flexibility in this dissertation¹³.

The supply of reserve capacity, $\{\mathbf{V}_g\}_{g=1\dots G}$, is in turn supposed to cover the demand for reserve capacity of the flexible heat pumps, $\{\mathbf{R}_b\}_{b=1\dots B}$, as well as the system-level uncertainty, $\tilde{\mathbf{w}}_{sys} = \{\delta w_{sys,k}\}_{k=0\dots K}$. This system-level uncertainty represents the uncertainty on the traditional demand, the uncertainty on the renewable power generation¹⁴, as well as the uncertainty related to the conventional generation, such as unplanned outages and the like. It is assumed to be Gaussian, with a zero mean, and variance $\Sigma_{sys,k}$.

Note that the operational decisions, or said differently, the strategy χ of each building (subscript b) at the demand side, or each generator (subscript g) at the supply side not only determine the demand for/supply of energy and reserve capacity, but also some other (more local) operational decisions that are not directly involved in the coupling constraints. These are represented by \times .

Each strategy χ belongs to a set of strategies X , which is defined by a number of equality and inequality constraints, constituting the subproblems of each building or generator. In the following sections, each of these subproblems is further elaborated on, thereby defining the demand side constraints (set by the demand side problem discussed in Section 9.2.1.1), as well as the supply side constraints, coupling constraints, and the objective function (set by the supply side problem discussed

¹¹ In contrast to the day-ahead, *expected* cost associated with this reserve capacity activation.

¹² The analysis considers the residual electricity demand, such that the uncertainty related to the renewable electricity generation can be incorporated in the system-level uncertainty.

¹³ In other words, the flexibility offered by among others white good appliances, battery storage, electric vehicles, or flexible industrial processes is neglected here.

¹⁴ Recall that the renewable power generation is incorporated in the residual, traditional demand.

in Section 9.2.1.2). The resulting OCP formulation of the integrated system-level optimization problem combining these subproblems is summarized in Section 9.2.1.3.

9.2.1.1 Demand side problem

The demand side problem determines the demand side constraints in the integrated system-level optimization problem. As the demand side is assumed to be a group of buildings equipped with heat pumps for space heating, each controlled by the SMPC^{ap} strategy (in interaction with the supply side), the demand side constraints correspond to an altered/extended (and repeated) version of the stochastic OCP formulation derived in Chapter 4¹⁵.

Since the stochastic OCP formulation (4.21) does not specify the heat supply system, this component model needs to be added to the OCP formulation. More particularly, the OCP formulation is extended with a slightly adapted version of the heat pump model described in Section 8.1.3.1. The required adaptations to the heat pump model include the following. First, the heat pump model considered in this chapter should merely consider space heating; the demand for space cooling and domestic hot water are omitted here. Second, for arguments of convenience, the assistance by an auxiliary resistance heater is neglected in this chapter. Finally, since this chapter considers a stochastic instead of a deterministic approach (as was the case in Chapter 8), the pre-processing step to determine the COP with the help of Equation (8.9), and the electric power input with the help of Equation (8.10), should now make use of the weather forecasts. However, the fact that these weather forecasts are uncertain, and hence turn the COP and the maximum electric power input into stochastic variables is neglected, as the COP and maximum electric power input are averaged out over the considered prediction horizon anyhow (as discussed in Section 8.1.3.1), making the exact value of these parameters at each time instant of less importance.

Taking into account the extensions and alterations introduced above, the following set of constraints defining the set of feasible strategies X_b for a particular building b is obtained¹⁶.

¹⁵ Note that the stochastic OCP formulation derived in Chapter 4 incorporates ADF. The equivalent case without ADF can be seen as a special form of this problem formulation, which is obtained by forcing the transformation matrix $\mathbf{T}_{\mathbf{u}_b}$ to be a zero matrix.

¹⁶ Note that in Equation (9.2), it is acknowledged that only one heat input is considered. Consequently, the index j is omitted, and the variable representing the heat inputs is converted from a vector $\mathbf{u}_{b,k}$ into a scalar $u_{b,k}$. The index b , on the other hand, is added, in order to account for the fact that a group of multiple, distinct buildings is considered in this chapter.

$$\bar{\mathbf{x}}_{b,k+1} = \bar{\mathbf{A}}_b \bar{\mathbf{x}}_{b,k} + \bar{\mathbf{B}}_b \bar{u}_{b,k} + \bar{\mathbf{E}}_b \bar{\mathbf{d}}_{b,k} \quad \forall k \quad (9.2a)$$

$$\begin{aligned} \Sigma_{\mathbf{x}_{b,k+1}}^r &= (\bar{\mathbf{x}}_{b,k}^T \otimes \mathbf{I}_{n_x}) \Sigma_{\mathbf{A}_b}^r + \bar{\mathbf{A}}_b \Sigma_{\mathbf{x}_{b,k}}^r + \\ &\quad \bar{u}_{b,k} \Sigma_{\mathbf{B}_b}^r + \bar{\mathbf{B}}_b \Sigma_{u_{b,k}}^r + \\ &\quad (\bar{\mathbf{d}}_{b,k}^T \otimes \mathbf{I}_{n_x}) \Sigma_{\mathbf{E}_b}^r + \bar{\mathbf{E}}_b \Sigma_{\mathbf{d}_{b,k}}^r \quad \forall k \end{aligned} \quad (9.2b)$$

$$\bar{x}_{b,i,k} + s_{b,i,k} \geq x_{b,i,k}^{min} + \Phi^{-1}(1 - \epsilon_{x_{b,i,k}}) q_{b,i,k} \quad \forall i, k \quad (9.2c)$$

$$\bar{x}_{b,i,k} - s_{b,i,k} \leq x_{b,i,k}^{max} - \Phi^{-1}(1 - \epsilon_{x_{b,i,k}}) q_{b,i,k} \quad \forall i, k \quad (9.2d)$$

$$q_{b,i,k} \geq \|\Sigma_{x_{b,i,k}}^r\|_2 \quad \forall i, k \quad (9.2e)$$

$$s_{b,i,k} \geq 0 \quad \forall i, k \quad (9.2f)$$

$$\bar{u}_{b,k} \geq 0 + \Phi^{-1}(1 - \epsilon_{u_{b,k}}) r_{b,k} \quad \forall k \quad (9.2g)$$

$$\bar{u}_{b,k} \leq u_{b,k}^{max} - \Phi^{-1}(1 - \epsilon_{u_{b,k}}) r_{b,k} \quad \forall k \quad (9.2h)$$

$$r_{b,k} \geq \|\Sigma_{u_{b,k}}^r\|_2 \quad \forall k \quad (9.2i)$$

$$\Sigma_{\mathbf{u}_b}^r = \mathbf{T}_{\mathbf{u}_b} \Sigma_{\mathbf{p}_b}^r \quad (9.2j)$$

$$\mathbf{x}_b(0) = \mathbf{x}_{b,0} \quad (9.2k)$$

$$u_b(0) = u_{b,0} \quad (9.2l)$$

$$\bar{u}_{b,k} = \bar{Q}_{sup,b,k} = \overline{COP}_{b,k}^{sh} \bar{P}_{hp,b,k}^{sh} \quad \forall k \quad (9.2m)$$

$$u_{b,k}^{max} = \overline{COP}_{b,k}^{sh} \bar{P}_{hp,b,k}^{sh,max} \quad \forall k \quad (9.2n)$$

Based on the OCP formulation described above, the demand for electric energy is equal to the heat pump electricity consumption during a time step Δt , as summarized by Equation (9.2o). The demand for reserve capacity, on the other hand, can be represented with the help of the auxiliary variable $r_{b,k}$, which is closely related to (i.e., bound from below by) the standard deviation of the stochastic demand $\bar{D}_{b,k}$. Note that $r_{b,k}$ is chosen as a proxy for the standard deviation (see also Footnote 2), instead of the root form $\Sigma_{D_{b,k}}^r$, since $r_{b,k}$ represents the uncertainty at a certain time step with the help of one single value, whereas in $\Sigma_{D_{b,k}}^r$, the uncertainty is distributed over multiple vector elements, making it less comprehensible. Since $r_{b,k}$ is tailored to the uncertainty on the heat input in Equation (9.2), it still needs to

be converted to an uncertainty related to the electricity demand. This can be done with the help of the COP, as expressed by Equation (9.2p).

$$\bar{D}_{b,k} = \bar{P}_{hp,b,k}^{sh} \Delta t \quad \forall k \quad (9.2o)$$

$$R_{b,k} = \frac{r_{b,k}}{COP_{b,k}^{sh}} \quad \forall k \quad (9.2p)$$

As already mentioned in Section 9.2.1, the demand for real-time flexibility is not accounted for, since the focus is on the day-ahead scheduling, and hence, the open-loop OCP is considered; the subsequent solution of the closed-loop OCP throughout the day is not further considered. This is justified if the closed-loop control merely comes down to the implementation of the optimized ADF strategy in real time, since in this case, the additional consideration of this real-time behavior does not add any new information to the discussion¹⁷.

In the integrated system-level optimization problem, the above-mentioned set of constraints is repeated multiple times to model the demand side flexibility of a limited number of distinct buildings. The demand of each of these buildings is scaled up by a constant factor, in order to obtain a higher share of flexible demand in the integrated system-level problem that can have a significant and observable impact on the electricity generation system.

9.2.1.2 Supply side problem

The supply side problem determines the supply side constraints, the coupling constraints, as well as the objective function of the integrated system-level optimization problem (9.1). The considered problem formulation is a stylized version of an economic dispatch problem, stripped down to its essence, where ramping constraints, minimum on- and off-times, and start-up costs are neglected. This problem aims to minimize the overall operating cost of the electricity generation while meeting the demand, subject to techno-economic constraints of the involved (aggregated) generating units.

A first important set of constraints determining the optimal schedule for the generating units consists of the coupling constraints imposing the required balance between supply and demand. It should be acknowledged that the coupling constraints are actually not a strict part of the supply side problem, but rather

¹⁷ Be aware that this argument does not hold if one decides to deviate from the prescribed reaction by the ADF strategy in real time. In this case, the demand projection in terms of the reference profile and associated uncertainty band is no longer valid. This implies that the control strategy for the building needs to be re-optimized, and that the consented DR strategy might be voided.

serve as a link between the demand and supply side problem. However, due to the specific approach we pursue to align the generator operation with the available bottom-up characterization of the uncertain demand, the technical constraints of the generators and the coupling constraints are intertwined, as will become clear throughout the discussion below.

For the coupling constraints, an explicit distinction needs to be made between the supply of and demand for electric energy on the one hand, and the supply of and demand for reserve capacity on the other hand.

The coupling constraint for the energy component can be straightforwardly expressed with the help of Equation (9.3), stating that the electricity generation under expected conditions should meet the expected demand¹⁸.

$$\sum_{g=1}^G \bar{S}_{g,k} = \sum_{b=1}^B \bar{D}_{b,k} + \bar{D}_{trad,k} \quad \forall k \quad (9.3)$$

In order to schedule the supply of reserve capacity, on the other hand, information about the real-time situation needs to be included in the open-loop OCP formulation of the supply side problem. This can be done by implementing an affine control scheme, in analogy with ADF incorporated in the SMPC^{ap} strategy at the demand side. By doing this, the generator output can be written as a function of the uncertain demand, thus exploiting its available substantiated, bottom-up characterization (described by Equations (9.2o) and (9.2p)). Following Bienstock et al. [175], all conventional generators are assumed to modulate their output $\{\tilde{P}_{gen,g,k}\}_{k=0\dots K} = \{\bar{P}_{gen,g,k} + \delta\dot{P}_{g,k}\}_{k=0\dots K}$ in response to real-time fluctuations in a proportional way with the help of the proportionality coefficients $\alpha_{g,k}$, as expressed by Equations (9.4a) to (9.4c), where these proportionality coefficients serve as additional optimization variables in the supply side problem.

$$\tilde{P}_{gen,g,k} = \bar{P}_{gen,g,k} + \alpha_{g,k} \left(\sum_{b=1}^B \frac{\delta D_{b,k}}{\Delta t} + \delta w_{sys,k} \right) \quad \forall g, k \quad (9.4a)$$

$$\alpha_{g,k} \geq 0 \quad \forall g, k \quad (9.4b)$$

$$\sum_{g=1}^G \alpha_{g,k} = 1 \quad \forall k \quad (9.4c)$$

¹⁸ If one wishes to include the curtailment of renewables, this equality constraint should be replaced by an inequality constraint, as the right hand side of Equation (9.3) might become negative in case of an overproduction of RES. This is nevertheless not further considered in this dissertation.

As such, the output of each generator becomes a function of the Gaussian random variables $\delta D_{b,k}$ and $\delta w_{sys,k}$. Because of its consequent stochasticity, the constraints regarding the output of a particular generator g can no longer be imposed as hard constraints, but instead need to be expressed as chance constraints, as done by Equations (9.5a) and (9.5b). To prevent a generator to produce power beyond its capacity cap_g , small values are assigned to $\epsilon_{\tilde{P}_{gen,g,k}}$ ¹⁹, so that the chance constraints closely resemble the original hard constraints.

$$P(\tilde{P}_{gen,g,k} \geq 0) \geq 1 - \epsilon_{\tilde{P}_{gen,g,k}} \quad \forall k \quad (9.5a)$$

$$P(\tilde{P}_{gen,g,k} \leq cap_g) \geq 1 - \epsilon_{\tilde{P}_{gen,g,k}} \quad \forall k \quad (9.5b)$$

Using Equation (9.4a) to further specify $\tilde{P}_{gen,g,k}$ in Equations (9.5a) and (9.5b), and reformulating the chance constraints into deterministic constraints following the same procedure as adopted in Chapter 4, the following expressions constraining the generator output are obtained.

$$\bar{P}_{gen,g,k} \geq 0 + \Phi^{-1}(1 - \epsilon_{\tilde{P}_{gen,g,k}}) V_{g,k} \quad \forall k \quad (9.6a)$$

$$\bar{P}_{gen,g,k} \leq cap_g - \Phi^{-1}(1 - \epsilon_{\tilde{P}_{gen,g,k}}) V_{g,k} \quad \forall k \quad (9.6b)$$

$$V_{g,k} \geq \alpha_{g,k} \frac{1}{\Delta t} \left\| \begin{array}{c} R_{1,k} \\ \vdots \\ R_{B,k} \\ \Delta t \sigma_{sys,k} \end{array} \right\|_2 \quad \forall k \quad (9.6c)$$

$$\alpha_{g,k} \geq 0 \quad \forall k \quad (9.6d)$$

Note that the elaboration of the 2-norm in Equation (9.6c) results in the more comprehensible expression for the reserve capacity given by Equation (9.7); the reformulation of this expression into the SOC constraint of Equation (9.6c) is nevertheless required to guarantee the convexity of the optimization problem.

$$V_{g,k}^2 \geq \alpha_{g,k}^2 \frac{1}{\Delta t^2} \left(\sum_{b=1}^B \Sigma_{D_{b,k}} + \Sigma_{sys,k} \Delta t^2 \right) \quad (9.7)$$

¹⁹ Throughout this dissertation, $\epsilon_{\tilde{P}_{gen,g,k}}$ is consistently equal to 0.999.

Based on Equations (9.6a) to (9.6d), the scheduled supply of electric energy and of reserve capacity can then be defined as follows.

$$\bar{S}_{g,k} = \bar{P}_{gen,g,k} \Delta t \quad \forall k \quad (9.8a)$$

$$V_{g,k} \quad \forall k \quad (9.8b)$$

Equations (9.6a) to (9.6d) represent a set of technical constraints (Equations (9.6a) and (9.6b)), and a set of balancing related constraints (Equations (9.6c) and (9.6d)). The summation of Equations (9.6c) and (9.6d) over all generators, in order to represent the overall provided reserve capacity, finally results in an additional coupling constraint, being Equation (9.9), supplementing Equation (9.3).

$$\sum_{g=1}^G V_{g,k} \geq \frac{1}{\Delta t} \left\| \begin{array}{c} R_{1,k} \\ \vdots \\ R_{B,k} \\ \Delta t \sigma_{sys,k} \end{array} \right\|_2 \quad \forall k \quad (9.9)$$

Now that the technical constraints and coupling constraints of the supply side problem are specified, the final aspect that still needs to be devised is the formulation of the objective function. As already stated above, the integrated system-level optimization problem aims to minimize the overall system operating cost. Given the considered problem setting, the relevant operating costs include the day-ahead (and hence, expected) costs of energy, c_g^{EN} , reserve capacity provision, c_g^{REp} , and reserve capacity activation, c_g^{REa} .

The day-ahead energy and reserve capacity activation costs for a particular generator g are both determined by the expected cost of the stochastic generation, expressed by Equation (9.10). The generation cost function c_g^{GEN} is assumed to be a quadratic function (characterized by three cost coefficients $c_{2,g}$, $c_{1,g}$ and $c_{0,g}$), in accordance with standard power system engineering practice [175, 176].

$$\begin{aligned} \mathbb{E}[c_g^{GEN}(\tilde{S}_{g,k})] &= \mathbb{E}\left[\frac{c_{2,g}}{2} \tilde{S}_{g,k}^2 + c_{1,g} \tilde{S}_{g,k} + c_{0,g}\right] \quad \forall k \\ &= \frac{c_{2,g}}{2} \mathbb{E}[\tilde{S}_{g,k}^2] + c_{1,g} \mathbb{E}[\tilde{S}_{g,k}] + c_{0,g} \quad \forall k \end{aligned} \quad (9.10)$$

Taking into account the definition of the stochastic generation as introduced by Equation (9.4a), the expected values $\mathbb{E}[\tilde{S}_{g,k}]$ and $\mathbb{E}[\tilde{S}_{g,k}^2]$ can be written as

$$\mathbb{E}[\tilde{S}_{g,k}] = \mathbb{E}\left[\bar{S}_{g,k} + \alpha_{g,k} \left(\sum_{b=1}^B \delta D_{b,k} + \delta w_{sys,k} \Delta t\right)\right] = \bar{S}_{g,k} \quad \forall k \quad (9.11a)$$

and

$$\begin{aligned}
\mathbb{E}[\tilde{S}_{g,k}^2] &= \mathbb{E} \left[\bar{S}_{g,k}^2 + \alpha_{g,k}^2 \left(\sum_{b=1}^B \delta D_{b,k} \right)^2 + \alpha_{g,k}^2 \left(\delta w_{sys,k} \Delta t \right)^2 + \right. \\
&\quad 2 \alpha_{g,k}^2 \left(\sum_{b=1}^B \delta D_{b,k} \right) \left(\delta w_{sys,k} \Delta t \right) + \\
&\quad \left. 2 \bar{S}_{g,k} \alpha_{g,k} \left(\sum_{b=1}^B \delta D_{b,k} \right) + 2 \bar{S}_{g,k} \alpha_{g,k} \left(\delta w_{sys,k} \Delta t \right) \right] \quad \forall k \\
&= \bar{S}_{g,k}^2 + \alpha_{g,k}^2 \left(\sum_{b=1}^B \Sigma_{D_{b,k}} + \Sigma_{sys,k} \Delta t^2 \right) \quad \forall k
\end{aligned} \tag{9.11b}$$

where it is acknowledged that $\delta w_{sys,k} \forall k$ and $\delta D_{b,k} \forall b, k$ are all independent stochastic random variables, and all have zero mean²⁰.

Consequently, the expected cost of the stochastic generation can be expressed as follows.

$$\begin{aligned}
\mathbb{E}[c_g^{GEN}(\tilde{S}_{g,k})] &= \frac{c_{2,g}}{2} \bar{S}_{g,k}^2 + c_{1,g} \bar{S}_{g,k} + c_{0,g} + \\
&\quad \frac{c_{2,g}}{2} \alpha_{g,k}^2 \left(\sum_{b=1}^B \Sigma_{D_{b,k}} + \Sigma_{sys,k} \Delta t^2 \right) \quad \forall k
\end{aligned} \tag{9.12}$$

By finally implementing Equation (9.7) into Equation (9.12), the following expressions for the day-ahead expected cost of energy c_g^{EN} , and the day-ahead expected cost of real-time reserve capacity activation c_g^{REa} for a particular generator g are obtained.

$$c_g^{EN} = \sum_{k=1}^K \frac{c_{2,g}}{2} \bar{S}_{g,k}^2 + c_{1,g} \bar{S}_{g,k} + c_{0,g} \tag{9.13a}$$

$$c_g^{REa} \geq \sum_{k=1}^K \frac{c_{2,g}}{2} V_{g,k}^2 \Delta t^2 \tag{9.13b}$$

²⁰ Due to the explicit distinction between the mean \bar{D}_b and uncertain portion δD_b of the stochastic variable \bar{D}_b , this uncertain portion δD_b can be interpreted as a segregated stochastic variable with zero mean and variance Σ_{D_b} .

The cost to keep aside spare capacity (i.e., reserve capacity provision), on the other hand, is assumed to be a percentage of the generation cost, as suggested by Pandžić et al. [177]; more particularly, the reserve capacity provision cost is taken equal to 30% of the average marginal generation cost [177]. This leads to the expression given by Equation (9.13c) for the day-ahead cost of reserve capacity provision c_g^{REp} . Note that this cost is based on the constraint tightening level $\Phi^{-1}(1 - \epsilon_{\dot{P}_{gen,g,k}}) V_{g,k}$ of the generator power constraints (Equations (9.6a) and (9.6b)), instead of $V_{g,k}$, as this expression reflects how much capacity actually needs to be kept aside.

$$\begin{aligned} c_g^{REp} &= \sum_{k=1}^K 0.30 \left(c_{2,g} \frac{cap_g}{2} + c_{1,g} \right) \left(\Phi^{-1}(1 - \epsilon_{\dot{P}_{gen,g,k}}) V_{g,k} \right) \\ &= \sum_{k=1}^K c_{3,g} \Phi^{-1}(1 - \epsilon_{\dot{P}_{gen,g,k}}) V_{g,k} \end{aligned} \quad (9.13c)$$

The summation of these three cost components for all involved electricity generation units characterizes the total system-level operating cost, and defines the objective function of the integrated system-level optimization problem.

$$\begin{aligned} \sum_{g=1}^G c_g^{EN} + c_g^{REa} + c_g^{REp} &\geq \\ &\sum_{g=1}^G \sum_{k=1}^K \frac{c_{2,g}}{2} \bar{S}_{g,k}^2 + c_{1,g} \bar{S}_{g,k} + c_{0,g} + \\ &\sum_{g=1}^G \sum_{k=1}^K \frac{c_{2,g}}{2} V_{g,k}^2 \Delta t^2 + \\ &\sum_{g=1}^G \sum_{k=1}^K c_{3,g} \Phi^{-1}(1 - \epsilon_{\dot{P}_{gen,g,k}}) V_{g,k} \end{aligned} \quad (9.14)$$

9.2.1.3 Resulting integrated system-level problem

The combination of the demand side constraints, supply side constraints, coupling constraints and objective function derived in Sections 9.2.1.1 and 9.2.1.2, results in the below mentioned accurate and detailed representation of the integrated system-level optimization problem. This OCP formulation will be used for the DR performance assessment in this dissertation, in order to verify the added value of the proposed SMPC^{ap} strategy for DR under uncertainty.

Optimal control problem formulation:

$$\min_{\substack{\{\chi_b\}_{b=1\dots B} \\ \{\chi_g\}_{g=1\dots G}}} \sum_{g=1}^G \sum_{k=1}^K \left(\left(\frac{c_{2,g}}{2} \bar{S}_{g,k}^2 + c_{1,g} \bar{S}_{g,k} + c_{0,g} \right) + \left(\frac{c_{2,g}}{2} V_{g,k}^2 \Delta t^2 \right) + \right. \quad (9.15)$$

$$\left. \left(c_{3,g} \Phi^{-1} (1 - \epsilon_{\dot{P}_{gen,g,k}}) V_{g,k} \right) \right) \quad (9.16)$$

with

$$\chi_b = (\bar{\mathbf{D}}_b, \mathbf{R}_b, \varkappa_b) \quad \forall b \quad (9.17a)$$

$$\bar{\mathbf{D}}_b = \left\{ \bar{P}_{hp,b,k}^{sh} \Delta t \right\}_{k=0\dots K} \quad \forall b \quad (9.17b)$$

$$\mathbf{R}_b = \left\{ \frac{r_{b,k}}{COP_{b,k}^{sh}} \right\}_{k=0\dots K} \quad \forall b \quad (9.17c)$$

$$\varkappa_b = \left\{ \{ \bar{\mathbf{x}}_{b,k} \}_{k=0\dots K+1}, \{ \Sigma_{\mathbf{x}_{b,k}}^r \}_{k=0\dots K+1}, \right. \\ \left. \{ \mathbf{q}_{b,k} \}_{k=0\dots K+1}, \{ \mathbf{s}_{b,k} \}_{k=0\dots K+1}, \right. \\ \left. \{ \bar{u}_{b,k} \}_{k=0\dots K}, \mathbf{T}_{\mathbf{u}_b} \right\} \quad \forall b \quad (9.17d)$$

$$\chi_g = (\bar{\mathbf{S}}_g, \mathbf{V}_g) \quad \forall g \quad (9.17e)$$

$$\bar{\mathbf{S}}_g = \{ \bar{P}_{gen,g,k} \Delta t \}_{k=0\dots K} \quad \forall g \quad (9.17f)$$

$$\mathbf{V}_g = \{ V_{g,k} \}_{k=0\dots K} \quad \forall g \quad (9.17g)$$

subject to demand side constraints $\chi_b \in X_b \quad \forall b$

$$\bar{\mathbf{x}}_{b,k+1} = \bar{\mathbf{A}}_b \bar{\mathbf{x}}_{b,k} + \bar{\mathbf{B}}_b \bar{u}_{b,k} + \bar{\mathbf{E}}_b \bar{\mathbf{d}}_{b,k} \quad \forall b, k \quad (9.18a)$$

$$\begin{aligned} \Sigma_{\mathbf{x}_{b,k+1}}^r &= (\bar{\mathbf{x}}_{b,k}^T \otimes \mathbf{I}_{n_x}) \Sigma_{\mathbf{A}_b}^r + \bar{\mathbf{A}}_b \Sigma_{\mathbf{x}_{b,k}}^r + \\ &\quad \bar{u}_{b,k} \Sigma_{\mathbf{B}_b}^r + \bar{\mathbf{B}}_b \Sigma_{u_{b,k}}^r + \\ &\quad (\bar{\mathbf{d}}_{b,k}^T \otimes \mathbf{I}_{n_x}) \Sigma_{\mathbf{E}_b}^r + \bar{\mathbf{E}}_b \Sigma_{\mathbf{d}_{b,k}}^r \quad \forall b, k \end{aligned} \quad (9.18b)$$

$$\bar{x}_{b,i,k} + s_{b,i,k} \geq x_{b,i,k}^{min} + \Phi^{-1}(1 - \epsilon_{x_{b,i,k}}) q_{b,i,k} \quad \forall b, i, k \quad (9.18c)$$

$$\bar{x}_{b,i,k} - s_{b,i,k} \leq x_{b,i,k}^{max} - \Phi^{-1}(1 - \epsilon_{x_{b,i,k}}) q_{b,i,k} \quad \forall b, i, k \quad (9.18d)$$

$$q_{b,i,k} \geq \|\Sigma_{x_{b,i,k}}^r\|_2 \quad \forall b, i, k \quad (9.18e)$$

$$s_{b,i,k} \geq 0 \quad \forall b, i, k \quad (9.18f)$$

$$\bar{u}_{b,k} \geq 0 + \Phi^{-1}(1 - \epsilon_{u_{b,k}}) r_{b,k} \quad \forall b, k \quad (9.18g)$$

$$\bar{u}_{b,k} \leq u_{b,k}^{max} - \Phi^{-1}(1 - \epsilon_{u_{b,k}}) r_{b,k} \quad \forall b, k \quad (9.18h)$$

$$r_{b,k} \geq \|\Sigma_{u_{b,k}}^r\|_2 \quad \forall b, k \quad (9.18i)$$

$$\Sigma_{\mathbf{u}_b}^r = \mathbf{T}_{\mathbf{u}_b} \Sigma_{\mathbf{p}_b}^r \quad (9.18j)$$

$$\mathbf{x}_b(0) = \mathbf{x}_{b,0} \quad \forall b \quad (9.18k)$$

$$u_b(0) = u_{b,0} \quad \forall b \quad (9.18l)$$

$$\bar{u}_{b,k} = \bar{Q}_{sup,b,k} = \overline{COP}_{b,k}^{sh} \bar{P}_{hp,b,k}^{sh} \quad \forall b, k \quad (9.18m)$$

$$u_{b,k}^{max} = \overline{COP}_{b,k}^{sh} \bar{P}_{hp,b,k}^{sh,max} \quad \forall b, k \quad (9.18n)$$

subject to supply side constraints $\chi_g \in X_g \quad \forall g$

$$\bar{P}_{gen,g,k} \geq 0 + \Phi^{-1}(1 - \epsilon_{\bar{P}_{gen,g,k}}) V_{g,k} \quad \forall g, k \quad (9.19a)$$

$$\bar{P}_{gen,g,k} \leq cap_g - \Phi^{-1}(1 - \epsilon_{\bar{P}_{gen,g,k}}) V_{g,k} \quad \forall g, k \quad (9.19b)$$

subject to coupling constraints

$$\sum_{g=1}^G \bar{S}_{g,k} = \sum_{b=1}^B \bar{D}_{b,k} + \bar{D}_{trad,k} \quad \forall k \quad (9.20a)$$

$$\sum_{g=1}^G V_{g,k} \geq \frac{1}{\Delta t} \left\| \begin{array}{c} R_{1,k} \\ \vdots \\ R_{B,k} \\ \Delta t \sigma_{sys,k} \end{array} \right\|_2 \quad \forall k \quad (9.20b)$$

Summary:

Simplifying the integrated system-level optimization problem to its essence leads to the concise representation expressed by Equation (9.21), serving as a refined version of Equation (9.1).

$$\min_{\substack{\{\chi_b\}_{b=1\dots B} \\ \{\chi_g\}_{g=1\dots G}}} \sum_{g=1}^G f_g(\bar{\mathbf{S}}_g, \mathbf{V}_g) \quad (9.21a)$$

with

$$f_g(\bar{\mathbf{S}}_g, \mathbf{V}_g) = \sum_{k=1}^K \left(\left(\frac{c_{2,g}}{2} \bar{S}_{g,k}^2 + c_{1,g} \bar{S}_{g,k} + c_{0,g} \right) + \left(\frac{c_{2,g}}{2} V_{g,k}^2 \Delta t^2 \right) + \left(c_{3,g} \Phi^{-1}(1 - \epsilon_{\dot{P}_{gen,g,k}}) V_{g,k} \right) \right) \quad \forall g \quad (9.21b)$$

subject to

Demand side constraints:

$$\chi_b = (\bar{\mathbf{D}}_b, \mathbf{R}_b, \varkappa_b) \in X_b \quad \forall b \quad (9.21c)$$

Supply side constraints:

$$\chi_g = (\bar{\mathbf{S}}_g, \mathbf{V}_g) \in X_g \quad \forall g \quad (9.21d)$$

Coupling constraints:

$$\sum_{g=1}^G \bar{S}_{g,k} = \sum_{b=1}^B \bar{D}_{b,k} + \bar{D}_{trad,k} \quad \forall k \quad (9.21e)$$

$$\sum_{g=1}^G V_{g,k} \geq \frac{1}{\Delta t} \left\| \begin{array}{c} R_{1,k} \\ \vdots \\ R_{B,k} \\ \Delta t \sigma_{sys,k} \end{array} \right\|_2 \quad \forall k \quad (9.21f)$$

9.2.2 Distributed solution strategy using ADMM

The integrated system-level optimization problem is a fairly large problem, with a large number of optimization variables (recall among others the discussions in Section 4.4 and Section 6.3.2). To ensure mathematical tractability, this section proposes a distributed solution approach for the integrated problem, splitting up the original problem into smaller subproblems, each of which are easier to manage, and can be solved in parallel.

A particular algorithm that is well suited for distributed convex optimization [178, 179], and which has been gaining increasing popularity in a DR context [121, 180, 181, 182], is the alternating direction method of multipliers. The general working principle of this algorithm is briefly explained in Intermezzo 9.1, after which the implementation of this algorithm to solve the integrated system-level optimization problem is discussed in detail in the remainder of this section.

Intermezzo 9.1

The alternating direction method of multipliers

The alternating direction method of multipliers (ADMM) is a simple but powerful algorithm that can be used to solve convex optimization problems of the form of Problem (9.22), where $f(\mathbf{y})$ and $g(\mathbf{z})$ represent convex functions, and Y and Z represent convex sets, that can be represented using convex equality and inequality constraints. The targeted problems are separable in the optimization variables \mathbf{y} and \mathbf{z} , except for the coupling constraints (9.22d) [178].

$$\min_{\mathbf{y}, \mathbf{z}} f(\mathbf{y}) + g(\mathbf{z}) \quad (9.22a)$$

$$s.t. \mathbf{y} \in Y \quad (9.22b)$$

$$\mathbf{z} \in Z \quad (9.22c)$$

$$\mathbf{F}\mathbf{y} + \mathbf{G}\mathbf{z} = \mathbf{h} \quad (\boldsymbol{\lambda}) \quad (9.22d)$$

The solution approach of ADMM makes use of the augmented Lagrangian $L_\rho(\mathbf{y}, \mathbf{z}, \boldsymbol{\lambda})$ of Problem (9.22), which is defined as follows.

$$L_\rho(\mathbf{y}, \mathbf{z}, \boldsymbol{\lambda}) = f(\mathbf{y}) + g(\mathbf{z}) + \boldsymbol{\lambda}^T (\mathbf{F}\mathbf{y} + \mathbf{G}\mathbf{z} - \mathbf{h}) + \frac{\rho}{2} \|\mathbf{F}\mathbf{y} + \mathbf{G}\mathbf{z} - \mathbf{h}\|_2^2 \quad (9.23)$$

Here, $\boldsymbol{\lambda}$ is the vector of dual variables, or Lagrange multipliers, associated with the coupling constraints (9.22d), and $\rho > 0$ is a (user-defined) penalty parameter.

ADMM solves Problem (9.22) in an iterative way, and in doing so, exploits its decomposability for the separable optimization variables \mathbf{y} and \mathbf{z} . The procedure to obtain the next ADMM-iterates starting from the current iterates $(\mathbf{y}^l, \mathbf{z}^l, \boldsymbol{\lambda}^l)$, can be summarized as follows.

y-minimization step:

$$\begin{aligned} \mathbf{y}^{l+1} &= \arg \min_{\mathbf{y} \in Y} L_\rho(\mathbf{y}, \mathbf{z}^l, \boldsymbol{\lambda}^l) \\ &= \arg \min_{\mathbf{y} \in Y} f(\mathbf{y}) + \boldsymbol{\lambda}^T \mathbf{F}\mathbf{y} + \frac{\rho}{2} \|\mathbf{F}\mathbf{y} + \mathbf{G}\mathbf{z}^l - \mathbf{h}\|_2^2 \end{aligned} \quad (9.24a)$$

z-minimization step:

$$\begin{aligned} \mathbf{z}^{l+1} &= \arg \min_{\mathbf{z} \in Z} L_\rho(\mathbf{y}^{l+1}, \mathbf{z}, \boldsymbol{\lambda}^l) \\ &= \arg \min_{\mathbf{z} \in Z} g(\mathbf{z}) + \boldsymbol{\lambda}^T \mathbf{G}\mathbf{z} + \frac{\rho}{2} \|\mathbf{F}\mathbf{y}^{l+1} + \mathbf{G}\mathbf{z} - \mathbf{h}\|_2^2 \end{aligned} \quad (9.24b)$$

dual variable update:

$$\boldsymbol{\lambda}^{l+1} = \boldsymbol{\lambda}^l + \rho(\mathbf{F}\mathbf{y}^{l+1} + \mathbf{G}\mathbf{z}^{l+1} - \mathbf{h}) \quad (9.24c)$$

The convergence of the iterative procedure towards the optimal solution is tracked with the help of the primal and dual residuals, i.e., the residuals for the primal and dual feasibility conditions, defined by Equations (9.25a) and (9.25b), respectively; the derivation of these expressions can be found in the work of Boyd et al. [178]. The primal residual is a measure for the satisfaction of the coupling constraint. The dual residual, on the other hand, indicates how much the optimization variables still change from one iteration to the next. As imposed by Equations (9.25c) and (9.25d), these residuals should be sufficiently small, in order for the iterative optimization to be terminated, indicating that the algorithm is converged to the global optimum.

$$\mathbf{res}_{prim}^{l+1} = \mathbf{F}\mathbf{y}^{l+1} + \mathbf{G}\mathbf{z}^{l+1} - \mathbf{h} \quad (9.25a)$$

$$\mathbf{res}_{dual}^{l+1} = \rho \mathbf{F}^T \mathbf{G} (\mathbf{z}^{l+1} - \mathbf{z}^l) \quad (9.25b)$$

$$\|\mathbf{res}_{prim}^{l+1}\|_2 \leq \epsilon_{prim} \quad (\text{with } \epsilon_{prim} > 0) \quad (9.25c)$$

$$\|\mathbf{res}_{dual}^{l+1}\|_2 \leq \epsilon_{dual} \quad (\text{with } \epsilon_{dual} > 0) \quad (9.25d)$$

The penalty parameter ρ has an important impact on the convergence of ADMM. To improve convergence in practice, and to make the performance of the ADMM procedure less dependent on the initially imposed value, the penalty parameter can be updated with the help of the scheme presented by Equation (9.26). This adaptive update scheme ensures that the norms of the primal and dual variables stay within a factor ν from one another while they both converge to zero [178].

$$\rho^{l+1} = \begin{cases} \tau^{incr} \rho^l & \text{if } \|\mathbf{res}_{prim}^l\|_2 > \nu \|\mathbf{res}_{dual}^l\|_2 \\ \rho^l / \tau^{decr} & \text{if } \|\mathbf{res}_{dual}^l\|_2 > \nu \|\mathbf{res}_{prim}^l\|_2 \\ \rho^l & \text{otherwise} \end{cases} \quad (9.26)$$

Here, $\nu > 1$, $\tau^{incr} > 1$ and $\tau^{decr} > 1$ serve as parameters, for which the following values are recommended: $\nu = 10$, and $\tau^{incr} = \tau^{decr} = 2$ [178].

^a Note that the augmented Lagrangian (in contrast to the optimization problem) is not separable for \mathbf{y} and \mathbf{z} . Nonetheless, ADMM ensures a decoupling of these optimization variables by alternately minimizing the augmented Lagrangian for \mathbf{y} and \mathbf{z} , respectively.

9.2.2.1 Reformulation of the integrated system-level optimization problem in ADMM form

The integrated system-level optimization problem in the form of Equation (9.21) does not comply with the required ADMM structure to allow for a decomposition of the problem into distinct subproblems for all different generators and buildings (due to the considered formulation of the coupling constraints, Equations (9.21e) and (9.21f)). This issue can be overcome by creating copies of the optimization variables involved in the coupling constraints, as for example done by Mhanna et al. [183] in the context of a quadratic second order cone constrained problem for optimal power flow. This duplication introduces additional auxiliary optimization variables $\mathbf{z}_g^{EN} = \{z_{g,k}^{EN}\}_{k=0\dots K} \forall g$, $\mathbf{z}_b^{EN} = \{z_{b,k}^{EN}\}_{k=0\dots K} \forall b$, $\mathbf{z}_g^{RE} = \{z_{g,k}^{RE}\}_{k=0\dots K} \forall g$, and $\mathbf{z}_b^{RE} = \{z_{b,k}^{RE}\}_{k=0\dots K} \forall b$, resulting in a reformulated problem in the required ADMM form, as presented by Equation (9.27). Here, the equality constraints establishing the duplication of the coupling variables can be considered as the renewed coupling constraints (Equations (9.27f) to (9.27i)). The original coupling constraints, on the other hand, are now fully attributed to the auxiliary optimization variables (Equations (9.27d) and (9.27e)). The problem formulation thus obtained is adequately separable for the primal and auxiliary variables, as we will further discuss below.

$$\min_{\{\chi_b\}_{b=1\dots B}, \mathbf{z}_{BU}^{EN}, \mathbf{z}_{BU}^{RE}, \{\chi_g\}_{g=1\dots G}, \mathbf{z}_{GE}^{EN}, \mathbf{z}_{GE}^{RE}} \sum_{g=1}^G f_g(\bar{\mathbf{S}}_g, \mathbf{V}_g) \quad (9.27a)$$

subject to

$$\chi_b = (\bar{\mathbf{D}}_b, \mathbf{R}_b, \varkappa_b) \in X_b \quad \forall b \quad (9.27b)$$

$$\chi_g = (\bar{\mathbf{S}}_g, \mathbf{V}_g) \in X_g \quad \forall g \quad (9.27c)$$

$$\sum_{g=1}^G \mathbf{z}_g^{EN} = \sum_{b=1}^B \mathbf{z}_b^{EN} + \bar{\mathbf{D}}_{trad} \quad (9.27d)$$

$$\sum_{g=1}^G z_{g,k}^{RE} \geq \frac{1}{\Delta t} \left\| \begin{array}{c} z_{1,k}^{RE} \\ \vdots \\ z_{B,k}^{RE} \end{array} \right\|_2 \quad \forall k \quad (9.27e)$$

$$\mathbf{z}_g^{EN} = \bar{\mathbf{S}}_g \quad (\boldsymbol{\lambda}_g^{EN}) \quad \forall g \quad (9.27f)$$

$$\bar{\mathbf{D}}_b = \mathbf{z}_b^{EN} \quad (\boldsymbol{\lambda}_b^{EN}) \quad \forall b \quad (9.27g)$$

$$\mathbf{z}_g^{RE} = \mathbf{V}_g \quad (\boldsymbol{\lambda}_g^{RE}) \quad \forall g \quad (9.27h)$$

$$\mathbf{R}_b = \mathbf{z}_b^{RE} \quad (\boldsymbol{\lambda}_b^{RE}) \quad \forall b \quad (9.27i)$$

with

$$\begin{aligned} \bar{\mathbf{S}}_{GE} &= [\bar{\mathbf{S}}_1 \dots \bar{\mathbf{S}}_G] & \bar{\mathbf{D}}_{BU} &= [\bar{\mathbf{D}}_1 \dots \bar{\mathbf{D}}_B] \\ \mathbf{V}_{GE} &= [\mathbf{V}_1 \dots \mathbf{V}_G] & \mathbf{R}_{BU} &= [\mathbf{R}_1 \dots \mathbf{R}_B] \\ \mathbf{Z}_{GE}^{EN} &= [\mathbf{z}_1^{EN} \dots \mathbf{z}_G^{EN}] & \mathbf{Z}_{BU}^{EN} &= [\mathbf{z}_1^{EN} \dots \mathbf{z}_B^{EN}] \\ \mathbf{Z}_{GE}^{RE} &= [\mathbf{z}_1^{RE} \dots \mathbf{z}_G^{RE}] & \mathbf{Z}_{BU}^{RE} &= [\mathbf{z}_1^{RE} \dots \mathbf{z}_B^{RE}] \\ \boldsymbol{\Lambda}_{GE}^{EN} &= [\boldsymbol{\lambda}_1^{EN} \dots \boldsymbol{\lambda}_G^{EN}] & \boldsymbol{\Lambda}_{BU}^{EN} &= [\boldsymbol{\lambda}_1^{EN} \dots \boldsymbol{\lambda}_B^{EN}] \\ \boldsymbol{\Lambda}_{GE}^{RE} &= [\boldsymbol{\lambda}_1^{RE} \dots \boldsymbol{\lambda}_G^{RE}] & \boldsymbol{\Lambda}_{BU}^{RE} &= [\boldsymbol{\lambda}_1^{RE} \dots \boldsymbol{\lambda}_B^{RE}] \end{aligned} \quad (9.27j)$$

The augmented Lagrangian L_ρ of Problem (9.27) is then defined by Equation (9.28)²¹.

$$\begin{aligned} L_\rho &= \sum_{g=1}^G f_g(\bar{\mathbf{S}}_g, \mathbf{V}_g) + \sum_{g=1}^G \left((\boldsymbol{\lambda}_g^{EN})^T (\mathbf{z}_g^{EN} - \bar{\mathbf{S}}_g) + \frac{\rho}{2} \|\mathbf{z}_g^{EN} - \bar{\mathbf{S}}_g\|_2^2 \right) + \\ &\quad \sum_{b=1}^B \left((\boldsymbol{\lambda}_b^{EN})^T (\bar{\mathbf{D}}_b - \mathbf{z}_b^{EN}) + \frac{\rho}{2} \|\bar{\mathbf{D}}_b - \mathbf{z}_b^{EN}\|_2^2 \right) + \\ &\quad \sum_{g=1}^G \left((\boldsymbol{\lambda}_g^{RE})^T (\mathbf{z}_g^{RE} - \mathbf{V}_g) + \frac{\rho}{2} \|\mathbf{z}_g^{RE} - \mathbf{V}_g\|_2^2 \right) + \\ &\quad \sum_{b=1}^B \left((\boldsymbol{\lambda}_b^{RE})^T (\mathbf{R}_b - \mathbf{z}_b^{RE}) + \frac{\rho}{2} \|\mathbf{R}_b - \mathbf{z}_b^{RE}\|_2^2 \right) \end{aligned} \quad (9.28)$$

²¹ Note that the local (i.e., not coupling) constraints should actually be included in the augmented Lagrangian via their indicator function, where the indicator function $I_{\mathcal{A}}$ of a subset \mathcal{A} of a set \mathcal{X} indicates whether an element x in \mathcal{X} belongs to \mathcal{A} ($I_{\mathcal{A}}(x) = 1$) or not ($I_{\mathcal{A}}(x) = 0$). Nevertheless, for the ease of notation, these indicator functions are omitted in Equation (9.28). The local constraints will later on be explicitly included for each of the subproblems aiming to minimize part of the augmented Lagrangian.

By regrouping the different terms of the augmented Lagrangian in Equation (9.28), it can be rewritten from the point of view of the primal optimization variables, as done in Equation (9.29a), as well as from the point of view of the auxiliary optimization variables, as done in Equation (9.29b). In these equations, O_1 and O_2 represent all terms that are not depending on the primal or auxiliary variables, respectively. Note that the reformulation from the point of view of the auxiliary variables is not a mere regrouping of terms, but also involves some additional (straightforward) manipulations regarding special products. As such, the reformulation more clearly indicates that the update of the auxiliary variables actually comes down to a Euclidean projection of the demand side and supply side variables onto the set described by the original coupling constraints.

$$L_\rho = \underbrace{\sum_{g=1}^G \left(f_g(\bar{\mathbf{S}}_g, \mathbf{V}_g) - (\boldsymbol{\lambda}_g^{EN})^T \bar{\mathbf{S}}_g - (\boldsymbol{\lambda}_g^{RE})^T \mathbf{V}_g + \frac{\rho}{2} \left\| \begin{matrix} \mathbf{z}_g^{EN} - \bar{\mathbf{S}}_g \\ \mathbf{z}_g^{RE} - \mathbf{V}_g \end{matrix} \right\|_2^2 \right)}_{L_\rho^g(\bar{\mathbf{S}}_g, \mathbf{V}_g, \mathbf{z}_g^{EN}, \mathbf{z}_g^{RE}, \boldsymbol{\lambda}_g^{EN}, \boldsymbol{\lambda}_g^{RE})} + \sum_{b=1}^B \left((\boldsymbol{\lambda}_b^{EN})^T \bar{\mathbf{D}}_b + (\boldsymbol{\lambda}_b^{RE})^T \mathbf{R}_b + \frac{\rho}{2} \left\| \begin{matrix} \bar{\mathbf{D}}_b - \mathbf{z}_b^{EN} \\ \mathbf{R}_b - \mathbf{z}_b^{RE} \end{matrix} \right\|_2^2 \right) + O_1 \quad (9.29a)$$

$$L_\rho^b(\bar{\mathbf{D}}_b, \mathbf{R}_b, \mathbf{z}_b^{EN}, \mathbf{z}_b^{RE}, \boldsymbol{\lambda}_b^{EN}, \boldsymbol{\lambda}_b^{RE})$$

$$= \frac{\rho}{2} \left(\underbrace{\sum_{g=1}^G \left\| \mathbf{z}_g^{EN} - \left(\bar{\mathbf{S}}_g - \frac{\boldsymbol{\lambda}_g^{EN}}{\rho} \right) \right\|_2^2 + \sum_{b=1}^B \left\| \left(\bar{\mathbf{D}}_b + \frac{\boldsymbol{\lambda}_b^{EN}}{\rho} \right) - \mathbf{z}_b^{EN} \right\|_2^2}_{L_\rho^{EN}(\bar{\mathbf{S}}_{GE}, \bar{\mathbf{D}}_{BU}, \mathbf{Z}_{GE}^{EN}, \mathbf{Z}_{BU}^{EN}, \boldsymbol{\Lambda}_{GE}^{EN}, \boldsymbol{\Lambda}_{BU}^{EN})} + \sum_{g=1}^G \left\| \mathbf{z}_g^{RE} - \left(\mathbf{V}_g - \frac{\boldsymbol{\lambda}_g^{RE}}{\rho} \right) \right\|_2^2 + \sum_{b=1}^B \left\| \left(\mathbf{R}_b + \frac{\boldsymbol{\lambda}_b^{RE}}{\rho} \right) - \mathbf{z}_b^{RE} \right\|_2^2 \right) +$$

$$L_\rho^{RE}(\mathbf{V}_{GE}, \mathbf{R}_{BU}, \mathbf{Z}_{GE}^{RE}, \mathbf{Z}_{BU}^{RE}, \boldsymbol{\Lambda}_{GE}^{RE}, \boldsymbol{\Lambda}_{BU}^{RE})$$

$$O_2 \quad (9.29b)$$

The iterative ADMM solution procedure for the integrated system-level optimization problem can then be set up as Problem (9.30). Note that the different steps are now more adequately named compared to Intermezzo 9.1, in order to make a clear distinction between the actual optimization variables of interest, and the auxiliary variables that were merely introduced to make the problem separable, and compliant with the required ADMM structure.

Primal variables update:

$$\begin{aligned}
 & [\{\chi_g^{l+1}\}_{g=1\dots G}, \{\chi_b^{l+1}\}_{b=1\dots B}] = \\
 & \arg \min \sum_{g=1}^G L_\rho^g(\bar{\mathbf{S}}_g, \mathbf{V}_g, \mathbf{z}_g^{EN,l}, \mathbf{z}_g^{RE,l}, \boldsymbol{\lambda}_g^{EN,l}, \boldsymbol{\lambda}_g^{RE,l}) + \\
 & \quad \sum_{b=1}^B L_\rho^b(\bar{\mathbf{D}}_b, \mathbf{R}_b, \mathbf{z}_b^{EN,l}, \mathbf{z}_b^{RE,l}, \boldsymbol{\lambda}_b^{EN,l}, \boldsymbol{\lambda}_b^{RE,l}) + O_1 \\
 & \text{s.t. } \{\chi_g \in X_g\}_{g=1\dots G} \\
 & \quad \{\chi_b \in X_b\}_{b=1\dots B} \tag{9.30a}
 \end{aligned}$$

$$\begin{aligned}
 \Rightarrow \forall g: \chi_g^{l+1} &= \arg \min L_\rho^g(\bar{\mathbf{S}}_g, \mathbf{V}_g, \mathbf{z}_g^{EN,l}, \mathbf{z}_g^{RE,l}, \boldsymbol{\lambda}_g^{EN,l}, \boldsymbol{\lambda}_g^{RE,l}) \\
 & \text{s.t. } \chi_g \in X_g \tag{9.30b}
 \end{aligned}$$

$$\begin{aligned}
 \Rightarrow \forall b: \chi_b^{l+1} &= \arg \min L_\rho^b(\bar{\mathbf{D}}_b, \mathbf{R}_b, \mathbf{z}_b^{EN,l}, \mathbf{z}_b^{RE,l}, \boldsymbol{\lambda}_b^{EN,l}, \boldsymbol{\lambda}_b^{RE,l}) \\
 & \text{s.t. } \chi_b \in X_b \tag{9.30c}
 \end{aligned}$$

Auxiliary variables update:

$$\begin{aligned}
 & [\mathbf{Z}_{BU}^{EN,l+1}, \mathbf{Z}_{BU}^{RE,l+1}, \mathbf{Z}_{GE}^{EN,l+1}, \mathbf{Z}_{GE}^{RE,l+1}] = \\
 & \arg \min L_\rho^{EN}(\bar{\mathbf{S}}_{GE}^{l+1}, \bar{\mathbf{D}}_{BU}^{l+1}, \mathbf{Z}_{GE}^{EN}, \mathbf{Z}_{BU}^{EN}, \boldsymbol{\Lambda}_{GE}^{EN,l}, \boldsymbol{\Lambda}_{BU}^{EN,l}) + \\
 & \quad L_\rho^{RE}(\mathbf{V}_{GE}^{l+1}, \mathbf{R}_{BU}^{l+1}, \mathbf{Z}_{GE}^{RE}, \mathbf{Z}_{BU}^{RE}, \boldsymbol{\Lambda}_{GE}^{RE,l}, \boldsymbol{\Lambda}_{BU}^{RE,l}) + O_2 \\
 & \text{s.t. } \sum_{g=1}^G \mathbf{z}_g^{EN} = \sum_{b=1}^B \mathbf{z}_b^{EN} + \bar{\mathbf{D}}_{trad} \\
 & \quad \sum_{g=1}^G z_{g,k}^{RE} \geq \frac{1}{\Delta t} \left\| \begin{array}{c} z_{1,k}^{RE} \\ \vdots \\ z_{B,k}^{RE} \\ \Delta t \sigma_{sys,k} \end{array} \right\|_2 \quad \forall k \tag{9.30d}
 \end{aligned}$$

$$\Rightarrow \begin{bmatrix} \mathbf{z}_{GE}^{EN,l+1} \\ \mathbf{z}_{BU}^{EN,l+1} \end{bmatrix} = \arg \min L_{\rho}^{EN}(\bar{\mathbf{S}}_G^{l+1}, \bar{\mathbf{D}}_B^{l+1}, \mathbf{z}_{GE}^{EN}, \mathbf{z}_{BU}^{EN}, \Lambda_{GE}^{EN,l}, \Lambda_{BU}^{EN,l})$$

$$s.t. \sum_{g=1}^G \mathbf{z}_g^{EN} = \sum_{b=1}^B \mathbf{z}_b^{EN} + \bar{\mathbf{D}}_{trad} \quad (9.30e)$$

$$\Rightarrow \begin{bmatrix} \mathbf{z}_{GE}^{RE,l+1} \\ \mathbf{z}_{BU}^{RE,l+1} \end{bmatrix} = \arg \min L_{\rho}^{RE}(\mathbf{V}_G^{l+1}, \mathbf{R}_B^{l+1}, \mathbf{z}_{GE}^{RE}, \mathbf{z}_{BU}^{RE}, \Lambda_{GE}^{RE,l}, \Lambda_{BU}^{RE,l})$$

$$s.t. \sum_{g=1}^G z_{g,k}^{RE} \geq \frac{1}{\Delta t} \left\| \begin{array}{c} z_{1,k}^{RE} \\ \vdots \\ z_{B,k}^{RE} \\ \Delta t \sigma_{sys,k} \end{array} \right\|_2 \quad \forall k \quad (9.30f)$$

Dual variables update:

$$\lambda_g^{EN,l+1} = \lambda_g^{EN,l} + \rho(\mathbf{z}_g^{EN,l+1} - \bar{\mathbf{S}}_g^{l+1}) \quad \forall g \quad (9.30g)$$

$$\lambda_b^{EN,l+1} = \lambda_b^{EN,l} + \rho(\bar{\mathbf{D}}_b^{l+1} - \mathbf{z}_b^{EN,l+1}) \quad \forall b \quad (9.30h)$$

$$\lambda_g^{RE,l+1} = \lambda_g^{RE,l} + \rho(\mathbf{z}_g^{RE,l+1} - \mathbf{V}_g^{l+1}) \quad \forall g \quad (9.30i)$$

$$\lambda_b^{RE,l+1} = \lambda_b^{RE,l} + \rho(\mathbf{R}_b^{l+1} - \mathbf{z}_b^{RE,l+1}) \quad \forall b \quad (9.30j)$$

The iterative solution procedure can be summarized in words as follows.

Thanks to the decomposability of the problem, the primal variables update breaks down into B individual subproblems for the different buildings, and G individual subproblems for the different generators, all of which can be solved in parallel²².

The auxiliary variables update, on the other hand, breaks down into two larger separable subproblems for each time step, one per original coupling constraint. These problems cannot be further simplified, since their exact aim is to bring all primal variables together, and make them comply with the original coupling constraints, which are not separable. Consequently, the auxiliary variables update can be considered as a more centralized two-part subproblem, which collects and brings together information of all different buildings and generators.

²² This specific form of ADMM, where more than two separable problems are involved, is also known as multi-block ADMM.

Throughout this iterative solution procedure, the auxiliary and dual variables serve as coordination signals for the generators and buildings, in order to ultimately align the supply and demand, while minimizing the overall system operating cost. Nevertheless, note that the communication of both the auxiliary and dual variables to a particular building or generator is redundant, because of the explicit relations between both, as expressed by Equations (9.30g) to (9.30j). Hence, in this work, it is chosen to only communicate the dual variables as independent coordination signals. This choice is prompted by their straightforward physical interpretation as proxies for energy and reserve capacity prices, as we will further discuss below. The associated auxiliary variables, on the other hand, can then be locally computed by each of the generators and buildings based on the dual variables with the help of Equation (9.31), which is a reformulation of Equations (9.30g) to (9.30j).

$$\begin{aligned}
 \mathbf{z}_b^{EN,l+1} &= \bar{\mathbf{D}}_b^{l+1} + \frac{\lambda^{EN,l} - \lambda^{EN,l+1}}{\rho}, & \mathbf{z}_b^{RE,l+1} &= \mathbf{R}_b^{l+1} + \frac{\lambda_b^{RE,l} - \lambda_b^{RE,l+1}}{\rho} \quad \forall b \\
 \mathbf{z}_g^{EN,l+1} &= \bar{\mathbf{S}}_g^{l+1} - \frac{\lambda^{EN,l} - \lambda^{EN,l+1}}{\rho}, & \mathbf{z}_g^{RE,l+1} &= \mathbf{V}_g^{l+1} - \frac{\lambda_{GE}^{RE,l} - \lambda_{GE}^{RE,l+1}}{\rho} \quad \forall g
 \end{aligned} \tag{9.31}$$

Although all subproblems defined in Problem (9.30) could be directly used for the iterative ADMM solution procedure, the auxiliary subproblems can still be further revised, improving the interpretability of the ADMM procedure.

9.2.2.2 Further revision of the auxiliary subproblems

The fact that the auxiliary subproblems can be further revised is particularly true for the update of the auxiliary variables related to the energy balancing constraint²³, Equation (9.30e). As we will devise below, this optimization problem can be rewritten in the form of two explicit expressions for $\mathbf{z}_g^{EN,l+1}$ and $\mathbf{z}_b^{EN,l+1}$. In addition, the dual variables $\{\lambda_g^{EN,l+1} \forall g\}$ and $\{\lambda_b^{EN,l+1} \forall b\}$ can be reduced to a single dual variable $\lambda^{EN,l}$, which can be interpreted as the price for electric energy.

Since the subproblem to determine the auxiliary variables related to the energy balancing constraint represents a Euclidean projection onto an affine set, it has a clear-cut closed-form solution [184], which is given by Equation (9.32). Note that this closed-form solution can also be straightforwardly derived by applying the

²³ Be aware that the further revision discussed in this section is tailored to the case where the energy balancing constraint is imposed as an equality constraint (only then, the particular derived closed-form solution holds), and hence, is not applicable if one wishes to account for the curtailment of RES.

method of Lagrange multipliers to the optimization problem defined by Equation (9.30e).

$$\mathbf{z}_g^{EN,l+1} = \bar{\mathbf{S}}_g^{l+1} - \frac{\lambda_g^{EN,l}}{\rho} - \frac{1}{G+B} \mathbf{IMB}^{l+1} \quad \forall g \quad (9.32a)$$

$$\mathbf{z}_b^{EN,l+1} = \bar{\mathbf{D}}_b^{l+1} + \frac{\lambda_b^{EN,l}}{\rho} + \frac{1}{G+B} \mathbf{IMB}^{l+1} \quad \forall b \quad (9.32b)$$

with

$$\begin{aligned} \mathbf{IMB}^{l+1} &= \sum_{g=1}^G \left(\bar{\mathbf{S}}_g^{l+1} - \frac{\lambda_g^{EN,l}}{\rho} \right) - \sum_{b=1}^B \left(\bar{\mathbf{D}}_b^{l+1} + \frac{\lambda_b^{EN,l}}{\rho} \right) - \bar{\mathbf{D}}_{trad} \\ &= \sum_{g=1}^G \bar{\mathbf{S}}_g^{l+1} - \sum_{b=1}^B \bar{\mathbf{D}}_b^{l+1} - \bar{\mathbf{D}}_{trad} - \frac{\sum_{g=1}^G \lambda_g^{EN,l} + \sum_{b=1}^B \lambda_b^{EN,l}}{\rho} \end{aligned} \quad (9.32c)$$

The insertion of these expressions for $\mathbf{z}_g^{EN,l+1}$ and $\mathbf{z}_b^{EN,l+1}$ into the associated updates of the dual variables, Equations (9.30g) and (9.30h), results in the renewed update equations for the energy related dual variables, given by Equations (9.33a) and (9.33b).

$$\begin{aligned} \lambda_g^{EN,l+1} &= \lambda_g^{EN,l} + \rho(\mathbf{z}_g^{EN,l+1} - \bar{\mathbf{S}}_g^{l+1}) \quad \forall g \\ &= \frac{1}{G+B} \underbrace{\left(\sum_{g=1}^G \lambda_g^{EN,l} + \sum_{b=1}^B \lambda_b^{EN,l} \right)}_{\lambda^{EN,l}} - \\ &\quad \frac{\rho}{G+B} \left(\sum_{g=1}^G \bar{\mathbf{S}}_g^{l+1} - \sum_{b=1}^B \bar{\mathbf{D}}_b^{l+1} - \bar{\mathbf{D}}_{trad} \right) \quad \forall g \\ &= \lambda^{EN,l} - \frac{\rho}{G+B} \left(\sum_{g=1}^G \bar{\mathbf{S}}_g^{l+1} - \sum_{b=1}^B \bar{\mathbf{D}}_b^{l+1} - \bar{\mathbf{D}}_{trad} \right) \quad \forall g \end{aligned} \quad (9.33a)$$

$$\begin{aligned} \lambda_b^{EN,l+1} &= \lambda_b^{EN,l} + \rho(\bar{\mathbf{D}}_b^{l+1} - \mathbf{z}_b^{EN,l+1}) \quad \forall b \\ &= \lambda^{EN,l} - \frac{\rho}{G+B} \left(\sum_{g=1}^G \bar{\mathbf{S}}_g^{l+1} - \sum_{b=1}^B \bar{\mathbf{D}}_b^{l+1} - \bar{\mathbf{D}}_{trad} \right) \quad \forall b \end{aligned} \quad (9.33b)$$

Equations (9.33a) and (9.33b) show that, irrespective of the initialization of $\{\lambda_g^{EN,0} \forall g\}$ and $\{\lambda_b^{EN,0} \forall b\}$, the dual variables $\{\lambda_g^{EN,l+1} \forall g\}$ and $\{\lambda_b^{EN,l+1} \forall b\}$ become equal after the first iteration step, and remain equal for the remainder of the solution procedure. Hence, all dual variables $\{\lambda_g^{EN,l} \forall g, \lambda_b^{EN,l} \forall b\}$ can be replaced by one dual variable $\lambda^{EN,l}$ in Equation (9.30), which is updated depending on the overall imbalance between the supply of and demand for electric energy.

This unique dual variable $\lambda^{EN,l}$ can be readily interpreted as the price for electric energy. Indeed, in general, the value of the dual variable at the optimal solution corresponds to the change in the optimal value of the objective function by relaxing the constraint by an infinitesimal unit [185]. Accordingly, the particular dual variable associated with the energy balance constraint in the integrated system-level optimization problem, which aims to minimize the overall operating cost, corresponds to the marginal cost of generating one extra unit of electric energy. The interpretation of this dual variable as the price for electric energy is moreover further substantiated by looking at the objective functions of the generator and building subproblems, given by Equation (9.29a), which clearly shows that the generators and buildings are exchanging commodities \bar{S}_g and \bar{D}_b at a particular price $\lambda_g^{EN,l} = \lambda_b^{EN,l} = \lambda^{EN,l}$.

Finally, note that based on the derived expression for $\lambda^{EN,l+1}$ in Equations (9.33a) and (9.33b), the closed-form solution of the update of the auxiliary variables related to the energy balancing constraint can be further simplified to Equations (9.34a) and (9.34b), serving as the final substitute of Equation (9.30e).

$$z_g^{EN,l+1} = \bar{S}_g^{l+1} - \frac{1}{G+B} \left(\sum_{g=1}^G \bar{S}_g^{l+1} - \sum_{b=1}^B \bar{D}_b^{l+1} - \bar{D}_{trad} \right) \quad \forall g \quad (9.34a)$$

$$z_b^{EN,l+1} = \bar{D}_b^{l+1} + \frac{1}{G+B} \left(\sum_{g=1}^G \bar{S}_g^{l+1} - \sum_{b=1}^B \bar{D}_b^{l+1} - \bar{D}_{trad} \right) \quad \forall b \quad (9.34b)$$

For the update of the auxiliary variables related to the reserve capacity balancing constraint, Equation (9.30f), on the other hand, no closed-form solution is derived in this dissertation. Although there exist closed-form solutions for projections onto second order cones (see e.g., [186]), the particular form considered in this dissertation is even more involved due to the presence of the constant $\Delta t \sigma_{sys,k}$ in the 2-norm in the constraint. Therefore, the auxiliary problem is retained in the form of Equation (9.30f), which is a well-manageable optimization problem with a low number of optimization variables.

Although no closed-form solution is derived here, before finalizing the discussion about the revision of the subproblems, it is still useful to consider the reserve

capacity related dual variables $\{\lambda_g^{RE,l} \forall g, \lambda_b^{RE,l} \forall b\}$, as was done for the energy related auxiliary problem. Due to the specific problem structure, the dual variables related to the reserve capacity balancing constraint cannot be reduced to a single dual variable²⁴. Nevertheless, in analogy with the aforementioned discussion regarding the energy related auxiliary problem, the dual variables can still be interpreted as price signals, steered by the imbalance between supply and demand, albeit this time with an additional, intermediate step. Indeed, the dual variables $\{\lambda_g^{RE,l} \forall g\}$ are now updated based on the imbalance between the projection of the demand for reserve capacity onto the set defined by the original coupling constraints, $\mathbf{z}_g^{RE,l+1}$, and the actual demand for reserve capacity, \mathbf{V}_g^{l+1} (which might not satisfy the original coupling constraint while searching for the optimal solution). Analogously, the dual variables $\{\lambda_b^{RE,l} \forall b\}$ are updated based on the imbalance between the actual demand for reserve capacity, \mathbf{R}_b^{l+1} , and the projected demand for reserve capacity, $\mathbf{z}_b^{RE,l+1}$. The balance between the projected supply and the projected demand is in turn enforced by solving the auxiliary problem related to the reserve capacity balancing constraint.

9.2.2.3 Resulting ADMM algorithm for the integrated system-level optimization problem

Taking all the aforementioned considerations into account, the final algorithm to solve Problem (9.21) in an efficient, distributed way is given by Algorithm 9.1. The ADMM procedure corresponding to Algorithm 9.1 is schematically represented in Figure 9.3 for one iteration step.

²⁴ It can be shown that $\{\lambda_g^{RE,l} \forall g\}$ can be reduced to one and the same dual variable for all generators, $\lambda_{GE}^{RE,l+1}$. For $\{\lambda_b^{RE,l} \forall b\}$, on the other hand, this does not hold.

Algorithm 9.1

The ADMM procedure for the integrated system-level optimization problem

Initialization

$$\boldsymbol{\lambda}^{EN,0}, \boldsymbol{\lambda}_b^{RE,0}, \boldsymbol{\lambda}_g^{RE,0}, \mathbf{z}_b^{EN,0}, \mathbf{z}_g^{EN,0}, \mathbf{z}_b^{RE,0}, \mathbf{z}_g^{RE,0} \leftarrow \mathbf{0}_K \quad \forall g, b$$

$$l \leftarrow 0$$

$$\text{while } \|\text{res}_{prim}^{l+1}\|_2 > \epsilon_{prim} \text{ and } \|\text{res}_{dual}^{l+1}\|_2 > \epsilon_{dual}$$

Primal variables update

Buildings

$$\forall b : \chi_b^{l+1} = \arg \min (\boldsymbol{\lambda}^{EN,l})^T \bar{\mathbf{D}}_b + (\boldsymbol{\lambda}_b^{RE,l})^T \mathbf{R}_b + \frac{\rho}{2} \left\| \begin{matrix} \bar{\mathbf{D}}_b - \mathbf{z}_b^{EN,l} \\ \mathbf{R}_b - \mathbf{z}_b^{RE,l} \end{matrix} \right\|_2^2$$

$$s.t. \quad \chi_b \in X_b$$

Generators

$$\forall g : \chi_g^{l+1} = \arg \min \sum_{k=1}^K \left(\frac{c_{2,g}}{2} \bar{S}_{g,k}^2 + c_{1,g} \bar{S}_{g,k} + c_{0,g} + \frac{c_{2,g}}{2} V_{g,k}^2 \Delta t^2 + c_{3,g} \left(\Phi^{-1}(1 - \epsilon_{\dot{P}_{gen,g,k}}) V_{g,k} \right) \right) - (\boldsymbol{\lambda}^{EN,l})^T \bar{\mathbf{S}}_g - (\boldsymbol{\lambda}_g^{RE,l})^T \mathbf{V}_g + \frac{\rho}{2} \left\| \begin{matrix} \mathbf{z}_g^{EN,l} - \bar{\mathbf{S}}_g \\ \mathbf{z}_g^{RE,l} - \mathbf{V}_g \end{matrix} \right\|_2^2$$

$$s.t. \quad \chi_g \in X_b$$

Auxiliary variables update

Energy

$$\mathbf{z}_b^{EN,l+1} = \bar{\mathbf{D}}_b^{l+1} + \frac{1}{G+B} \left(\sum_{g=1}^G \bar{\mathbf{S}}_g^{l+1} - \sum_{b=1}^B \bar{\mathbf{D}}_b^{l+1} - \bar{\mathbf{D}}_{trad} \right) \quad \forall b$$

$$\mathbf{z}_g^{EN,l+1} = \bar{\mathbf{S}}_g^{l+1} - \frac{1}{G+B} \left(\sum_{g=1}^G \bar{\mathbf{S}}_g^{l+1} - \sum_{b=1}^B \bar{\mathbf{D}}_b^{l+1} - \bar{\mathbf{D}}_{trad} \right) \quad \forall g$$

Reserve capacity

$$\forall k : [z_{1,k}^{RE,l+1}, \dots, z_{G,k}^{RE,l+1}, z_{1,k}^{RE,l+1}, \dots, z_{B,k}^{RE,l+1}] =$$

$$\arg \min_{\mathbf{z}} \sum_{g=1}^G \left\| z_{g,k}^{RE,l} - \left(V_{g,k}^{l+1} - \frac{\lambda_{g,k}^{RE,l}}{\rho} \right) \right\|_2^2 +$$

$$\sum_{b=1}^B \left\| \left(R_{b,k}^{l+1} + \frac{\lambda_{b,k}^{RE,l}}{\rho} \right) - z_{b,k}^{RE} \right\|_2^2$$

$$s.t. \quad \sum_{g=1}^G z_{g,k}^{RE} \geq \frac{1}{\Delta t} \left\| \begin{array}{c} z_{1,k}^{RE} \\ \vdots \\ z_{B,k}^{RE} \\ \Delta t \sigma_{sys,k} \end{array} \right\|_2$$

Dual variables update**Energy**

$$\lambda^{EN,l+1} = \lambda^{EN,l} - \frac{\rho}{G+B} \left(\sum_{g=1}^G \bar{\mathbf{S}}_g^{l+1} - \sum_{b=1}^B \bar{\mathbf{D}}_b^{l+1} - \bar{\mathbf{D}}_{trad} \right)$$

Reserve capacity

$$\lambda_g^{RE,l+1} = \lambda_g^{RE,l} + \rho (\mathbf{z}_g^{RE,l+1} - \mathbf{V}_g^{l+1}) \quad \forall g$$

$$\lambda_b^{RE,l+1} = \lambda_b^{RE,l} + \rho (\mathbf{R}_b^{l+1} - \mathbf{z}_b^{RE,l+1}) \quad \forall b$$

Continuation

$$\| \mathbf{res}_{prim}^{l+1} \|_2 = \left\| \begin{array}{c} \mathbf{z}_g^{EN,l+1} - \bar{\mathbf{S}}_g^{l+1} \\ \bar{\mathbf{D}}_b^{l+1} - \mathbf{z}_b^{EN,l+1} \\ \mathbf{z}_g^{RE,l+1} - \mathbf{V}_g^{l+1} \\ \mathbf{R}_b^{l+1} - \mathbf{z}_b^{RE,l+1} \end{array} \right\|_2$$

$$\| \mathbf{res}_{dual}^{l+1} \|_2 = \left\| \begin{array}{c} \rho (\mathbf{z}_g^{EN,l+1} - \mathbf{z}_g^{EN,l}) \\ \rho (\mathbf{z}_b^{EN,l+1} - \mathbf{z}_b^{EN,l}) \\ \rho (\mathbf{z}_g^{RE,l+1} - \mathbf{z}_g^{RE,l}) \\ \rho (\mathbf{z}_b^{RE,l+1} - \mathbf{z}_b^{RE,l}) \end{array} \right\|_2$$

$$l \leftarrow l + 1$$

end

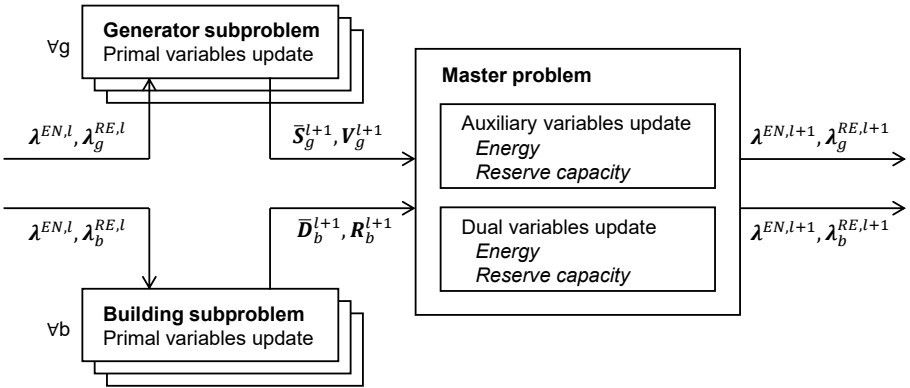


Figure 9.3: Schematic representation of all different (primal/auxiliary/dual) update steps within one iteration of the distributed ADMM procedure, illustrating its hierarchical structure.

Figure 9.3 clearly shows that due to the implementation of ADMM, the global, integrated system-level optimization problem discussed in Section 9.2.1 breaks down into a hierarchical structure. This hierarchical structure can be interpreted as a day-ahead coordination framework between a master problem (i.e., the update of the auxiliary variables as well as of the dual variables/prices), which collects and brings together information about all different buildings and generators, and individual subproblems for all participants (i.e., the update of the primal variables for all distinct generators and buildings), which individually optimize their operating schedule for the upcoming day based on the prices they receive. The exchange of the dual variables (i.e., price information) between the master problem and the generator and building subproblems is used to converge towards the optimal solution. As such, the ADMM procedure can be viewed as a form of tâtonnement or price adjustment process, where the price is increased or decreased depending on whether there is an excess demand or supply, respectively, ultimately aiming to converge towards a balance between the supply of and demand for electric energy as well as between the supply of and demand for reserve capacity [121, 178, 187].

This hierarchical coordination framework can be interpreted as a solid basis for more dedicated research regarding system operation, market design, consumer coordination and tariff structures for DR under uncertainty. Indeed, additional modifications and extensions are required to improve the validity of the coordination framework, such as a correct representation of all underlying markets and associated market mechanisms, and the inclusion of all relevant market players (such as aggregators). Although this is not further pursued in this dissertation, it is recommended as a valuable track of future research.

In a next step, the integrated system-level optimization problem is solved in Section 9.3 to investigate the beneficial impact of the coordination of the demand for reserve capacity in addition to the demand for electric energy on the overall system operating cost.

9.3 Case study

In this section, the added value of the proposed SMPC^{ap} strategy for DR under uncertainty is evaluated. This is done by comparing the overall system operating cost, obtained by solving the integrated system-level optimization problem, for two cases: one where the demand side is controlled by the proposed SMPC^{ap} strategy incorporating ADF, and one where ADF, and thus also the coordination of the demand for reserve capacity, is prohibited.

The considered flexible demand side in this study consists of the nine residential buildings for which the parametric uncertainty was characterized in Chapter 5; since the focus is on the day-ahead scheduling, only the open-loop stochastic OCP is considered, meaning that all these buildings are represented by their reference SSM combined with the corresponding covariance matrix. All buildings are equipped with a compression heat pump, which is sized according to the nominal heat demand with an additional safety factor of 1.5, to account for the additive as well as parametric uncertainties. For the installed heat emission system, both radiators and floor heating are looked at, albeit in two distinct analyses, in order to be able to distinguish the added value of the SMPC^{ap} strategy for DR under uncertainty for either of these cases.

All buildings are assumed to be subject to the same weather conditions, for which the weather data of 2016 are used. The expected value and covariance of the weather forecasts are again determined by applying the methods described in Chapter 5.

Regarding the occupant behavior, each of the nine buildings is combined with a different²⁵ StROBe profile, in order to further increase the diversification (and hence representativeness) of the demand side. This StROBe profile is this time not only used to define the internal heat gains (where the expected value and covariance of the internal heat gains are again determined as prescribed in Chapter 5), but also the indoor temperature set-points, serving as the lower thermal comfort bound. In contrast to previously considered case studies²⁶, the maximum allowed temperature also plays an important role here, as it defines the allowable temperature fluctuations when the building is occupied, thereby impeding the operational freedom

²⁵ Different, both in terms of magnitude, and in terms of timing.

²⁶ Recall that in all previously considered case studies (except for Chapter 8), the upper thermal comfort bound was of minor importance, since the control strategy was aiming to minimize the energy use, and consequently, was trying to stick to the lower temperature bound.

of the control strategy for DR. The upper temperature bound is determined as follows²⁷: $T_{ia}^{max} = \max(\{T_{ia,k}^{min}\}_{k=0\dots K+1}) + \Delta T_{DR}$, where ΔT_{DR} defines the DR temperature band²⁸. In this work, ΔT_{DR} is set equal to 4 °C [24]. This choice is further substantiated in Intermezzo 9.2.

Each of the nine considered buildings is either controlled by the SMPC^{ap} strategy incorporating ADF, developed in this dissertation, or by an equivalent strategy where ADF is disabled; both strategies consider a risk-averseness level regarding thermal comfort of $1 - \epsilon = 0.99$. The demand determined by these control strategies is for each building scaled up by a constant factor, in order to guarantee that the demand side flexibility can have a significant impact on the electricity generation system. To maximize insight, three different scaling factors, representing different market penetration levels, are considered, being 1000, 10,000 or 100 000. This leads to a demand side consisting of 9000, 90 000 or 900 000 flexible heat pumps²⁹, representing a heat pump market penetration level of approximately 0.2, 2 or 20%, respectively. As these heat pumps can either be coupled to radiators or floor heating, and can either be controlled by a strategy with or without ADF, a total number of 12 scenarios for the flexible demand side are considered, which are summarized in Figure 9.4. For each of these scenarios, the integrated system-level optimization problem is being solved, in order to determine the overall system operating cost. The analysis is supplemented with one additional scenario, without any heating demand, serving as a reference. Note that this final scenario can be calculated by centrally solving the integrated system-level optimization problem (9.21), with $\bar{D}_b = \mathbf{R}_b = \mathbf{0}_K \forall b$; no distributed solution strategy is required in this case.

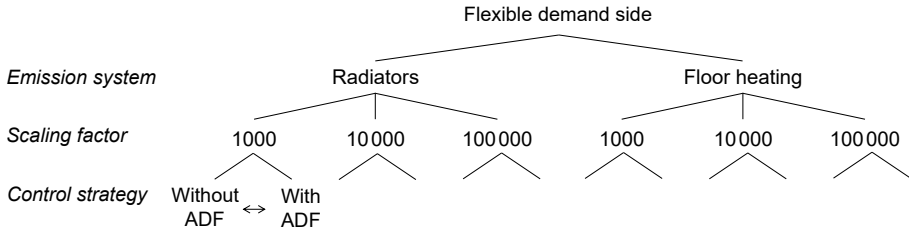


Figure 9.4: The different scenarios for the flexible demand side as part of the integrated system-level problem.

²⁷ The chosen approach acknowledges that the maximum allowed temperature for DR merely needs to be based on the temperature set-points during the occupied period.

²⁸ This approach implies that only upward flexibility is considered in this dissertation.

²⁹ These numbers should be weighed against the total number of households in Belgium, amounting to $\approx 5\,000\,000$ in 2021 [188].

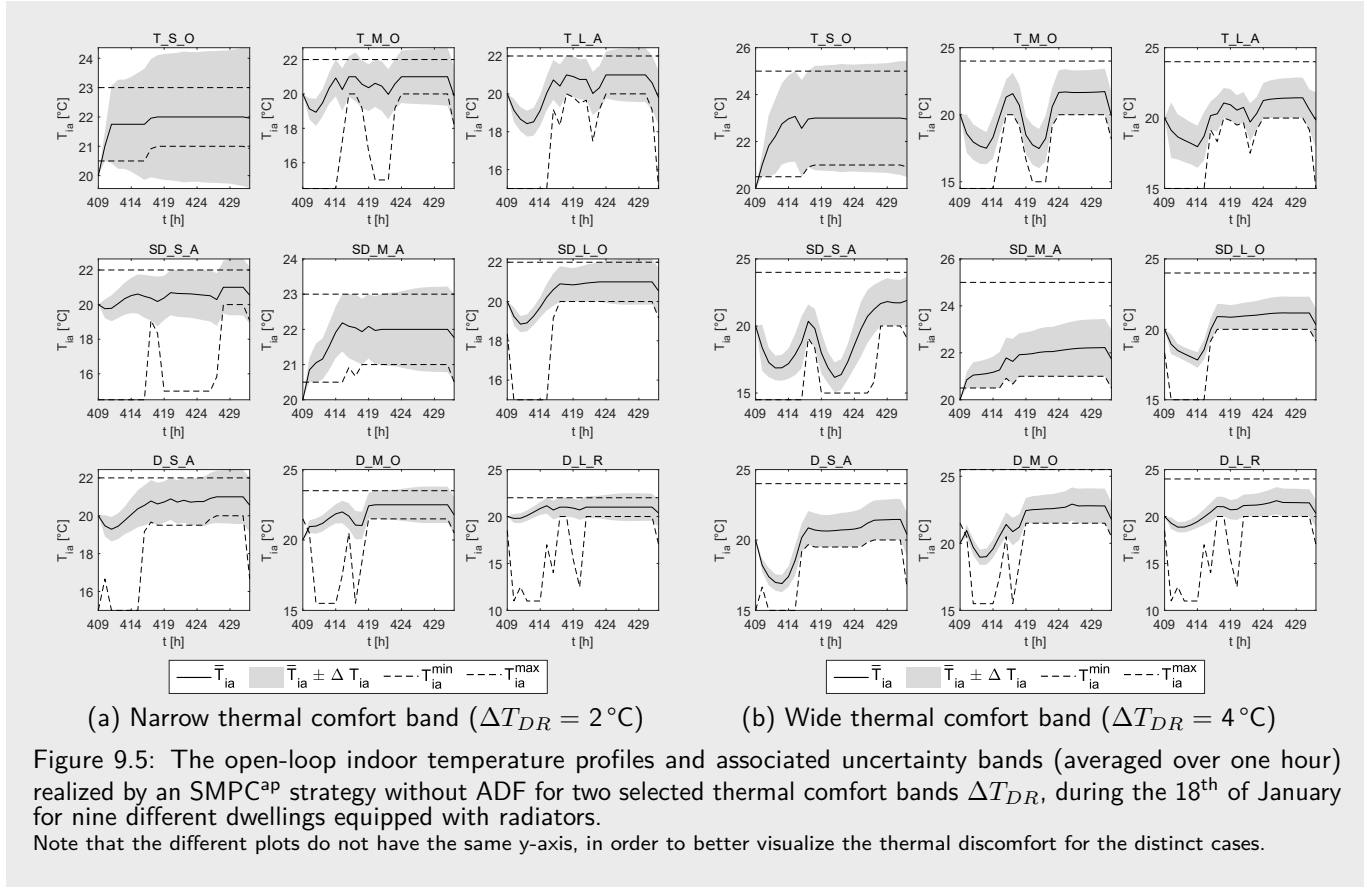
Intermezzo 9.2

Selection of the DR temperature band

In this work, the DR temperature band ΔT_{DR} is set equal to 4°C . Although narrower DR temperature bands are possible (see e.g., [18, 189]), this would hamper a fair comparison between the case without and with ADF. This statement is clarified by Figure 9.5, which shows the temperature profiles obtained from a small, illustrative analysis, where all buildings considered in this case study are equipped with radiators and controlled by an SMPC^{ap} strategy without ADF, aiming to minimize the energy use^a during the 18th of January 2016. As can be seen from the left hand side of Figure 9.5, a DR temperature band $\Delta T_{DR} < 4^\circ\text{C}$ is not able to guarantee thermal comfort towards the end of the prediction horizon, resulting in a control-in-the-middle approach, where the uncertainty band surrounding the reference temperature profile equally violates the lower and upper bound. The energy use, and thus also the operational cost, associated with this control-in-the-middle approach are unfairly low, especially when comparing them with the energy use and operational cost associated with an SMPC^{ap} strategy incorporating ADF which does succeed to guarantee thermal comfort. A relaxation of the upper comfort bound by increasing the DR temperature range would push the reference profile upwards, to prevent the uncertainty band from crossing the lower temperature bound, leading to a duly higher energy use for the SMPC^{ap} strategy without ADF.

One important drawback of allowing a wide DR temperature band is that it can result in large temperature fluctuations, which might be perceived as uncomfortable. The ASHRAE standard 55-2004 for example prescribes that the rate of change of the indoor temperature should be limited to 2.1°C in 1 h, although larger changes might be tolerated if these fluctuations are under the direct control of the user [190]. Here, it might be argued that the temperature adjustments for DR purposes correspond to the latter category. However, it should be stressed that this is a significant assumption.

^a Be aware that the objective function minimizing energy use is only considered in this small, illustrative analysis. For the actual case study, the objective functions of the building subproblems correspond to Equations (9.29a) and (9.30c).



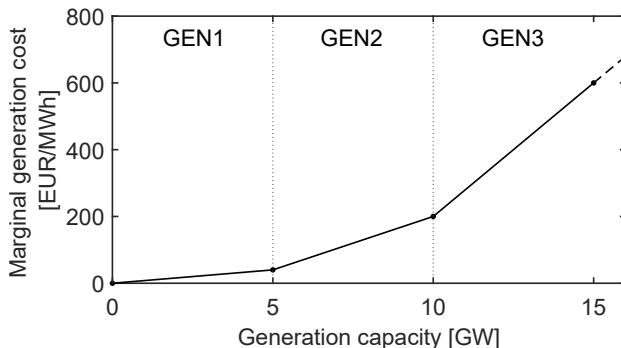


Figure 9.6: The convex approximation of the merit order curve in the form of a piece-wise, linear function, with three segments, used to characterize the supply side. The supply side is assumed to consist of three aggregated generators, GEN1, GEN2 and GEN3, each representing a group of technologies.

The fixed, traditional demand, supplementing the flexible demand of the heat pumps, is taken equal to the total load profile of the Belgian power system, reduced by the renewable supply. To ensure consistency, the used time series are also based on data for the year 2016, and are collected from the ENTSOE Transparency Platform [191]. The time series of the renewable supply is rescaled in accordance with the currently installed capacities. Finally, the system-level uncertainty is assumed to be fixed, with $3\sigma_{sys}$ equal to 1 GW. This value reflects the largest contingency in the Belgian power system, being either the loss of a nuclear power plant, or the outage of the NEMO-link between Belgium and the UK serving as an important transmission asset [192].

The supply side considered in this case study is inspired by the Belgian power system, such that it reflects the same orders of magnitude. It is modeled by a convex approximation of the merit order curve in the form of a piece-wise, linear function, with three segments³⁰, as shown in Figure 9.6. As such, three aggregated generators (GEN1, GEN2 and GEN3) are discerned. The first two aggregated generators each represent a group of technologies with a total capacity of 5 GW; the capacity of the third, most expensive generator, on the other hand, is unbounded, to prevent feasibility issues. The cost coefficients $c_{2,g}$, $c_{1,g}$ and $c_{0,g}$ describing the day-ahead expected cost of energy (see Equation (9.13b)) for each of these aggregated generators are summarized in Table 9.1. Table 9.1 also shows the cost

³⁰ The points demarcating the different segments of the piece-wise linear approximation of the merit order curve are (0,0), (5,40), (10,200) and (15,600), where the first value corresponds to the generation capacity (expressed in GW), and the second one to the marginal generation cost (expressed in EUR/MWh).

Table 9.1: The cost coefficients describing the day-ahead cost of electric energy ($c_{2,g}$, $c_{1,g}$ and $c_{0,g}$) and reserve capacity provision ($c_{3,g}$) of the three aggregated generators constituting the supply side of the integrated system-level problem.

| | GEN1 | GEN2 | GEN3 |
|-----------------------------------|-------|-------|------|
| $c_{0,g}$ [EUR] | 0 | 0 | 0 |
| $c_{1,g}$ [EUR/MWh] | 0 | 40 | 200 |
| $c_{2,g}$ [EUR/MWh ²] | 0.008 | 0.032 | 0.08 |
| $c_{3,g}$ [EUR/MW] | 6 | 36 | 120 |

Table 9.2: The four representative days for which the integrated system-level optimization problem is solved. The system behavior over the entire heating season can be appraised with the help of the weighting factors associated with each representative day.

| Day index | Date | Weighting factor |
|-----------|-----------------------------------|------------------|
| 18 | 18 th of January 2016 | 8.0 |
| 60 | 29 th of February 2016 | 73.3 |
| 86 | 26 th of March 2016 | 34.1 |
| 307 | 2 nd of November 2016 | 95.6 |

coefficients for the day-ahead cost of reserve capacity provision, which is assumed to be 30%³¹ of the average marginal generation cost [177].

To maintain tractability, the system-level operating cost is calculated for a set of representative days, rather than for each distinct day of the entire heating season (1st of October – 1st of April). These representative days are determined with the method of Poncelet et al. [193], based on the time series for the ambient temperature, solar heat gains and residual loads throughout the heating season, resulting in a final set of four days, summarized in Table 9.2. With the help of the weighting factors defined in Table 9.2, these four days can be used to appraise the system behavior over the entire heating season. The associated weather conditions and non-flexible residual load profiles are depicted in Figure 9.7 for the four representative days.

For each of the four representative days, the operating schedules for all generators and buildings are determined for hourly time steps, over a time span of 24 hours.

³¹ Be aware that the chosen percentage has an important impact on the trade-off between the supply of energy and the supply of reserve capacity. Consequently, the presented results should be interpreted in light of this choice.

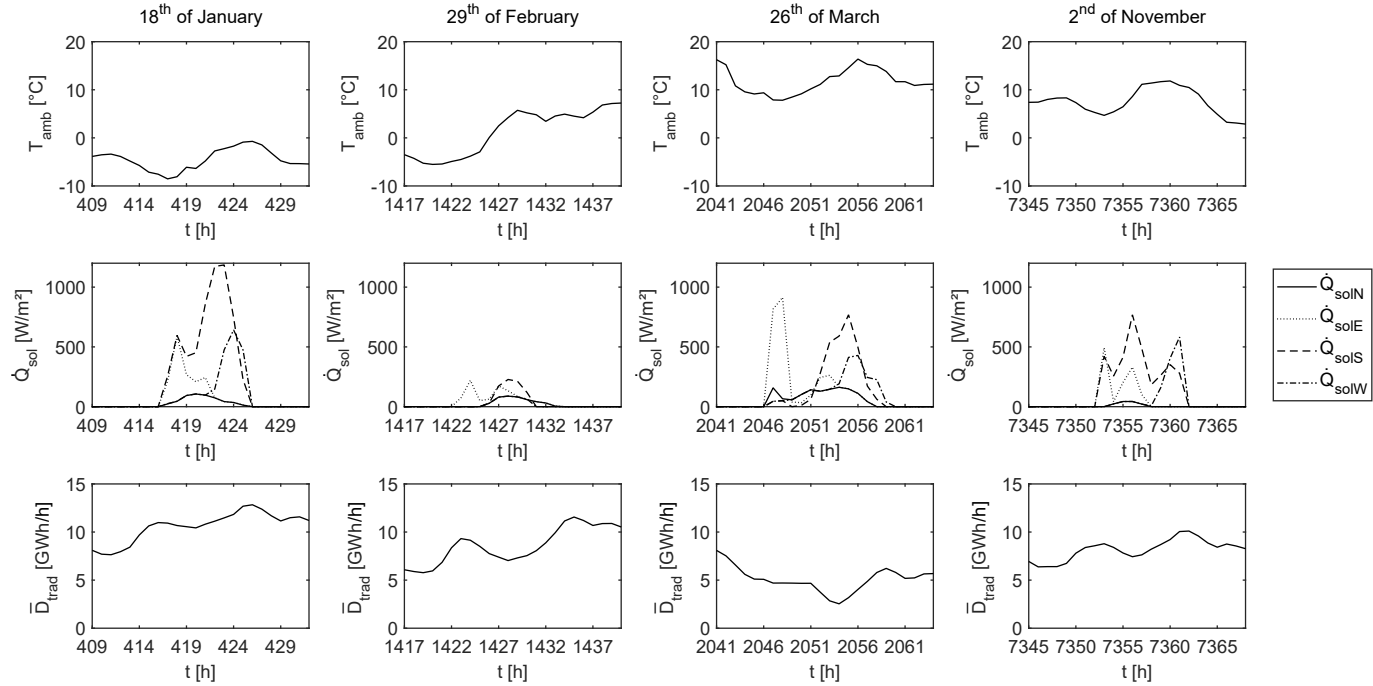


Figure 9.7: The time profiles of the weather conditions (i.e., ambient temperature and solar heat gains) and of the non-flexible, residual load during the four representative days for which the integrated system-level optimization problem is being solved.

Although only the first 24 hours of the building response matter for the balance between supply and demand, it should be acknowledged that buildings typically have time constants that well exceed this time span. Therefore, the prediction horizon of the building subproblems is prolonged to 60 hours (again restricted by the characteristics of the available disturbance forecasts). In line with this, also the coordination signals (prices) need to be prolonged. To avoid end-of-horizon effects, the value at the end of the day is retained for the remainder of the prolonged prediction horizon.

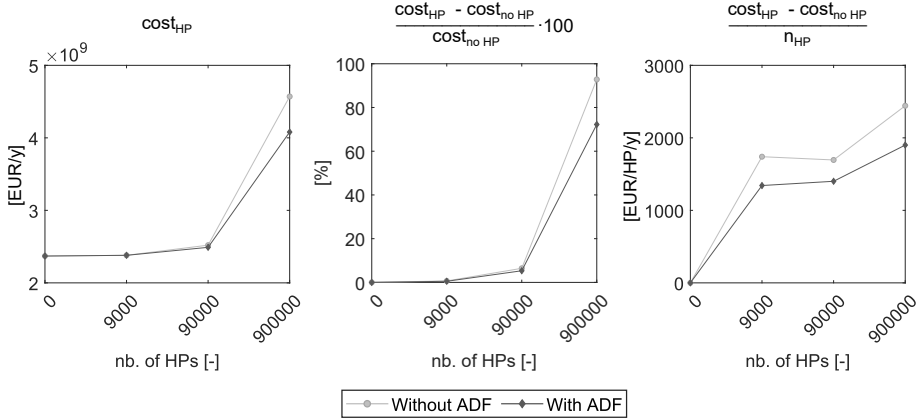
Finally, the convergence related parameters for the ADMM procedure are set as follows. The primal and dual stopping criteria are set to 10^{-3} , the maximum number of iterations is set to 400, the initial value for the penalty parameter ρ is set to 1, and it is updated according to the adaptive scheme discussed in Intermezzo 9.1.

9.4 Results and discussion

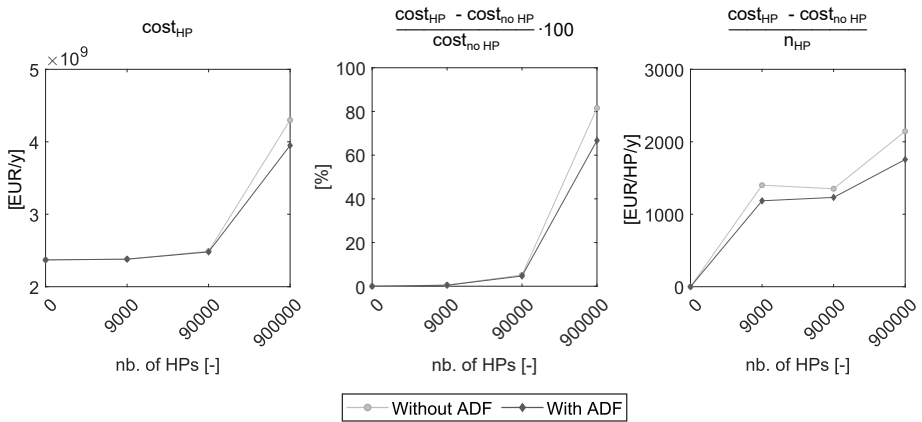
As we will illustrate below, the day-ahead coordination of the demand for reserve capacity, in addition to the demand for energy, enables a reduction of the system-level operating cost compared to the case where only the energy demand is coordinated; in the considered stylized case studies, cost reductions up to 10.7% are achieved. These results indicate the added value of using the proposed SMPC^{ap} strategy for DR under uncertainty.

Figure 9.8 compares the system operating cost for the entire heating season in case the flexible demand side in the integrated system-level optimization problem is controlled by the proposed SMPC^{ap} strategy, or by an equivalent strategy without ADF. As explained in Section 9.3, the analysis is performed for the case where all buildings are equipped with radiators (Figure 9.8a), and the case where the buildings are equipped with underfloor heating (Figure 9.8b). In both Figures 9.8a and 9.8b, the system operating cost is shown from three different points of view. The leftmost plots show the absolute operating cost, the plots in the middle show the relative cost increase compared to the reference case without heat pumps, and the rightmost plots depict the additional cost per heat pump compared to the same reference case. Within each plot, different market penetration levels of the flexible heat pumps are considered.

All plots in Figure 9.8 clearly indicate that the day-ahead coordination of the demand for reserve capacity, in addition to the demand for energy, enables an operating cost reduction, which becomes more significant for increasing heat pump market penetration levels. This indicates that the implementation of the proposed SMPC^{ap} strategy for DR under uncertainty contributes to a more cost-efficient electrification of the residential space heating sector, thus substantiating its added value.



(a) In case of radiators.



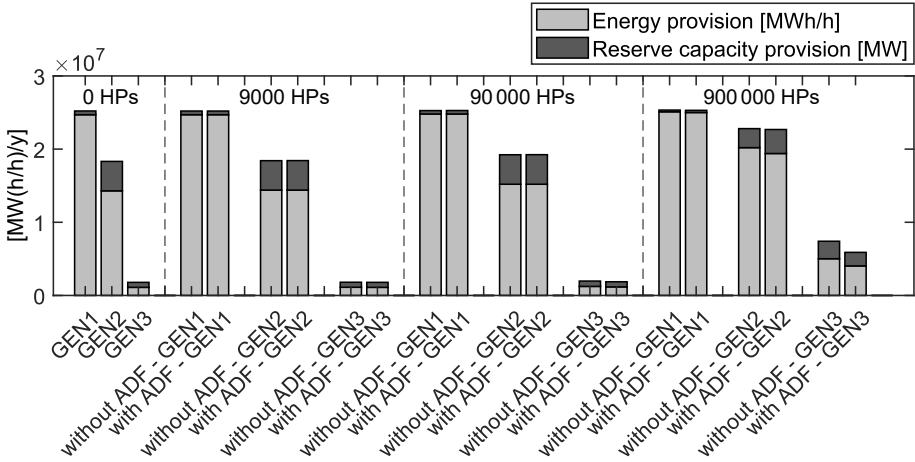
(b) In case of floor heating.

Figure 9.8: The comparison of the total system operating cost over the entire heating season in case the demand side in the integrated system-level optimization problem is controlled by the proposed SMPC^{ap} strategy, or by an equivalent strategy without ADF, for increasing heat pump market penetration levels. The figure shows the absolute operating cost, the relative cost increase compared to the reference case without flexible heat pumps, and the absolute additional cost per heat pump compared to the reference case.

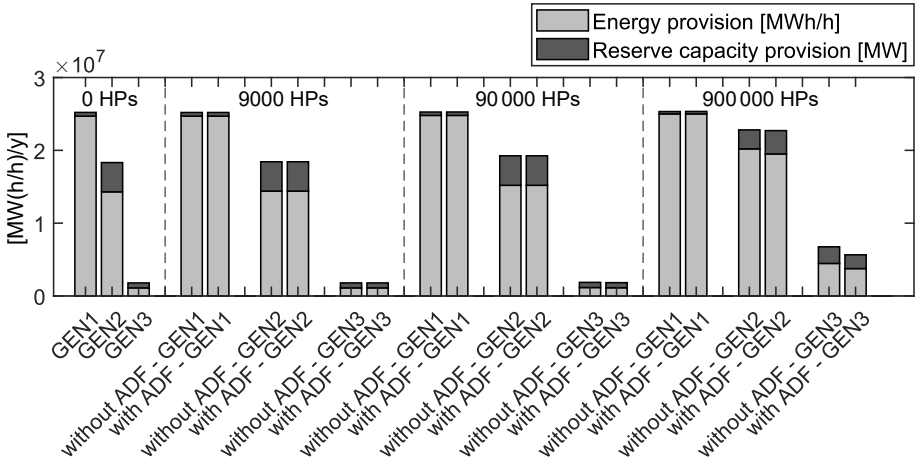
A comparison of Figures 9.8a and 9.8b demonstrates that the cost reductions induced by using the SMPC^{ap} strategy incorporating ADF are most pronounced for a demand side equipped with radiators. In the case of a flexible demand side consisting of 9000, 90 000 or 900 000 heat pumps combined with radiators, the incorporation of ADF can induce an operating cost reduction of 0.2%, 1.1% or 10.7%, respectively, relative to the case without ADF; for the analogous case with floor heating, on the other hand, relative cost reductions of 0.1%, 0.4% and 8.1% can be attained by incorporating ADF. In absolute terms, for a flexible demand side consisting of 9000, 90 000 or 900 000 heat pumps combined with radiators, the cost per heat pump per year³² is thanks to the incorporation of ADF reduced from 1747 EUR/HP/y to 1347 EUR/HP/y (reduction of 400 EUR/HP/y), from 1699 EUR/HP/y to 1404 EUR/HP/y (reduction of 295 EUR/HP/y), and from 2450 EUR/HP/y to 1907 EUR/HP/y (reduction of 543 EUR/HP/y); for the analogous case with floor heating, the cost per heat pump is reduced from 1407 EUR/HP/y to 1190 EUR/HP/y (reduction of 217 EUR/HP/y), from 1355 EUR/HP/y to 1235 EUR/HP/y (reduction of 120 EUR/HP/y), and 2151 EUR/HP/y to 1761 EUR/HP/y (reduction of 390 EUR/HP/y), respectively. The difference between the attainable gains for a demand side equipped with radiators or with floor heating is to be expected, since radiators are fast, responsive systems, which predominantly interact with the indoor air, meaning that their shift in operation is limited compared to the slower floor heating systems that interact through the building thermal mass, and hence have much larger time constants [130, 153]. Consequently, an additional degree of freedom for these kind of systems can still induce a more significant improvement of the system operation.

To be able to better understand the trends observed in Figure 9.8, Figure 9.9 shows the supply side operation determining the costs depicted in Figure 9.8. Figure 9.9 shows that for low market penetration levels (i.e., 9000 or 90 000 flexible heat pumps), the changes in operation of the different generators due to the additional coordination of the demand for reserve capacity are very small. Consequently, the marginal costs for the provision of energy and reserve capacity remain quasi unaltered, explaining the rather flat trends for the intermediate market penetration levels in the rightmost plots in Figure 9.8. However, for the highest heat pump market penetration levels, the additional demand side flexibility made available by the SMPC^{ap} strategy with ADF is able to trigger significant changes at the supply side. Indeed, Figure 9.9 clearly shows that for the case where the flexible demand side is controlled by an SMPC^{ap} strategy incorporating ADF, the third, most expensive generating unit (GEN3) is considerably less used. In the case of a flexible demand side consisting of 900 000 heat pumps combined with radiators, the total energy supply by GEN3 over the entire heating season is reduced by 19.5%, and the reserve capacity provision is reduced by 22.7% relative to the case without

³² It is assumed that the heat pumps only operate during the heating season, such that the operating cost during the heating season coincides with the yearly cost.



(a) In case of radiators.



(b) In case of floor heating.

Figure 9.9: Comparison of the optimized supply of electric energy and reserve capacity provision by the three aggregated generating facilities over the entire heating season in case the flexible demand side in the integrated system-level optimization problem is controlled by the proposed SMPC^{ap} strategy, or by an equivalent strategy without ADF, for increasing heat pump market penetration levels.

ADF; the energy supply by GEN2, on the other hand, is reduced by 4.1%, whereas the reserve capacity provision is increased by 26.2%. For the analogous case with floor heating, the energy supply by GEN3 is reduced by 15.8%, and the reserve capacity provision is reduced by 16.9%; the energy supply by GEN2 is reduced by 3.4%, whereas the reserve capacity provision is increased by 23.0%.

Supplementing the information depicted in Figure 9.9, Table 9.3 moreover illustrates that GEN3 is not only used less in terms of overall supply, but also in terms of instantaneous capacity (except for the 18th of January 2016 for the demand side equipped with radiators). This observation suggests that the day-ahead coordination of the demand for reserve capacity, in addition to the demand for energy, is not only able to reduce the operating cost, but also might enable a reduction of the required generation capacity, and hence, of the associated investment cost³³. The attainable peak capacity reduction is the largest for a demand side equipped with floor heating, as floor heating systems are able to better spread their operation in time thanks to the large time constants, thereby reducing demand peaks, which directly affects the required peak capacity at the supply side.

These different aspects regarding the altered supply side operation are also clearly visible in Figure 9.10, showing the time-dependent stochastic³⁴ generation profiles (averaged over one hour) of the three aggregated generating facilities during the 29th of February, in case the flexible demand side consists of 900 000 heat pumps (arbitrarily chosen as an example). For the cases with ADF, the energy profiles are clearly shifted downwards for GEN3; moreover, around $t = 1417$ h and $t = 1427$ h, it can be observed that the more expensive reserve capacity provided by GEN3 is replaced by cheaper reserve capacity provided by GEN2. Finally, the peaks in required capacity are also slightly lower in case ADF is enabled.

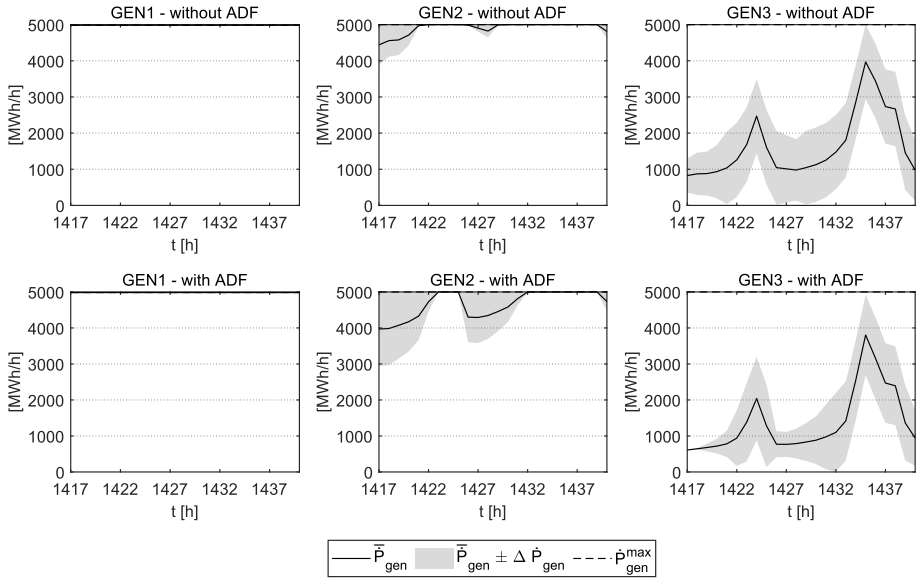
The above discussed changes regarding the supply side operation are enabled by the fundamentally different system behavior induced by incorporating ADF at the flexible demand side, as already discussed in detail in Section 9.1, and as again illustrated by Figure 9.11, showing the open-loop indoor temperature profiles and heat input profiles realized by an SMPC^{ap} strategy without or with ADF on the 29th of February for the detached, small, ageing dwelling as part of the flexible demand side in the integrated system-level problem; note that the depicted situation is arbitrarily chosen as an example. The incorporation of ADF allows for a less conservative control strategy. Hence, the energy demand is reduced, obviating the deployment of the more expensive generation units. On top of that, the uncertainty

³³ However, keep in mind that these cost reductions should be weighed against the investments in communication, measurement and control, required to enable DR [34], which are nevertheless not further considered in this dissertation.

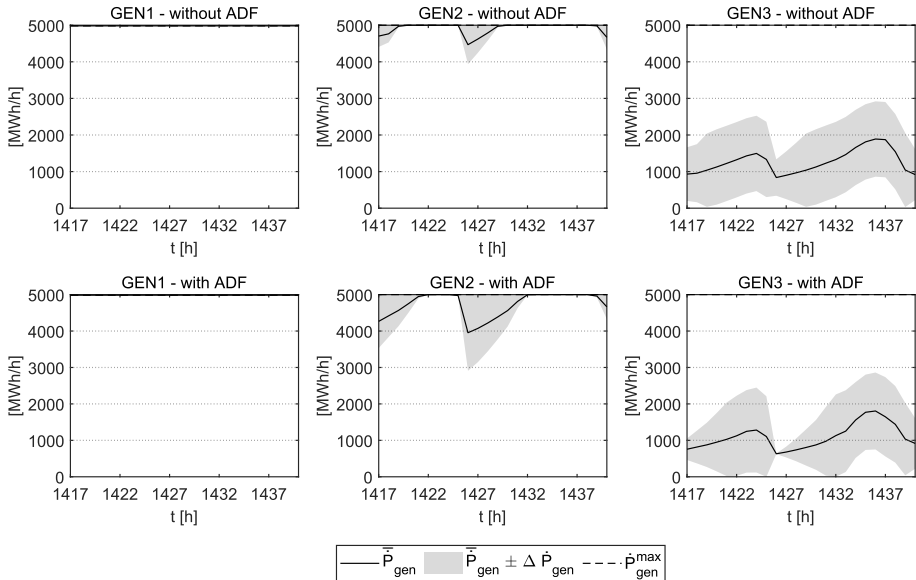
³⁴ Recall from the discussion in Section 9.1 that the shown uncertainty band surrounding the profile of the expected energy supply corresponds to the constraint tightening level of the generator power constraints, and thus reflects how much reserve capacity needs to be kept aside.

Table 9.3: The attainable reduction in peak capacity (in MW) required by the three aggregated generating facilities for the combined supply of energy and upward reserve capacity, by incorporating ADF in the demand side control strategy, in case the flexible demand side in the integrated system-level optimization problem consists of 900 000 flexible heat pumps, either equipped with radiators or with floor heating.

| Representative day index | Heat emission system | GEN1 - without ADF | | | GEN1 - with ADF | | | GEN2 - without ADF | | | GEN2 - with ADF | | | GEN3 - without ADF | | | GEN3 - with ADF | | | | | |
|--------------------------|----------------------|--------------------|-----------------|---------|--------------------|-----------------|---------|--------------------|-----------------|---------|--------------------|-----------------|---------|--------------------|-----------------|---------|-----------------|-----|---------|--------|--------|----------|
| | | GEN1 - without ADF | GEN1 - with ADF | | GEN2 - without ADF | GEN2 - with ADF | | GEN3 - without ADF | GEN3 - with ADF | | GEN3 - without ADF | GEN3 - with ADF | | GEN3 - without ADF | GEN3 - with ADF | | | | | | | |
| 18 | Radiators | 5000.0 | 5000.0 | → -0.0% | 5000.0 | 5000.0 | → -0.0% | 6500.0 | 6500.0 | → -0.0% | 5000.0 | 5000.0 | → -0.0% | 5000.0 | 4922.1 | → -1.6% | 0.0 | 0.0 | → -0.0% | 2087.3 | 1802.9 | → -13.6% |
| 60 | Radiators | 5000.0 | 5000.0 | → -0.0% | 5000.0 | 5000.0 | → -0.0% | 5000.0 | 5000.0 | → -0.0% | 5000.0 | 5000.0 | → -0.0% | 5000.0 | 4922.1 | → -1.6% | 0.0 | 0.0 | → -0.0% | 2087.3 | 1802.9 | → -13.6% |
| 86 | Radiators | 5000.0 | 5000.0 | → -0.0% | 4427.3 | 4427.3 | → -0.0% | 0.0 | 0.0 | → -0.0% | 5000.0 | 5000.0 | → -0.0% | 5000.0 | 4922.1 | → -1.6% | 0.0 | 0.0 | → -0.0% | 2087.3 | 1802.9 | → -13.6% |
| 307 | Radiators | 5000.0 | 5000.0 | → -0.0% | 5000.0 | 5000.0 | → -0.0% | 5000.0 | 5000.0 | → -0.0% | 5000.0 | 5000.0 | → -0.0% | 5000.0 | 4922.1 | → -1.6% | 0.0 | 0.0 | → -0.0% | 2087.3 | 1802.9 | → -13.6% |
| 18 | Floor heating | 5000.0 | 5000.0 | → -0.0% | 5000.0 | 5000.0 | → -0.0% | 6440.9 | 6129.8 | → -4.8% | 5000.0 | 5000.0 | → -0.0% | 5000.0 | 4922.1 | → -1.6% | 0.0 | 0.0 | → -0.0% | 2920.1 | 2862.5 | → -2.0% |
| 60 | Floor heating | 5000.0 | 5000.0 | → -0.0% | 5000.0 | 5000.0 | → -0.0% | 5000.0 | 5000.0 | → -0.0% | 5000.0 | 5000.0 | → -0.0% | 5000.0 | 4922.1 | → -1.6% | 0.0 | 0.0 | → -0.0% | 2920.1 | 2862.5 | → -2.0% |
| 86 | Floor heating | 5000.0 | 5000.0 | → -0.0% | 4855.1 | 4855.1 | → -0.0% | 0.0 | 0.0 | → -0.0% | 5000.0 | 5000.0 | → -0.0% | 5000.0 | 4922.1 | → -1.6% | 0.0 | 0.0 | → -0.0% | 2920.1 | 2862.5 | → -2.0% |
| 307 | Floor heating | 5000.0 | 5000.0 | → -0.0% | 5000.0 | 5000.0 | → -0.0% | 5000.0 | 5000.0 | → -0.0% | 5000.0 | 5000.0 | → -0.0% | 5000.0 | 4922.1 | → -1.6% | 0.0 | 0.0 | → -0.0% | 2920.1 | 2862.5 | → -2.0% |



(a) In case of radiators.



(b) In case of floor heating.

Figure 9.10: Comparison of the open-loop stochastic generation profiles (averaged over one hour) of the three aggregated generating facilities during the 29th of February, in case the flexible demand side in the integrated system-level optimization problem, consisting of 900 000 flexible heat pumps, is controlled by the proposed SMPC^{ap} strategy, or by an equivalent strategy without ADF.

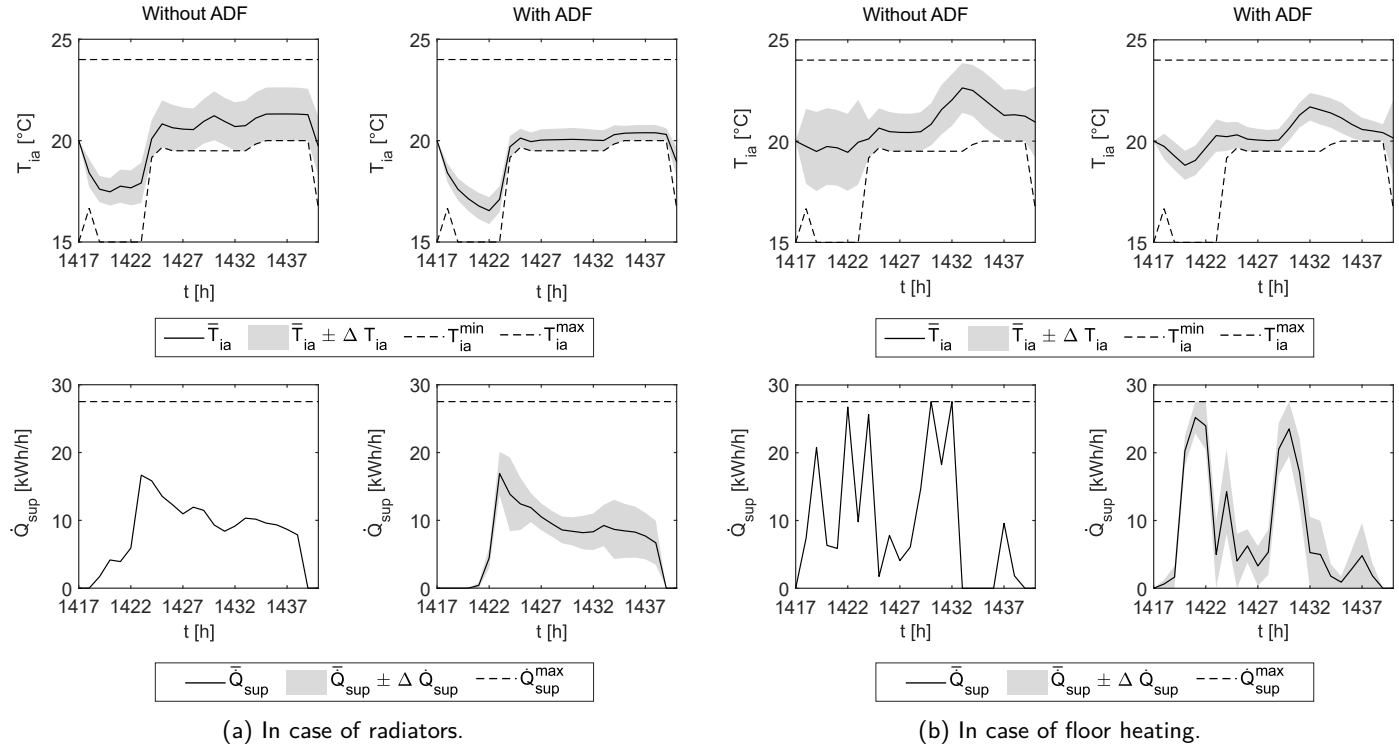


Figure 9.11: The open-loop indoor temperature profiles and heat input profiles (averaged over one hour) realized by an SMPC^{AP} strategy without or with ADF during the 29th of February for the detached, small, ageing dwelling.

on the temperature can be reduced in exchange for an increased uncertainty on the heat input³⁵. Consequently, the demand for energy can be partly traded for demand for reserve capacity, allowing the more expensive supply of energy to be replaced by cheaper supply of reserve capacity.

Finally, Figure 9.11 also clearly demonstrates the exploitation of the flexibility offered by the DR temperature band. This is especially visible for the case where the flexible demand side is equipped with floor heating and is controlled by the SMPC^{ap} strategy with ADF, where the stochastic temperature profile no longer necessarily sticks to the lower bound, such that a more desirable demand profile can be obtained to improve the system-level performance. What is also interesting to see is that in all cases in Figure 9.11, the uncertainty band surrounding the mean temperature profile does not yet simultaneously hit the lower and upper temperature bounds at the end of the prediction horizon. This implies that there is still additional operational flexibility available. Note that this remaining operational flexibility could not only be used to further adapt the profile of the demand for energy and reserve capacity, but can moreover also be exploited for reserve provision [117,194]. Although this aspect could be straightforwardly incorporated in the integrated system-level optimization problem, and in the associated hierarchical coordination framework, with the help of the worst-case reserve activation calculation proposed by Bruninx [117,119], it is not further considered in this dissertation. Instead, it is recommended as an interesting extension for future studies.

9.5 Conclusion

As a third MPC application domain, this chapter investigates the added value of using the SMPC^{ap} strategy for DR under uncertainty.

To this end, first, the impact of the SMPC^{ap} strategy on the resulting demand profile is evaluated. It is shown that due to the incorporation of ADF in the open-loop control problem, the SMPC^{ap} strategy is not only able to optimize the demand for energy, but also the demand for reserve capacity and real-time flexibility. In other words, an additional degree of freedom is unlocked, which can be exploited in a DR context.

In a next step, it is investigated whether the coordination of the stochastic demand of a group of TCLs managed by the proposed SMPC^{ap} strategy (thus exploiting the new degree of freedom) can benefit the energy system as a whole compared to an equivalent case without ADF, where the coordination of the demand for reserve capacity and real-time flexibility is disabled; the latter strategy can be considered

³⁵ Recall that by enabling ADF, the uncertainty on the heat input/demand becomes controllable.

as the current state-of-the-art for DR with MPC under uncertainty, albeit with the additional consideration of parametric uncertainties. In this context, an integrated system-level optimization problem is considered, linking the demand side with the supply side, and aiming for a minimal system operating cost. The considered cost components include the day-ahead expected cost of electric energy, reserve capacity provision, and reserve capacity activation.

To ensure mathematical tractability, a distributed solution approach is proposed, using the alternating direction method of multipliers. By implementing this distributed solution strategy, the integrated system-level optimization problem is converted into an hierarchical coordination framework that is communicating prices as a coordination signal to the different buildings and generators, to converge towards a balance between supply and demand. Although additional modifications and extensions are required to improve the framework, it is a solid basis for more dedicated research regarding system operation, market design, consumer coordination and tariff structures for DR under uncertainty.

The integrated system-level optimization problem is subsequently adopted in a case study, considering an electrification scenario of the residential heating sector. The flexible demand side, supplementing a fixed demand side characterized by a non-flexible demand and fixed system-level uncertainty, is constituted by a group of heterogeneous buildings equipped with compression heat pumps for space heating, each controlled by either the proposed SMPC^{ap} strategy, or by an equivalent strategy without ADF. To maximize insight, different heat emission systems, and different market penetration levels are considered. The supply side, on the other hand, is constituted by three aggregated electricity generating facilities, whose techno-economical characteristics are inspired by the Belgian power system. To maintain tractability, the integrated system-level optimization problem is solved for a set of four representative days (18th of January 2016, 29th of February 2016, 26th of March 2016 and 2nd of November 2016), which can be used to appraise the system behavior over the entire heating season.

The results of this case study illustrate that the day-ahead coordination of the demand for reserve capacity, in addition to the demand for energy, enables a reduction of the system-level operating cost. The attainable gains in operating cost become more significant as the heat pump market penetration level increases, and are most prominent for a demand side where all buildings are equipped with radiators. In that case, relative cost reductions up to 10.7% are attainable, compared to 8.1% in case of floor heating. In absolute terms, the cost per heat pump per year can be reduced from 2450 EUR/HP/y to 1907 EUR/HP/y for a demand side consisting of 900 000 flexible heat pumps coupled to radiators, and from 2151 EUR/HP/y to 1761 EUR/HP/y for an analogous demand side equipped with floor heating. Besides, it is shown that also a reduction in the required generation capacity might be achieved, impacting the system investment cost. These beneficial effects are

shown to be caused by the fundamentally different demand side behavior induced by the proposed SMPC^{ap} strategy, allowing for reduced conservatism, and for a possible interchange of the demand for electric energy and the demand for reserve capacity, compared to an equivalent strategy without ADF. This modified demand side behavior induced by the SMPC^{ap} strategy enables a more cost-efficient use of the available generating facilities and guarantees a more cost-efficient electrification of the residential space heating sector, thus indicating the added value of the SMPC^{ap} strategy developed in this dissertation for DR under uncertainty, and for integrating heat pumps into our future electricity systems.

Chapter 10

Conclusions and suggestions for future work

Since real-time uncertainty realizations are known to give rise to increased energy costs and comfort violations if not properly accounted for, the prevalent, deterministic model predictive control (MPC) approach needs to be replaced by a control strategy that explicitly hedges against the detrimental impact of uncertainties. Where the current state-of-the-art has primarily focused on the uncertainty on the disturbance forecasts, i.e., weather conditions and occupant behavior, this dissertation acknowledges that also uncertainty on the building model parameters is plausible, and hence, should be additionally accounted for. This is especially relevant when considering the implementation of MPC involving the older, existing building stock, e.g., in case of a large-scale roll-out of smart meters and controllers.

Therefore, the main goal of this dissertation is to develop and assess a stochastic MPC (SMPC) strategy for building climate control and demand response (DR) under combined additive (disturbance forecast) and parametric (model) uncertainty, more specifically referred to as the SMPC^{3P} strategy.

In this final chapter, the main findings and conclusions regarding this development and assessment are summarized in Section 10.1. This is done by answering the research questions defined in Chapter 1, where the discussion subsequently considers the research questions related to the SMPC development (Section 10.1.1), the SMPC assessment at building level (Section 10.1.2), and the SMPC assessment at system level (Section 10.1.3). Moreover, the main contributions of this work regarding each of these three aspects are highlighted. Finally, possible future research tracks are suggested in Section 10.2.

10.1 Conclusions

10.1.1 Development of the SMPC^{ap} strategy

RQ1: How does the conventional deterministic OCP formulation for building climate control need to be reformulated in order to explicitly account for additive (disturbance forecast) and parametric (model) uncertainties?

To cope with additive and parametric uncertainties, this dissertation develops a chance constrained SMPC with affine disturbance feedback (ADF) in a convex formulation. For the SMPC strategy to be able to hedge against both additive and parametric uncertainties, the conventional deterministic optimal control problem (OCP) formulation tailored to the class of systems represented by a linear time-invariant state space model (SSM), discussed in Chapter 2, is reformulated in Chapter 4, by explicitly taking into account the impact of uncertainties in all relevant parts of the OCP, being the state space equation, the state constraints and the input constraints. Consequently, the states and inputs are transformed into stochastic variables, characterized by a mean and covariance. The hard state and input constraints are in turn transformed into probabilistic chance constraints, for which an analytical reformulation is derived. To reduce conservatism, the analytically reformulated chance constraints are combined with ADF, mimicking the closed-loop behavior of the MPC strategy in the open-loop optimal control problem. As such, uncertainty on the system states can be exchanged for uncertainty on the inputs, where the latter represents the possibly required real-time modifications of the control strategy to react against uncertainty manifestations.

The derivation of the convex stochastic OCP formulation, explicitly accounting for both additive and parametric uncertainties, requires three main assumptions. First, it is assumed that the conventional deterministic OCP formulation is convex. Second, the products of stochastic variables are neglected, in order to ensure mathematical tractability. Finally, the chance constraints are reformulated for every distinct state and input based on their marginal distribution, which is assumed to be normal. Although especially the latter two assumptions entail important simplifications, the results in Chapter 6 show that despite these assumptions, the developed SMPC^{ap} approach is still able to guarantee improved thermal comfort compared to the state-of-the-art, and this at a limited increase in energy cost.

One important downside of the presented SMPC^{ap} approach is its limited scalability. To allow for a reaction against the parametric uncertainty via ADF, the uncertainty on each of the SSM elements has to be repeated for each time step in the latent variable $\tilde{\mathbf{p}}$, which markedly increases the problem size.

RQ 2: How can all relevant uncertainties affecting the building indoor climate be appropriately mathematically modeled in order to include them in the stochastic OCP formulation?

Chapter 5 derives a substantiated characterization (in terms of a mean value and associated covariance matrix) of the uncertainty on the building model parameters, on the weather forecasts, and on the occupant behavior forecasts.

The model parameter uncertainty is derived with the help of the probabilistic building characterization method of De Jaeger et al. [62, 63]. This method generates a statistical characterization of the building envelope based on the building location, geometry and construction year, without additional on-site data collection, by leveraging governmental databases of the energy performance of buildings. With the help of the theoretical physics-based modeling approach of Reynders et al. [132], this information can be subsequently converted into a reduced order one-zone four-states RC model, from which the uncertainty on the parameters of the building model in state-space form can be straightforwardly derived. This approach results in a worst-case estimation of the parametric uncertainty, acknowledging the possible lack of information about the building envelope, e.g., in case the older, existing building stock is involved. This point of view is especially relevant when aiming for a fast, widespread adoption of MPC (instead of only in deep renovations and/or new homes), and is fundamentally different from what is done in current research, where the uncertainty characterization is typically derived based on detailed (building-specific) information and/or experts' knowledge.

To come up with a substantiated estimate of the weather forecast uncertainty, this dissertation builds further on the work of Lambrichts [148]. Based on real measurement data and weather forecasts, mean vectors and covariance matrices describing the forecast errors are derived. As such, the presented uncertainty characterization takes into account the auto- and cross-correlation of the forecast errors, which are most often disregarded.

However, the uncertainty on the occupant-related disturbance forecasts, and on the internal heat gains in particular, is much harder to characterize, due to the complex nature of human behavior, but also due to the lack of measured profiles. As a workaround, a yearly profile, simulated with the open web tool StROBe (Stochastic Residential Occupancy Behaviour) of Baetens et al. [146], is used to deduce a daily average profile and associated variance, to get a loose representation of the occupancy-related uncertainty. Clearly, the uncertainty characterization of the occupant behavior is of inferior quality compared to the uncertainty characterization of the building model parameters and weather forecasts. Nevertheless, this does not detract from the general purpose of this dissertation, which is to develop and assess an SMPC strategy that is able to cope with different types of discrepancies between the actual situation and the model assumptions.

Main contributions related to the SMPC development (RQ 1 and RQ 2)

Regarding the SMPC development, our main contribution is the derivation of a novel convex chance constrained stochastic OCP formulation incorporating ADF, which enables the explicit quantification, and manipulation of both the mean and covariance of the system states and inputs, to guarantee a better control performance under combined additive and parametric uncertainties. The presented approach is tailored to the class of systems represented by a linear time-invariant SSM.

The implementation of the developed SMPC^{ap} strategy is enabled by a substantiated characterization of the parametric uncertainty, which is derived based on the building geometry, location and age, without intensive on-site data collection, by combining the probabilistic building characterization method of De Jaeger et al. [62,63], with the theoretical physics-based building modeling approach of Reynders et al. [132].

10.1.2 Assessment of the potential added value of the SMPC^{ap} strategy at building level

RQ 3: Does the SMPC^{ap} strategy guarantee a thermal comfort improvement compared to the current-practice deterministic MPC (DMPC) strategy, and the state-of-the-art SMPC^a strategy only accounting for additive uncertainties, and at what cost is this improvement obtained?

The results of the case study in Chapter 6 indicate that the enhanced uncertainty anticipation of the developed SMPC^{ap} strategy brings about an improvement in thermal comfort compared to the current-practice DMPC strategy and the state-of-the-art SMPC^a strategy, and this at the expense of a limited increase in energy use; for all considered cases, 90% of the thermal comfort improvement compared to the DMPC strategy can be attained with a relative increase of at most 9% in energy use, irrespective of the installed heat emission system. Apart from the increased energy use, also the increased computational complexity should be taken into account as an additional cost.

The thermal comfort gains are shown to be most prominent in buildings equipped with floor heating and characterized by the combination of a large model uncertainty and a large nominal heat demand. Also for buildings equipped with radiators, irrespective of the magnitude of the nominal heat demand and/or model uncertainty, thermal comfort can be improved by implementing the developed SMPC^{ap} strategy, although the thermal comfort gains compared to the MPC^a strategy are smaller

here. This can be explained by the fact that the SMPC^{ap} strategy is hampered to fully distinguish itself from the SMPC^a approach in this case, for three reasons, namely i) because of the small time constants associated with radiators, ii) because the stochastic OCP is re-solved for every subsequent time step, and iii) because the heat supply system is oversized. These three aspects all limit the added value of a correct uncertainty anticipation, which is the most important asset of the SMPC^{ap} approach. Finally, for buildings with a small heat demand equipped with floor heating, the thermal comfort gains by switching to a stochastic approach (either an SMPC^a or an SMPC^{ap} strategy) are shown to be negligible; in this case, the combination of the large time constants and the overestimation of the heat demand already implicitly triggers a considerable amount of anticipation, even without actually hedging against the impact of uncertainties.

RQ 4: Does the SMPC^{ap} strategy allow for obtaining a more appropriate, yet robust, sizing of the heating system when embedded in an integrated optimal control and design (IOCD) approach?

In an exploratory case study, the suitability of incorporating the SMPC^{ap} strategy in an IOCD approach for obtaining a more appropriate, yet robust, heat supply system size is demonstrated, by comparing it to an IOCD approach incorporating the current state-of-the-art PB MPC strategy, the DMPC strategy, the SMPC^a strategy or the SMPC^{ap} strategy. Rather than fully implementing a nested design-control optimization, the outer optimization loop steering the design decisions is replaced by a set of predetermined design scenarios, focusing on high-level decisions about the size of the heat supply system. For the lower-level control loop, the different MPC approaches are considered and compared.

The case study shows that the incorporation of the developed SMPC^{ap} strategy in an IOCD approach leads to a robust sizing of the heat supply system, able to truly guarantee thermal comfort under combined additive and parametric uncertainty for (almost) all possible building realizations. Moreover, the results of the case study demonstrate that the SMPC^{ap} strategy (as well as the SMPC^a strategy) allows for a more appropriate system sizing (i.e., a right-sizing, rather than an over-/undersizing of the system) compared to the DMPC strategy. Since the SMPC^{ap} strategy already explicitly takes into account the possibly required real-time reactions to uncertainty manifestations when optimizing its open-loop control strategy (via ADF), it deploys the available thermal power in a better way, and consequently does not require spare capacity in the form of an oversized system to be able to accommodate these real-time changes, in contrast to the DMPC strategy.

Main contributions related to the SMPC assessment at building level (RQ 3 and RQ 4)

Regarding the SMPC assessment at building level, our main contribution is the demonstration of the added value of the developed SMPC^{ap} strategy, compared to the state-of-the-art, for both building climate control under uncertainty, and integrated optimal control and design under uncertainty.

Moreover, we also pinpoint for which specific cases/conditions this added value is most pronounced. This is especially the case for situations where a correct anticipation is crucial, i.e., for systems with large time constants, for properly (not over-)sized heating systems, and for situations where longer intervals are considered between (re)solving the OCP.

Finally, we also clearly indicate at which cost this added value is obtained, being an increase in energy use as well as in computational complexity (see RQ 1).

10.1.3 Assessment of the potential added value of the SMPC^{ap} strategy at system level

RQ 5: How does the proposed SMPC^{ap} strategy alter the demand profile, and how can this altered demand profile be coordinated for the benefit of the central energy system?

Since the SMPC^{ap} strategy is not only able to optimize the demand for energy, but also the demand for reserve capacity and real-time flexibility (thanks to the incorporation of ADF), an additional degree of freedom is unlocked, which can be exploited in a DR context.

To investigate whether the central energy system can benefit from the coordination of the stochastic demand of a group of TCLs managed by the developed SMPC^{ap} strategy (thus exploiting the unlocked degree of freedom) compared to an equivalent case without ADF, where the coordination of the demand for reserve capacity and real-time flexibility is disabled, an integrated system-level optimization problem is set up, linking the demand side with the supply side, and aiming to minimize the overall system operating cost. To ensure mathematical tractability, a distributed solution approach is proposed, using the alternating direction method of multipliers (ADMM). By implementing this distributed solution strategy, the integrated system-level optimization problem is converted into a hierarchical coordination framework

that sends prices as a coordination signal to the different buildings and generators, to work towards a balance between supply and demand under uncertainty.

With the help of a case study, considering an electrification scenario of the residential heating sector, it is shown that the coordination of the stochastic demand of a group of compression heat pumps for space heating, managed by the developed SMPC^{ap} strategy (thus exploiting the unlocked degree of freedom) can lower the overall system operating cost compared to an equivalent case without ADF, where the coordination of the demand for reserve capacity and real-time flexibility is disabled; the latter strategy can be considered as the current state-of-the-art for DR with MPC under uncertainty, albeit with the additional consideration of parametric uncertainties. It is shown that the attainable gains in operating cost become more significant as the heat pump market penetration level increases, and are most prominent for a demand side where all buildings are equipped with radiators; in that case, relative cost reductions up to 10.7% are attainable. Moreover, it is shown that a reduction in the required generation capacity might be achieved, impacting the system investment cost. These results demonstrate that the widespread implementation of the developed SMPC^{ap} strategy can aid a more cost-efficient electrification of the residential space heating sector.

Main contributions related to the SMPC assessment at system level (RQ 5)

Regarding the SMPC assessment at system level, a first important contribution is the development of a hierarchical coordination framework for DR under combined additive and parametric uncertainty, leveraging the developed SMPC^{ap} strategy. This framework not only balances the supply of and demand for energy, but also (simultaneously) the demand for and supply of reserve capacity, while guaranteeing end-user thermal comfort. As such, a trade-off between the degree of uncertainty management at building versus at system level is enabled. The developed coordination framework is an important stepping stone for future research regarding system operation, market design, consumer coordination and tariff structures for DR under uncertainty.

A second important contribution is the demonstration of the added value of the developed SMPC^{ap} strategy, compared to the state-of-the-art, for demand response under uncertainty. Here, we showed that the modified demand side behavior induced by the SMPC^{ap} strategy, allowing for an optimization of the load uncertainty, enables a more cost-efficient operation of the available generating facilities and hence, guarantees a more cost-efficient electrification of the residential space heating sector. The largest operating cost reductions were shown to be achievable for a demand side equipped with radiators.

10.2 Suggestions for future work

Based on the findings of this dissertation, several paths for future research are recommended.

A first interesting future research track would be to combine the SMPC^{ap} strategy developed in this dissertation with **machine learning** to derive the stochastic building model and/or the additive uncertainty representation. In this setting, the uncertainty characterizations derived in this dissertation can serve as substantiated initial guesses, which can be subsequently updated in an online fashion. This could either be done in a simulation environment, focusing on closed-loop simulations with more detailed emulator models, or even in a real-life setting. As this adaptive, learning-based SMPC^{ap} approach allows for a trade-off between model complexity and uncertainty management, it may enable a more widespread adoption of MPC, where the focus can be extended beyond new homes and/or deep renovations, since a detailed characterization of the building envelope might no longer be a strict requisite.

Future research may also focus on (the re-thinking of) the required **regulation and market design** to leverage flexible demand, given the insight that the uncertain demand can be split up in an interchangeable demand for energy and for reserve capacity. To this end, the developed hierarchical coordination framework can be further extended with a more correct representation of the relevant markets and market mechanisms.

In this context, it might be relevant to supplement the day-ahead analysis considered in this dissertation with the consideration of the intraday and real-time operational stage, where consumers can still further adapt/optimize their demand in real time within the operational limits set by the purchased electric energy and reserve capacity, in order to additionally participate in short-term markets (e.g., intraday markets, real-time markets or balancing settlement schemes).

Also the consideration of all important market players (such as aggregators) and their business models would be of great value. Here, a particularly interesting future research track might be the development of a monetary remuneration scheme to reward the DR participants, where it might be required to make a distinction between the coordination signal/prices used by an aggregator to steer the demand, and the actually charged end-user tariff, in order to prevent consumers from being exposed to extremely high or fluctuating prices [34].

Finally, it would be interesting to extend the presented research regarding optimal control, optimal design, and demand response under uncertainty, to energy systems involving district heating and cooling networks, or even **multi-energy vector systems**. This can be achieved by altering the considered heat supply system in the buildings and by adding more energy conversion and (thermal/electric)

storage models in the stochastic OCP formulation, by adapting the local and coupling constraints to correctly represent the underlying physics for these cases (it will for example no longer necessarily be required that demand and supply are quasi-instantaneously balanced), and by adapting the communicated variables (the demand can for example be expressed in terms of temperatures and mass flow rates, rather than in terms of energy, in case of a district heating and cooling network). In this context, it would also be interesting to consider the impact of collective conversion or storage assets as additional (competing) flexibility providers.

Appendix

Appendix A

Parametric uncertainty characterization for a two-zones nine-states building model

Data-driven estimation of parametric uncertainty of reduced order RC models for building climate control

Anke Uytterhoeven^{1,2}, Ina De Jaeger^{1,3}, Kenneth Bruninx^{1,2},
Dirk Saelens^{1,3}, Lieve Helsen^{1,2}
¹EnergyVille, Genk, Belgium

²KU Leuven, Mechanical Engineering Department, Leuven, Belgium

³KU Leuven, Civil Engineering Department, Leuven, Belgium

Abstract

Current model predictive control (MPC) applications for residential space heating typically rely upon accurate building models, obtained via extensive data acquisition and/or experts' knowledge. However, in the context of older residential buildings, one needs to rely upon sparse, publicly available data. Therefore, the aim of this paper is to come up with an estimate of the parametric uncertainty of building controller models in case neither detailed information about the building thermal properties nor experts' knowledge is available. In addition, the impact of this uncertainty on the optimal space heating strategy is investigated. The results show that the considered approach gives rise to rather large parametric uncertainty. The obtained variation in model parameters is shown to markedly affect the optimal space heating control, both in terms of dynamic effects (i.e., peak demand and timing) and yearly energy use, thereby indicating the need for improved data acquisition and/or dedicated control strategies that operate robustly under uncertainty.

Key innovations

Data-driven, worst case estimation of the parametric uncertainty of building models based on sparse, publicly available data.

Practical implications

This contribution highlights that the lack of information about the thermal performance of older residential buildings gives rise to non-negligible uncertainty on building energy simulation models and on controller models derived therefrom. To cope with this, improved data acquisition and/or dedicated robustified control strategies are needed.

Introduction

Model predictive control is gaining widespread attention as an advanced control strategy for residential heating systems, and heat pumps in particular, since it can systematically improve thermal comfort with simultaneous energy and/or cost savings, as well as

enable the provision of services to the rest of the energy system (Serale et al. (2018); Drgoňa et al. (2020); Oldewurtel et al. (2010); Avci et al. (2013); Bianchini et al. (2016)).

The performance of any MPC strategy is dependent on the accuracy of the mathematical model describing the thermal loads and the forecasts of disturbances, such as weather and user behavior. Deviating model parameters and inaccurate predictions are shown to result in increased energy costs and comfort violations if not properly accounted for (Bengea et al. (2011); Oldewurtel et al. (2010, 2012)). Nevertheless, the uncertainty on the building model parameters in MPC is only occasionally explicitly addressed (Oldewurtel et al. (2010); Maasoumy et al. (2014); Tanaskovic et al. (2017); Nagpal et al. (2020)). The main reason is that current research often employs accurate physics-based building models, obtained via extensive data acquisition combined with experts' knowledge, for which the feedback mechanism of the receding horizon implementation of MPC offers sufficient robustness against the small remaining uncertainties.

In contrast, in case of a large-scale implementation of MPC, a lack of information is plausible, especially if also the older, existing building stock is involved. In that case, the parametric uncertainty of the controller model can become non-negligible, and additional measures might be necessary (Ioannou and Itard (2015)). However, precisely because of the lack of information, a scientifically sound characterization of the building model and associated parametric uncertainty, as well as an assessment of the impact of the uncertainty, is a challenging task. In this context, one may opt for statistical, data-driven building characterization methods (De Jaeger et al. (2021)), which leverage publicly available data, to generate high-quality controller models.

Given the aforementioned challenges and trends, the aim, and main novelty, of this paper is to come up with a substantiated, data-driven estimate of the parametric uncertainty when deriving a physics-based building controller model, to be used in MPC, starting from publicly available data (i.e., location, geom-

etry and construction year). Since neither detailed, building-specific information on the thermal properties nor experts' knowledge is incorporated, this can be seen as a worst-case assessment. In addition, this paper investigates the impact of the obtained variation in model parameters on the energy demand profile determined by optimal control, and on the resulting yearly energy use, via a Monte Carlo analysis. This is a first step in assessing the importance of building model parametric uncertainty regarding MPC performance.

The following research questions will be answered.

RQ1 What statistical variation in the parameters of a building controller model is to be expected when merely starting from publicly available data?

RQ2 How does the optimal energy demand profile, and related to that, the yearly energy use alter for this variation in building model parameters?

In the next section, the methodology to convert publicly available information into a building controller model is explained, as well as the set-up of the optimal control problem in which the building controller model will be incorporated. Subsequently, nine existing buildings are presented as case studies for which the parametric uncertainty is determined. Next, the obtained variation in building model parameters, and in energy use, is discussed and compared for these nine dwellings. Finally, the conclusions are drawn.

Methods

Figure 1 summarizes the workflow of the paper.

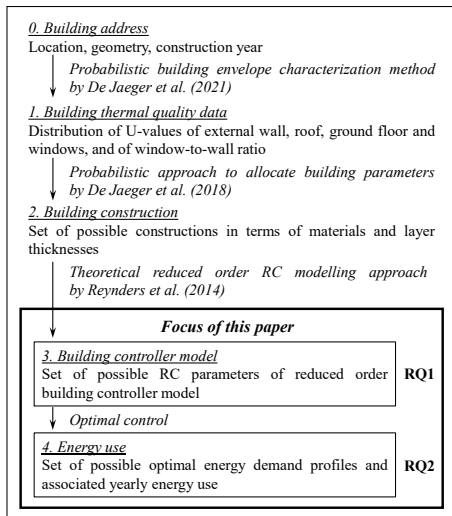


Figure 1: The workflow of the paper.

1. Extracting building thermal quality data

To be able to answer the first research question, the publicly available data need to be transformed into a

building controller model. This can be achieved via following procedure.

Based on the building location, geometry and construction year (where the latter two characteristics can be derived from the building address based on geospatial and cadastral data), information on the building thermal properties can be obtained with the help of the probabilistic building envelope characterization method developed by De Jaeger et al. (2021). This method generates distributions of the U-values of the external walls, roof, ground floor and windows, as well as of the window-to-wall ratio (WWR), by applying a quantile regression method on the Flemish energy performance certificates database, which contains building envelope thermal quality data of Flemish single-family dwellings. The correlations between the different variables are included by building multivariate distributions from the distinct marginal distributions, and by subsequently drawing correlated samples of the U-values and WWR on building level. These correlated samples can be seen as possible realizations of a specific dwelling with a fixed location, geometry and age.

Since this paper focusses on building models to be used in advanced controllers for residential heat pumps, only the realizations with a sufficiently low nominal heat demand¹ are considered (i.e., $\dot{Q}_{nom} < 15$ kW), restricting the considered domain of the obtained distributions.

2. Converting building thermal quality data to building construction

In order to be able to derive a building controller model, the obtained U-values and WWR need to be converted to material layers composing the building envelope. Following De Jaeger et al. (2018), we derive the building construction, in terms of materials and layer thicknesses, by gradually adjusting an initial (heavy-weight) construction, representative for Flemish buildings, with predefined upgrades until the targeted U-values are reached. More specifically, for the roof and for the ground floor, these adjustments imply gradually adding insulation. For the wall, first, the thickness of the heavy masonry composing the internal walls is increased up to a maximum value, after which a non-ventilated air cavity is provided between the internal and external walls; finally, if needed, an insulation layer with appropriate thickness is added between the internal walls and the air cavity. For the windows, the most appropriate glazing out of a list of discrete options is chosen.

This conversion process is repeated for the domain of the distribution of the U-values and WWR obtained in the previous step, leading to a set of possible constructions for a dwelling with a fixed location, geometry and age.

¹The nominal heat demand is quantified following NBN EN 12831 (NBN (2017)).

3. Converting building construction to building controller model

The building controller model can be obtained based on the specified construction, by using a theoretical, physics-based modeling approach. In this paper, the approach of Reynders et al. (2014) is used, resulting in a reduced order RC model, with a model structure as shown in Figure 2.

The model represents a residential dwelling with two thermal zones: a day zone, consisting of all rooms in which the occupants are active during the day, and a night zone, mainly consisting of the bedrooms. Figure 2 shows all states representing the building structure, being the temperatures – in both zones (indicated by either 'D' or 'N') – of the indoor air, T_i , of the external walls (or of the combination of the external walls and roof in case of the night zone), T_w , of the interior walls, T_{wi} and of the floors, T_f . Also the associated thermal capacities and resistances (same indices) are shown. The windows are not represented by an individual state, because of their negligible thermal mass compared to the massive building structure; as such, the resistance $R_{inf,win}$ not only refers to the heat losses via infiltration/ventilation, but also to the transmission losses via the windows and doors. Also the external boundary conditions are included in Figure 2, being the ambient and ground temperature. Note that the heat inputs, emitted by low-temperature radiators, solar gains and internal gains are not explicitly shown; they are all distributed over the capacities of all different states by using distribution coefficients (Reynders et al. (2014)).

The building model RC parameters are related to the building construction as follows. The thermal capacities, representing the active thermal mass, are determined by the material layers within the insulation barrier. In line with this, the thermal resistances of the external walls and ground floor are split in two components: an internal resistance (index 1) up to, but excluding, the insulation layer, and an external resistance (index 2). For the internal walls, the thermal resistance is taken equal to 50% of the total resistance of the wall, since the thermal mass is equally accessible from both sides. Finally, the UA-values of the windows and doors are combined with the ventilation and infiltration losses to represent an additional thermal resistance.

By repeating the model identification for the whole set of possible constructions, the resulting set of RC parameters may be interpreted as a statistical characterization of the building controller model.

To summarize the whole conversion process, Table 1 clarifies the relation between the probabilistic U-values and WWR, and the RC parameters of the building controller model, illustrating the probabilistic character of the latter.

4. Using building controller model to determine energy use via optimal control

To understand how the variations in building controller model parameters translate to variations in optimal energy use, a Monte Carlo analysis (MCA) is performed. As such, an optimal space heating strategy is determined for a large set of possible building controller models that may be representative for a specific dwelling with a fixed geometry, location and age.

The formulation of the considered optimal control problem (OCP), aiming at guaranteeing thermal comfort at minimal energy use, is shown below.

$$\min_{\mathbf{u}_t} \sum_{t=1}^n ((\mathbf{1}_n^T \cdot \mathbf{u}_t) \cdot \Delta t + c \cdot s_t)$$

$$s.t. \quad \mathbf{T}_{t+1} = f_{RC}(\mathbf{T}_t, \mathbf{u}_t, \mathbf{d}_t, \Delta t) \quad \forall t = 1 \dots n$$

$$T_{zone,t} + s_t \geq \underline{T}_{zone,t} \quad \forall t = 1 \dots n$$

$$T_{zone,t} - s_t \leq \overline{T}_{zone,t} \quad \forall t = 1 \dots n$$

$$\mathbf{1}_n^T \cdot \mathbf{u}_t \leq u_{max,t} \quad \forall t = 1 \dots n$$

where $\mathbf{1}_n$ is an all-ones vector of size n

In this OCP, \mathbf{u}_t represents the thermal power inputs delivered by the heating system to the low-temperature radiators in the day and night zone during time step Δt , in order to keep the temperature of each zone $T_{zone,t}$ in between its comfort limits $\underline{T}_{zone,t}$ and $\overline{T}_{zone,t}$. The imposed thermal comfort requirements can not always be satisfied, especially during mid-season and summer months, when, e.g., overheating can occur if no cooling system is present. To prevent the model from becoming infeasible in these cases, the comfort constraints are relaxed with the help of a slack variable s_t that is penalized in the objective function at a very high cost c . The heat inputs are in turn limited by a maximum power bound, taken equal to the nominal heat demand of the building; as such, the heating system is assumed to be ideal, with a 100% efficiency and perfect modulation. The final important constraint is set by the building dynamics, determining the temperatures \mathbf{T}_{t+1} of all states representing the building structure based on the building RC model f_{RC} , the preceding building temperatures \mathbf{T}_t , the heat inputs \mathbf{u}_t , the disturbances \mathbf{d}_t (such as weather and occupant behavior), and the length of the time step Δt .

The optimization considered in this paper spans a whole year, with an additional week for initialization purposes². The time step is equal to one hour. Perfect predictions of the disturbances are assumed, resulting in a theoretical bound on the performance that any real controller can achieve³. For the weather

²For the one-week initialization problem, cyclic boundary conditions are imposed.

³Note that the absence of a receding horizon approach with closed-loop disruptions is why the considered implementation is referred to as optimal control, rather than as MPC.

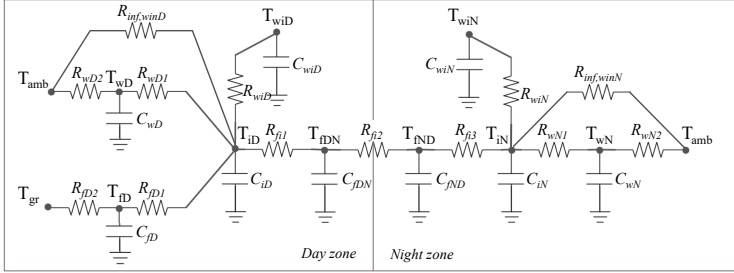


Figure 2: The model structure of the reduced order RC model, where a residential building is modeled as two zones (a day and night zone), represented by nine states (adapted from Reynders et al. (2014)).

Table 1: The dependency of the RC parameters on the U-values and WWR, illustrating their probabilistic character.

| | $R_{inf,winD}$ | $R_{wD}(1/2)$ | R_{wiD} | $R_{fD}(1/2)$ | $R_{fi}(1/2/3)$ | $R_{inf,winN}$ | $R_{wN}(1/2)$ | R_{wiN} | C_{wD} | C_{wiD} | C_{fD} | C_{fDN} | C_{iD} | C_{wN} | C_{wiN} | C_{fND} | C_{iN} |
|-----------------------|----------------|---------------|-----------|---------------|-----------------|----------------|---------------|-----------|----------|-----------|----------|-----------|----------|----------|-----------|-----------|----------|
| $U_{external\ walls}$ | | x | | | | | x | | x | | | | | | x | | |
| $U_{ground\ floor}$ | | | | x | | | | | | | | | | | | | |
| U_{roof} | | | | | | | x | | | | | | | | x | | |
| $U_{windows}$ | x | | | | | x | | | | | | | | | | | |
| WWR | x | x | | | | x | x | | x | | | | | | x | | |

data (i.e., ambient temperature and solar heat gains), measurement data of the year 2016 of the Vliet test building of the KU Leuven Laboratory of Building Physics, located in Leuven (Belgium), are used. For the occupancy behavior (i.e., internal heat gains and comfort requirements in terms of setpoint temperatures for different zones), profiles characterizing a four-person household are generated with the help of the StROBe toolbox of Baetens and Saelens (2016).

Case study

To maximize insight, the statistical characterization of a building controller model and its subsequent application in an optimal control problem is repeated for multiple dwellings for which the main characteristics determining the thermal quality (i.e., geometry and construction year) are sufficiently different.

Nine buildings of varying age (old (<1950), ageing (1950-1990) or more recent (>1990)) are selected from the suburban residential areas of the City of Genk in Flanders (Belgium). For each building type (i.e., terraced, semi-detached and detached), three buildings are selected with a varying floor area, ranging from small, over medium, to large. Their main characteristics are summarized in Table 2.

As a final remark, it should be noted that all buildings are assumed to have the same air infiltration rate of 0.4 h^{-1} ; this assumption is based on the fact that, in case of renovation, the decrease of infiltration is compensated by the introduction of mechanical ventilation, which is assumed to result in a similar total

air change rate.

For each dwelling in Table 2, 100 correlated samples of the U-values and WWR are generated, leading to 100 possible building controller models per considered dwelling.

Results and discussion

In this section, the uncertainty of the building model parameters derived from publicly available data is determined, together with its impact on the optimal space heating strategy. Since the different uncertain variables have different orders of magnitude, the whole assessment is done in terms of the standardized coefficient of variation (CV)⁴.

RQ1 - Variation in building model parameters

Figure 3 and 4 respectively show the distributions of the U-values and WWR, and the resulting set of RC parameters for the nine considered dwellings; in order not to overload Figure 4, only the most important uncertain parameters characterizing the day zone are shown. To be able to analyze the results, first, a proper understanding of the uncertainty on the building thermal properties is needed, followed by an in-depth assessment of how this uncertainty propagates into the model parameters.

When comparing the thermal properties of the different dwellings, an interesting trend can be observed (Figure 3). Because of the imposed cap on the nom-

⁴The coefficient of variation is equal to the ratio of the standard deviation to the mean, and serves as a unit-independent statistical measure of the dispersion of a variable.

Table 2: Overview of the main characteristics of the nine studied dwellings. The label refers to the building type, size, and age, and will be used throughout the paper.

| label | building type [-] | net floor | protected | ground floor | façade | roof | construction |
|--------|----------------------|---------------------------|-----------------------------|---------------------------|---------------------------|---------------------------|---------------|
| | | area [m ²] | volume [m ³] | area [m ²] | area [m ²] | area [m ²] | year [-] |
| T_S_O | terraced (T) | 129 (S) | 406 | 87 | 80 | 95 | <1950 (O) |
| T_M_O | terraced (T) | 193 (M) | 531 | 97 | 92 | 116 | <1950 (O) |
| T_L_A | terraced (T) | 244 (L) | 844 | 145 | 116 | 161 | 1950-1990 (A) |
| SD_S_A | semi-detached (SD) | 155 (S) | 546 | 96 | 171 | 101 | 1950-1990 (A) |
| SD_M_A | semi-detached (SD) | 210 (M) | 692 | 105 | 140 | 122 | 1950-1990 (A) |
| SD_L_O | semi-detached (SD) | 275 (L) | 742 | 200 | 226 | 154 | <1950 (O) |
| D_S_A | detached (D) | 163 (S) | 559 | 94 | 202 | 112 | 1950-1990 (A) |
| D_M_O | detached (D) | 260 (M) | 716 | 139 | 181 | 187 | <1950 (O) |
| D_L_R | detached (D) | 301 (L) | 752 | 151 | 167 | 173 | > 1990 (R) |

inal heat demand, the total heat loss coefficient of transmission (i.e., the total sum of the UA-values of the building), presented in the last plot of Figure 3, spans approximately the same range for all considered dwellings (although terraced dwellings can have slightly smaller heat losses because of the smaller total loss area). These similar UA-values break down in small buildings with a large range of admissible U-values, or in larger, renovated buildings, for which only the lowest U-values are allowed. Due to this effect, the nine considered dwellings can also be interpreted as nine cases of increasing confidence about the building thermal quality. This is confirmed by Table 3 and Figure 5. Figure 5 clearly shows that this effect predominantly manifests itself for the U-value of the external walls (CV 0.30–0.61) and roof (CV 0.43–0.99). For the U-value of the ground floor (CV 0.31–0.49), the tendency is less clear, since the low probability of invasive floor renovations leads to more similar distributions for all dwellings, which is confirmed by Figure 3. Also for the windows (CV 0.23–0.30), the difference in uncertainty is less pronounced, since window glazing can only have a limited number of discrete U-value options; the significantly lower absolute value of the CV of the U-value of the window compared to the other U-values, on the other hand, can be explained by the significantly higher average U-value for windows compared to opaque parts.

The minimal bounds of the CV ranges for all U-values are of the same order (~ 0.3) as the values reported in literature for older buildings (Ioannou and Itard (2015)), and as such, can be roughly considered as expected values of the uncertainty for existing, (partly) renovated, heavy-weight dwellings. It should be stressed that these expected values are worst case estimates, since the followed approach relies upon very limited building-specific information.

When converting the U-values of the different construction elements into RC parameters for a particular dwelling, the uncertainty is affected by the different processing operations. First, the uncertainty

is altered due to the conversion of U-values into UA-values describing the heat transfer with the surroundings. This operation only has an impact in case of a variable area (i.e., for the external walls and windows due to the variable WWR); otherwise, the mean and standard deviation are simply scaled by the same factor. Next, the split up of the heat transfer by setting apart the material layers inside and outside the insulation barrier further impacts the CV. Finally, an inverting operation is needed, since the heat transfer coefficients are related to the inverse of the R and C parameters. However, the inverting operation is not considered here, since it results in distorted distributions with increased skewness due to exacerbated outliers, thereby making the analysis more difficult.

For the external walls, the CV of the UA-value is slightly increased compared to the U-value due to the impact of the WWR, resulting in a variation between 0.31 and 0.62 (see Table 3). The internal resistance $1/R_{wD1}$ and the capacitance $1/C_{wD}$ are hardly impacted by this uncertainty, with a CV in the order of 10^{-2} . This is to be expected, since the large differences in U(A)-values are mainly attributed to different insulation levels of the exterior, whereas the inner parts don't change much when converting U-values to layers and materials with the method of De Jaeger et al. (2018). Hence, the uncertainty is mainly transferred to the external resistance $1/R_{wD2}$, as can also clearly be seen in Figure 5. Remarkably, the conversion from U to $1/R$ results in an even higher CV for all nine cases, with values ranging from 0.40 to 0.93. For the analogous resistances and capacitances in the night zone, similar and even more pronounced effects are visible, since here, also the uncertainty of the U-value of the roof is incorporated.

For the ground floor, the uncertainty of the U-values does not affect the internal resistance $1/R_{fD1}$ (CV = 0), since the corresponding material layers, tiles and screed, are fixed. The external resistance $1/R_{fD2}$, on the other hand, has a mildly varying CV ranging from 0.22 to 0.32, which is a clear decrease compared to the CV of the U-value.

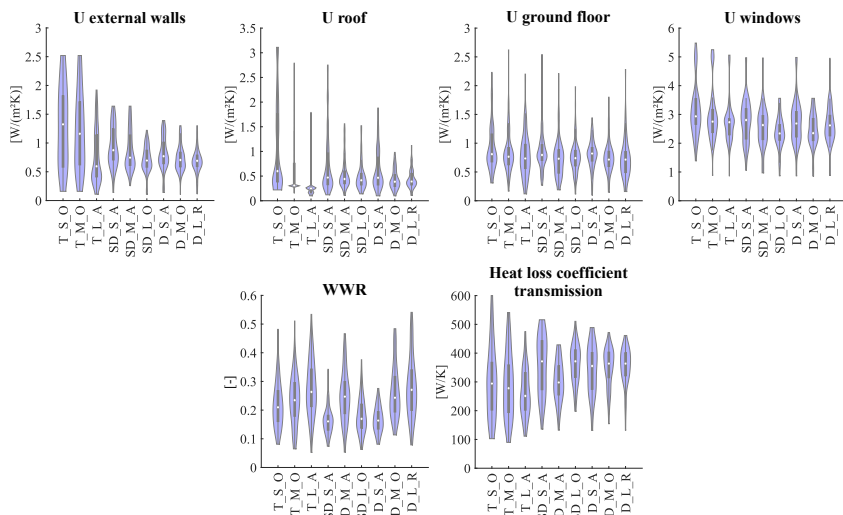


Figure 3: The distribution of the U -values, window-to-wall ratio and heat loss coefficient of transmission for the nine considered dwellings.

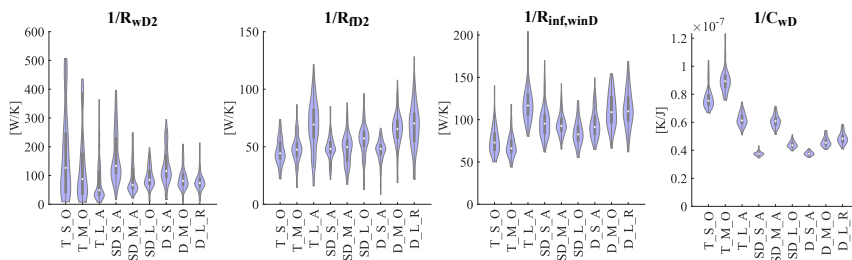


Figure 4: The distribution of the inverse of the most significant uncertain RC parameters characterizing the day zone of the nine considered dwellings.

Finally, for the windows and doors, the CV of the UA-value is increased compared to the U -value due to the varying WWR, resulting in a CV in the range of 0.35 up to 0.46. This uncertainty is then absorbed by the resistances $1/R_{inf,winD}$ and $1/R_{inf,winN}$, resulting in a CV between 0.14 and 0.21, and 0.14 and 0.22, respectively. This reduction in CV is due to the fact that $R_{inf,win}$ does not only account for transmission losses via windows and doors, but also for infiltration losses, which are assumed to be known.

The key takeaway from the analysis above is the insight in how the uncertainty on the building thermal properties propagates into the building model parameters for the different construction elements. It should nevertheless be stressed that these insights depend on i) the underlying input data (being the energy performance data of the Flemish building stock), ii) the subsequent processing (being the methods of De Jaeger et al. (2018) and De Jaeger et al. (2021)), and iii) the imposed building model structure (being the 9-state reduced order RC model developed by Reynders et al.

(2014)). In order to further consolidate the presented results, a more differentiated assessment is recommended, where the uncertainty on the $U(A)$ -values and derived model parameters is further explored for different U -value distributions, and for other building model structures.

RQ2 - Variation in optimal energy demand profile and yearly energy use

Figure 6 illustrates how the different realizations of the detached, midsize, old dwelling result in different energy demand profiles for a particular day (start of January). The different model realizations entail different estimates of the time constants of the building, thereby requiring a different heat supply to the radiator system, both in terms of timing, and in terms of peak demand. The difference in peak demand between the considered 100 possible dwelling realizations exceeds 4 kW for the shown 24h-profile.

The yearly energy use for the 100 dwelling realizations of the D_M_O case ranges from 9757 kWh to

Table 3: The coefficient of variation of the U -values and window-to-wall ratio, the UA -values, and the RC parameters for the nine considered dwellings.

| | U external walls | | U roof | | U ground floor | | U windows | | WWR | | UA external walls | | UA windows | | $1/R_{wD1}$ | $1/R_{wD2}$ | $1/R_{wN1}$ | $1/R_{wN2}$ | $1/R_{fD1}$ | $1/R_{fD2}$ | $1/R_{inf,winD}$ | $1/R_{inf,winN}$ | $1/C_{wD}$ | $1/C_{wN}$ |
|--------|------------------|------|--------|------|----------------|------|-----------|------|------|------|-------------------|---|------------|------|-------------|-------------|-------------|-------------|-------------|-------------|------------------|------------------|------------|------------|
| T.S.O | 0.52 | 0.83 | 0.43 | 0.28 | 0.37 | 0.54 | 0.42 | 0.08 | 0.86 | 0.03 | 1.27 | 0 | 0.24 | 0.21 | 0.22 | 0.10 | 0.08 | | | | | | | |
| T.M.O | 0.55 | 0.99 | 0.42 | 0.30 | 0.36 | 0.57 | 0.43 | 0.09 | 0.93 | 0.03 | 0.84 | 0 | 0.24 | 0.21 | 0.21 | 0.10 | 0.08 | | | | | | | |
| T.L.A | 0.61 | 0.96 | 0.49 | 0.26 | 0.34 | 0.62 | 0.46 | 0.07 | 0.90 | 0.02 | 0.77 | 0 | 0.32 | 0.20 | 0.20 | 0.07 | 0.06 | | | | | | | |
| SD.S.A | 0.37 | 0.84 | 0.42 | 0.27 | 0.27 | 0.37 | 0.38 | 0.04 | 0.54 | 0.02 | 0.74 | 0 | 0.22 | 0.20 | 0.20 | 0.04 | 0.03 | | | | | | | |
| SD.M.A | 0.39 | 0.57 | 0.45 | 0.28 | 0.35 | 0.40 | 0.39 | 0.07 | 0.60 | 0.02 | 0.44 | 0 | 0.28 | 0.14 | 0.14 | 0.07 | 0.06 | | | | | | | |
| SD.L.O | 0.30 | 0.58 | 0.37 | 0.23 | 0.34 | 0.31 | 0.36 | 0.05 | 0.40 | 0.02 | 0.33 | 0 | 0.24 | 0.17 | 0.17 | 0.05 | 0.05 | | | | | | | |
| D.S.A | 0.35 | 0.64 | 0.31 | 0.28 | 0.27 | 0.36 | 0.35 | 0.04 | 0.48 | 0.02 | 0.46 | 0 | 0.22 | 0.18 | 0.18 | 0.04 | 0.03 | | | | | | | |
| D.M.O | 0.30 | 0.46 | 0.36 | 0.23 | 0.35 | 0.31 | 0.35 | 0.07 | 0.41 | 0.02 | 0.33 | 0 | 0.23 | 0.18 | 0.18 | 0.07 | 0.06 | | | | | | | |
| D.L.R | 0.31 | 0.43 | 0.47 | 0.24 | 0.38 | 0.34 | 0.36 | 0.08 | 0.44 | 0.02 | 0.35 | 0 | 0.30 | 0.19 | 0.19 | 0.08 | 0.06 | | | | | | | |

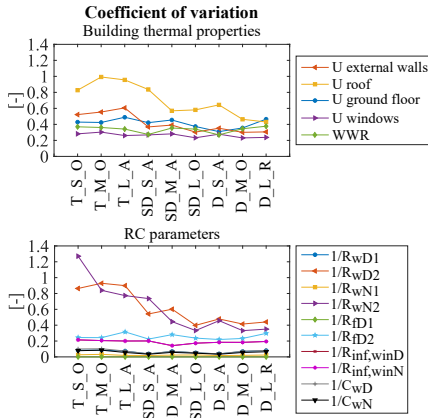


Figure 5: The coefficient of variation of the U -values and of (the inverse of) the derived RC parameters for the nine considered dwellings.

26702 kWh, resulting in a CV of 0.22. For the other considered dwellings, the CV is higher; their variation in yearly energy use is summarized in Figure 7.

The substantial variation in resulting space heating control strategies, both in terms of dynamic effects and total yearly energy use, is a first indication that the obtained uncertainty characterization is not accurate enough to be directly used for deterministic building level control, and that additional data acquisition (e.g., via experts or learning) narrowing down the range of feasible model parameters, and/or an adapted control strategy explicitly accounting for the uncertainty, is needed. This will be further investigated in future research; this follow-up work will first assess in more detail the impact of the uncertainty on the MPC performance in terms of thermal comfort and cost by considering a closed loop receding horizon approach correcting for model mismatch by

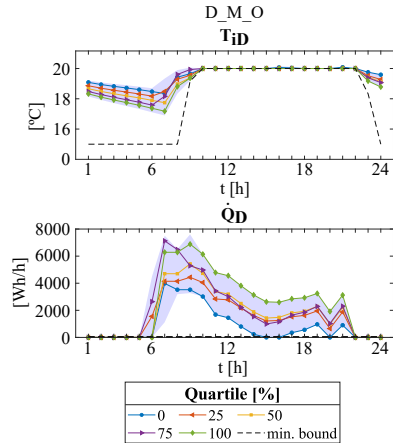


Figure 6: 24h-profiles of the indoor temperature T_{iD} and heat input Q_D (averaged over 1 hour) for the day zone for five dwelling realizations of the detached, midsize, old dwelling; the blue shaded area indicates the range of solutions spanned by all possible dwelling realizations.

state updates. Subsequently, it will be investigated to what extent the detrimental effects can be alleviated by an adapted, robustified control strategy that is incorporating the uncertainty characterization derived in this paper.

Summary and conclusion

For older residential buildings, a lack of information about the building thermal properties hampers the construction of accurate building simulation or controller models. As a worst case estimation, this work investigates the uncertainty if building controller models for model predictive control applications are derived based on sparse, publicly available data.

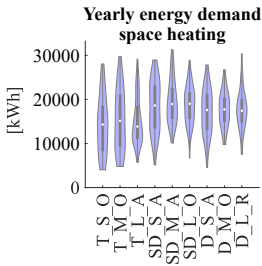


Figure 7: The distribution of the optimized yearly energy demand for space heating for the nine considered dwellings.

The proposed approach first uses the method of De Jaeger et al. (2018) to determine distributions of the building thermal properties based on statistical data of the energy performance of the Flemish residential heavy-weight building stock. A detailed comparison of the results for nine disparate, (partly) renovated dwellings shows that the proposed approach results in rather large distributions for the thermal properties. A coefficient of variation in the order of 0.3 is observed as a minimal bound for all U-values for all considered dwellings. The uncertainty on the U-values of the ground floor and windows is found to fluctuate around the same value, whereas the uncertainty on the U-values of the external walls and roof can vary considerably.

The obtained building thermal properties are subsequently converted into a 9-states reduced order RC model. Since the exact set of building model parameters depends on the imposed building model structure, the most important takeaway is the insight in how the uncertainty on the building thermal properties propagates into RC model parameters, rather than exact values for the parametric uncertainty. It is observed that the uncertainty is predominantly transferred to the external resistances containing the insulation layer; more specifically, for the ground floor and windows, the coefficient of variation decreases when moving from U to 1/R, whereas for the external walls and roof, it increases.

Finally, the derived uncertainty is shown to affect the optimal control strategy, both in terms of dynamic effects and yearly energy use, thereby indicating the need for improved data acquisition and/or dedicated control strategies under uncertainty; this will be more detailedly investigated in future research.

Acknowledgements

This work was supported by KU Leuven (C2 Research Project C24/16/018 'Energy Storage as a Disruptive Technology in the Energy System of the Future'), the Flemish Institute for Technological Research (VITO), and the Research Foundation – Flanders (FWO) (doctoral mandate 11D0318N and post-doctoral mandate 12J3320N).

References

- Avci, M., M. Erkok, A. Rahmani, and S. Asfour (2013). Model predictive HVAC load control in buildings using real-time electricity pricing. *Energy and Buildings* 60, 199–209.
- Baetens, R. and D. Saelens (2016). Modelling uncertainty in district energy simulations by stochastic residential occupant behaviour. *Journal of Building Performance Simulation* 9(4), 431–447.
- Bengea, S., V. Adetola, K. Kang, M. J. Liba, D. Vrabie, R. Bitmead, and S. Narayanan (2011). Parameter estimation of a building system model and impact of estimation error on closed-loop performance. In *50th IEEE Conference on Decision and Control and European Control Conference, 2011, Orlando, FL, USA*, pp. 5137–5143. IEEE.
- Bianchini, G., M. Casini, A. Vicino, and D. Zarrilli (2016). Demand-response in building heating systems: A Model Predictive Control approach. *Applied Energy* 168, 159–170.
- De Jaeger, I., J. Lago, and D. Saelens (2018). A probabilistic approach to allocate building parameters within district energy simulations. In *Proceedings of the Urban Energy Simulation Conference, 2018, Glasgow, Scotland*. University of Strathclyde.
- De Jaeger, I., J. Lago, and D. Saelens (2021). A probabilistic building characterization method for district energy simulations. *Energy and Buildings* 230, 110566.
- Drgoňa, J., J. Arroyo, I. C. Figueroa, D. Blum, K. Arendt, D. Kim, E. P. Ollé, J. Oravec, M. Wetter, D. L. Vrabie, et al. (2020). All you need to know about model predictive control for buildings. *Annual Reviews in Control*.
- Ioannou, A. and L. C. Itard (2015). Energy performance and comfort in residential buildings: Sensitivity for building parameters and occupancy. *Energy and Buildings* 92, 216–233.
- Maasoumy, M., M. Razmara, M. Shahbakhti, and A. S. Vincentelli (2014). Handling model uncertainty in model predictive control for energy efficient buildings. *Energy and Buildings* 77, 377–392.
- Nagpal, H., A. Staino, and B. Basu (2020). Robust model predictive control of HVAC systems with uncertainty in building parameters using linear matrix inequalities. *Advances in Building Energy Research* 14(3), 338–354.
- NBN (2017). NBN EN 12831-1: Energy performance of buildings - Method for calculation of the design heat load - Part 1: Space heating load.
- Oldewurtel, F., D. Gyalistras, M. Gwerder, C. Jones, A. Parisio, V. Stauch, B. Lehmann, and M. Morari (2010). Increasing energy efficiency in building climate control using weather forecasts and model predictive control. In *Climate RHEVA World Congress, 2010, Antalya, Turkey*.
- Oldewurtel, F., A. Parisio, C. N. Jones, D. Gyalistras, M. Gwerder, V. Stauch, B. Lehmann, and M. Morari (2012). Use of model predictive control and weather forecasts for energy efficient building climate control. *Energy and Buildings* 45, 15–27.
- Oldewurtel, F., A. Ulbig, A. Parisio, G. Andersson, and M. Morari (2010). Reducing peak electricity demand in building climate control using real-time pricing and model predictive control. In *49th IEEE conference on decision and control (CDC), Atlanta, GA, USA*, pp. 1927–1932. IEEE.
- Reynders, G., J. Diriken, and D. Saelens (2014). Bottom-up modeling of the Belgian residential building stock: influence of model complexity. In *Proceedings of the 9th International Conference on System Simulation in Buildings, 2014, Liège, Belgium*, pp. 1–19. University of Liège.
- Serale, G., M. Fiorentini, A. Capozzoli, D. Bernardini, and A. Bemporad (2018). Model predictive control (MPC) for enhancing building and HVAC system energy efficiency: Problem formulation, applications and opportunities. *Energies* 11(3), 631.
- Tanaskovic, M., D. Sturzenegger, R. Smith, and M. Morari (2017). Robust adaptive model predictive building climate control. *IFAC-PapersOnLine* 50(1), 1871–1876.

Bibliography

- [1] Eurostat, “Energy consumption in households,” 2018. https://ec.europa.eu/eurostat/statistics-explained/index.php?title=Energy_consumption_in_households. Accessed: 2021-04-22.
- [2] European Commission, “Communication from the Commission to the European Parliament, the Council, the European Economic and Social Committee and the Committee of the Regions. An EU Strategy on Heating and Cooling,” 2016. <https://eur-lex.europa.eu/legal-content/EN/TXT/HTML/?uri=CELEX:52016DC0051>. Accessed: 2021-05-17.
- [3] European Commission, “Directive 2010/31/EU of the European Parliament and of the Council of 19 May 2010 on the energy performance of buildings,” 2010. <https://eur-lex.europa.eu/legal-content/EN/TXT/?uri=CELEX:32010L0031>. Accessed: 2021-05-17.
- [4] European Commission, “Directive 2012/27/EU of the European Parliament and of the Council of 25 October 2012 on energy efficiency, amending Directives 2009/125/EC and 2010/30/EU and repealing Directives 2004/8/EC and 2006/32/EC,” 2012. <https://eur-lex.europa.eu/legal-content/EN/TXT/HTML/?uri=CELEX:32012L0027>. Accessed: 2021-05-17.
- [5] European Commission, “Directive 2018/844 of the European Parliament and of the Council of 30 May 2018 amending Directive 2010/31/EU on the energy performance of buildings and Directive 2012/27/EU on energy efficiency,” 2018. <https://eur-lex.europa.eu/legal-content/EN/TXT/HTML/?uri=CELEX:32018L0844>. Accessed: 2021-05-17.
- [6] European Commission, “Directive (EU) 2018/2001 of the European Parliament and of the Council of 11 December 2018 on the promotion of the use of energy from renewable sources,” 2018. <https://eur-lex.europa.eu/legal-content/EN/TXT/HTML/?uri=CELEX:32018L2001>. Accessed: 2021-05-17.

- [7] European Commission, "Energy performance of buildings directive." https://ec.europa.eu/energy/topics/energy-efficiency/energy-efficient-buildings/energy-performance-buildings-directive_en. Accessed: 2021-08-12.
- [8] European Commission, "Communication from the Commission to the European Parliament, the Council, the European Economic and Social Committee and the Committee of the Regions. A Renovation Wave for Europe - greening our buildings, creating jobs, improving lives," 2020. <https://eur-lex.europa.eu/legal-content/EN/TXT/HTML/?uri=CELEX:52020DC0662>. Accessed: 2021-08-12.
- [9] D. Connolly, H. Lund, B. Mathiesen, S. Werner, B. Möller, U. Persson, T. Boermans, D. Trier, P. Østergaard, and S. Nielsen, "Heat Roadmap Europe: Combining district heating with heat savings to decarbonise the EU energy system," *Energy Policy*, vol. 65, pp. 475–489, 2014.
- [10] C. Reidhav and S. Werner, "Profitability of sparse district heating," *Applied Energy*, vol. 85, no. 9, pp. 867–877, 2008.
- [11] B. Mathiesen, D. Drysdale, H. Lund, S. Paardekooper, I. Ridjan, D. Connolly, J. Thellufsen, and J. Jensen, *Future Green Buildings: A Key to Cost-Effective Sustainable Energy Systems*. Department of Development and Planning, Aalborg University, Denmark, 2016.
- [12] G. Serale, M. Fiorentini, A. Capozzoli, D. Bernardini, and A. Bemporad, "Model predictive control (MPC) for enhancing building and HVAC system energy efficiency: Problem formulation, applications and opportunities," *Energies*, vol. 11, no. 3, p. 631, 2018.
- [13] H. Thieblemont, F. Haghghat, R. Ooka, and A. Moreau, "Predictive control strategies based on weather forecast in buildings with energy storage system: A review of the state-of-the art," *Energy and Buildings*, vol. 153, pp. 485–500, 2017.
- [14] A. Mirakhorli and B. Dong, "Occupancy behavior based model predictive control for building indoor climate—a critical review," *Energy and Buildings*, vol. 129, pp. 499–513, 2016.
- [15] Boydens, W. and Helsen, L. and Olesen, B. W. and Ferkl, L. and Laverge, J., *Renewable and Storage-integrated Systems to Supply Comfort in Buildings: pre-design and control for hybridGEOTABS projects*. A&S/books, 2021.
- [16] M. Anda and J. Temmen, "Smart metering for residential energy efficiency: The use of community based social marketing for behavioural change and smart grid introduction," *Renewable Energy*, vol. 67, pp. 119–127, 2014. Renewable Energy for Sustainable Development and Decarbonisation.

- [17] D. Fischer and H. Madani, "On heat pumps in smart grids: A review," *Renewable and Sustainable Energy Reviews*, vol. 70, pp. 342–357, 2017.
- [18] G. Reynders, T. Nuytten, and D. Saelens, "Potential of structural thermal mass for demand-side management in dwellings," *Building and Environment*, vol. 64, pp. 187–199, 2013.
- [19] R. G. Junker, A. G. Azar, R. A. Lopes, K. B. Lindberg, G. Reynders, R. Relan, and H. Madsen, "Characterizing the energy flexibility of buildings and districts," *Applied energy*, vol. 225, pp. 175–182, 2018.
- [20] A. Arteconi, N. Hewitt, and F. Polonara, "State of the art of thermal storage for demand-side management," *Applied Energy*, vol. 93, pp. 371–389, 2012.
- [21] R. Belmans, J. Büscher, C. de Jonghe, P. de Pauw, P. de Raedemaeker, C. Devellder, S. Grosjean, E. Hendrix, J. Lemmens, G. Palmers, M. Strobbe, I. Van Vaerenbergh, and P. Vingerhoets, "De eindgebruiker centraal in de energietransitie (in Dutch)," *KVAB Standpunt 44*, 2016.
- [22] G. Strbac, "Demand side management: Benefits and challenges," *Energy Policy*, vol. 36, no. 12, pp. 4419–4426, 2008. Foresight Sustainable Energy Management and the Built Environment Project.
- [23] R. Halvgaard, N. K. Poulsen, H. Madsen, and J. B. Jørgensen, "Economic model predictive control for building climate control in a smart grid," in *3rd IEEE PES Conference on Innovative Smart Grid Technologies (ISGT) 2012, Washington D.C., USA*, pp. 1–6, IEEE Power and Energy Society (PES), 2012.
- [24] D. Patteeuw, K. Bruninx, A. Arteconi, E. Delarue, W. D'haeseleer, and L. Helsen, "Integrated modeling of active demand response with electric heating systems coupled to thermal energy storage systems," *Applied Energy*, vol. 151, pp. 306–319, 2015.
- [25] M. Dahl Knudsen and S. Petersen, "Demand response potential of model predictive control of space heating based on price and carbon dioxide intensity signals," *Energy and Buildings*, vol. 125, pp. 196–204, 2016.
- [26] G. Bianchini, M. Casini, A. Vicino, and D. Zarrilli, "Demand-response in building heating systems: A Model Predictive Control approach," *Applied Energy*, vol. 168, pp. 159–170, 2016.
- [27] H. Lund, S. Werner, R. Wiltshire, S. Svendsen, J. E. Thorsen, F. Hvelplund, and B. V. Mathiesen, "4th Generation District Heating (4GDH): Integrating smart thermal grids into future sustainable energy systems," *Energy*, vol. 68, pp. 1–11, 2014.

- [28] M. D. Knudsen and S. Petersen, "Model predictive control for demand response of domestic hot water preparation in ultra-low temperature district heating systems," *Energy and Buildings*, vol. 146, pp. 55–64, 2017.
- [29] H. Cai, C. Ziras, S. You, R. Li, K. Honoré, and H. W. Bindner, "Demand side management in urban district heating networks," *Applied Energy*, vol. 230, pp. 506–518, 2018.
- [30] D. Romanchenko, E. Nyholm, M. Odenberger, and F. Johnsson, "Impacts of demand response from buildings and centralized thermal energy storage on district heating systems," *Sustainable Cities and Society*, vol. 64, p. 102510, 2021.
- [31] P. Siano, "Demand response and smart grids—a survey," *Renewable and Sustainable Energy Reviews*, vol. 30, pp. 461–478, 2014.
- [32] M. Avci, M. Erkoç, A. Rahmani, and S. Asfour, "Model predictive HVAC load control in buildings using real-time electricity pricing," *Energy and Buildings*, vol. 60, pp. 199–209, 2013.
- [33] R. Belmans, B. Beusen, B. Boesmans, W. Cardinaels, B. Claessens, S. Claessens, P. Coomans, R. Dhulst, W. De Meyer, J. Degraeve, C. Develder, B. Dupont, W. Foubert, J. Gordelbeke, F. Hoornaert, S. Iacovella, J. Jargstorf, R. Jahn, K. Kessels, W. Labeeuw, P. Muyters, S. Penninck, R. Ponnette, D. Six, S. Stoffels, J. Stragier, M. Strobbe, K. Van Daele, P. Van Dievel, P. Van Poppel, D. Vanbeveren, C. Vangrunderbeek, K. Vanthournout, G. Verbeek, P. Verboven, and P. Vingerhoets, "Linear: The Report. Demand Response for Families," tech. rep., 2014. https://www.energyville.be/sites/energyville/files/downloads/2020/boekje_linear_okt_2014_boekje_web.pdf. Accessed: 2021-08-17.
- [34] N. O'Connell, P. Pinson, H. Madsen, and M. O'Malley, "Benefits and challenges of electrical demand response: A critical review," *Renewable and Sustainable Energy Reviews*, vol. 39, pp. 686–699, 2014.
- [35] A. Afram and F. Janabi-Sharifi, "Theory and applications of HVAC control systems – A review of model predictive control (MPC)," *Building and Environment*, vol. 72, pp. 343–355, 2014.
- [36] J. Drgoňa, J. Arroyo, I. C. Figueroa, D. Blum, K. Arendt, D. Kim, E. P. Ollé, J. Oravec, M. Wetter, D. L. Vrabie, and L. Helsen, "All you need to know about model predictive control for buildings," *Annual Reviews in Control*, vol. 50, pp. 190–232, 2020.

- [37] C. D. Korkas, S. Baldi, I. Michailidis, and E. B. Kosmatopoulos, "Occupancy-based demand response and thermal comfort optimization in microgrids with renewable energy sources and energy storage," *Applied Energy*, vol. 163, pp. 93–104, 2016.
- [38] F. Oldewurtel, A. Ulbig, A. Parisio, G. Andersson, and M. Morari, "Reducing peak electricity demand in building climate control using real-time pricing and model predictive control," in *49th IEEE conference on decision and control (CDC) 2010, Atlanta, GA, USA*, pp. 1927–1932, IEEE, 2010.
- [39] C. Verhelst, *Model Predictive Control of Ground Coupled Heat Pump Systems in Office Buildings*. PhD thesis, KU Leuven, Belgium, 2012.
- [40] L. Sugden, "Smart grids create new opportunities for heat pumps," *The REHVA European HVAC Journal*, vol. 49, pp. 20–22, 2012.
- [41] J. Wang, P. Li, K. Fang, and Y. Zhou, "Robust optimization for household load scheduling with uncertain parameters," *Applied Sciences*, vol. 8, no. 4, p. 575, 2018.
- [42] S. Benghea, V. Adetola, K. Kang, M. J. Liba, D. Vrabie, R. Bitmead, and S. Narayanan, "Parameter estimation of a building system model and impact of estimation error on closed-loop performance," in *50th IEEE Conference on Decision and Control (CDC) 2011 and European Control Conference (ECC) 2011, Orlando, FL, USA*, pp. 5137–5143, IEEE, 2011.
- [43] F. Oldewurtel, D. Gyalistras, M. Gwerder, C. Jones, A. Parisio, V. Stauch, B. Lehmann, and M. Morari, "Increasing energy efficiency in building climate control using weather forecasts and model predictive control," in *Clima - REHVA World Congress 2010, Antalya, Turkey*, Federation of European Heating, Ventilation and Air Conditioning Associations (REHVA) and Turkish Society of HVAC and Sanitary Engineers (TTMD), 2010.
- [44] F. Oldewurtel, A. Parisio, C. N. Jones, D. Gyalistras, M. Gwerder, V. Stauch, B. Lehmann, and M. Morari, "Use of model predictive control and weather forecasts for energy efficient building climate control," *Energy and Buildings*, vol. 45, pp. 15–27, 2012.
- [45] S. Goyal, H. A. Ingley, and P. Barooah, "Effect of various uncertainties on the performance of occupancy-based optimal control of HVAC zones," in *51st IEEE Conference on Decision and Control (CDC) 2012, Maui, Hawaii*, pp. 7565–7570, IEEE, 2012.
- [46] G. Lankeshwara, R. Sharma, R. Yan, and T. K. Saha, "Control algorithms to mitigate the effect of uncertainties in residential demand management," *Applied Energy*, vol. 306, p. 117971, 2022.

- [47] C. A. Correa-Florez, A. Michiorri, and G. Kariniotakis, "Comparative analysis of adjustable robust optimization alternatives for the participation of aggregated residential prosumers in electricity markets," *Energies*, vol. 12, no. 6, p. 1019, 2019.
- [48] Y. Long, S. Liu, L. Xie, and K. H. Johansson, "A scenario-based distributed stochastic MPC for building temperature regulation," in *10th IEEE International Conference on Automation Science and Engineering (CASE) 2014, Taipei, Taiwan*, pp. 1091–1096, IEEE, 2014.
- [49] A. Parisio, D. Varagnolo, M. Molinari, G. Pattarello, L. Fabietti, and K. H. Johansson, "Implementation of a scenario-based MPC for HVAC systems: an experimental case study," *IFAC Proceedings Volumes*, vol. 47, no. 3, pp. 599–605, 2014.
- [50] D. Ioli, A. Falsone, and M. Prandini, "Energy management of a building cooling system with thermal storage: a randomized solution with feedforward disturbance compensation," in *American Control Conference (ACC) 2016, Boston, MA, USA*, pp. 2346–2351, IEEE, 2016.
- [51] Y. Ma, J. Matuško, and F. Borrelli, "Stochastic model predictive control for building HVAC systems: Complexity and conservatism," *IEEE Transactions on Control Systems Technology*, vol. 23, no. 1, pp. 101–116, 2014.
- [52] J. Zhang and T. Ohtsuka, "Stochastic model predictive control using simplified affine disturbance feedback for chance-constrained systems," *IEEE Control Systems Letters*, vol. 5, no. 5, pp. 1633–1638, 2020.
- [53] X. Zhang, G. Schildbach, D. Sturzenegger, and M. Morari, "Scenario-based MPC for energy-efficient building climate control under weather and occupancy uncertainty," in *European Control Conference (ECC) 2013, Zurich, Switzerland*, pp. 1029–1034, European Control Association (EUCA), 2013.
- [54] A. Ioannou and L. C. Itard, "Energy performance and comfort in residential buildings: Sensitivity for building parameters and occupancy," *Energy and Buildings*, vol. 92, pp. 216–233, 2015.
- [55] W. Tian, Y. Heo, P. De Wilde, Z. Li, D. Yan, C. S. Park, X. Feng, and G. Augenbroe, "A review of uncertainty analysis in building energy assessment," *Renewable and Sustainable Energy Reviews*, vol. 93, pp. 285–301, 2018.
- [56] H. Nagpal, A. Staino, and B. Basu, "Robust model predictive control of HVAC systems with uncertainty in building parameters using linear matrix inequalities," *Advances in Building Energy Research*, vol. 14, no. 3, pp. 338–354, 2020.

- [57] M. Maasoumy, M. Razmara, M. Shahbakhti, and A. S. Vincentelli, "Handling model uncertainty in model predictive control for energy efficient buildings," *Energy and Buildings*, vol. 77, pp. 377–392, 2014.
- [58] M. Tanaskovic, D. Sturzenegger, R. Smith, and M. Morari, "Robust adaptive model predictive building climate control," *IFAC-PapersOnLine*, vol. 50, no. 1, pp. 1871–1876, 2017.
- [59] S. Yang, M. P. Wan, W. Chen, B. F. Ng, and D. Zhai, "An adaptive robust model predictive control for indoor climate optimization and uncertainties handling in buildings," *Building and Environment*, vol. 163, p. 106326, 2019.
- [60] I. De Jaeger, *On the Impact of Input Data Uncertainty on the Reliability of Urban Building Energy Models*. PhD thesis, KU Leuven, Belgium, 2021.
- [61] M. Killian and M. Kozek, "Ten questions concerning model predictive control for energy efficient buildings," *Building and Environment*, vol. 105, pp. 403–412, 2016.
- [62] I. De Jaeger, J. Lago, and D. Saelens, "A probabilistic approach to allocate building parameters within district energy simulations," in *Urban Energy Simulation Conference 2018, Glasgow, Scotland*, University of Strathclyde, Scotland, 2018.
- [63] I. De Jaeger, J. Lago, and D. Saelens, "A probabilistic building characterization method for district energy simulations," *Energy and Buildings*, vol. 230, p. 110566, 2021.
- [64] P. Huang, G. Huang, and Y. Wang, "HVAC system design under peak load prediction uncertainty using multiple-criterion decision making technique," *Energy and Buildings*, vol. 91, pp. 26–36, 2015.
- [65] G. Mavromatidis, K. Orehounig, and J. Carmeliet, "A review of uncertainty characterisation approaches for the optimal design of distributed energy systems," *Renewable and Sustainable Energy Reviews*, vol. 88, pp. 258–277, 2018.
- [66] Y. Sun, M. Elizondo, S. Lu, and J. C. Fuller, "The impact of uncertain physical parameters on hvac demand response," *IEEE Transactions on Smart Grid*, vol. 5, no. 2, pp. 916–923, 2014.
- [67] S. Petersen and K. W. Bundgaard, "The effect of weather forecast uncertainty on a predictive control concept for building systems operation," *Applied Energy*, vol. 116, pp. 311–321, 2014.

- [68] NBN, "NBN EN ISO 7730:2005 - Ergonomics of the thermal environment - Analytical determination and interpretation of thermal comfort using calculation of the PMV and PPD indices and local thermal comfort criteria," 2005.
- [69] NBN, "NBN EN ISO 15251:2007 - Indoor environmental input parameters for design and assessment of energy performance of buildings addressing indoor air quality, thermal environment, lighting and acoustics," 2007.
- [70] F. Jorissen, W. Boydens, and L. Helsen, "Methodology for integrated optimal control and design of buildings," in *REHVA Annual Meeting Conference Low Carbon Technologies in HVAC 2018, Brussels, Belgium*, Federation of European Heating, Ventilation and Air Conditioning Associations (REHVA) and Royal Association of Heating, Ventilation and Climate Control Technology (ATIC), 2018.
- [71] B. van der Heijde, *Optimal Integration of Thermal Energy Storage and Conversion in Fourth Generation Thermal Networks*. PhD thesis, KU Leuven, Belgium, 2019.
- [72] W. Gang, S. Wang, F. Xiao, and D. Gao, "Robust optimal design of building cooling systems considering cooling load uncertainty and equipment reliability," *Applied Energy*, vol. 159, pp. 265–275, 2015.
- [73] W. Gang, S. Wang, K. Shan, and D. Gao, "Impacts of cooling load calculation uncertainties on the design optimization of building cooling systems," *Energy and Buildings*, vol. 94, pp. 1–9, 2015.
- [74] E. Djunaedy, K. Van den Wymelenberg, B. Acker, and H. Thimmana, "Oversizing of HVAC system: signatures and penalties," *Energy and Buildings*, vol. 43, no. 2-3, pp. 468–475, 2011.
- [75] Y. Sun, L. Gu, C. J. Wu, and G. Augenbroe, "Exploring HVAC system sizing under uncertainty," *Energy and Buildings*, vol. 81, pp. 243–252, 2014.
- [76] K. Bettgenhäuser, M. Offermann, T. Boermans, M. Bosquet, J. Grözinger, B. von Manteuffel, and N. Surmeli, "Heat pump implementation scenarios until 2030," tech. rep., 2013.
- [77] IEA, "Heat pumps tracking report," 2021. <https://www.iea.org/reports/heat-pumps>. Accessed: 2021-11-06.
- [78] A. Parisio, D. Varagnolo, D. Risberg, G. Pattarello, M. Molinari, and K. H. Johansson, "Randomized model predictive control for HVAC systems," in *BuildSys 2013: 5th ACM Workshop on Embedded Systems For Energy-Efficient Buildings 2013, Rome, Italy*, pp. 1–8, Association for Computing Machinery (ACM), 2013.

- [79] F. Oldewurtel, A. Parisio, C. N. Jones, M. Morari, D. Gyalistras, M. Gwerder, V. Stauch, B. Lehmann, and K. Wirth, "Energy efficient building climate control using stochastic model predictive control and weather predictions," in *American Control Conference (ACC) 2010, Baltimore, MD, USA*, pp. 5100–5105, IEEE, 2010.
- [80] H. Brohus, P. Heiselberg, A. Simonsen, and K. Sørensen, "Uncertainty of energy consumption assessment of domestic buildings," in *Building Simulation (BS) Conference 2009, Glasgow, Scotland*, International Building Performance Simulation Association (IBPSA), 2009.
- [81] H. Brohus, C. Frier, P. Heiselberg, and F. Haghighat, "Quantification of uncertainty in predicting building energy consumption: A stochastic approach," *Energy and Buildings*, vol. 55, pp. 127–140, 2012.
- [82] F. Oldewurtel, *Stochastic model predictive control for energy efficient building climate control*. PhD thesis, ETH Zurich, Switzerland, 2011.
- [83] L. Peeters, R. De Dear, J. Hensen, and W. D'haeseleer, "Thermal comfort in residential buildings: Comfort values and scales for building energy simulation," *Applied Energy*, vol. 86, no. 5, pp. 772–780, 2009.
- [84] A. Mesbah, "Stochastic model predictive control: An overview and perspectives for future research," *IEEE Control Systems Magazine*, vol. 36, no. 6, pp. 30–44, 2016.
- [85] M. Prandini, S. Garatti, and J. Lygeros, "A randomized approach to stochastic model predictive control," in *51st IEEE Conference on Decision and Control (CDC) 2012, Maui, Hawaii*, pp. 7315–7320, IEEE, 2012.
- [86] X. Zhang, S. Grammatico, G. Schildbach, P. Goulart, and J. Lygeros, "On the sample size of randomized MPC for chance-constrained systems with application to building climate control," in *European Control Conference (ECC) 2014, Strasbourg, France*, pp. 478–483, European Control Association (EUCA), 2014.
- [87] L. Hewing, K. P. Wabersich, and M. N. Zeilinger, "Recursively feasible stochastic model predictive control using indirect feedback," *Automatica*, vol. 119, p. 109095, 2020.
- [88] M. Wallace, P. Mhaskar, J. House, and T. I. Salsbury, "Offset-free model predictive control of a heat pump," *Industrial & Engineering Chemistry Research*, vol. 54, no. 3, pp. 994–1005, 2015.
- [89] S. Herzog, D. Atabay, J. Jungwirth, and V. Mikulovic, "Self-adapting building models for model predictive control," in *Building Simulation (BS) Conference*

- 2013, *Chambéry, France*, pp. 2489–2493, International Building Performance Association (IBPSA), 2013.
- [90] F. Smarra, A. Jain, T. De Rubeis, D. Ambrosini, A. D’Innocenzo, and R. Mangharam, “Data-driven model predictive control using random forests for building energy optimization and climate control,” *Applied energy*, vol. 226, pp. 1252–1272, 2018.
- [91] M. Farina, L. Giulioni, and R. Scattolini, “Stochastic linear model predictive control with chance constraints—a review,” *Journal of Process Control*, vol. 44, pp. 53–67, 2016.
- [92] F. Oldewurtel, C. N. Jones, A. Parisio, and M. Morari, “Stochastic model predictive control for building climate control,” *IEEE Transactions on Control Systems Technology*, vol. 22, no. 3, pp. 1198–1205, 2013.
- [93] M. Farina and R. Scattolini, “Model predictive control of linear systems with multiplicative unbounded uncertainty and chance constraints,” *Automatica*, vol. 70, pp. 258–265, 2016.
- [94] A. Nemirovski and A. Shapiro, “Convex approximations of chance constrained programs,” *SIAM Journal on Optimization*, vol. 17, no. 4, pp. 969–996, 2007.
- [95] G. C. Calafiore and L. El Ghaoui, “On distributionally robust chance-constrained linear programs,” *Journal of Optimization Theory and Applications*, vol. 130, no. 1, pp. 1–22, 2006.
- [96] S. Peng, *Chance constrained problem and its applications*. PhD thesis, Université Paris Saclay (COMUE), France; Xi’an Jiaotong University, China, 2019.
- [97] M. Maasoumy and A. Sangiovanni-Vincentelli, “Optimal control of building HVAC systems in the presence of imperfect predictions,” in *5th Dynamic Systems and Control Conference (DSCC) 2012 and 11th Motion and Vibration Conference (MOVIC) 2012, Fort Lauderdale, FL, USA*, vol. 45301, pp. 257–266, American Society of Mechanical Engineers (ASME) and Japan Society of Mechanical Engineers (JSME), 2012.
- [98] A. Parisio, M. Molinari, D. Varagnolo, and K. H. Johansson, “A scenario-based predictive control approach to building HVAC management systems,” in *9th IEEE International Conference on Automation Science and Engineering (CASE) 2013, Madison, Wisconsin, USA*, pp. 428–435, IEEE, 2013.
- [99] J. Drgoňa, M. Kvasnica, M. Klaučo, and M. Fikar, “Explicit stochastic MPC approach to building temperature control,” in *52nd IEEE Conference on Decision and Control (CDC) 2013, Florence, Italy*, pp. 6440–6445, IEEE, 2013.

- [100] F. Oldewurtel, C. N. Jones, and M. Morari, "A tractable approximation of chance constrained stochastic MPC based on affine disturbance feedback," in *47th IEEE Conference on Decision and Control (CDC) 2008, Cancun, Mexico*, pp. 4731–4736, IEEE, 2008.
- [101] Y. Ma, S. Vichik, and F. Borrelli, "Fast stochastic MPC with optimal risk allocation applied to building control systems," in *51st IEEE Conference on Decision and Control (CDC) 2012, Maui, Hawaii*, pp. 7559–7564, IEEE, 2012.
- [102] X. Geng and L. Xie, "Data-driven decision making in power systems with probabilistic guarantees: Theory and applications of chance-constrained optimization," *Annual Reviews in Control*, vol. 47, pp. 341–363, 2019.
- [103] R. Evins, "A review of computational optimisation methods applied to sustainable building design," *Renewable and Sustainable Energy Reviews*, vol. 22, pp. 230–245, 2013.
- [104] C. A. Correa-Florez, A. Michiorri, and G. Kariniotakis, "Robust optimization for day-ahead market participation of smart-home aggregators," *Applied energy*, vol. 229, pp. 433–445, 2018.
- [105] J. L. Mathieu, M. G. Vayá, and G. Andersson, "Uncertainty in the flexibility of aggregations of demand response resources," in *39th Annual Conference of the IEEE Industrial Electronics Society (IECON) 2013, Vienna, Austria*, pp. 8052–8057, IEEE, 2013.
- [106] Y. Zhang, S. Shen, and J. L. Mathieu, "Distributionally robust chance-constrained optimal power flow with uncertain renewables and uncertain reserves provided by loads," *IEEE Transactions on Power Systems*, vol. 32, no. 2, pp. 1378–1388, 2016.
- [107] J. Hu and J. Cao, "Demand Response Optimal Dispatch and Control of TCL and PEV Agents with Renewable Energies," *Fractal and Fractional*, vol. 5, no. 4, p. 140, 2021.
- [108] T. Dengiz, P. Jochem, and W. Fichtner, "Uncertainty handling control algorithms for demand response with modulating electric heating devices," in *IEEE PES innovative smart grid technologies Europe (ISGT-Europe) 2019, Bucharest, Romania*, pp. 1–5, IEEE Power and Energy Society (PES), 2019.
- [109] Z. Chen, L. Wu, and Y. Fu, "Real-time price-based demand response management for residential appliances via stochastic optimization and robust optimization," *IEEE transactions on smart grid*, vol. 3, no. 4, pp. 1822–1831, 2012.
- [110] H. Li, Z. Wan, and H. He, "Real-time residential demand response," *IEEE Transactions on Smart Grid*, vol. 11, no. 5, pp. 4144–4154, 2020.

- [111] G. Liu, Y. Xu, and K. Tomsovic, "Bidding strategy for microgrid in day-ahead market based on hybrid stochastic/robust optimization," *IEEE Transactions on Smart Grid*, vol. 7, no. 1, pp. 227–237, 2015.
- [112] M. Vrakopoulou, J. L. Mathieu, and G. Andersson, "Stochastic optimal power flow with uncertain reserves from demand response," in *2014 47th Hawaii International Conference on System Sciences*, pp. 2353–2362, IEEE, 2014.
- [113] M. Vrakopoulou, B. Li, and J. L. Mathieu, "Chance constrained reserve scheduling using uncertain controllable loads part i: Formulation and scenario-based analysis," *IEEE Transactions on Smart Grid*, vol. 10, no. 2, pp. 1608–1617, 2017.
- [114] S. Frank and S. Rebennack, "An introduction to optimal power flow: Theory, formulation, and examples," *IIE transactions*, vol. 48, no. 12, pp. 1172–1197, 2016.
- [115] N. Good, E. Karangelos, A. Navarro-Espinosa, and P. Mancarella, "Optimization under uncertainty of thermal storage-based flexible demand response with quantification of residential users' discomfort," *IEEE Transactions on Smart Grid*, vol. 6, no. 5, pp. 2333–2342, 2015.
- [116] X. Kou, F. Li, J. Dong, M. Olama, M. Starke, Y. Chen, and H. Zandi, "A Comprehensive Scheduling Framework using SP-ADMM for Residential Demand Response with Weather and Consumer Uncertainties," *IEEE Transactions on Power Systems*, 2020.
- [117] K. Bruninx, Y. Dvorkin, E. Delarue, W. D'haeseleer, and D. S. Kirschen, "Valuing demand response controllability via chance constrained programming," *IEEE Transactions on Sustainable Energy*, vol. 9, no. 1, pp. 178–187, 2017.
- [118] K. Bruninx, H. Pandžić, H. Le Cadre, and E. Delarue, "On the interaction between aggregators, electricity markets and residential demand response providers," *IEEE Transactions on Power Systems*, vol. 35, no. 2, pp. 840–853, 2019.
- [119] K. Bruninx, *Improved modeling of unit commitment decisions under uncertainty*. PhD thesis, KU Leuven, Belgium, 2016.
- [120] K. Garifi, K. Baker, B. Touri, and D. Christensen, "Stochastic model predictive control for demand response in a home energy management system," in *2018 IEEE Power and Energy Society General Meeting (PESGM)*, pp. 1–5, IEEE, 2018.
- [121] M. Diekerhof, F. Peterssen, and A. Monti, "Hierarchical distributed robust optimization for demand response services," *IEEE Transactions on Smart Grid*, vol. 9, no. 6, pp. 6018–6029, 2017.

- [122] C. E. Rasmussen and C. K. I. Williams, *Gaussian Processes for Machine Learning*. Massachusetts Institute of Technology, 2006. Appendix A: Mathematical background.
- [123] W. K. Klein Haneveld, M. H. van der Vlerk, and W. Romeijnders, *Chance Constraints*, pp. 115–138. Cham: Springer International Publishing, 2020.
- [124] C. A. Thilker, R. G. Junker, P. Bacher, J. B. Jørgensen, and H. Madsen, “Model Predictive Control Based on Stochastic Grey-Box Models,” *Towards Energy Smart Homes: Algorithms, Technologies, and Applications*, pp. 329–380, 2021.
- [125] C. A. Thilker, H. Madsen, and J. B. Jørgensen, “Advanced forecasting and disturbance modelling for model predictive control of smart energy systems,” *Applied Energy*, vol. 292, 116889, 2021.
- [126] G. Reynders, J. Diriken, and D. Saelens, “Quality of grey-box models and identified parameters as function of the accuracy of input and observation signals,” *Energy and Buildings*, vol. 82, pp. 263–274, 2014.
- [127] P. Bacher and H. Madsen, “Identifying suitable models for the heat dynamics of buildings,” *Energy and Buildings*, vol. 43, no. 7, pp. 1511–1522, 2011.
- [128] H. Harb, N. Boyanov, L. Hernandez, R. Streblow, and D. Müller, “Development and validation of grey-box models for forecasting the thermal response of occupied buildings,” *Energy and Buildings*, vol. 117, pp. 199–207, 2016.
- [129] A. Tindale, “Third-order lumped-parameter simulation method,” *Building Services Engineering Research and Technology*, vol. 14, no. 3, pp. 87–97, 1993.
- [130] G. Reynders, *Quantifying the impact of building design on the potential of structural storage for active demand response in residential buildings*. PhD thesis, KU Leuven, Belgium, 2015.
- [131] D. Patteeuw, *Demand response for residential heat pumps in interaction with the electricity generation system*. PhD thesis, KU Leuven, Belgium, 2016.
- [132] G. Reynders, J. Diriken, and D. Saelens, “Bottom-up modeling of the Belgian residential building stock: influence of model complexity,” in *9th International Conference on System Simulation in Buildings (SSB) 2014, Liège, Belgium*, pp. 1–19, University of Liège, Belgium, 2014.
- [133] M. Gouda, S. Danaher, and C. Underwood, “Low-order model for the simulation of a building and its heating system,” *Building Services Engineering Research and Technology*, vol. 21, no. 3, pp. 199–208, 2000.

- [134] O. Gutschker, "Parameter identification with the software package LORD," *Building and Environment*, vol. 43, no. 2, pp. 163 – 169, 2008. Outdoor Testing, Analysis and Modelling of Building Components.
- [135] M. J. Jiménez, H. Madsen, and K. K. Andersen, "Identification of the main thermal characteristics of building components using MATLAB," *Building and Environment*, vol. 43, no. 2, pp. 170–180, 2008.
- [136] I. A. Macdonald, *Quantifying the effects of uncertainty in building simulation*. PhD thesis, University of Strathclyde, Scotland, 2002.
- [137] NBN, "NBN EN 12831-1: Energy performance of buildings - Method for calculation of the design heat load - Part 1: Space heating load," 2017.
- [138] M. Sourbron, *Dynamic Thermal Behaviour of Buildings with Concrete Core Activation*. PhD thesis, KU Leuven, Belgium, 2012.
- [139] A. Uytterhoeven, I. De Jaeger, K. Bruninx, D. Saelens, and L. Helsen, "Data-driven estimation of parametric uncertainty of reduced order RC models for building climate control," in *Building Simulation (BS) Conference 2021, Bruges, Belgium*, International Building Performance Association (IBPSA), 2021.
- [140] S. S. Shapiro and M. B. Wilk, "An analysis of variance test for normality (complete samples)," *Biometrika*, vol. 52, no. 3/4, pp. 591–611, 1965.
- [141] N. M. Razali, Y. B. Wah, *et al.*, "Power comparisons of Shapiro-Wilk, Kolmogorov-Smirnov, Lilliefors and Anderson-Darling tests," *Journal of statistical modeling and analytics*, vol. 2, no. 1, pp. 21–33, 2011.
- [142] K. D. Hopkins and D. L. Weeks, "Tests for normality and measures of skewness and kurtosis: Their place in research reporting," *Educational and Psychological Measurement*, vol. 50, no. 4, pp. 717–729, 1990.
- [143] MathWorks Help Center, "Matlab documentation: Kurtosis." <https://www.mathworks.com/help/stats/kurtosis.html>. Accessed: 2021-09-25.
- [144] MathWorks Help Center, "Matlab documentation: Skewness." <https://www.mathworks.com/help/stats/skewness.html>. Accessed: 2021-09-25.
- [145] H.-Y. Kim, "Statistical notes for clinical researchers: assessing normal distribution (2) using skewness and kurtosis," *Restorative dentistry & endodontics*, vol. 38, no. 1, pp. 52–54, 2013.
- [146] R. Baetens and D. Saelens, "Modelling uncertainty in district energy simulations by stochastic residential occupant behaviour," *Journal of Building Performance Simulation*, vol. 9, no. 4, pp. 431–447, 2016.

- [147] H. Brohus, C. Frier, and P. K. Heiselberg, "Stochastic load models based on weather data," tech. rep., 2002.
- [148] W. Lambrichts, "Model Predictive Control of Residential Heating: Accounting for Uncertainties on Weather and Occupancy Behaviour," Master's thesis, KU Leuven, Belgium, 2020.
- [149] O. Guerra-Santin and L. Itard, "Occupants' behaviour: determinants and effects on residential heating consumption," *Building Research & Information*, vol. 38, no. 3, pp. 318–338, 2010.
- [150] A. E.-D. Mady, G. Provan, C. Ryan, and K. Brown, "Stochastic model predictive controller for the integration of building use and temperature regulation," in *AAAI Conference on Artificial Intelligence 2011, San Francisco, CA, USA*, vol. 25, Association for the Advancement of Artificial Intelligence (AAAI), 2011.
- [151] I. Atmaca, O. Kaynakli, and A. Yigit, "Effects of radiant temperature on thermal comfort," *Building and environment*, vol. 42, no. 9, pp. 3210–3220, 2007.
- [152] F. Jorissen, *Toolchain for Optimal Control and Design of Energy Systems in Buildings*. PhD thesis, KU Leuven, Belgium, 2018.
- [153] Z. Wang, B. Lin, and Y. Zhu, "Modeling and measurement study on an intermittent heating system of a residence in Cambridgeshire," *Building and Environment*, vol. 92, pp. 380–386, 2015.
- [154] E. Bee, A. Prada, P. Baggio, and E. Psimopoulos, "Air-source heat pump and photovoltaic systems for residential heating and cooling: Potential of self-consumption in different European climates," in *Building Simulation (BS) Conference 2019, Rome, Italy*, vol. 12, pp. 453–463, International Building Performance Association (IBPSA), 2019.
- [155] L. Schibuola, M. Scarpa, and C. Tambani, "Demand response management by means of heat pumps controlled via real time pricing," *Energy and Buildings*, vol. 90, pp. 15–28, 2015.
- [156] U. I. Dar, I. Sartori, L. Georges, and V. Novakovic, "Advanced control of heat pumps for improved flexibility of net-zeb towards the grid," *Energy and Buildings*, vol. 69, pp. 74–84, 2014.
- [157] C. Verhelst, F. Logist, J. Van Impe, and L. Helsen, "Study of the optimal control problem formulation for modulating air-to-water heat pumps connected to a residential floor heating system," *Energy and Buildings*, vol. 45, pp. 43–53, 2012.

- [158] Photovoltaic-software.com, "Photovoltaic-software.com." <https://photovoltaic-software.com/principle-ressources/how-calculate-solar-energy-power-pv-systems>. Accessed: 2019-04-02.
- [159] S. Dubey, J. N. Sarvaiya, and B. Seshadri, "Temperature dependent photovoltaic (PV) efficiency and its effect on PV production in the world—a review," *Energy Procedia*, vol. 33, pp. 311–321, 2013.
- [160] Organisatie Duurzame Energie, "Code van goede praktijk voor de toepassing van warmtepompsystemen in de woningbouw (in Dutch)," 2004.
- [161] D. Patteuw, K. Bruninx, E. Delarue, L. Helsen, and W. D'haeseleer, "Short-term demand response of flexible electric heating systems: an integrated model," *Working Paper WP2014-28*, 2014.
- [162] L. W. Turner, "Energy Fact Sheet: Heat Pumps for Residential Heating and Cooling: Some Questions and Answers," *Agricultural Engineering Energy Series*, vol. 26, 1979. https://uknowledge.uky.edu/aees_reports/26.
- [163] Daikin Europe N.V., "Altherma, in: Technical Data Heat Pump: Altherma ERLQ008CV3."
- [164] IEE Project TABULA, "Typology Approach for Building Stock Energy Assessment." <https://episcopes.eu/iee-project/tabula/>. Accessed: 2021-01-14.
- [165] W. Cyx, N. Renders, M. Van Holm, and S. Verbeke, "IEE TABULA-typology approach for building stock energy assessment," tech. rep., 2011.
- [166] A. K. Yadav and S. Chandel, "Tilt angle optimization to maximize incident solar radiation: A review," *Renewable and Sustainable Energy Reviews*, vol. 23, pp. 503–513, 2013.
- [167] G. Qiu and S. Riffat, "Optimum tilt angle of solar collectors and its impact on performance," *International journal of ambient energy*, vol. 24, no. 1, pp. 13–20, 2003.
- [168] R. Salenbien, K. Allaerts, and J. Desmedt, "Technologische beschrijving en selectie van het elektrisch aanbod (in Dutch)," *Studie uitgevoerd in het kader van het IWT-VIS traject Smart Geotherm*, 2012.
- [169] Engie - Paul D., "Wat is de ideale hellingshoek van een dak voor zonnepanelen? (in Dutch)," 2020. <https://www.engie.be/nl/blog/zonnepanelen/ideale-hellingshoek-dak-zonnepanelen/>. Accessed: 2021-10-16.

- [170] Dark Sky, "Dark Sky API." <https://darksky.net/dev>. Accessed: 2020-05-20.
- [171] T. Winters, "Hernieuwbare productie van sanitair warm water in Vlaanderen: een energetische, economische en ecologische vergelijking (in Dutch)," Master's thesis, KU Leuven, Belgium, 2019.
- [172] Viessmann, "Technische gegevens Vitocell 100-V (in Dutch)," 2018. https://www.viessmann.nl/content/dam/vi-brands/NL/pdfs%20boilers/vitocell_100-v/5712831-NL%20TG%20VITOCCELL%20100-V%20CVA,%20CVAA,%20CVAA-A%205-2018.pdf/_jcr_content/renditions/original./5712831-NL%20TG%20VITOCCELL%20100-V%20CVA,%20CVAA,%20CVAA-A%205-2018.pdf. Accessed: 2021-10-11.
- [173] Viessmann, "EPB-Produktkenwaarden Leveringsprogramma 2015 (in Dutch)," 2015. <https://adoc.pub/viesmann-epb-produktkenwaarden-leveringsprogramma-planningsa.html>. Accessed: 2021-10-11.
- [174] K. Bruninx, D. Patteeuw, E. Delarue, L. Helsen, and W. D'haeseleer, "Short-term demand response of flexible electric heating systems: The need for integrated simulations," in *10th International Conference on the European Energy Market (EEM) 2012, Stockholm, Sweden*, pp. 1–10, IEEE, 2012.
- [175] D. Bienstock, M. Chertkov, and S. Harnett, "Chance-constrained optimal power flow: Risk-aware network control under uncertainty," *SIAM Review*, vol. 56, no. 3, pp. 461–495, 2014.
- [176] M. Zivic Djurovic, A. Milacic, and M. Krsulja, "A simplified model of quadratic cost function for thermal generators," in *23rd International DAAAM Symposium 2012, Zadar, Croatia*, vol. 23, pp. 25–28, 2012.
- [177] K. Pandžić, K. Bruninx, and H. Pandžić, "Managing risks faced by strategic battery storage in joint energy-reserve markets," *IEEE Transactions on Power Systems*, vol. 36, no. 5, pp. 4355–4365, 2021.
- [178] S. Boyd, N. Parikh, E. Chu, B. Peleato, and J. Eckstein, *Distributed optimization and statistical learning via the alternating direction method of multipliers*, vol. 3. Now Publishers Inc, 2011.
- [179] J. Eckstein and W. Yao, "Augmented Lagrangian and alternating direction methods for convex optimization: A tutorial and some illustrative computational results," *RUTCOR Research Reports*, vol. 32, no. 3, p. 44, 2012.
- [180] J. Arroyo, S. Gowri, F. De Ridder, and L. Helsen, "Flexibility quantification in the context of flexible heat and power for buildings," in *REHVA Annual*

- Meeting Conference Low Carbon Technologies in HVAC 2018, Brussels, Belgium*, Federation of European Heating, Ventilation and Air Conditioning Associations (REHVA) and Royal Association of Heating, Ventilation and Climate Control Technology (ATIC), 2018.
- [181] X. Kou, F. Li, J. Dong, M. Starke, J. Munk, Y. Xue, M. Olama, and H. Zandi, "A scalable and distributed algorithm for managing residential demand response programs using alternating direction method of multipliers (admm)," *IEEE Transactions on Smart Grid*, vol. 11, no. 6, pp. 4871–4882, 2020.
- [182] A. Mercurio, A. Di Giorgio, and F. Purificato, "Optimal fully electric vehicle load balancing with an ADMM algorithm in smart grids," in *21st Mediterranean Conference on Control and Automation (MED) 2013, Crete, Greece*, pp. 119–124, IEEE, 2013.
- [183] S. Mhanna, G. Verbič, and A. C. Chapman, "Accelerated Methods for the SOCP-Relaxed Component-Based Distributed Optimal Power Flow," in *Power Systems Computation Conference (PSCC) 2018, Dublin, Ireland*, pp. 1–7, IEEE Power and Energy Society (PES), 2018.
- [184] J. Plesník, "Finding the orthogonal projection of a point onto an affine subspace," *Linear algebra and its applications*, vol. 422, no. 2-3, pp. 455–470, 2007.
- [185] S. Boyd, S. P. Boyd, and L. Vandenberghe, *Convex optimization*. Cambridge University Press, 2004.
- [186] Q. Peng and S. H. Low, "Distributed optimal power flow algorithm for radial networks, i: Balanced single phase case," *IEEE Transactions on Smart Grid*, vol. 9, no. 1, pp. 111–121, 2016.
- [187] H. Höschle, *Capacity Mechanisms in Future Electricity Markets*. PhD thesis, KU Leuven, Belgium, 2018.
- [188] Statbel (Algemene Directie Statistiek - Statistics Belgium), "Aantal huishoudens volgens type - Populatie 01/01/2021 (in Dutch)." https://statbel.fgov.be/sites/default/files/files/documents/bevolking/5.1%20Structuur%20van%20de%20bevolking/pop-typeHH_NLv2.xlsx. Accessed: 2021-11-03.
- [189] G. Reynders, J. Diriken, and D. Saelens, "Generic characterization method for energy flexibility: Applied to structural thermal storage in residential buildings," *Applied energy*, vol. 198, pp. 192–202, 2017.
- [190] ASHRAE, "ANSI/ASHRAE Standard 55-2004 - Thermal Environmental Conditions for Human Occupancy," 2004.

- [191] The European Network of Transmission System Operators for Electricity (ENTSO-E), "ENTSO-E Transparency Platform." <https://transparency.entsoe.eu/>. Accessed: 2021-09-13.
- [192] Elia, "Adequacy and flexibility study for Belgium 2020–2030," tech. rep., 2019.
- [193] K. Poncelet, H. Höschle, E. Delarue, A. Virag, and W. D'haeseleer, "Selecting representative days for capturing the implications of integrating intermittent renewables in generation expansion planning problems," *IEEE Transactions on Power Systems*, vol. 32, no. 3, pp. 1936–1948, 2016.
- [194] G. De Zotti, S. A. Pourmousavi, H. Madsen, and N. K. Poulsen, "Ancillary services 4.0: A top-to-bottom control-based approach for solving ancillary services problems in smart grids," *IEEE Access*, vol. 6, pp. 11694–11706, 2018.

Curriculum

Anke Uytterhoeven

°July 4, 1994 in Bonheiden, Belgium

Work experience

| | |
|-----------|---|
| 2017–2022 | PhD researcher and teaching assistant Division of Applied Mechanics and Energy Conversion, Department of Mechanical Engineering, KU Leuven, Leuven, Belgium Project: C2 research project C24/16/018 <i>"Energy Storage as a Disruptive Technology in the Energy System of the Future"</i> |
| 2016 | Student job as technology engineer Atlas Copco, Wilrijk, Belgium |
| 2015 | Internship Atlas Copco, Wilrijk, Belgium |

Education

- | | |
|-----------|---|
| 2015–2017 | Master of Science in Mechanical Engineering KU Leuven, Leuven, Belgium <i>Magna cum laude</i> |
| 2012–2015 | Bachelor of Science in Mechanical and Chemical Engineering KU Leuven, Leuven, Belgium <i>Magna cum laude</i> |
| 2006–2012 | Greek-Mathematics Sint-Ursula-Instituut, O.-L.-V.-Waver, Belgium |

Miscellaneous

- | | |
|-----------|--|
| 2017–2021 | Board member of Flemish Organization of Sustainable Energy ODE Vlaanderen, Brussels, Belgium |
| 2010–2012 | Student council president Sint-Ursula-Instituut, O.-L.-V.-Waver, Belgium |

List of publications

Articles submitted to peer-reviewed academic journals

- [1] A. Uytterhoeven, R. Van Rompaey, K. Bruninx, D. Saelens, and L. Helsen, "Chance Constrained Stochastic MPC for Building Climate Control Under Combined Parametric and Additive Uncertainty," submitted to *Journal of Building Performance Simulation*, July 2021.
Status: referee comments received, minor revision in progress.

Articles planned to be submitted to peer-reviewed academic journals

- [2] A. Uytterhoeven, R. Van Rompaey, K. Bruninx, and L. Helsen, "Distributed Optimization of the Stochastic Load of Residential Heat Pumps for Demand Response," in progress, to be submitted to *Applied Energy*.

Articles published in conference proceedings

- [3] A. Uytterhoeven, G. Deconinck, A. Arteconi, and L. Helsen, "Hybrid heat pump scenarios as a transition towards more flexible buildings," in *Proceedings of the 10th International Conference on System Simulation in Buildings (SSB) 2018, Liège, Belgium*, Université de Liège, Belgium, 2018.
- [4] A. Uytterhoeven, I. De Jaeger, K. Bruninx, D. Saelens, and L. Helsen, "Data-driven estimation of parametric uncertainty of reduced order RC models for building climate control," in *Proceedings of the Building Simulation (BS) Conference 2021, Bruges, Belgium*, International Building Performance Association (IBPSA), 2021.

Presentations at international scientific conferences

- [5] A. Uytterhoeven, G. Deconinck, A. Arteconi, and L. Helsen, "Hybrid heat pump scenarios as a transition towards more flexible buildings," presented at *10th International Conference on System Simulation in Buildings (SSB) 2018, Liège, Belgium, 10-12 December 2018*.
- [6] A. Uytterhoeven, A. Arteconi, and L. Helsen, "Decentralized storage and demand response: impact on renewable share in grids and buildings," presented at *World Sustainable Energy Days 2019, Wels, Austria, 27 February – 1 March 2019*.
- [7] A. Uytterhoeven, K. Bruninx, G. Deconinck, A. Arteconi, and L. Helsen, "Leveraging residential thermal loads in local energy communities – the role of demand response aggregators," presented at *Intelligent Building Operations Workshop 2019, Colorado Boulder, United States, 7-9 August 2019*.
- [8] A. Uytterhoeven, I. De Jaeger, K. Bruninx, D. Saelens, and L. Helsen, "Data-driven estimation of parametric uncertainty of reduced order RC models for building climate control," presented at *Building Simulation (BS) Conference 2021, Bruges, Belgium, 1-3 September 2021*.

Science Outreach

- [9] A. Uytterhoeven, and L. Helsen, "The added value of heat pumps for grid stability via demand response," presented at *11th Heat Pump Symposium 2018, Ghent, Belgium, 11 October 2018*.
- [10] L. Helsen, M. Jones, and A. Uytterhoeven, "HP Forum 2019 Opening Session - Introducing the call of the youth on energy and climate," presented at *HP Forum 2019, Brussels, Belgium, 15-16 May 2019*.
- [11] A. Uytterhoeven, A. Arteconi, and L. Helsen, "De digitale meter en warmtepompen. Verhoging zelfverbruik & gevolgen voor dimensionering (in Dutch)," presented at *General Assembly Meeting Flemish Heat Pump Platform 2019, Kortenberg, Belgium, 24 May 2019*.
- [12] A. Uytterhoeven, G. Deconinck, A. Arteconi, and L. Helsen, "The Added Value of Heat Pumps for Grid Stability via Demand Response," in *IEA Heat Pumping Technologies Magazine, vol 37, no2, August 2019*, Heat Pump Centre, 2019.

FACULTY OF ENGINEERING SCIENCE
DEPARTMENT OF MECHANICAL ENGINEERING
THERMAL SYSTEMS SIMULATION
Celestijnenlaan 300 box 2421
B-3001 Leuven
<http://the.sysi.be>

